UiT
THE ARCTIC
UNIVERSITY
OF NORWAY

FACULTY OF SCIENCE AND TECHNOLOGY
DEPARTMENT OF MATHEMATICS AND STATISTICS

Deforming the vacuum

On the physical origin and numerical calculation of the Casimir effect

—

Karl Øyvind Mikalsen
MAT-3900 Master's Thesis in Mathematics, May 2014

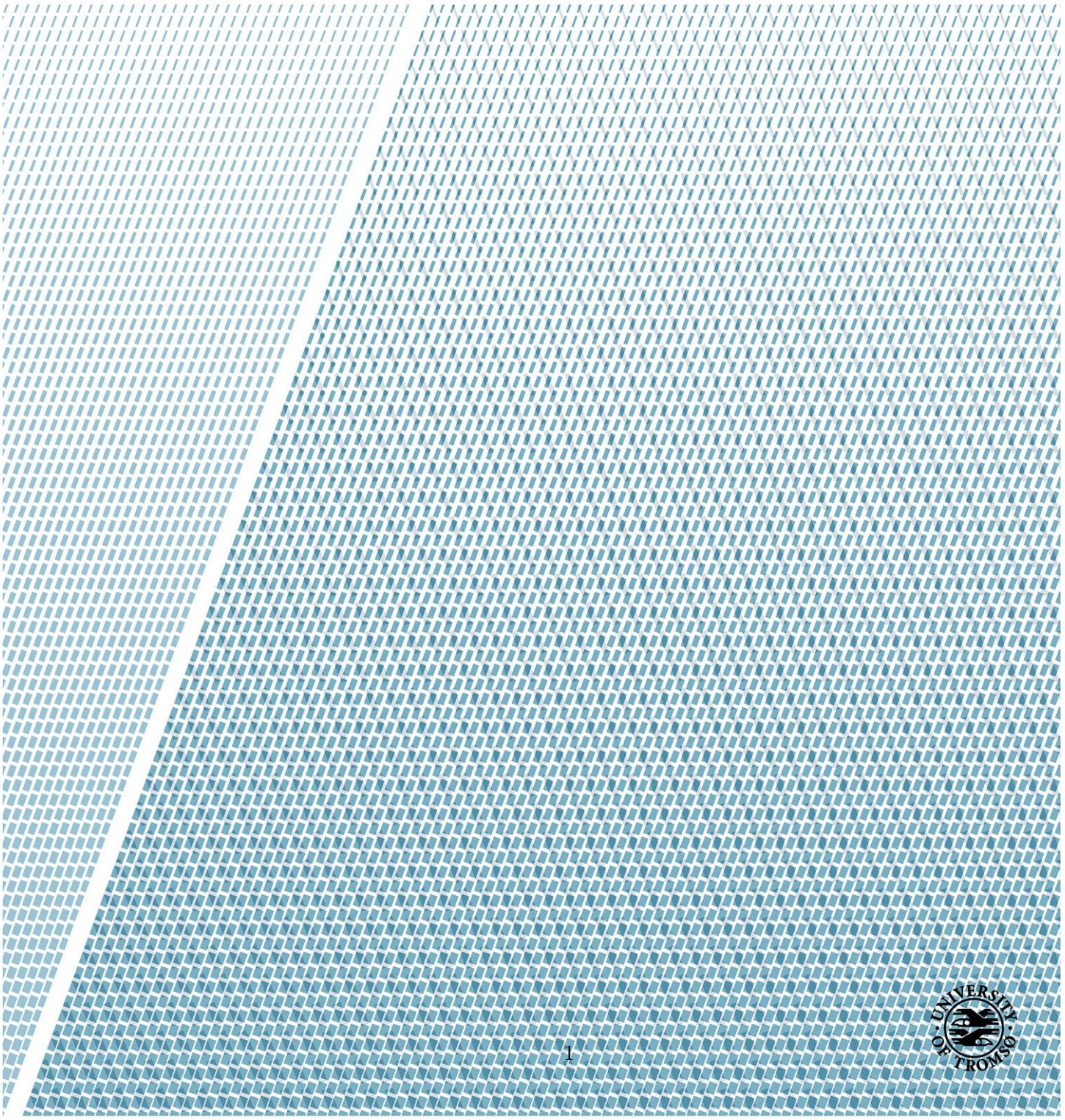

Abstract

A new method for calculating the Casimir force between compact objects was introduced in May 2012 by Per Jakobsen and Isak Kilen [1]. In this method a regularization procedure is used to reduce the pressure to the solution of an integral equation defined on the boundaries of the objects. In this thesis the method is further developed by extending from a 2D to a 3D massless scalar field, subject to Dirichelet boundary conditions on the boundaries of the objects. The method is implemented numerically and tested on configurations consisting of plates, spheres and ellipsoids. We compare the method to the functional integral method and the method of mode summation where possible.

Our results are in accordance with what I. Kilen found; the method correctly predicts the geometry dependence of the Casimir force, but the size of the force is off by a factor of two.

Acknowledgements

This thesis concludes my master's degree in applied mathematics at UiT The Arctic University of Norway. First and foremost I would like to express my sincere gratitude to my supervisor Per Jakobsen for the excellent guidance he has provided throughout this study. This thesis wouldn't have been written without his advices and support. I would like to thank Hugues Verdure for his help with computer support. Also other staff and fellow students at the Institute of Mathematics and Statistics deserves to be thanked for their help and support.

Contents

Chapter 1

Introduction

1.1 The Casimir effect

The typical example of the *Casimir force* is an attractive force between uncharged, parallel, conducting metal plates in vacuum and zero temperature. This force was first predicted by Casimir in 1948 [2]. He assumed that the vacuum between the plates was filled with an electromagnetic field and predicted that the force per area is a function of the separation distance a,

$$\frac{F(a)}{A} = -\frac{\pi^2}{240}\frac{\hbar c}{a^4}. \tag{1.1}$$

The minus sign indicates that the plates attract each other. This result was derived using a method based on *mode summation*. Conceptually this method is simple, one uses the fact that a quantized electromagnetic field can be decomposed into an infinite number of quantum harmonic oscillators, which usually are called modes. By assigning a zero-point energy of $\frac{1}{2}\hbar\omega$ to each mode (photon) of the quantized field, the ground state energy of the electromagnetic field can be found by summing over zero-point energies of the field determined by Dirichelet boundary conditions where the plates are located;

$$E = \frac{\hbar}{2}\sum_n \omega_n. \tag{1.2}$$

This sum is divergent, but by subtracting the energy without the presence of boundaries and giving a proper definition to the sums, Casimir was able to extract a finite result, the *Casimir energy* for this geometry. When the Casimir energy is known, the *Casimir force* can be found by taking the derivative of the energy with respect to a parameter, in this case with respect to the separation distance a. Because of this relationship, one often only refers to the *Casimir effect*. As we can see from equation (1.1), the force decreases rapidly as the separation between the plates increases. This indicates that the Casimir effect is only measurable at small length scales, typically nano-meter and micro-meter.

In general, the Casimir force is usually thought of as a force arising when the zero point fluctuations of a quantum field are modified by the presence of static or slowly moving objects. The Casimir energy is obtained by taking the difference between the energy of the field when the objects are present and when the objects are removed to infinite separation. This effect has been seen as a physical consequence directly due to zero-point fluctuations. However, it should be mentioned that the Casimir effect does not prove the "reality" of the vacuum energy of the zero point fluctuations. It has been explained without reference to such fluctuations. For example, in 1975, Schwinger explained the Casimir effect in the source theory language [3]. Nevertheless, it is a fact that the Casimir effect can be, and usually is, explained using quantum fluctuations.

The Casimir force has similarities with the *van der Waals* force. Both effects are of quantum origin (the forces depend on $\hbar$) and can cause an *attractive* force between two neutral objects. A difference is that the Casimir force in addition may be *repulsive*. The attractive or repulsive character of the Casimir force depends on the geometry of the objects, the number of spatial dimensions and whether the quantum field between the objects is bosonic or fermionic etc. An other important difference is that the Casmir force is relativistic (the force depends on the speed of light c), while the van der Waals force is non-relativistic.

1.2 Measurements and applications of the Casimir effect

Even though the Casimir force was predicted theoretically in 1948, it should take almost 50 years before the first successful measurement of the force was done. In fact, Casimir's paper for a long time remained largely unknown, but from the 1970s it has received more and more attention and especially the last 15-20 years, the Casimir effect has been intensely investigated. The first reported attempt to measure the force was in 1958. Then Sparnaay et al. tried to measure the Casimir force between two parallel plates. However, due to systematic errors, the measurements had a 100 % uncertainty and all Sparnaay could conclude was that "the observed attractions do not contradict Casimir's theoretical prediction" [4]. The first successful measurement was completed in 1997 by S.K. Lamoreaux [5]. Since the configuration of two parallel plates is difficult to use experimentally, he instead measured the force between a plate and a sphere. He obtained results in agreement with theory at the level of 5% . In 1998 Mohideen and Roy [6] measured the Casimir force, also between a plate and a sphere, but even more accurately than Lamoreaux. Their experiment differed from theoretical predictions by less than 2 %.

As today's electrical devices become smaller and more and more devices are invented using nanotechnology, the need for understanding and taking benefit of the Casimir effect increases. Nanoelectromechanical systems (NEMS) and microelectromechanical

systems (MEMS) are terms used to describe nanofabricated devices. These devices can function as sensors, routers and actuators (devices that convert an electrical signal into a mechanical output). Accelerometers and gyroscopes in cars, and microphones in portable devices are examples of such electromechanical systems. The Casimir force typically become influential at distances below a micron and therefore it has to be taken into consideration when designing such devices. A tendency of MEMS devices is that the moving components frequently jump into contact with the fixed electrodes and adhere to them. This phenomenon is called stiction, and leads to loss of functionality. It has been recognized that the Casimir force is primary cause to stiction [7]. Careful analysis of the Casimir force is necessary to design devices that avoid such problems. It could be that it is possible to take advantage of the fact that the Casimir force in some cases is repulsive to resolve the problem of stiction. It has also been suggested that repulsive Casimir forces could allow quantum levitation of objects and lead to a new class of nanoscale devices with ultra-low static friction [8]. We see that the Casimir effect both can provide new functionality and be a hindrance. In any case, this should be a motivation for more study the effect, both theoretically and experimentally.

1.3 Methods for calculating the Casimir force

As mentioned above, especially after the successful measurements of the Casimir effect in 97 and 98, many methods for calculating the Casimir effect have been developed. In this section we discuss some methods that are of particular interest for us.

The classical method for calculating the Casimir force is the method of mode summation that Casimir used in his original work. This method has now been further developed and use highly advanced mathematical methods like the argument principle and zeta function regularization. An advantage of this method is that it can be used to calculate the Casimir effect exactly. Mode summation works very well for the case Casimir considered; perfectly conducting parallel plates, vacuum and zero temperature. However, as one move away from this configuration, the method becomes progressively more difficult to apply. The problem is that one has to find the full frequency spectrum $\{\omega_n\}_{n=1}^{\infty}$, and for non-symmetric configurations this is hopeless do analytically. To obtain the required precision numerically is also very hard. We are left with the configurations where it is possible to solve the mode equations using separation of variables. Typical examples are symmetric configurations such as two parallel plates, two concentric spheres or cylinders. In fact, even for very symmetric situations such as two concentric spheres, the method is very hard to apply. The reason is that extracting a finite Casimir energy of the sum in equation (1.2) is also a very hard problem in general. For practical applications of the Casimir effect, it is not enough to restrict only to symmetric configurations. Therefore general methods that applies to arbitrary configurations are needed. However, when

developing new methods, it is useful to test the method on configurations where the Casimir effect can be obtained by mode summation.

A method that applies to non-planar configurations is the *proximity force approximation* (PFA). For many years, using PFA was the only practical way to compute the Casimir effect for other configurations than parallel plates [9]. Essentially, this is a method for treating curved surfaces as flat. The surfaces of the interacting objects are divided into pairs of small parallel plates. By extending the plates to infinity, Casimir's original result can be applied to each of the pairs. Taking the sum over the contributions from each of the pairs, one obtains the total Casimir energy or force. However, this approximation is only valid for very small separations and therefore the applicability of the PFA is limited.

Whereas it is hard to apply numerical methods using mode summation, there has in the 21th century been developed methods that don't require knowledge about the mode spectrum and are adapted for using modern numerical tools. An example is a method based on functional integrals developed by T.Emig [10], [11], [12], [13]. An advantage of the method is that it can be applied to arbitrary configurations of objects, different boundary conditions and quantum fields. This method, which is based on Feynman's idea to integrate over weighted classical paths, has been further developed by P. Jakobsen and I. Kilen [1]. We refer to it as the *functional integral method* (FIM) and give a brief description of the method here. First, the Casimir energy is related to a functional integral, which turns out to be of Gaussian type since the field equations are linear. By discretizing the boundaries of the conductors, using a free-space Green's function and defining a complete, orthonormal set of functions on the boundaries, the Casimir energy can be expressed in terms of a determinant of a finite matrix. In order to find this matrix, one has to find inverses and products of other matrices. This method has been highly successful for calculating the Casimir effect in situations where mode summation doesn't apply. However, since the method involves calculation of a determinant of a matrix that easily become very large, it is hard to make an effective implementation of the method, for example using parallelization.

All the methods we have considered till now output the Casimir energy. The energy is related to the pressure (or force) on the objects via a derivative. Thus, if one use a numerical method and wants to calculate the force or pressure, a minimum of two evaluations of the energy is required. However, there exist methods for calculating the pressure directly. A possibility is to use Green's functions, which are related to the pressure via some derivatives. The pressure has to be calculated on the boundaries of the conductors, but the Green's functions are extremely singular here, and therefore one obtain an infinite pressure if no *regularization* is used. The problem with infinities seems to be unavoidable in all methods for calculating the Casimir effect. There are many ways dealing with these infinite expressions, but a common word for all such methods

is regularization. The pressure that is obtained directly from the Green's function is a sum of the self pressure and the interaction pressure. Whereas it is the interaction pressure that causes the force on the objects, the self pressure doesn't contribute to the total force and is infinite in general. A major part of the regularization procedure will be to extract out the interaction pressure such that a finite pressure is obtained. This appears to be the same kind of problem that one meets in the mode summation approach, but there is an important difference; in the Green's function approach it is possible to apply a regularization procedure that is more or less independent of the geometry of the objects. One can therefore regularize before using numerical methods on the regularized equations. An implication is that the Green's function approach isn't stuck to symmetric situations, it applies to arbitrary configurations. In 2006 a numerical approach using Green's functions based on the finite difference time domain (FDTD) method from computational electromagnetics was introduced [14]. With this method it is possible to calculate the Casimir force for complex geometries. When using FDTD, the entire problem space is gridded, also the space between the objects. However, the Green's functions only have to be calculated on the boundaries of the objects and therefore it seems like this approach involves unnecessary calculations.

We should keep in mind that the problem sizes easily become so large that the numerical calculations become hard to perform, even on nowadays supercomputers. Therefore unnecessary calculations should be avoided. I. Kilen and P. Jakobsen introduced a new Green's function approach in 2012 [1], the *boundary integral method* (BIM), where the Casimir pressure is calculated on the boundaries only. This method applies to arbitrary configurations and is most efficient when used on linear equations and boundaries with piecewise linear material coefficients. In the BIM, the Casimir pressure is found by solving a set of boundary integral equations. The equations are regularized before they are discretized and solved numerically. Computationally the BIM is based on filling and solving a set of linear equations, which is a problem that has the advantage that it can be programmed in parallel. In addition, if the boundaries of the objects of interest are symmetric, the computational load for this method can be reduced enormously. So far, the method has been investigated for the case of a 2D massless scalar field subject to Dirichelet boundary conditions. I. Kilen found that in this case it is possible to find fully regularized boundary integral equations for the pressure, but that a factor of two was missing. He found that this missing factor was geometry independent and concluded that it was lost somewhere in the theory.

1.4 Layout and aims

The object of this thesis is to extend the boundary integral method (BIM) from two to three spatial dimensions. We consider the case of a massless scalar field subject

to Dirichelet boundary conditions. We will investigate whether it is possible to fully regularize the boundary integral equations, before solving them numerically, also in the three dimensional case. If so, we expect that there is still a missing factor. The question is whether this factor has the same value as in 2D, or whether it depends on the number of dimensions. We will further investigate the theory of the method and hopefully find the source of this missing factor. The method will be compared to the functional integral method and the method of mode summation for different configurations.

In chapter 2 the theory for the boundary integral method (BIM) is developed. First we define the Green's function using the scalar field. We derive some of its properties and show that it actually is a Green's function, i.e. that it is the inverse of the differential operator in the scalar field equation. The stress tensor will be used to show that the Casimir force is related to the Green's function via a double normal derivative. In order to find this quantity, we formulate the differential equation for the Green's function as a boundary integral equation. This equation is regularized through a process that involves several steps. We discretize and formulate the regularized boundary integral equations as a system of linear equations that will be solved numerically. Explicit expressions for all the matrix elements will be derived and discussed. At last, we show that there is a great potential of reducing the computational load, if the configuration of objects is symmetric.

The functional integral method (FIM) will be discussed in chapter 3. First a formula that relates the Casimir energy to the transition amplitude is found. The transition amplitude is expressed as a functional integral over an exponential. After implementing both spatial and periodic BCs, using the classical equations of motion, a change of variables and some more steps, we will be able to solve the functional integral exactly. The regularization involves subtraction of self-interaction terms. Finally we arrive at a formula for the Casimir energy that will involve an integral over a determinant of a matrix. This matrix contains all the information about the geometry of the problem. The integral will be calculated numerically and therefore we derive expressions for the matrix elements.

In chapter 4 the method of mode summation is used to derive simple formulas for the Casimir energy for two symmetric configurations. For the parallel plates configuration, we derive the energy using two different methods. The first is based on the argument principle, whereas the second method is regularized using zeta functions. The second configuration is two concentric spheres. Applying mode summation to this configuration is more advanced. The regularization will involve several steps such as frequency cutoffs, zeta function regularization and the argument principle.

Chapter 5 gives a general relation between the Casimir energy and the Casimir force. For the configurations where the method of mode summation and/or the functional integral method will be applied, we use this relation to derive explicit expressions for

the force. Chapter 6 describe the numerical implementations of the BIM and FIM. We also discuss the complexity of the two methods.

We are going to test the implementation of the BIM on different configurations. The BIM is compared to the FIM and the exact solution found using mode summation where possible. First will the flat configuration consisting of two parallel plates be considered. We thereafter test the method on configurations where the objects have a constant, non-zero curvature; two concentric spheres and two adjacent spheres. Configurations consisting of objects with varying curvature (ellipsoids) will also be considered. The results of these tests, and a discussion, are presented in chapter 7. We also compare our results to the results Isak Kilen obtained. In chapter 8 we conclude on the validity of the boundary integral method.

In appendix A some Gaussian integrals are calculated. The final result in this appendix is used in the functional integral method.

For the special configuration consisting of two parallel plates, we discretize the boundaries of the objects using two different methods. We use both a structured grid of squares and an unstructured grid consisting of triangles. The latter is a special case of a *triangulation*, which we will discuss in more detail in appendix B. The reason for triangulating the surfaces is that such a discretization is much more flexible than structured grids in fitting to objects of arbitrarily shape. Therefore we will for all other configurations only use triangulations. However, by using two different discretizations on the plates, we can test the importance of the discretization in the implementations of the BIM and FIM. The results of these comparisons are also given in chapter 7.

Appendix C lists up programs we have developed and/or used in our implementation of the BIM and FIM, and give a short explanation of them. The reason for including this appendix is to make it easier to re-use our implementations of the BIM and the FIM.

1.5 Configuration of objects

The theory of the BIM will be developed for a configuration of objects that consists of r static, compact, perfect conductors of arbitrarily shape. Let Q_α denote the boundary of the conductor V_α. The boundary Q_α is idealized; it will be assumed that Q_α consists of an ideal metal which is uncharged and perfectly conducting. Let V_0 denote the complement to the compact conductors. Thus

$$V_0 = \mathbb{R}^3 - \sum_{\alpha=1}^{r} V_\alpha. \tag{1.3}$$

The space V_0 is assumed to consist of a vacuum. Our boundary integral equations will be derived under the assumption that the temperature is at absolute zero. The vacuum

in V_0 will consist of the simplest example of a three dimensional relativistic field that is possible find, namely a massless scalar field $\hat{\varphi}$ in its ground state. The fact that the objects are perfectly conducting means that we can assign the Dirichelet boundary conditions

$$\hat{\varphi}|_{Q_\alpha} = 0, \quad \alpha = 1, ..., r, \tag{1.4}$$

at the boundaries Q_α. These boundary conditions simulate perfectly conducting boundaries from the electromagnetic case and we will also for the scalar field case call these boundary conditions perfectly conducting.

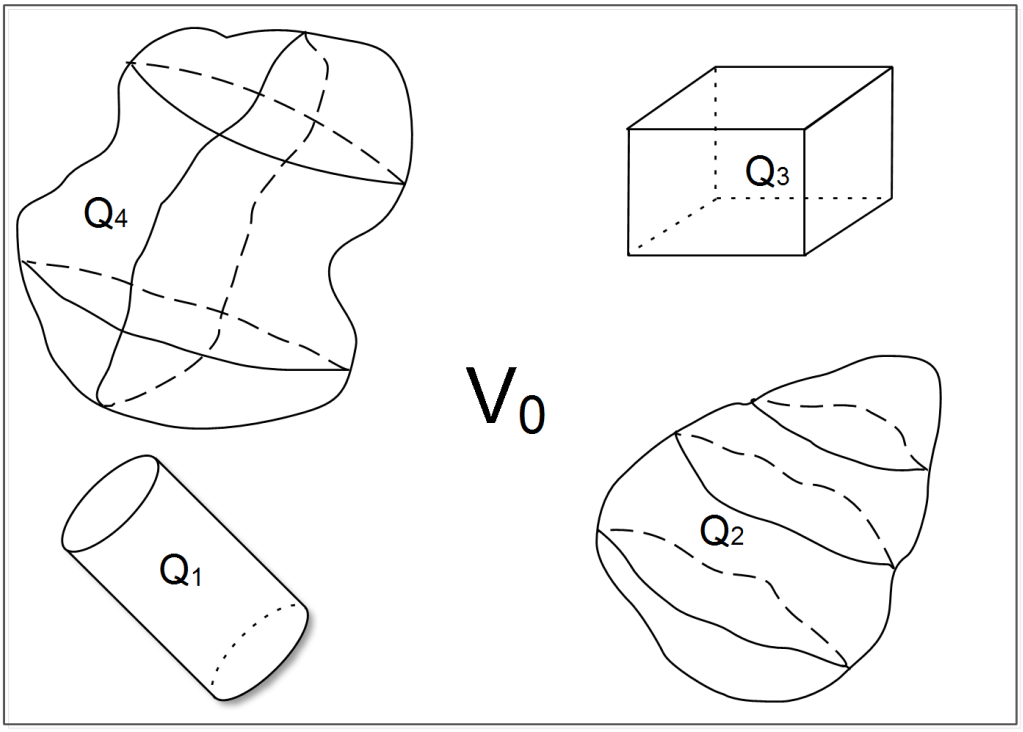

FIGURE 1.1: Possible configuration of compact objects.

Chapter 2

Boundary integral method

2.1 Green's function

In this section we define our Green's function. We derive some of its properties and show that it actually is a Green's function for the scalar field equation.

The massless scalar field $\hat{\varphi}$ that fills the region $V_0 = \mathbb{R}^3 - \sum_{\alpha=1}^{r} V_\alpha$ is determined by the field equation

$$\begin{aligned} \hat{\varphi}_{tt} - \nabla^2 \hat{\varphi} &= 0 \\ \hat{\varphi}|_{Q_j} &= 0, \end{aligned} \tag{2.1}$$

where Q_j is the boundary of the object V_j. In order to simplify the equations, natural units are selected, i.e $\hbar = c = k = 1$, where k is the *Boltzmann* constant. The fields $\hat{\varphi}$ and $\hat{\varphi}_t$ satisfy the *equal time commutation relations*

$$\begin{aligned} [\hat{\varphi}(\boldsymbol{x}, t), \hat{\varphi}(\boldsymbol{x'}, t)] = [\hat{\varphi}_t(\boldsymbol{x}, t), \hat{\varphi}_t(\boldsymbol{x'}, t)] = 0, \\ [\hat{\varphi}_t(\boldsymbol{x}, t), \hat{\varphi}(\boldsymbol{x'}, t)] = i\delta(\boldsymbol{x} - \boldsymbol{x'}). \end{aligned} \tag{2.2}$$

In order to obtain a Green's function that decay exponentially instead of oscillatory, we transform to imaginary time, $t = -is$. The time derivative changes as $\partial_t = \partial_s \frac{ds}{dt} = i\partial_s$ and the equation for the quantized field $\hat{\varphi}$ becomes

$$\begin{aligned} \hat{\varphi}_{ss} + \nabla^2 \hat{\varphi} &= 0 \\ \hat{\varphi}|_{Q_j} &= 0, \end{aligned} \tag{2.3}$$

and commutation relations

$$\begin{aligned} [\hat{\varphi}(\boldsymbol{x}, s), \hat{\varphi}(\boldsymbol{x'}, s)] = [\hat{\varphi}_s(\boldsymbol{x}, s), \hat{\varphi}_s(\boldsymbol{x'}, s)] = 0, \\ [\hat{\varphi}_s(\boldsymbol{x}, s), \hat{\varphi}(\boldsymbol{x'}, s)] = \delta(\boldsymbol{x} - \boldsymbol{x'}). \end{aligned} \tag{2.4}$$

In the Heisenberg picture the field operator $\hat{\varphi}(\boldsymbol{x}, s)$ satisfies the equation of motion

$$\frac{d}{ds}\hat{\varphi}(\boldsymbol{x}, s) = [\hat{H}, \hat{\varphi}(\boldsymbol{x}, s)], \tag{2.5}$$

where $\hat{H}$ is the Hamiltonian for the system. The conductors are assumed to be stationary so that $\hat{H}$ is time independent, i.e. independent of s. Equation (2.5) is formally solved by

$$\hat{\varphi}(\boldsymbol{x}, s) = e^{s\hat{H}}\hat{\varphi}(\boldsymbol{x})e^{-s\hat{H}}, \tag{2.6}$$

where $\hat{\varphi}(\boldsymbol{x}) = \hat{\varphi}(\boldsymbol{x}, 0)$

The basic Green's function $\mathcal{D}$ is defined by

$$\mathcal{D}(\boldsymbol{x}, s, \boldsymbol{x'}, s') = \left\langle T[\hat{\varphi}(\boldsymbol{x}, s)\hat{\varphi}(\boldsymbol{x'}, s')] \right\rangle. \tag{2.7}$$

I.e $\mathcal{D}$ is the expectation value of the time ordered product of the field $\hat{\varphi}$ in it's ground state. It is assumed that the quantum field is in a state of thermal equilibrium at temperature T. We will at the end of this section let the temperature go to zero, but to start with, we consider a general temperature T. Given thermal equilibrium, the *density matrix* is $\hat{\rho} = \frac{1}{Z}e^{-\beta\hat{H}}$. Defining $\beta = 1/T$ and using the property $\left\langle \hat{A} \right\rangle = \mathrm{Tr}(\hat{\rho}\hat{A})$, we get

$$\mathcal{D}(\boldsymbol{x}, s, \boldsymbol{x'}, s') = \frac{1}{Z}\mathrm{Tr}\left(e^{-\beta\hat{H}}T[\hat{\varphi}(\boldsymbol{x}, s)\hat{\varphi}(\boldsymbol{x'}, s')]\right), \tag{2.8}$$

where $Z = \mathrm{Tr}\left(e^{-\beta\hat{H}}\right)$ is the partition function. The derivations that follow will only relate to the time domain. In order to simplify the notation, the abbreviation

$$\mathcal{D}(s, s') = \mathcal{D}(\boldsymbol{x}, s, \boldsymbol{x'}, s') \tag{2.9}$$

will be used, meaning that the two spatial arguments are $\boldsymbol{x}$ and $\boldsymbol{x'}$. Define

$$\begin{aligned} \mathcal{D}^+(s, s') &= \left\langle \hat{\varphi}(\boldsymbol{x}, s)\hat{\varphi}(\boldsymbol{x'}, s') \right\rangle, \\ \mathcal{D}^-(s, s') &= \left\langle \hat{\varphi}(\boldsymbol{x'}, s')\hat{\varphi}(\boldsymbol{x}, s) \right\rangle. \end{aligned} \tag{2.10}$$

Thus the Green's function can be written as

$$\mathcal{D}(s, s') = \begin{cases} \mathcal{D}^+(s, s') & s > s' \\ \mathcal{D}^-(s, s') & s < s'. \end{cases} \tag{2.11}$$

We will now derive some properties of the Green's function. Equation (2.6) is used to show that the Green's function is periodic in β;

$$\begin{aligned}
\mathcal{D}^+(s+\beta, s') &= \frac{1}{Z}\mathrm{Tr}\left(e^{-\beta\hat{H}}e^{(s+\beta)\hat{H}}\hat{\varphi}(\boldsymbol{x})e^{-(s+\beta)\hat{H}}\hat{\varphi}(\boldsymbol{x'}, s')\right) \\
&= \frac{1}{Z}\mathrm{Tr}\left(e^{s\hat{H}}\hat{\varphi}(\boldsymbol{x})e^{-s\hat{H}}e^{-\beta\hat{H}}\hat{\varphi}(\boldsymbol{x'}, s')\right) \\
&= \frac{1}{Z}\mathrm{Tr}\left(\hat{\varphi}(\boldsymbol{x}, s)e^{-\beta\hat{H}}\hat{\varphi}(\boldsymbol{x'}, s')\right) \\
&= \frac{1}{Z}\mathrm{Tr}\left(e^{-\beta\hat{H}}\hat{\varphi}(\boldsymbol{x'}, s')\hat{\varphi}(\boldsymbol{x}, s)\right) \\
&= \mathcal{D}^-(s, s'),
\end{aligned} \tag{2.12}$$

where a property of traces of matrices is used; $\mathrm{Tr}(ABC) = \mathrm{Tr}(CAB) = \mathrm{Tr}(BCA)$. Using similar reasoning, we get

$$\mathcal{D}^-(s, s'+\beta) = \mathcal{D}^+(s, s'). \tag{2.13}$$

Equations (2.12) and (2.13) are known as the Kubo-Martin-Schwinger (KMS) boundary conditions. The fact that $\hat{H}$ is time independent gives

$$\begin{aligned}
\mathcal{D}^+(s, s') &= \frac{1}{Z}\mathrm{Tr}\left(e^{-\beta\hat{H}}\hat{\varphi}(\boldsymbol{x}, s)\hat{\varphi}(\boldsymbol{x'}, s')\right) \\
&= \frac{1}{Z}\mathrm{Tr}\left(e^{-\beta\hat{H}}e^{s\hat{H}}\hat{\varphi}(\boldsymbol{x})e^{-s\hat{H}}e^{s'\hat{H}}\hat{\varphi}(\boldsymbol{x'})e^{-s'\hat{H}}\right) \\
&= \frac{1}{Z}\mathrm{Tr}\left(e^{-\beta\hat{H}}e^{(s-s')\hat{H}}\hat{\varphi}(\boldsymbol{x})e^{-(s-s')\hat{H}}\hat{\varphi}(\boldsymbol{x'})\right) \\
&= \mathcal{D}^+(s-s', 0).
\end{aligned} \tag{2.14}$$

Similar calculations give that

$$\mathcal{D}^-(s, s') = \mathcal{D}^-(s-s', 0). \tag{2.15}$$

Based on the above properties, we introduce a slightly modified Green's function

$$\mathcal{D}(s) = \begin{cases} \mathcal{D}^+(s, 0) & s > 0 \\ \mathcal{D}^-(s, 0) & s < 0. \end{cases} \tag{2.16}$$

Equations (2.14) and (2.15) give that

$$\mathcal{D}(s-s') = \mathcal{D}(s, s') \quad \forall s, s' \in \mathbb{R}. \tag{2.17}$$

Thus there is a close relationship between the two Green's functions.

Now let $|n\rangle$ be a complete set of eigenstates for $\hat{H}$, i.e $\hat{H}|n\rangle = E_n|n\rangle$. For $s > 0$ we have

$$\begin{aligned}\mathcal{D}(s) = \mathcal{D}^+(s,0) &= \frac{1}{Z}\mathrm{Tr}\left(e^{-\beta\hat{H}}e^{s\hat{H}}\hat{\varphi}(\boldsymbol{x})e^{-s\hat{H}}\hat{\varphi}(\boldsymbol{x'})\right) \\ &= \frac{1}{Z}\sum_n \left\langle n \left| e^{-\beta\hat{H}}e^{s\hat{H}}\hat{\varphi}(\boldsymbol{x})e^{-s\hat{H}}\hat{\varphi}(\boldsymbol{x'})\right| n\right\rangle \\ &= \frac{1}{Z}\sum_{nn'} e^{-(\beta-s)E_n}e^{-sE_{n'}}\left\langle n|\hat{\varphi}(\boldsymbol{x})|n'\right\rangle\left\langle n'|\hat{\varphi}(\boldsymbol{x'})|n\right\rangle.\end{aligned} \tag{2.18}$$

Observe that when $s > \beta$, we get exponential growth and the series doesn't converge. Thus $\mathcal{D}(s)$ only exists for $s \leq \beta$. Similar calculations for $s < 0$ give

$$\mathcal{D}(s) = \frac{1}{Z}\sum_{nn'} e^{-(\beta+s)E_n}e^{sE_{n'}}\left\langle n|\hat{\varphi}(\boldsymbol{x'})|n'\right\rangle\left\langle n'|\hat{\varphi}(\boldsymbol{x})|n\right\rangle. \tag{2.19}$$

Thus $\mathcal{D}(s)$ only exists for $s \geq -\beta$. Combining the two latest results, we get that $\mathcal{D}(s)$ only exists for $s \in [-\beta, \beta]$. We apply the KMS conditions and get

$$\mathcal{D}(s+\beta) = \mathcal{D}^+(s+\beta,0) = \mathcal{D}^-(s,0) = \mathcal{D}(s). \tag{2.20}$$

Thus $\mathcal{D}(s)$ is determined by its values on $[-\beta, 0]$. By definition, we then extend $\mathcal{D}(s)$ to all s as a function of period β.

We now show that $\mathcal{D}(s)$ is a Green's function for the scalar field equation (2.3). First note that

$$\mathcal{D}(s) = \theta(s)\left\langle\hat{\varphi}(\boldsymbol{x},s)\hat{\varphi}(\boldsymbol{x'},0)\right\rangle + \theta(-s)\left\langle\hat{\varphi}(\boldsymbol{x'},0)\hat{\varphi}(\boldsymbol{x},s)\right\rangle, \tag{2.21}$$

where θ is the Heaviside step function. Differentiate with respect to s, use the fact that $\theta'(s) = \delta(s)$ and the commutation relations (2.4) to get

$$\begin{aligned}\partial_s\mathcal{D}(s) &= \delta(s)\left\langle\hat{\varphi}(\boldsymbol{x},s)\hat{\varphi}(\boldsymbol{x'},0)\right\rangle + \theta(s)\left\langle\partial_s\hat{\varphi}(\boldsymbol{x},s)\hat{\varphi}(\boldsymbol{x'},0)\right\rangle \\ &\quad - \delta(s)\left\langle\hat{\varphi}(\boldsymbol{x'},0)\hat{\varphi}(\boldsymbol{x},s)\right\rangle + \theta(-s)\left\langle\hat{\varphi}(\boldsymbol{x'},0)\partial_s\hat{\varphi}(\boldsymbol{x},s)\right\rangle \\ &= \delta(s)[\hat{\varphi}(\boldsymbol{x},s),\hat{\varphi}(\boldsymbol{x'},0)] + \theta(s)\left\langle\partial_s\hat{\varphi}(\boldsymbol{x},s)\hat{\varphi}(\boldsymbol{x'},0)\right\rangle + \theta(-s)\left\langle\hat{\varphi}(\boldsymbol{x'},0)\partial_s\hat{\varphi}(\boldsymbol{x},s)\right\rangle \\ &= \theta(s)\left\langle\partial_s\hat{\varphi}(\boldsymbol{x},s)\hat{\varphi}(\boldsymbol{x'},0)\right\rangle + \theta(-s)\left\langle\hat{\varphi}(\boldsymbol{x'},0)\partial_s\hat{\varphi}(\boldsymbol{x},s)\right\rangle.\end{aligned} \tag{2.22}$$

Differentiate once more, use the defining equation (2.3) and the commutation relations (2.4) to get

$$\begin{aligned}\partial_{ss}\mathcal{D}(s) &= \delta(s)\left\langle\partial_s\hat{\varphi}(\boldsymbol{x},s)\hat{\varphi}(\boldsymbol{x'},0)\right\rangle + \theta(s)\left\langle\partial_{ss}\hat{\varphi}(\boldsymbol{x},s)\hat{\varphi}(\boldsymbol{x'},0)\right\rangle \\ &\quad - \delta(s)\left\langle\hat{\varphi}(\boldsymbol{x'},0)\partial_s\hat{\varphi}(\boldsymbol{x},s)\right\rangle + \theta(-s)\left\langle\hat{\varphi}(\boldsymbol{x'},0)\partial_{ss}\hat{\varphi}(\boldsymbol{x},s)\right\rangle \\ &= \delta(s)[\partial_s\hat{\varphi}(\boldsymbol{x},s),\hat{\varphi}(\boldsymbol{x'},0)] - \nabla^2\left(\theta(s)\left\langle\hat{\varphi}(\boldsymbol{x},s)\hat{\varphi}(\boldsymbol{x'},0)\right\rangle + \theta(-s)\left\langle\hat{\varphi}(\boldsymbol{x'},0)\hat{\varphi}(\boldsymbol{x},s)\right\rangle\right) \\ &= \delta(s)\delta(\boldsymbol{x}-\boldsymbol{x'}) - \nabla^2\mathcal{D}(s).\end{aligned} \tag{2.23}$$

Thus the equation for the Green's function becomes

$$\partial_{ss}\mathcal{D}(\boldsymbol{x},\boldsymbol{x'},s)+\nabla^2\mathcal{D}(\boldsymbol{x},\boldsymbol{x'},s)=\delta(s)\delta(\boldsymbol{x}-\boldsymbol{x'}). \tag{2.24}$$

We see that $\mathcal{D}$ is a Green's function for the scalar field equation (2.3). Using the boundary condition $\hat{\varphi}|_{Q_j}=0$, the defining equation for $\mathcal{D}$ and equation (2.17), we obtain the boundary condition

$$\mathcal{D}(\boldsymbol{x},\boldsymbol{x'},s)=0, \qquad \boldsymbol{x}\in Q_j \text{ or } \boldsymbol{x'}\in Q_j. \tag{2.25}$$

We have showed that the Green's function $\mathcal{D}(\boldsymbol{x},\boldsymbol{x'},s)$ is periodic in s with period $\beta=1/T$. Thus $\mathcal{D}(\boldsymbol{x},\boldsymbol{x'},s)$ can be written as a Fourier series. However, in this thesis we only consider situations where the temperature is zero, i.e T $\to 0$. Thus the period of the Fourier series will be infinite and therefore $\mathcal{D}(\boldsymbol{x},\boldsymbol{x'},s)$ can be written using a Fourier transform in s. We obtain the equation

$$\begin{aligned}\nabla^2\mathcal{D}(\boldsymbol{x},\boldsymbol{x'},\omega)-\omega^2\mathcal{D}(\boldsymbol{x},\boldsymbol{x'},\omega)&=\delta(\boldsymbol{x}-\boldsymbol{x'}),\\ \mathcal{D}(\boldsymbol{x},\boldsymbol{x'},\omega)&=0, \qquad \boldsymbol{x}\in Q_j \text{ or } \boldsymbol{x'}\in Q_j.\end{aligned} \tag{2.26}$$

2.2 Relation between the Casimir force and the Green's function

In the following section an expression for the Casimir force on conductor i will be derived. Both tensor notation and dyadic notation is used in the derivation. Partial derivatives are written two different ways; $\partial_0=\partial_t$, $\partial_1=\partial_x$, $\partial_2=\partial_y$, $\partial_3=\partial_z$. We start by deriving a relation between the classical stress tensor and the momentum density. Then we do a quantization and use the quantized stress tensor to find an expression for the force.

The *Lagrangian density* for the "un-quantized" version of field equation (2.1), i.e the classical wave equation

$$\varphi_{tt}-\nabla^2\varphi=0, \tag{2.27}$$

is given by

$$\mathcal{L}(\varphi)=\frac{1}{2}\left(\varphi_t^2-\nabla\varphi^2\right)=\frac{1}{2}\partial^\mu\varphi\partial_\mu\varphi. \tag{2.28}$$

Using Noether's theorem, the *stress-energy tensor* is given by

$$T^{\mu\nu}=\frac{\partial\mathcal{L}}{\partial(\partial_\mu\varphi)}\partial^\nu\varphi-\eta^{\mu\nu}\mathcal{L}, \quad \mu,\nu=0,1,2,3, \tag{2.29}$$

where $\eta^{\mu\nu}$ is the Minowski metric with signature $\{+,-,-,-\}$. Insert equation (2.28) into (2.29) to obtain

$$T^{\mu\nu}=\partial^\mu\varphi\partial^\nu\varphi-\frac{1}{2}\eta^{\mu\nu}\partial^\rho\varphi\partial_\rho\varphi. \tag{2.30}$$

The conservation equations are

$$\partial_\mu T^{\mu\nu} = 0, \tag{2.31}$$

where $\nu = 0$ gives conservation of energy and $\nu = 1, 2, 3$ gives conservation of momentum. The equation for conservation of energy can be written as

$$\partial_t \mathcal{H} + \nabla \cdot \boldsymbol{S}_e = 0, \tag{2.32}$$

where

$$\mathcal{H} = T^{00} = \frac{1}{2}\left[\varphi_t^2 + \nabla\varphi \cdot \nabla\varphi\right] = \frac{1}{2}\left[\varphi_t^2 + \mathrm{Tr}(\nabla\varphi\nabla\varphi)\right] \tag{2.33}$$

is the *energy density* or the *Hamiltonian density* and

$$\boldsymbol{S}_e = -\varphi_t \nabla\varphi \tag{2.34}$$

is the *energy flux tensor*. The equations for conservation of momentum become

$$\partial_t \boldsymbol{p} + \nabla \cdot S = 0 \tag{2.35}$$

where

$$\boldsymbol{p} = \varphi_t \nabla\varphi \tag{2.36}$$

is the *momentum density* and S, given by

$$S(\boldsymbol{x}, t) = -\nabla\varphi\nabla\varphi + \frac{1}{2}\mathrm{Tr}(\nabla\varphi\nabla\varphi)I - \frac{1}{2}\varphi_t^2 I, \tag{2.37}$$

is the *momentum flux* or the *stress tensor*. I.e. S is a 2-tensor and in our case it has been written as a matrix. However, we are working with the quantized scalar field $\hat{\varphi}$ and must therefore do a quantization. Start by doing a rotation into the complex plane, $t = -is$. Observe that the stress tensor can be written as

$$\begin{aligned} S(\boldsymbol{x}, s) &= \left(-\nabla\nabla + \frac{1}{2}\mathrm{Tr}(\nabla\nabla)I + \frac{1}{2}\partial_s^2 I\right)\varphi(x, s)\varphi(x, s) \\ &= \left(-\nabla\nabla + \frac{1}{2}\mathrm{Tr}(\nabla\nabla)I + \frac{1}{2}\partial_s^2 I\right)\frac{1}{2}\left\{\varphi(\boldsymbol{x}, s), \varphi(\boldsymbol{x}, s)\right\}, \end{aligned} \tag{2.38}$$

where $\{A, B\} = AB + BA$ is the anti commutator. The *quantum stress tensor* S_q will be defined via the *point splitting* method ([15], [16]). We start by quantizing the fields by letting $\varphi \to \hat{\varphi}$ and then replacing one of the fields $\hat{\varphi}(\boldsymbol{x}, s)$ by $\hat{\varphi}(\boldsymbol{x}', s')$, where $(\boldsymbol{x}', s')$ is a nearby point. The corresponding operator ∇ is replaced by ∇'. By ∇' is meant the derivative w.r.t. to the primed variables. We let $(\boldsymbol{x}', s')$ approach $(\boldsymbol{x}, s)$ and take the

vacuum expectation value;

$$S_q(\boldsymbol{x},s) = \lim_{(\boldsymbol{x}',s')\to(\boldsymbol{x},s)} \left(-\nabla\nabla' + \frac{1}{2}\mathrm{Tr}(\nabla\nabla')I + \frac{1}{2}\partial_s\partial_{s'}I\right)\frac{1}{2}\mathcal{D}^{(1)}(\boldsymbol{x},s,\boldsymbol{x}',s'), \tag{2.39}$$

where $\mathcal{D}^{(1)}(\boldsymbol{x},s,\boldsymbol{x}',s')$ is the *Hadamard's Green's function*, given by

$$\mathcal{D}^{(1)}(\boldsymbol{x},s,\boldsymbol{x}',s') = \left\langle\{\hat{\varphi}(\boldsymbol{x},s),\hat{\varphi}(\boldsymbol{x}',s')\}\right\rangle = \mathcal{D}^{(+)}(\boldsymbol{x},s,\boldsymbol{x}',s') + \mathcal{D}^{(-)}(\boldsymbol{x},s,\boldsymbol{x}',s'), \tag{2.40}$$

and the functions $\mathcal{D}^{(\pm)}(\boldsymbol{x},s,\boldsymbol{x}',s')$ are defined in equation (2.10).

A property of the Heaviside step function, θ, is that

$$\theta(x) + \theta(-x) = 1, \quad \forall\, x. \tag{2.41}$$

Using this property and by adding and subtracting the same quantities, we can relate the Hadamard Green's function $\mathcal{D}^{(1)}$ to the Green's function $\mathcal{D}$, given in equation (2.7);

$$\begin{aligned}\mathcal{D}^{(1)}(\boldsymbol{x},s,\boldsymbol{x}',s') &= \big(\theta(s-s') + \theta(s'-s)\big)\left\langle\{\hat{\varphi}(\boldsymbol{x},s),\hat{\varphi}(\boldsymbol{x}',s')\}\right\rangle \\ &= 2\left(\theta(s-s')\left\langle\hat{\varphi}(\boldsymbol{x},s),\hat{\varphi}(\boldsymbol{x}',s')\right\rangle + \theta(s'-s)\left\langle\hat{\varphi}(\boldsymbol{x}',s'),\hat{\varphi}(\boldsymbol{x},s)\right\rangle\right) \\ &\quad - \theta(s-s')\langle[\hat{\varphi}(\boldsymbol{x},s),\hat{\varphi}(\boldsymbol{x}',s')]\rangle + \theta(s'-s)\langle[\hat{\varphi}(\boldsymbol{x},s),\hat{\varphi}(\boldsymbol{x}',s')]\rangle \\ &= 2\mathcal{D}(\boldsymbol{x},s,\boldsymbol{x}',s') - \mathcal{D}^R(\boldsymbol{x},s,\boldsymbol{x}',s') - \mathcal{D}^A(\boldsymbol{x},s,\boldsymbol{x}',s'),\end{aligned} \tag{2.42}$$

where

$$\mathcal{D}^R(\boldsymbol{x},s,\boldsymbol{x}',s') = \theta(s-s')\langle[\hat{\varphi}(\boldsymbol{x},s),\hat{\varphi}(\boldsymbol{x}',s')]\rangle \tag{2.43}$$

$$\mathcal{D}^A(\boldsymbol{x},s,\boldsymbol{x}',s') = -\theta(s'-s)\langle[\hat{\varphi}(\boldsymbol{x},s),\hat{\varphi}(\boldsymbol{x}',s')]\rangle. \tag{2.44}$$

$\mathcal{D}^R$ is the *retarded Green's function* and $\mathcal{D}^A$ is the *advanced Green's function*. However, because of the commutation relations (2.4), both are zero in the limit $(\boldsymbol{x}',s') \to (\boldsymbol{x},s)$. Thus

$$S_q(\boldsymbol{x},s) = \lim_{(\boldsymbol{x}',s')\to(\boldsymbol{x},s)} \left(-\nabla\nabla' + \frac{1}{2}\mathrm{Tr}(\nabla\nabla')I + \frac{1}{2}\partial_s\partial_{s'}I\right)\mathcal{D}(\boldsymbol{x},s,\boldsymbol{x}',s'). \tag{2.45}$$

By letting $\tau = s - s'$, we can use the property of the Green's function $\mathcal{D}$ given in equation (2.17); $\mathcal{D}(\boldsymbol{x},s,\boldsymbol{x}',s') = \mathcal{D}(\boldsymbol{x},\boldsymbol{x}',s-s')$. S_q changes into

$$S_q(\boldsymbol{x}) = \lim_{\substack{\boldsymbol{x}'\to\boldsymbol{x}\\ \tau\to 0}} \left(-\nabla\nabla' + \frac{1}{2}\mathrm{Tr}(\nabla\nabla')I - \frac{1}{2}\partial_{\tau\tau}I\right)\mathcal{D}(\boldsymbol{x},\boldsymbol{x}',\tau). \tag{2.46}$$

A Fourier transform in τ results in

$$S_q(\boldsymbol{x},\omega) = \lim_{\boldsymbol{x}'\to\boldsymbol{x}} \left(-\nabla\nabla' + \frac{1}{2}\mathrm{Tr}(\nabla\nabla')I + \frac{1}{2}\omega^2 I\right)\mathcal{D}(\boldsymbol{x},\boldsymbol{x}',\omega). \tag{2.47}$$

The quantum stress tensor can be expressed via its Fourier components by taking the inverse Fourier transform and evaluating at zero

$$S_q(\boldsymbol{x}) = \left[\frac{1}{2\pi} \int_{-\infty}^{\infty} d\omega \, e^{i\omega\tau} S_q(\boldsymbol{x}, \omega) \right]_{\tau=0} = \frac{1}{2\pi} \int_{-\infty}^{\infty} d\omega \, S_q(\boldsymbol{x}, \omega). \tag{2.48}$$

From classical mechanics we know the relation between force and momentum through a time-derivative. Using the equation of momentum conservation (2.35) and the divergence theorem, the expression for the net force on conductor i becomes

$$\boldsymbol{F}_i = \partial_t \int_{V_i} dV \, \boldsymbol{p}(\boldsymbol{x}, t) = - \int_{V_i} dV \, \nabla \cdot S_q(\boldsymbol{x}, t) = - \oint_{Q_i} dA \, \boldsymbol{n} \cdot \, S_q(\boldsymbol{x}), \tag{2.49}$$

where $\boldsymbol{n}$ is the unit normal pointing from the boundary Q_i into V_0. The total system is assumed to be stationary, and therefore the sum of all forces is zero: $\sum \boldsymbol{F}_j = 0$.

The expression for the force can be simplified considerably using the boundary conditions. At any point on the surface Q_i it is possible to find two tangent vectors, $\boldsymbol{t}_1$ and $\boldsymbol{t}_2$, such that they span the tangent plane. Together with the unit normal $\boldsymbol{n}$ they span $\mathbb{R}^3$. With respect to this basis the unit vectors are

$$\boldsymbol{e}_i = (\boldsymbol{e}_i \cdot \boldsymbol{t}_1)\boldsymbol{t}_1 + (\boldsymbol{e}_i \cdot \boldsymbol{t}_2)\boldsymbol{t}_2 + (\boldsymbol{e}_i \cdot \boldsymbol{n})\boldsymbol{n}, \quad i = 1, 2, 3. \tag{2.50}$$

The gradient changes to

$$\nabla \to (\boldsymbol{t}_1 \cdot \nabla)\boldsymbol{t}_1 + (\boldsymbol{t}_2 \cdot \nabla)\boldsymbol{t}_2 + (\boldsymbol{n} \cdot \nabla)\boldsymbol{n} = \boldsymbol{t}_1 \partial_{\boldsymbol{t}_1} + \boldsymbol{t}_2 \partial_{\boldsymbol{t}_2} + \boldsymbol{n} \partial_{\boldsymbol{n}}, \tag{2.51}$$

and the double gradient becomes

$$\begin{aligned} \nabla\nabla' = {} & \boldsymbol{t}_1\boldsymbol{t}_1' \partial_{\boldsymbol{t}_1\boldsymbol{t}_1'} + \boldsymbol{t}_1\boldsymbol{t}_2' \partial_{\boldsymbol{t}_1\boldsymbol{t}_2'} + \boldsymbol{t}_2\boldsymbol{t}_1' \partial_{\boldsymbol{t}_2\boldsymbol{t}_1'} + \boldsymbol{t}_2\boldsymbol{t}_2' \partial_{\boldsymbol{t}_2\boldsymbol{t}_2'} + \boldsymbol{t}_1\boldsymbol{n}' \partial_{\boldsymbol{t}_1\boldsymbol{n}'} \\ & + \boldsymbol{n}\boldsymbol{t}_1' \partial_{\boldsymbol{n}\boldsymbol{t}_1'} + \boldsymbol{t}_2\boldsymbol{n}' \partial_{\boldsymbol{t}_2\boldsymbol{n}'} + \boldsymbol{n}\boldsymbol{t}_2' \partial_{\boldsymbol{n}\boldsymbol{t}_2'} + \boldsymbol{n}\boldsymbol{n}' \partial_{\boldsymbol{n}\boldsymbol{n}'}. \end{aligned} \tag{2.52}$$

Remember the boundary condition for the Green's function,

$$\mathcal{D}(\boldsymbol{x}, \boldsymbol{x}', \omega) = 0, \quad \boldsymbol{x} \in Q_j \text{ or } \boldsymbol{x}' \in Q_j, \quad j = 1, ..., r. \tag{2.53}$$

Thus for $\boldsymbol{x}, \boldsymbol{x}' \in Q_i$;

$$\partial_{\boldsymbol{t}_1} \mathcal{D} = \partial_{\boldsymbol{t}_1'} \mathcal{D} = \partial_{\boldsymbol{t}_2} \mathcal{D} = \partial_{\boldsymbol{t}_2'} \mathcal{D} = 0, \tag{2.54}$$

which gives

$$\nabla\nabla' \mathcal{D}(\boldsymbol{x}, \boldsymbol{x}', \omega) = \boldsymbol{n}\boldsymbol{n}' \partial_{\boldsymbol{n}\boldsymbol{n}'} \mathcal{D}(\boldsymbol{x}, \boldsymbol{x}', \omega), \quad \boldsymbol{x}, \boldsymbol{x}' \in Q_i. \tag{2.55}$$

Under the assumption that $\boldsymbol{x}, \boldsymbol{x}' \in Q_i$, we can insert equations (2.53) and (2.55) into the defining equation of the stress tensor (2.47). It then changes into

$$\begin{aligned} S_q(\boldsymbol{x}, \omega) &= \lim_{\boldsymbol{x}' \to \boldsymbol{x}} \left(-\boldsymbol{n}\boldsymbol{n}' + \frac{1}{2}\mathrm{Tr}(\boldsymbol{n}\boldsymbol{n}')I \right) \partial_{\boldsymbol{n}\boldsymbol{n}'} \mathcal{D}(\boldsymbol{x}, \boldsymbol{x}', \omega) \\ &= \left(-\boldsymbol{n}\boldsymbol{n} + \frac{1}{2}\mathrm{Tr}(\boldsymbol{n}\boldsymbol{n})I \right) \partial_{\boldsymbol{n}\boldsymbol{n}} \mathcal{D}(\boldsymbol{x}, \boldsymbol{x}, \omega). \end{aligned} \tag{2.56}$$

The expression for the force changes into

$$\begin{aligned} \boldsymbol{F}_i &= -\oint_{Q_i} dA_{\boldsymbol{x}} \boldsymbol{n} \cdot \int_{-\infty}^{\infty} \frac{d\omega}{2\pi} S_q(\boldsymbol{x}, \omega) \\ &= -\frac{1}{2\pi} \oint_{Q_i} dA_{\boldsymbol{x}} \boldsymbol{n} \cdot \int_{-\infty}^{\infty} d\omega \left(-\boldsymbol{n}\boldsymbol{n} + \frac{1}{2}\mathrm{Tr}(\boldsymbol{n}\boldsymbol{n})I \right) \partial_{\boldsymbol{n}\boldsymbol{n}} \mathcal{D}(\boldsymbol{x}, \boldsymbol{x}, \omega) \\ &= \frac{1}{4\pi} \oint_{Q_i} dA_{\boldsymbol{x}} \boldsymbol{n} \int_{-\infty}^{\infty} d\omega \, \partial_{\boldsymbol{n}\boldsymbol{n}} \mathcal{D}(\boldsymbol{x}, \boldsymbol{x}, \omega), \end{aligned} \tag{2.57}$$

where we have used that $\boldsymbol{n} \cdot \boldsymbol{n}\boldsymbol{n} = \boldsymbol{n}$, $\mathrm{Tr}(\boldsymbol{n}\boldsymbol{n}) = \|\boldsymbol{n}\|^2 = 1$ and $\boldsymbol{n} \cdot I = \boldsymbol{n}$. Thus the unregularized force on object i is

$$\boldsymbol{F}_i = \iint_{Q_i} dA_{\boldsymbol{x}} \, \boldsymbol{n}(\boldsymbol{x}) \, P(\boldsymbol{x}), \tag{2.58}$$

where $\boldsymbol{n}(\boldsymbol{x})$ is the unit normal pointing into the region V_0 and the pressure, P, on surface i, is given by

$$P(\boldsymbol{x}) = \frac{1}{4\pi} \int_{-\infty}^{\infty} d\omega \, \partial_{\boldsymbol{n}\boldsymbol{n}} \mathcal{D}(\boldsymbol{x}, \boldsymbol{x}, \omega) \tag{2.59}$$

Positive pressure means that the force is pointing in the same direction as the normal.

2.3 Boundary integral equation for the pressure density

We have now related the Casimir force to the Green's function $\mathcal{D}(\boldsymbol{x}, \boldsymbol{x}, \omega)$ through a double normal derivative. The quantity $\partial_{\boldsymbol{n}\boldsymbol{n}}\mathcal{D}$ will be referred to as the pressure density. This section will be used to derive a boundary integral equation for the pressure density. In order to derive such an equation, we return to the PDE that describes the Green's function (2.26). Start by taking the gradient with respect to the primed variable to obtain

$$\nabla^2 \boldsymbol{\mathcal{E}}(\boldsymbol{x}, \boldsymbol{x}', \omega) - \omega^2 \boldsymbol{\mathcal{E}}(\boldsymbol{x}, \boldsymbol{x}', \omega) = \nabla' \delta(\boldsymbol{x} - \boldsymbol{x}'), \tag{2.60}$$

where the definition

$$\boldsymbol{\mathcal{E}}(\boldsymbol{x},\boldsymbol{x'},\omega) = \nabla'\mathcal{D}(\boldsymbol{x},\boldsymbol{x'},\omega) \tag{2.61}$$

is used. Since $\mathcal{D}(\boldsymbol{x},\boldsymbol{x'},\omega) = 0$ for $\boldsymbol{x},\boldsymbol{x'} \in Q_j$, the boundary condition

$$\boldsymbol{\mathcal{E}}(\boldsymbol{x},\boldsymbol{x'},\omega) = \mathbf{0}, \quad \boldsymbol{x} \in Q_j \tag{2.62}$$

holds. In order to find a boundary integral formulation of the problem, we introduce the free Green's function D_0,

$$D_0(\boldsymbol{x},\boldsymbol{x''},\omega) = -\frac{e^{-|\omega|\|\boldsymbol{x}-\boldsymbol{x''}\|}}{4\pi\|\boldsymbol{x}-\boldsymbol{x''}\|}, \tag{2.63}$$

which satisfies the differential equation

$$LD_0(\boldsymbol{x},\boldsymbol{x''},\omega) = \delta(\boldsymbol{x}-\boldsymbol{x''}). \tag{2.64}$$

L is the differential operator given by

$$L = \nabla^2 - \omega^2, \tag{2.65}$$

which is same as the Helmholtz operator $\nabla^2 + k^2$ for $k = i\omega$. Thus we see that D_0 is a Green's function that satisfies equation (2.26), but not the boundary conditions.

Hereafter abbreviations such as for example $\mathcal{D}(\boldsymbol{x},\boldsymbol{x''})$ will be used for the Fourier components $\mathcal{D}(\boldsymbol{x},\boldsymbol{x''},\omega)$. Using the fact that $\nabla^2\boldsymbol{\mathcal{E}} = (\nabla^2\mathcal{E}_x, \nabla^2\mathcal{E}_y, \nabla^2\mathcal{E}_z)$, we can apply *Green's second identity* on each component to produce an integral formulation of the boundary value problem (2.60), (2.62);

$$\begin{aligned}
&\iiint_{V_0} dV_{\boldsymbol{x}} \left\{ D_0(\boldsymbol{x},\boldsymbol{x''})L\boldsymbol{\mathcal{E}}(\boldsymbol{x},\boldsymbol{x'}) - \boldsymbol{\mathcal{E}}(\boldsymbol{x},\boldsymbol{x'})LD_0(\boldsymbol{x},\boldsymbol{x''}) \right\} \\
&\quad = \iiint_{V_0} dV_{\boldsymbol{x}} \left\{ D_0(\boldsymbol{x},\boldsymbol{x''})\nabla^2\boldsymbol{\mathcal{E}}(\boldsymbol{x},\boldsymbol{x'}) - \boldsymbol{\mathcal{E}}(\boldsymbol{x},\boldsymbol{x'})\nabla^2 D_0(\boldsymbol{x},\boldsymbol{x''}) \right\} \\
&\quad = -\sum_{\alpha} \oiint_{Q_\alpha} d\boldsymbol{A}_{\boldsymbol{x}} \cdot \left\{ D_0(\boldsymbol{x},\boldsymbol{x''})\nabla\boldsymbol{\mathcal{E}}(\boldsymbol{x},\boldsymbol{x'}) - \boldsymbol{\mathcal{E}}(\boldsymbol{x},\boldsymbol{x'})\nabla D_0(\boldsymbol{x},\boldsymbol{x''}) \right\},
\end{aligned} \tag{2.66}$$

where $\boldsymbol{x'},\boldsymbol{x''} \in V_0$. The notation $\nabla\boldsymbol{\mathcal{E}}$ means taking the gradient of each component of $\boldsymbol{\mathcal{E}}$. In the second term the dyadic product is used. The dot-product of a vector and a 2-tensor will produce a vector. The minus sign appears because $d\boldsymbol{A}_{\boldsymbol{x}} = dA_{\boldsymbol{x}}\boldsymbol{n}$, and $\boldsymbol{n}$ is defined such that it points out of each of the surfaces Q_α and into V_0. Inserting

equations (2.60) and (2.64) give

$$\begin{aligned}\iiint_{V_0} dV_{\boldsymbol{x}} \ \left\{D_0(\boldsymbol{x},\boldsymbol{x}'')\nabla'\delta(\boldsymbol{x}-\boldsymbol{x}') - \boldsymbol{\mathcal{E}}(\boldsymbol{x},\boldsymbol{x}')\delta(\boldsymbol{x}-\boldsymbol{x}'')\right\} \\ = -\sum_\alpha \oiint_{Q_\alpha} d\boldsymbol{A}_{\boldsymbol{x}} \cdot \left\{D_0(\boldsymbol{x},\boldsymbol{x}'')\nabla\boldsymbol{\mathcal{E}}(\boldsymbol{x},\boldsymbol{x}') - \boldsymbol{\mathcal{E}}(\boldsymbol{x},\boldsymbol{x}')\nabla D_0(\boldsymbol{x},\boldsymbol{x}'')\right\}.\end{aligned} \tag{2.67}$$

Inserting the boundary condition $\boldsymbol{\mathcal{E}}(\boldsymbol{x},\boldsymbol{x}') = 0$ for $\boldsymbol{x} \in Q_j$ and using the properties of the Dirac delta, we obtain the integral identity

$$\iiint_{V_0} dV_{\boldsymbol{x}} D_0(\boldsymbol{x},\boldsymbol{x}'')\nabla'\delta(\boldsymbol{x}-\boldsymbol{x}') = \boldsymbol{\mathcal{E}}(\boldsymbol{x}'',\boldsymbol{x}') - \sum_\alpha \oiint_{Q_\alpha} dA_{\boldsymbol{x}}\, D_0(\boldsymbol{x},\boldsymbol{x}'')\partial_{\boldsymbol{n}}\boldsymbol{\mathcal{E}}(\boldsymbol{x},\boldsymbol{x}'), \tag{2.68}$$

where $\boldsymbol{x}', \boldsymbol{x}'' \in V_0$. This integral equation is satisfied by any solution to equation (2.60). However, we don't have to solve the equation in the entire region V_0 since the pressure only acts on the conductors. Therefore we are going to let $\boldsymbol{x}', \boldsymbol{x}''$ approach the boundaries Q_k. It turns out that it isn't a trivial thing to take these limits, but we can start by observing that if we let $\boldsymbol{x}''$ approach the boundary, Q_j, of conductor j, then $\boldsymbol{\mathcal{E}}(\boldsymbol{x}'',\boldsymbol{x}') = 0$. This term disappears from equation (2.68) and we obtain

$$-\iiint_{V_0} dV_{\boldsymbol{x}} D_0(\boldsymbol{x},\boldsymbol{x}'')\nabla'\delta(\boldsymbol{x}-\boldsymbol{x}') = \sum_\alpha \oiint_{Q_\alpha} dA_{\boldsymbol{x}}\, D_0(\boldsymbol{x},\boldsymbol{x}'')\partial_{\boldsymbol{n}}\boldsymbol{\mathcal{E}}(\boldsymbol{x},\boldsymbol{x}'), \tag{2.69}$$

where $\boldsymbol{x}'' \in Q_j$ and $\boldsymbol{x}' \in V_0$. The free Green's function D_0 has a pole of order one at $\boldsymbol{x} = \boldsymbol{x}''$. Therefore the integrals in the equation have singularities at the points $\boldsymbol{x} = \boldsymbol{x}''$. However, as we will see in the next section, these can be made sense of as principal value integrals. Remember that we want to use our boundary integral equation to find the pressure density, $\partial_{\boldsymbol{nn}}\mathcal{D}$, on the boundaries of the conductors. We now have an equation for $\partial_{\boldsymbol{n}}\boldsymbol{\mathcal{E}}$, but because of the close relation between the function $\partial_{\boldsymbol{n}}\boldsymbol{\mathcal{E}}$ and $\partial_{\boldsymbol{nn}}\mathcal{D}$, it is an easy task to manipulate equation (2.69) such that it contains $\partial_{\boldsymbol{nn}}\mathcal{D}$. We let $\boldsymbol{x}'$ approach the boundary Q_i of conductor i and (initially) ignore the problems that arise on the left hand side if $i = j$ and $\boldsymbol{x}' \to \boldsymbol{x}''$. As we did in the previous section, we change basis to normal and tangent vectors at $\boldsymbol{x}'$ such that the gradient ∇' becomes

$$\nabla' \to \boldsymbol{t}_1'\partial_{\boldsymbol{t}_1'} + \boldsymbol{t}_2'\partial_{\boldsymbol{t}_2'} + \boldsymbol{n}'\partial_{\boldsymbol{n}'}. \tag{2.70}$$

The boundary condition $\mathcal{D}(\boldsymbol{x},\boldsymbol{x}') = 0$, for $\boldsymbol{x}' \in Q_i$, gives

$$\begin{aligned}\partial_{\boldsymbol{n}}\boldsymbol{\mathcal{E}}(\boldsymbol{x},\boldsymbol{x}') = \partial_{\boldsymbol{n}}\nabla'\mathcal{D}(\boldsymbol{x},\boldsymbol{x}') &\to \partial_{\boldsymbol{n}}(\boldsymbol{t}_1'\partial_{\boldsymbol{t}_1'} + \boldsymbol{t}_2'\partial_{\boldsymbol{t}_2'} + \boldsymbol{n}'\partial_{\boldsymbol{n}'})\mathcal{D}(\boldsymbol{x},\boldsymbol{x}') \\ &= \partial_{\boldsymbol{n}}\boldsymbol{n}'\partial_{\boldsymbol{n}'}\mathcal{D}(\boldsymbol{x},\boldsymbol{x}') = \boldsymbol{n}'\partial_{\boldsymbol{nn}'}\mathcal{D}(\boldsymbol{x},\boldsymbol{x}').\end{aligned} \tag{2.71}$$

We now consider what happens to the left hand side of equation (2.69) when $\boldsymbol{x}' \to Q_i$ (still omitting the special case $\boldsymbol{x}' \to \boldsymbol{x}''$). Observe that L is a selfadjoint operator that

acts on the space of functions

$$\mathcal{M} = \left\{ f : V_0 \to \mathbb{R} \;\middle|\; f(\boldsymbol{x}) = 0 \text{ for } \boldsymbol{x} \in Q_k,\ \ k = 1, 2, ..., r \right\}. \tag{2.72}$$

Assume $\left\{ \phi_\lambda \;\middle|\; \phi_\lambda \in \mathcal{M} \right\}$ is a complete set of eigenfunctions for L. Then for $f \in \mathcal{M}$, we have that

$$f(\boldsymbol{x}) = \sum_\lambda \langle f | \phi_\lambda \rangle \, \phi_\lambda(\boldsymbol{x}) = \sum_\lambda \int dV_{\boldsymbol{x}'} f(\boldsymbol{x}') \phi_\lambda(\boldsymbol{x}') \phi_\lambda(\boldsymbol{x}). \tag{2.73}$$

Formally this can be done for the Dirac-delta function as well, s.t. for $\boldsymbol{x}, \boldsymbol{x}' \in Q_k$ we have

$$\delta(\boldsymbol{x} - \boldsymbol{x}') = \sum_\lambda \phi_\lambda(\boldsymbol{x}) \phi_\lambda(\boldsymbol{x}'). \tag{2.74}$$

Using the expansion of the gradient ∇', we get

$$\begin{aligned} \nabla' \delta(\boldsymbol{x} - \boldsymbol{x}') &= \sum_\lambda \phi_\lambda(\boldsymbol{x}) \nabla' \phi_\lambda(\boldsymbol{x}') \to \sum_\lambda \phi_\lambda(\boldsymbol{x}) (\boldsymbol{t}_1' \partial_{\boldsymbol{t}_2'} + \boldsymbol{t}_2' \partial_{\boldsymbol{t}_2'} + \boldsymbol{n}' \partial_{\boldsymbol{n}'}) \phi_\lambda(\boldsymbol{x}') \\ &= \sum_\lambda \phi_\lambda(\boldsymbol{x}) \boldsymbol{n}' \partial_{\boldsymbol{n}'} \phi_\lambda(\boldsymbol{x}') = \boldsymbol{n}' \partial_{\boldsymbol{n}'} \delta(\boldsymbol{x} - \boldsymbol{x}'). \end{aligned} \tag{2.75}$$

Thus the left hand side of equation (2.83) changes to

$$\begin{aligned} -\iiint_{V_0} dV_{\boldsymbol{x}} D_0(\boldsymbol{x}, \boldsymbol{x}'') \nabla' \delta(\boldsymbol{x} - \boldsymbol{x}') &= -\iiint_{V_0} dV_{\boldsymbol{x}} D_0(\boldsymbol{x}, \boldsymbol{x}'') \boldsymbol{n}' \partial_{\boldsymbol{n}'} \delta(\boldsymbol{x} - \boldsymbol{x}') \\ = -\boldsymbol{n}' \partial_{\boldsymbol{n}'} \iiint_{V_0} dV_{\boldsymbol{x}} D_0(\boldsymbol{x}, \boldsymbol{x}'') \delta(\boldsymbol{x} - \boldsymbol{x}') &= -\boldsymbol{n}' \partial_{\boldsymbol{n}'} D_0(\boldsymbol{x}', \boldsymbol{x}'') \end{aligned} \tag{2.76}$$

where $\boldsymbol{n}'$ is the normal vector pointing from the boundary Q_i and into V_0. We see that $\boldsymbol{n}'$ is common to both sides of the equation and can be cancelled. Thus we get the boundary integral equation

$$-\partial_{\boldsymbol{n}'} D_0(\boldsymbol{x}', \boldsymbol{x}'') = \sum_\alpha \oiint_{Q_\alpha} dA_{\boldsymbol{x}} \, D_0(\boldsymbol{x}, \boldsymbol{x}'') \partial_{\boldsymbol{n}\boldsymbol{n}'} \mathcal{D}(\boldsymbol{x}, \boldsymbol{x}'), \tag{2.77}$$

where $\boldsymbol{x}' \in Q_i$, $\boldsymbol{x}'' \in Q_j$, $i, j = 1, ..., r$ and assuming that $\boldsymbol{x}' \neq \boldsymbol{x}''$.

2.4 Regularization of the boundary integral equation

As we have already indicated, the boundary integral equation (2.77) can't be solved w.r.t the pressure density, $\partial_{\boldsymbol{n}\boldsymbol{n}'} \mathcal{D}$, as it stands. We have to define how to integrate over the infinity that occurs on the right hand side at $\boldsymbol{x} = \boldsymbol{x}''$ and how to treat the singularity that occurs on the left hand side when $\boldsymbol{x}'$ approaches $\boldsymbol{x}''$. This will be a big part of the regularization of the equation. In addition, the regularization consists of subtracting the

self-pressure contribution from $\partial_{\boldsymbol{nn'}}\mathcal{D}(\boldsymbol{x},\boldsymbol{x}')$. We will return to this at the end of the section.

The first part of the regularization will be to define how the integrals on the right hand side shall be calculated. Remember that we let $\boldsymbol{x}'' \to Q_j$, thus the j-th integral has a singularity when $\boldsymbol{x} = \boldsymbol{x}''$. The other integrals can be treated as ordinary integrals. In order to define how to perform the j-th integral, we start by extending the surface Q_j to $Q_j^\epsilon \cup D_\epsilon$, where D_ϵ is the hemisphere with radius ϵ, centered around $\boldsymbol{x}''$ (see figure 2.1). Q_j^ϵ is almost the same surface as Q_j, only a disk with a radius ϵ and center in $\boldsymbol{x}''$ is removed. To get back to the original surface Q_j is simply a matter of letting the radius go to zero. A parametrization of the hemisphere is given by

$$\boldsymbol{X}(\varphi,\theta) = \boldsymbol{x}'' + \epsilon\left(\sin\varphi\cos\theta, \sin\varphi\sin\theta, \cos\varphi\right), \quad \varphi_1 \le \varphi \le \varphi_1 + \frac{\pi}{2},\ 0 \le \theta < 2\pi \tag{2.78}$$

and φ_1 is a constant. Without loss of generality, we can assume that $\varphi_1 = 0$. A parametrization of the normal vector is

$$\boldsymbol{N}(\varphi,\theta) = \boldsymbol{X}_\theta \times \boldsymbol{X}_\varphi = \epsilon^2 sin\varphi\left(\sin\varphi\cos\theta, \sin\varphi\sin\theta, \cos\varphi\right) = \epsilon^2 sin\varphi\, \boldsymbol{n}, \tag{2.79}$$

where $\boldsymbol{n}$ is the unit normal, pointing out of the hemisphere.

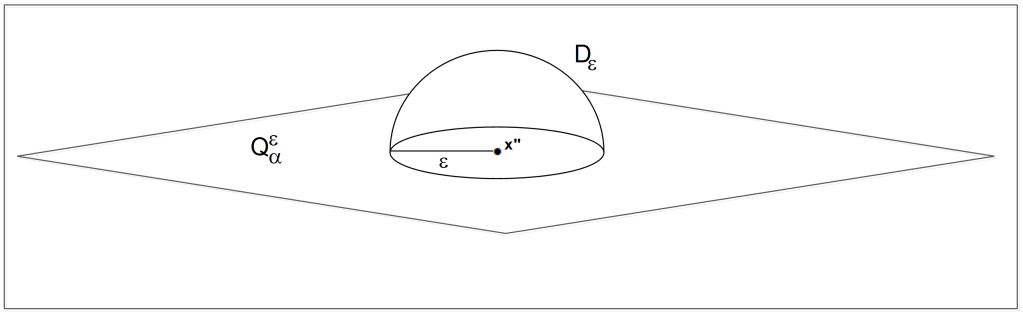

FIGURE 2.1: The extended surface around the singularity at $\boldsymbol{x''}$

The j-th integral on the right hand side in the boundary integral equation (2.77), we define as the integral over Q_j^ϵ and D_ϵ, where the radius ϵ goes to zero:

$$\lim_{\epsilon\to 0}\iint_{Q_j^\epsilon} dA_{\boldsymbol{x}} D_0(\boldsymbol{x},\boldsymbol{x}'')\partial_{\boldsymbol{nn'}}\mathcal{D}(\boldsymbol{x},\boldsymbol{x}') + \lim_{\epsilon\to 0}\iint_{D_\epsilon} dA_{\boldsymbol{x}} D_0(\boldsymbol{x},\boldsymbol{x}'')\partial_{\boldsymbol{nn'}}\mathcal{D}(\boldsymbol{x},\boldsymbol{x}'). \tag{2.80}$$

By definition, the integral over Q_j^ϵ is a principal value integral when $\epsilon \to 0$. The contribution from integrating over the hemisphere D_ϵ is

$$\begin{aligned}\iint\limits_{D_\epsilon} dA_{\boldsymbol{x}} D_0(\boldsymbol{x},\boldsymbol{x}'')\partial_{\boldsymbol{n}\boldsymbol{n}'}\mathcal{D}(\boldsymbol{x},\boldsymbol{x}') &= \int_0^{\pi/2} d\varphi \int_0^{2\pi} d\theta\, \|\boldsymbol{N}\|\, D_0(\boldsymbol{X},\boldsymbol{x}'')\partial_{\boldsymbol{n}\boldsymbol{n}'}\mathcal{D}(\boldsymbol{X},\boldsymbol{x}') \\ &= \int_0^{\pi/2} d\varphi\, \sin(\varphi) \int_0^{2\pi} d\theta\, \epsilon^2 \frac{e^{-|\omega|\epsilon}}{4\pi\epsilon}\partial_{\boldsymbol{n}\boldsymbol{n}'}\mathcal{D}(\boldsymbol{X},\boldsymbol{x}'). \quad (2.81)\end{aligned}$$

But

$$\lim_{\epsilon\to 0} \epsilon^2 \frac{e^{-|\omega|\epsilon}}{4\pi\epsilon} = \lim_{\epsilon\to 0} \epsilon \frac{e^{-|\omega|\epsilon}}{4\pi} = 0. \quad (2.82)$$

Thus the integral over the hemisphere D_ϵ gives no contribution and therefore the j-th integral reduces to a principal value integral over Q_j. The boundary integral equation (2.77) now can be written

$$-\partial_{\boldsymbol{n}'} D_0(\boldsymbol{x}',\boldsymbol{x}'') = \sum_\alpha PV_{\boldsymbol{x}''} \iint\limits_{Q_\alpha} dA_{\boldsymbol{x}} D_0(\boldsymbol{x},\boldsymbol{x}'')\partial_{\boldsymbol{n}\boldsymbol{n}'}\mathcal{D}(\boldsymbol{x},\boldsymbol{x}'), \quad (2.83)$$

where $\boldsymbol{x}' \in Q_i$, $\boldsymbol{x}'' \in Q_j$, $i,j = 1,...,r$. Only the integral over Q_j is a principal value integral.

The next step is to define how to take the limit $\boldsymbol{x}' \to \boldsymbol{x}''$ so that we don't get an infinity on the left hand side of the equation for $\boldsymbol{x}' = \boldsymbol{x}''$. Observe that if we start with equation (2.69) where $\boldsymbol{x}' \in V_0$, $\boldsymbol{x}'' \in Q_i$ and takes the limit $\boldsymbol{x}' \to \boldsymbol{x}''$ along some arbitrary path in V_0, then some of the steps that led to equation (2.83) aren't valid and one doesn't get rid of the infinity on the left hand side. However, as we remember from the derivation of the expression of the force (equation (2.57)), the limit $\boldsymbol{x}' \to \boldsymbol{x}$ was taken with both $\boldsymbol{x} \in Q_i$ and $\boldsymbol{x}' \in Q_i$. Thus letting $\boldsymbol{x}'$ approach any point, but not $\boldsymbol{x}''$, at the boundary Q_i and then taking the limit $\boldsymbol{x}' \to \boldsymbol{x}''$ along the surface Q_i, is the only interesting limit for us. Doing it this way, we can use equation (2.83) as a starting point when we shall take the limit $\boldsymbol{x}' \to \boldsymbol{x}''$.

Notice that the free Green's function D_0, given by equation (2.63), only depends on the distance $\|\boldsymbol{x}' - \boldsymbol{x}''\|$. The gradient of a function g: $\mathbb{R}^n \to \mathbb{R}$ that only depends of the distance $r = \|\boldsymbol{r}\|$ is given by

$$\nabla g(r) = \frac{\boldsymbol{r}}{r}\frac{d}{dr} g(r). \quad (2.84)$$

Therefore the left hand side of equation (2.83) can be written as

$$\begin{aligned}-\partial_{\boldsymbol{n}'} D_0(\boldsymbol{x}',\boldsymbol{x}'') = -\boldsymbol{n}' \cdot \nabla' D_0(\boldsymbol{x}',\boldsymbol{x}'') &= -\boldsymbol{n}' \cdot \frac{1}{4\pi}\left[\frac{\boldsymbol{r}}{r}\frac{d}{dr}\frac{e^{-\omega r}}{r}\right]_{\boldsymbol{r}=\boldsymbol{x}'-\boldsymbol{x}''} \\ &= -\boldsymbol{n}' \cdot \left(\boldsymbol{x}' - \boldsymbol{x}''\right) \frac{e^{-\omega\|\boldsymbol{x}'-\boldsymbol{x}''\|}}{4\pi\|\boldsymbol{x}'-\boldsymbol{x}''\|^3}\left(1 + \omega\|\boldsymbol{x}'-\boldsymbol{x}''\|\right).\end{aligned} \quad (2.85)$$

In two dimensions the corresponding equation to (2.85) has a $\|\boldsymbol{x}' - \boldsymbol{x}''\|^2$ dependence in the denominator. In that case it is possible to show that $\partial_{\boldsymbol{n}'} D_0(\boldsymbol{x}', \boldsymbol{x}'')$ is finite also in the limit $\boldsymbol{x}' \to \boldsymbol{x}''$. I. Kilen showed that this factor is proportional to the curvature when $\boldsymbol{x}' \to \boldsymbol{x}''$ in his thesis [1].

In our case we have a $\|\boldsymbol{x}' - \boldsymbol{x}''\|^3$ dependence in the denominator and therefore it seems like we haven't resolved anything by first letting $\boldsymbol{x}' \to Q_i$. There is still an infinity in $\partial_{\boldsymbol{n}'} D_0(\boldsymbol{x}', \boldsymbol{x}'')$ when we take the limit $\boldsymbol{x}' \to \boldsymbol{x}''$. This is a clear difference from the two dimensional case. The quantity $\partial_{\boldsymbol{n}'} D_0(\boldsymbol{x}', \boldsymbol{x}'')$ must be regularized even more.

Observe that for parallel plates, because of orthogonality, $\boldsymbol{n}' \perp (\boldsymbol{x}' - \boldsymbol{x}'')$, the quantity $\partial_{\boldsymbol{n}'} D_0(\boldsymbol{x}', \boldsymbol{x}'')$ is zero. It turns out that this fact also will help us in situations where the boundaries are surfaces with curvature. The reason is that the surfaces Q_k will be discretized into pieces that are flat, i.e without curvature. The flat pieces will be triangles. When $\boldsymbol{x}'$ and $\boldsymbol{x}''$ are on the same triangle, the normal $\boldsymbol{n}'$ is orthogonal to $\boldsymbol{x}' - \boldsymbol{x}''$ and the contribution is zero. When $\boldsymbol{x}'$ and $\boldsymbol{x}''$ are on different triangles, the contribution from the left hand side can be calculated using equation (2.85). Because $\boldsymbol{x}'$ and $\boldsymbol{x}''$ are on different triangles, we know that the denominator isn't zero and the contribution from the left hand side is finite. Thus the discretization removes the singularity and is therefore the final regularization of $\partial_{\boldsymbol{n}'} D_0(\boldsymbol{x}', \boldsymbol{x}'')$. However, we should keep in mind that, especially when the resolution of the discretization is high and the objects are very curved and the two sources $\boldsymbol{x}'$ and $\boldsymbol{x}''$ are placed on two neighbouring triangles, that both the nominator and the denominator are close to zero. We will discuss this behaviour in more detail after having introduced how we are going to discretize the equations.

Our boundary value equation (2.83) has now been regularized s.t. the expression on the left hand side is finite for all $\boldsymbol{x}' \in Q_i, \boldsymbol{x}'' \in Q_j$ and the integrals on the right hand side are treated as principal value integrals when integrating over singularities in the free Green's function D_0. However, we haven't arrived at our fully regularized boundary integral equations yet. The final part of the regularization will be to separate the interaction pressure from the self pressure.

Assume that $\boldsymbol{x}$ and $\boldsymbol{x}''$ belong to different surfaces Q_k and Q_l. Observe that when $\omega \to \infty$, the free Green's function $D_0(\boldsymbol{x}, \boldsymbol{x}'', \omega) \to 0$ (see equation (2.63)). This make the equations (2.83) decouple into separate equations for each surface Q_j for high frequencies. We denote the solutions of the resulting equations by $\mathcal{P}_i(\boldsymbol{x}, \boldsymbol{x}')$, where the equations are

$$-\partial_{\boldsymbol{n}'} D_0(\boldsymbol{x}', \boldsymbol{x}'') = PV_{\boldsymbol{x}''} \iint_{Q_i} dA_{\boldsymbol{x}} D_0(\boldsymbol{x}, \boldsymbol{x}'') \mathcal{P}_i(\boldsymbol{x}, \boldsymbol{x}') \quad \boldsymbol{x}', \boldsymbol{x}'' \in Q_i,\ i = 1, .., r. \tag{2.86}$$

Since $\mathcal{P}_i(\boldsymbol{x}, \boldsymbol{x}')$ is the self pressure on surface i, the equations (2.86) will be called the *self pressure equations*. Physically, the self pressure isn't measurable. Our final regularization will therefore be to subtract the self pressure contribution from equation (2.83).

This will remove the high frequency contribution from the force and the resulting force will be redefined as the correct force for our problem.

By subtracting $\iint_{Q_i} dA_{\boldsymbol{x}} D_0(\boldsymbol{x}, \boldsymbol{x}'')\mathcal{P}_i(\boldsymbol{x}, \boldsymbol{x}')$ from both sides of equation (2.83), introducing $Q = \cup_k Q_k$ and interchanging the left and right hand side of the equation, we get

$$\iint\limits_{Q} dA_{\boldsymbol{x}} D_0(\boldsymbol{x}, \boldsymbol{x}'')\mathcal{P}(\boldsymbol{x}, \boldsymbol{x}') = -\partial_{\boldsymbol{n}'} D_0(\boldsymbol{x}', \boldsymbol{x}'') - \iint\limits_{Q_i} dA_{\boldsymbol{x}} D_0(\boldsymbol{x}, \boldsymbol{x}'')\mathcal{P}_i(\boldsymbol{x}, \boldsymbol{x}') \tag{2.87}$$

where $\boldsymbol{x}' \in Q_i$ and $\boldsymbol{x}'' \in Q_j$ for $i, j = 1, 2, ..., r$. The integrals over Q_j are principal value integrals and the regularized density, $\mathcal{P}$, is given by

$$\mathcal{P}(\boldsymbol{x}, \boldsymbol{x}') = \begin{cases} \partial_{\boldsymbol{n}\boldsymbol{n}'}\mathcal{D}(\boldsymbol{x}, \boldsymbol{x}') - \mathcal{P}_i(\boldsymbol{x}, \boldsymbol{x}'), & \boldsymbol{x}, \boldsymbol{x}' \in Q_i \\ \partial_{\boldsymbol{n}\boldsymbol{n}'}\mathcal{D}(\boldsymbol{x}, \boldsymbol{x}'), & \boldsymbol{x} \in Q_j, \boldsymbol{x}' \in Q_i, \quad j \neq i. \end{cases} \tag{2.88}$$

This is our final boundary integral equation, which is fully regularized. It can be solved and investigated using standard analytical or numerical methods. We will return to how we are going to do this shortly.

When we have solved equation (2.87) for all ω's that contributes to the density components $\mathcal{P}(\boldsymbol{x}, \boldsymbol{x}', \omega)$, we get the regularized pressure,

$$P(\boldsymbol{x}) = \frac{1}{4\pi} \int_{-\infty}^{\infty} d\omega\, \mathcal{P}(\boldsymbol{x}, \boldsymbol{x}, \omega). \tag{2.89}$$

The fact that $D_0(\boldsymbol{x}, \boldsymbol{x}'', \omega)$ is an even function in ω implies that $\mathcal{P}(\boldsymbol{x}, \boldsymbol{x}, \omega)$ is even in ω and therefore the regularized pressure can be written as

$$P(\boldsymbol{x}) = \frac{1}{2\pi} \int\limits_{0}^{\infty} d\omega\, \mathcal{P}(\boldsymbol{x}, \boldsymbol{x}, \omega). \tag{2.90}$$

Finally, the regularized force is found by

$$\boldsymbol{F}_i = \oiint\limits_{Q_i} dA_{\boldsymbol{x}}\, \boldsymbol{n}(\boldsymbol{x})P(\boldsymbol{x}) = \oiint\limits_{Q_i} dA_{\boldsymbol{x}}\, \boldsymbol{n}(\boldsymbol{x}) \frac{1}{2\pi} \int\limits_{0}^{\infty} d\omega\, \mathcal{P}(\boldsymbol{x}, \boldsymbol{x}, \omega). \tag{2.91}$$

2.5 Discretization of the regularized boundary integral equation

It can be convenient to separate ordinary integrals and principal value integrals, and also to separate between whether $\boldsymbol{x}'$ and $\boldsymbol{x}''$ belong to the same surface or not. Using the self-pressure equation (2.86), the fully regularized boundary integral equation (2.87)

can for $\boldsymbol{x}', \boldsymbol{x}'' \in Q_i$ be written as

$$PV_{\boldsymbol{x}''} \iint\limits_{Q_i} dA_{\boldsymbol{x}} D_0(\boldsymbol{x}, \boldsymbol{x}'')\mathcal{P}(\boldsymbol{x}, \boldsymbol{x}') + \sum_{\alpha \neq i} \iint\limits_{Q_\alpha} dA_{\boldsymbol{x}} D_0(\boldsymbol{x}, \boldsymbol{x}'')\mathcal{P}(\boldsymbol{x}, \boldsymbol{x}') = 0. \tag{2.92}$$

For $\boldsymbol{x}' \in Q_i$, $\boldsymbol{x}'' \in Q_j$, $i \neq j$, we have

$$\begin{aligned} &PV_{\boldsymbol{x}''} \iint\limits_{Q_j} dA_{\boldsymbol{x}} D_0(\boldsymbol{x}, \boldsymbol{x}'')\mathcal{P}(\boldsymbol{x}, \boldsymbol{x}') + \sum_{\alpha \neq j} \iint\limits_{Q_\alpha} dA_{\boldsymbol{x}} D_0(\boldsymbol{x}, \boldsymbol{x}'')\mathcal{P}(\boldsymbol{x}, \boldsymbol{x}') \\ &= -\partial_{\boldsymbol{n}'} D_0(\boldsymbol{x}', \boldsymbol{x}'') - \iint\limits_{Q_i} dA_{\boldsymbol{x}} D_0(\boldsymbol{x}, \boldsymbol{x}'')\mathcal{P}_i(\boldsymbol{x}, \boldsymbol{x}'), \end{aligned} \tag{2.93}$$

where $\mathcal{P}_i(\boldsymbol{x}, \boldsymbol{x}')$ is the self pressure, found by solving equation (2.86). These equations will be solved numerically using *the method of moments*, which is a numerical technique used to convert the integral equations into a linear system that can be solved numerically. For the test configuration consisting of two parallel plates, two different discretizations are used; both standard grids of squares and triangulations consisting of triangles. For all other configurations we only discretize using triangulations.

To simplify the notation of the linear systems that appear, the following definitions will be helpful: Given a discretization of the surface Q_i, let S_k^i be the k^{th} triangle or square and $\boldsymbol{s}_k$ the "center of mass" of S_k^i.

Define

$$x_{kk'}^{ij} = \mathcal{P}(\boldsymbol{s}_k, \boldsymbol{s}_{k'}) \quad \text{for } \boldsymbol{s}_k \in S_k^i \text{ and } \boldsymbol{s}_{k'} \in S_{k'}^j \tag{2.94}$$

$$a_{kk''}^{ij} = \iint\limits_{S_k^i} dA_{\boldsymbol{x}} D_0(\boldsymbol{x}, \boldsymbol{s}_{k''}), \quad \text{for } \boldsymbol{s}_{k''} \in S_{k''}^j, \tag{2.95}$$

where the integral in equation (2.95) is a principal value integral when $i = j$ and $k = k''$. Further, define

$$y_{k'k''}^{ij} = -\partial_{\boldsymbol{n}'} D_0(\boldsymbol{s}_{k'}, \boldsymbol{s}_{k''}) \quad \text{for } \boldsymbol{s}_{k'} \in S_{k'}^i \text{ and } \boldsymbol{s}_{k''} \in S_{k''}^j \tag{2.96}$$

$$b_{kk'}^{ii} = \mathcal{P}_i(\boldsymbol{s}_k, \boldsymbol{s}_{k'}) \quad \text{for } \boldsymbol{s}_k \in S_k^i \text{ and } \boldsymbol{s}_{k'} \in S_{k'}^i. \tag{2.97}$$

To illustrate the efficiency of the above notation, let us see how the integrals in equations (2.92) and (2.93) will change:

$$\begin{aligned} &\iint\limits_{Q_i} dA_{\boldsymbol{x}} D_0(\boldsymbol{x}, \boldsymbol{s}_{k''})\mathcal{P}(\boldsymbol{x}, \boldsymbol{s}_{k'}) = \sum_k \iint\limits_{S_k^i} dA_{\boldsymbol{x}} D_0(\boldsymbol{x}, \boldsymbol{s}_{k''})\mathcal{P}(\boldsymbol{x}, \boldsymbol{s}_{k'}) \\ &\approx \sum_k \left(\iint\limits_{S_k^i} dA_{\boldsymbol{x}} D_0(\boldsymbol{x}, \boldsymbol{s}_{k''}) \right) \mathcal{P}(\boldsymbol{s}_k, \boldsymbol{s}_{k'}) = \sum_k a_{kk''}^{ij} x_{kk'}^{ij}. \end{aligned} \tag{2.98}$$

Remember that we are considering a configuration consisting of r conductors. Discretizing the boundaries $\{Q_k\}_{k=1}^r$ and using the above notation, equations (2.92) and (2.93) can be approximated by the system

$$\begin{aligned}
&\sum_k a_{kk''}^{11} x_{kk'}^{1i} + ... + a_{kk''}^{i1} x_{kk'}^{ii} + ... + a_{kk''}^{r1} x_{kk'}^{ri} = y_{k'k''}^{i1} - \sum_k a_{kk''}^{i1} b_{kk'}^{ii} \\
&\qquad\qquad\qquad\qquad \vdots \\
&\sum_k a_{kk''}^{1,i-1} x_{kk'}^{1i} + ... + a_{kk''}^{i,i-1} x_{kk'}^{ii} + ... + a_{kk''}^{r,i-1} x_{kk'}^{ri} = y_{k'k''}^{i,i-1} - \sum_k a_{kk''}^{i,i-1} b_{kk'}^{ii} \\
&\sum_k a_{kk''}^{1i} x_{kk'}^{1i} + ... + a_{kk''}^{ii} x_{kk'}^{ii} + ... + a_{kk''}^{ri} x_{kk'}^{ri} = 0 \\
&\sum_k a_{kk''}^{1,i+1} x_{kk'}^{1i} + ... + a_{kk''}^{i,i+1} x_{kk'}^{ii} + ... + a_{kk''}^{r,i+1} x_{kk'}^{ri} = y_{k'k''}^{i,i+1} - \sum_k a_{kk''}^{i1} b_{kk'}^{ii} \\
&\qquad\qquad\qquad\qquad \vdots \\
&\sum_k a_{kk''}^{1r} x_{kk'}^{1i} + ... + a_{kk''}^{ir} x_{kk'}^{ii} + ... + a_{kk''}^{rr} x_{kk'}^{ri} = y_{k'k''}^{ir} - \sum_k a_{kk''}^{ir} b_{kk'}^{ii}.
\end{aligned} \tag{2.99}$$

The self pressure equation (2.86), for object i, becomes

$$\sum_k a_{kk''}^{ii} b_{kk'}^{ii} = y_{k'k''}^{ii}. \tag{2.100}$$

We express this linear system of equations as a product of block matrices. Define

$$A^{ij} = \left(a_{kk''}^{ij}\right)^T = \left(a_{k''k}^{ij}\right), \tag{2.101}$$

$$X^{ij} = \left(x_{kk'}^{ij}\right), \tag{2.102}$$

$$Y^{ij} = \left(y_{k'k''}^{ij}\right)^T = \left(y_{k''k'}^{ij}\right), \tag{2.103}$$

$$B^{ii} = \left(b_{kk'}^{ii}\right). \tag{2.104}$$

The above equations (2.99) can be expressed as

$$\begin{bmatrix}
A^{11} & \cdots & \cdots & A^{i1} & \cdots & \cdots & A^{r1} \\
\vdots & \ddots & & \vdots & & & \vdots \\
A^{1,i-1} & & \ddots & \vdots & & & A^{r,i-1} \\
A^{1i} & \cdots & \cdots & A^{ii} & \cdots & \cdots & A^{ri} \\
A^{1,i+1} & & & \vdots & \ddots & & A^{r,i+1} \\
\vdots & & & \vdots & & \ddots & \vdots \\
A^{ri} & \cdots & \cdots & A^{ri} & \cdots & \cdots & A^{rr}
\end{bmatrix}
\begin{bmatrix}
X^{1i} \\ \vdots \\ X^{i-1,i} \\ X^{ii} \\ X^{i+1,i} \\ \vdots \\ X^{ri}
\end{bmatrix}
=
\begin{bmatrix}
Y^{i1} - A^{i1}B^{ii} \\ \vdots \\ Y^{i,i-1} - A^{i,i-1}B^{ii} \\ 0 \\ Y^{i,i+1} - A^{i,i+1}B^{ii} \\ \vdots \\ Y^{ir} - A^{ir}B^{ii}
\end{bmatrix}, \tag{2.105}$$

for $i = 1, 2, ..., r$. These are r block matrix equations for r block matrix unknowns. The self pressure is given by

$$A^{ii}B^{ii} = Y^{ii}, \quad i = 1, 2, ..., r. \tag{2.106}$$

For the special configuration consisting of two objects, equations (2.105) turns into

$$\begin{bmatrix} A^{11} & A^{21} \\ A^{12} & A^{22} \end{bmatrix} \begin{bmatrix} X^{11} \\ X^{21} \end{bmatrix} = \begin{bmatrix} 0 \\ Y^{12} - A^{12}B^{11} \end{bmatrix} \tag{2.107}$$

and

$$\begin{bmatrix} A^{11} & A^{21} \\ A^{12} & A^{22} \end{bmatrix} \begin{bmatrix} X^{12} \\ X^{22} \end{bmatrix} = \begin{bmatrix} Y^{21} - A^{21}B^{22} \\ 0 \end{bmatrix}, \tag{2.108}$$

where B^{ii} is given by

$$A^{ii}B^{ii} = Y^{ii}, \quad i = 1, 2. \tag{2.109}$$

For each ω, the self pressure is found by solving for B^{ii}. After this, the matrices X^{ii} are found, where the diagonal elements contribute to the pressure.

The next two sections show how to calculate the elements of the matrices A^{ij} and Y^{ij} for the two different discretizations that we are going to use.

2.6 Matrix elements for the square discretization of the parallel plates

Fix a coordinate system such that the plates are lying in the planes $z = z_1 = -\frac{a}{2}$ and $z = z_2 = \frac{a}{2}$. Let the plates have length L in both x- and y-direction. Fix two grids such that S^i_{kl} is the square with center in $\boldsymbol{s}_{kl} = ((k - \frac{1}{2})h, (l - \frac{1}{2})h, z_i)$ and edges of length $h = \frac{L}{N}$, where N is the number of squares in both x- and y-direction. A problem with this discretization is that we get four-double lower indices such as for example $a^{ij}_{klk''l''}$, but we want to work with matrix elements. A way to resolve this is to let $m = k + N(l-1)$ and $m'' = k'' + N(l'' - 1)$. Then m and m' run from 1 to N^2 and the elements transforms as $a^{ij}_{klk''l''} \to a^{ij}_{mm''}$. Finally, we rename the dummy-indices m and m'' s.t. we get $a^{ij}_{kk''}$.

2.6.1 Matrix elements $y^{ij}_{k'k''}$

The matrix elements $y^{ij}_{k'k''}$ are given by equations (2.96) and (2.85). Thus

$$\begin{aligned} y^{ij}_{k'k''} &= -\partial_{\boldsymbol{n'}} D_0(\boldsymbol{s}_{k'}, \boldsymbol{s}_{k''}) \\ &= -\boldsymbol{n'} \cdot (\boldsymbol{s}_{k'} - \boldsymbol{s}_{k''}) \frac{e^{-\omega\|\boldsymbol{s}_{k'} - \boldsymbol{s}_{k''}\|}}{4\pi\|\boldsymbol{s}_{k'} - \boldsymbol{s}_{k''}\|^3} \left(1 + \omega\|\boldsymbol{s}_{k'} - \boldsymbol{s}_{k''}\|\right). \end{aligned} \tag{2.110}$$

When $i = j$, the normal vector $\boldsymbol{n'}$ is orthogonal to $\boldsymbol{s}_{k'} - \boldsymbol{s}_{k''}$ and therefore

$$y^{ii}_{k'k''} = 0. \tag{2.111}$$

This means that $Y^{11} = Y^{22} = 0$ and the unique solutions of the self pressure equations (2.106) are

$$B^{11} = B^{22} = 0. \tag{2.112}$$

I.e. the self pressure is zero on the parallel plates.

When $i \neq j$, we have that $\boldsymbol{n'} \cdot (\boldsymbol{s}_{k'} - \boldsymbol{s}_{k''}) = -a$. Thus

$$y^{ij}_{k'k''} = \frac{a}{4\pi} \frac{e^{-\omega\|\boldsymbol{s}_{k'} - \boldsymbol{s}_{k''}\|}}{\|\boldsymbol{s}_{k'} - \boldsymbol{s}_{k''}\|^3} \left(1 + \omega\|\boldsymbol{s}_{k'} - \boldsymbol{s}_{k''}\|\right), \qquad i \neq j. \tag{2.113}$$

2.6.2 Matrix elements $a^{ij}_{kk''}$

When $k \neq k''$, the elements are approximated by the midpoint rule

$$a^{ij}_{kk''} = \iint\limits_{S^i_k} dA_{\boldsymbol{x}} D_0(\boldsymbol{x}, \boldsymbol{s}_{k''}) = -\frac{1}{4\pi} \iint\limits_{S^i_k} dA_{\boldsymbol{x}} \frac{e^{-\omega\|\boldsymbol{x} - \boldsymbol{s}_{k''}\|}}{\|\boldsymbol{x} - \boldsymbol{s}_{k''}\|} \approx -\frac{h^2}{4\pi} \frac{e^{-\omega\|\boldsymbol{s}_k - \boldsymbol{s}_{k''}\|}}{\|\boldsymbol{s}_k - \boldsymbol{s}_{k''}\|}. \tag{2.114}$$

When $i = j$ and $k = k''$, we have to integrate over the singularity at $\boldsymbol{x} = \boldsymbol{s}_k$. Remember from the derivation in section 2.4 that we can treat this integral as a principal value integral because the contribution from integrating over the hemisphere D_ϵ is zero, thus

$$a^{ii}_{kk} = PV_{\boldsymbol{s}_k} \iint\limits_{S^i_k} dA_{\boldsymbol{x}} D_0(\boldsymbol{x}, \boldsymbol{s}_k) = -\frac{1}{4\pi} PV_{\boldsymbol{s}_k} \iint\limits_{S^i_k} dA_{\boldsymbol{x}} \frac{e^{-\omega\|\boldsymbol{x} - \boldsymbol{s}_k\|}}{\|\boldsymbol{x} - \boldsymbol{s}_k\|}. \tag{2.115}$$

It is possible to make this integral independent of i and k by choosing a two dimensional coordinate system, lying in the plane $z = z_i$, such that the center of mass, $\boldsymbol{s}_k$, of the square S^i_k is in the origin $\mathbf{0} = (0, 0)$, and the edges of S^i_k are parallel to the coordinate axes. Thus

$$a^{ii}_{kk} = -\frac{1}{4\pi} PV \iint\limits_{S} dA_{\boldsymbol{x}} \frac{e^{-\omega\|\boldsymbol{x}\|}}{\|\boldsymbol{x}\|} \equiv -\frac{1}{4\pi} \lim_{\epsilon \to 0} \iint\limits_{S_\epsilon} dA \frac{e^{-\omega\|\boldsymbol{x}\|}}{\|\boldsymbol{x}\|}, \tag{2.116}$$

where $S = [-\frac{h}{2}, \frac{h}{2}] \times [-\frac{h}{2}, \frac{h}{2}]$ and S_ϵ is the remaining part of the square S when the part which is inside the hemisphere D_ϵ of radius ϵ and with center in the origin is removed.

It will now be helpful to define a function f, given by

$$f(r; \omega) = \frac{e^{-\omega r}}{r}. \tag{2.117}$$

This function is closely related to the free Green's function D_0. Using f, we get

$$a_{kk}^{ii} = -\frac{1}{4\pi} PV \iint_S dA\, f(\|\boldsymbol{x}\|;\omega). \tag{2.118}$$

In order to solve the above integral (2.118), the divergence theorem will be used. Therefore we must find a function $\boldsymbol{g}$ s.t $f(r;\omega) = \nabla \cdot \boldsymbol{g}(\boldsymbol{r};\omega)$. Try with $\boldsymbol{g}(\boldsymbol{r};\omega) = \boldsymbol{r}h(r;\omega)$. Then

$$\begin{aligned} \nabla \cdot \boldsymbol{g}(\boldsymbol{r};\omega) &= \nabla \cdot (\boldsymbol{r}h(r;\omega)) = (\nabla \cdot \boldsymbol{r})h(r;\omega) + \boldsymbol{r} \cdot \nabla h(r;\omega) \\ &= 2h(r;\omega) + \boldsymbol{r} \cdot \frac{\boldsymbol{r}}{r} h'(r;\omega) = 2h(r;\omega) + rh'(r;\omega). \end{aligned} \tag{2.119}$$

In order to find $h(r;\omega)$, we have to solve the first order linear ODE given by

$$2h(r;\omega) + rh'(r;\omega) = \frac{e^{-\omega r}}{r}. \tag{2.120}$$

The solution, found using standard methods, is

$$h(r;\omega) = \frac{1}{\omega r^2}\left(C - e^{-\omega r}\right), \quad C \in \mathbb{R}, \tag{2.121}$$

and therefore

$$\boldsymbol{g}(\boldsymbol{r};\omega) = \boldsymbol{r}h(r;\omega) = \frac{\boldsymbol{r}}{\omega r^2}\left(C - e^{-\omega r}\right), \quad C \in \mathbb{R}. \tag{2.122}$$

We are free to choose the constant C, but remember that we are going to integrate over ω from 0 to ∞. Observe that the choice $C = 1$ gives

$$\lim_{\omega \to 0} \boldsymbol{g}(\boldsymbol{r};\omega) = \lim_{\omega \to 0} \frac{\boldsymbol{r}}{\omega r^2}\left(1 - e^{-\omega r}\right) = \frac{\boldsymbol{r}}{r} \tag{2.123}$$

Thus $C = 1$ makes sure that $\boldsymbol{g}(\boldsymbol{r};0)$ is finite, and we therefore define $\boldsymbol{g}$ by

$$\boldsymbol{g}(\boldsymbol{r};\omega) = \frac{\boldsymbol{r}}{\omega r^2}\left(1 - e^{-\omega r}\right). \tag{2.124}$$

The diagonal elements change to

$$a_{kk}^{ii} = -\frac{1}{4\pi} PV \iint_S dA\, \nabla \cdot \boldsymbol{g}(\boldsymbol{x};\omega). \tag{2.125}$$

The divergence theorem gives

$$a_{kk}^{ii} = -\frac{1}{4\pi} \lim_{\epsilon \to 0} \oint_{\partial S_\epsilon} ds\, \boldsymbol{n} \cdot \boldsymbol{g}(\boldsymbol{x};\omega) = -\frac{1}{4\pi} \left(\oint_{\partial S} ds\, \boldsymbol{n} \cdot \boldsymbol{g}(\boldsymbol{x};\omega) + \lim_{\epsilon \to 0} \oint_{C_\epsilon} ds\, \boldsymbol{n} \cdot \boldsymbol{g}(\boldsymbol{x};\omega) \right), \tag{2.126}$$

where $\partial S_\epsilon = \partial S \cup C_\epsilon$ is the boundary of S_ϵ. ∂S is the boundary of the square S and C_ϵ is the boundary of the hemisphere D_ϵ. A parametrization of the circle C_ϵ, correctly oriented, is given by

$$C_\epsilon : \quad \boldsymbol{\gamma}(\theta) = \epsilon\left(\cos\theta, -\sin\theta\right), \quad \theta \in [0, 2\pi]. \tag{2.127}$$

The contribution from the second integral in equation (2.126) is

$$\begin{aligned} -\frac{1}{4\pi}\oint_{C_\epsilon} ds\, \boldsymbol{n}\cdot\boldsymbol{g}(\boldsymbol{x};\omega) &= -\frac{1}{4\pi}\int_0^{2\pi} d\theta\, \epsilon\boldsymbol{n}\cdot\frac{\boldsymbol{\gamma}(\theta)}{\omega\|\boldsymbol{\gamma}(\theta)\|^2}\left(1-e^{-\omega\|\boldsymbol{\gamma}(\theta)\|}\right) \\ &= -\frac{1}{4\pi}\int_0^{2\pi} d\theta\, \frac{\epsilon^2}{\omega\epsilon^2}\left(1-e^{-\omega\epsilon}\right) \\ &= -\frac{1}{2\omega}\left(1-e^{-\omega\epsilon}\right) \overset{\epsilon\to 0}{\longrightarrow} 0. \end{aligned} \tag{2.128}$$

Thus there is no contribution from integrating around the circle C_ϵ when $\epsilon \to 0$, and therefore

$$a^{ii}_{kk} = -\frac{1}{4\pi}\oint_{\partial S} ds\, \boldsymbol{n}\cdot\boldsymbol{g}(\boldsymbol{x};\omega), \tag{2.129}$$

where $\partial S = C_1 \cup C_2 \cup C_3 \cup C_4$ is the boundary of the square S. A parametrization of ∂S is introduced;

$$\begin{aligned} C_1 : &\quad \boldsymbol{\gamma}_1(t) = \left(t, -\tfrac{h}{2}\right), \quad t \in \left[-\tfrac{h}{2}, \tfrac{h}{2}\right], \quad \boldsymbol{n}_1 = (0,-1), \\ C_2 : &\quad \boldsymbol{\gamma}_2(t) = \left(\tfrac{h}{2}, t\right), \quad t \in \left[-\tfrac{h}{2}, \tfrac{h}{2}\right], \quad \boldsymbol{n}_2 = (1,0), \\ C_3 : &\quad \boldsymbol{\gamma}_3(t) = \left(-t, \tfrac{h}{2}\right), \quad t \in \left[-\tfrac{h}{2}, \tfrac{h}{2}\right], \quad \boldsymbol{n}_3 = (0,1), \\ C_4 : &\quad \boldsymbol{\gamma}_4(t) = \left(-\tfrac{h}{2}, -t\right) \quad t \in \left[-\tfrac{h}{2}, \tfrac{h}{2}\right] \quad \boldsymbol{n}_4 = (-1,0). \end{aligned} \tag{2.130}$$

Observe that $\boldsymbol{n}_i \cdot \boldsymbol{\gamma}_i(t) = \frac{h}{2}$ and $\|\boldsymbol{\gamma}_i(t)\| = \sqrt{t^2 + \left(\frac{h}{2}\right)^2}$ for $i = 1,2,3,4$. Thus

$$\begin{aligned} a^{ii}_{kk} &= -\frac{1}{4\pi}\int_{-h/2}^{h/2} dt \sum_{i=1}^{4} \boldsymbol{n}_i \cdot \frac{\boldsymbol{\gamma}_i(t)}{\omega\|\boldsymbol{\gamma}_i(t)\|^2}\left(1-e^{-\omega\|\boldsymbol{\gamma}_i(t)\|}\right) \\ &= -\frac{h}{2\pi\omega}\int_{-h/2}^{h/2} dt\, \frac{1-e^{-\omega\sqrt{t^2+(\frac{h}{2})^2}}}{t^2+(\frac{h}{2})^2}. \end{aligned} \tag{2.131}$$

This integral is calculated numerically, using a Gaussian quadrature or the midpoint rule.

2.7 Matrix elements for the triangle discretization

Consider a general configuration of r compact objects. Assume that the boundaries of the objects have been triangulated by m_i triangles on each of the r surfaces. Let the triangles S_k^i be represented by their vertices $\boldsymbol{x}_{1_k}, \boldsymbol{x}_{2_k}, \boldsymbol{x}_{3_k}$, which are oriented counter clockwise when looking at the surface Q_i. Let $\boldsymbol{s}_k$ be the center of mass of each triangle, i.e. $\boldsymbol{s}_k = \frac{1}{3}(\boldsymbol{x}_{1_k} + \boldsymbol{x}_{2_k} + \boldsymbol{x}_{3_k})$. A_k^i is defined as the area of the triangle S_k^i.

2.7.1 Matrix elements $y_{k'k''}^{ij}$

The matrix elements $y_{k'k''}^{ij}$ are given by exactly the same expression as they were for the square discretization;

$$y_{k'k''}^{ij} = -\boldsymbol{n}' \cdot (\boldsymbol{s}_{k'} - \boldsymbol{s}_{k''}) \frac{e^{-\omega\|\boldsymbol{s}_{k'} - \boldsymbol{s}_{k''}\|}}{4\pi\|\boldsymbol{s}_{k'} - \boldsymbol{s}_{k''}\|^3} (1 + \omega\|\boldsymbol{s}_{k'} - \boldsymbol{s}_{k''}\|). \tag{2.132}$$

In particular, when $i = j$ and $k' = k''$, we have that

$$y_{k'k'}^{ii} = 0 \tag{2.133}$$

because the limit $\boldsymbol{s}_{k'} \to \boldsymbol{s}_{k''}$ is taken with both $\boldsymbol{s}_{k'} \in S_{k'}^i$ and $\boldsymbol{s}_{k''} \in S_{k'}^i$, and therefore $\boldsymbol{n}' \cdot (\boldsymbol{s}_{k'} - \boldsymbol{s}_{k''}) = 0$.

2.7.2 Matrix elements $a_{kk''}^{ij}$

When $i = j$ and $k \neq k''$, or $i \neq j$, the matrix elements are approximated by the midpoint rule;

$$a_{kk''}^{ij} = \iint\limits_{S_k^i} dA_{\boldsymbol{x}} D_0(\boldsymbol{x}, \boldsymbol{s}_{k''}) = -\frac{1}{4\pi} \iint\limits_{S_k^i} dA_{\boldsymbol{x}} \frac{e^{-\omega\|\boldsymbol{x} - \boldsymbol{s}_{k''}\|}}{\|\boldsymbol{x} - \boldsymbol{s}_{k''}\|} \approx -\frac{A_k^i}{4\pi} \frac{e^{-\omega\|\boldsymbol{s}_k - \boldsymbol{s}_{k''}\|}}{\|\boldsymbol{s}_k - \boldsymbol{s}_{k''}\|}. \tag{2.134}$$

When $i = j$ and $k = k''$, the elements are represented via principal value integrals;

$$a_{kk}^{ii} = PV_{\boldsymbol{s}_k} \iint\limits_{S_k^i} dA_{\boldsymbol{x}} D_0(\boldsymbol{x}, \boldsymbol{s}_k) = -\frac{1}{4\pi} PV_{\boldsymbol{s}_k} \iint\limits_{S_k^i} dA_{\boldsymbol{x}} \frac{e^{-\omega\|\boldsymbol{x} - \boldsymbol{s}_k\|}}{\|\boldsymbol{x} - \boldsymbol{s}_k\|}. \tag{2.135}$$

Since the integrand only depends on $\|\boldsymbol{x} - \boldsymbol{s}_k\|$, we can choose coordinates such that the integral simplifies. The coordinate choice will be made such that the triangle S_k^i is lying in the xy-plane with the vertex $\boldsymbol{x}_{\boldsymbol{1_k}}$ in the origin and the vertex $\boldsymbol{x}_{\boldsymbol{2_k}}$ on the positive part of the x axis. See figure 2.2.

Define

$$\begin{aligned} \boldsymbol{r_k} &= \boldsymbol{x}_{\boldsymbol{2_k}} - \boldsymbol{x}_{\boldsymbol{1_k}}, \\ \boldsymbol{q_k} &= \boldsymbol{x}_{\boldsymbol{3_k}} - \boldsymbol{x}_{\boldsymbol{1_k}}. \end{aligned} \tag{2.136}$$

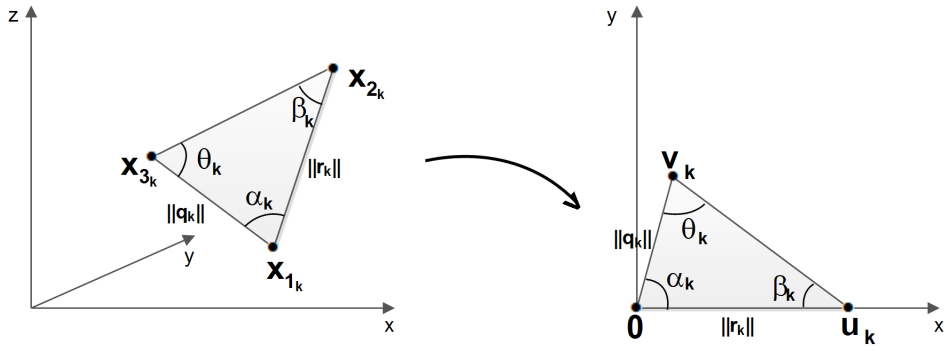

FIGURE 2.2: Change of coordinates.

The coordinates are chosen such that

$$\begin{aligned} \boldsymbol{x_{1_k}} &\to \mathbf{0} = (0,0), \\ \boldsymbol{x_{2_k}} &\to \boldsymbol{u_k} = (u_k, 0), \\ \boldsymbol{x_{3_k}} &\to \boldsymbol{v_k} = (v_k, w_k), \end{aligned} \tag{2.137}$$

where

$$\|\boldsymbol{u_k}\| = u_k = \|\boldsymbol{r_k}\| \tag{2.138}$$

and

$$\boldsymbol{v_k} = (v_k, w_k) = \|\boldsymbol{q_k}\|(\cos\alpha_k, \sin\alpha_k) = \frac{1}{\|\boldsymbol{r_k}\|}(\boldsymbol{r_k}\cdot\boldsymbol{q_k}, \|\boldsymbol{r_k}\times\boldsymbol{q_k}\|). \tag{2.139}$$

In equation (2.139) the identities

$$\boldsymbol{a}\cdot\boldsymbol{b} = \|\boldsymbol{a}\|\|\boldsymbol{b}\|\cos\alpha, \tag{2.140}$$

$$\|\boldsymbol{a}\times\boldsymbol{b}\| = \|\boldsymbol{a}\|\|\boldsymbol{b}\|\sin\alpha \tag{2.141}$$

are used. α is the angle between the vectors $\boldsymbol{a}$ and $\boldsymbol{b}$. In these coordinates, the triangle S_k^i has the vertexes $\mathbf{0}$, $\boldsymbol{u_k}$ and $\boldsymbol{v_k}$. The center of mass becomes

$$\boldsymbol{s_k} = \frac{1}{3}(\boldsymbol{u_k} + \boldsymbol{v_k}). \tag{2.142}$$

The diagonal elements are given by

$$a_{kk}^{ii} = -\frac{1}{4\pi} PV_{\boldsymbol{s_k}} \iint\limits_{S_k^i} dA_{\boldsymbol{x}} \frac{e^{-\omega\|\boldsymbol{x}-\boldsymbol{s}_k\|}}{\|\boldsymbol{x}-\boldsymbol{s}_k\|} = -\frac{1}{4\pi} PV_{\boldsymbol{s_k}} \iint\limits_{S_k^i} dA_{\boldsymbol{x}} f(\|\boldsymbol{x}-\boldsymbol{s}_k\|;\omega). \tag{2.143}$$

By definition of the principal value integral, we have that

$$a_{kk}^{ii} = -\frac{1}{4\pi} \lim_{\epsilon \to 0} \iint\limits_{S_{k,\epsilon}^i} dA_{\boldsymbol{x}} f(\|\boldsymbol{x} - \boldsymbol{s}_k\|; \omega), \tag{2.144}$$

where $S_{k,\epsilon}^i$ is the remaining part of the triangle S_k^i when the part which is inside the hemisphere $D_{k,\epsilon}^i$ of radius ϵ, centered around $\boldsymbol{s_k}$, is removed. Now, use the fact that $f(r;\omega) = \nabla \cdot \boldsymbol{g}(\boldsymbol{r};\omega)$ and the divergence theorem to obtain

$$a_{kk}^{ii} = -\frac{1}{4\pi} \left(\oint\limits_{\partial S_k^i} dl\, \boldsymbol{n} \cdot \boldsymbol{g}(\boldsymbol{x} - \boldsymbol{s}_k; \omega) + \lim_{\epsilon \to 0} \oint\limits_{C_{k,\epsilon}^i} dl\, \boldsymbol{n} \cdot \boldsymbol{g}(\boldsymbol{x} - \boldsymbol{s}_k; \omega) \right), \tag{2.145}$$

where $\partial S_k^i = C_{1_k} \cup C_{2_k} \cup C_{3_k}$ is the boundary of the triangle S_k^i. $C_{k,\epsilon}^i$ is the boundary of the hemisphere $D_{k,\epsilon}^i$. Similar calculations as we did for the squares, show that integrating around the circle $C_{k,\epsilon}^i$ give no contribution. Thus

$$a_{kk}^{ii} = -\frac{1}{4\pi\omega} \oint\limits_{\partial S_k^i} dl_{\boldsymbol{x}}\, \boldsymbol{n} \cdot \frac{\boldsymbol{x} - \boldsymbol{s_k}}{\|\boldsymbol{x} - \boldsymbol{s_k}\|^2} \left(1 - e^{-\omega \|\boldsymbol{x} - \boldsymbol{s_k}\|}\right). \tag{2.146}$$

A parametrization of ∂S_k^i is

$$\begin{aligned} C_{1_k}: &\quad \boldsymbol{\gamma_{1_k}}(t) = \boldsymbol{u_k} t, \quad t \in [0,1], \\ C_{2_k}: &\quad \boldsymbol{\gamma_{2_k}}(t) = \boldsymbol{u_k} + (\boldsymbol{v_k} - \boldsymbol{u_k}) t, \quad t \in [0,1] \\ C_{3_k}: &\quad \boldsymbol{\gamma_{3_k}}(t) = \boldsymbol{v_k}(1-t), \quad t \in [0,1]. \end{aligned} \tag{2.147}$$

Observe that

$$\begin{aligned} dl\, \boldsymbol{n_{1_k}} &= dt\, \|\boldsymbol{\gamma}'_{\boldsymbol{1_k}}(t)\| \boldsymbol{n_{1_k}} = dt\, (0, -u_k), \\ dl\, \boldsymbol{n_{2_k}} &= dt\, \|\boldsymbol{\gamma}'_{\boldsymbol{2_k}}(t)\| \boldsymbol{n_{2_k}} = dt\, (w_k, u_k - v_k), \\ dl\, \boldsymbol{n_{3_k}} &= dt\, \|\boldsymbol{\gamma}'_{\boldsymbol{3_k}}(t)\| \boldsymbol{n_{3_k}} = dt\, (-w_k, v_k), \end{aligned} \tag{2.148}$$

and

$$\|\boldsymbol{\gamma}'_{\boldsymbol{j_k}}(t)\| \boldsymbol{n_{j_k}} \cdot (\boldsymbol{\gamma_{j_k}}(t) - \boldsymbol{s_k}) = \frac{u_k w_k}{3}, \quad j = 1,2,3. \tag{2.149}$$

Inserting this and the parametrization into (2.146), we get

$$a_{kk}^{ii} \approx -\frac{A_k^i}{6\pi\omega} \int\limits_0^1 dt \sum_{j=1}^{3} \frac{1 - e^{-\omega \|\boldsymbol{\gamma_{j_k}}(t) - \boldsymbol{s_k}\|}}{\|\boldsymbol{\gamma_{j_k}}(t) - \boldsymbol{s_k}\|^2}, \tag{2.150}$$

where

$$A_k^i = \frac{u_k w_k}{2} \tag{2.151}$$

is the area of the triangle S_k^i. $\boldsymbol{s_k}$ is the center of mass defined in equation (2.142). The coordinates of the vertices $\boldsymbol{u_k}$ and $\boldsymbol{v_k}$ are given in equations (2.136),(2.137), (2.138) and (2.139). The integral in equation (2.150) is calculated numerically using a Gaussian quadrature or the midpoint rule.

2.8 Dependence on curvature and resolution in the self-pressure

In this section we discuss how the self-pressure depend on curvature and number of triangles in the discretization. The discretized self pressure equation is according to equation (2.106)

$$A^{ii}B^{ii} = Y^{ii}. \tag{2.152}$$

Thus we have to consider the matrix elements $a^{ii}_{kk''}$ and $y^{ii}_{k'k''}$. The main influence to the right hand side will come when the two sources $\boldsymbol{x'}$ and $\boldsymbol{x''}$ are placed on two neighbouring triangles S_k^i and S_{k+1}^i. The configuration of the two triangles that makes the matrix element $y^{ii}_{k,k+1}$ become as large as possible, is illustrated in the two figures 2.3 and 2.4.

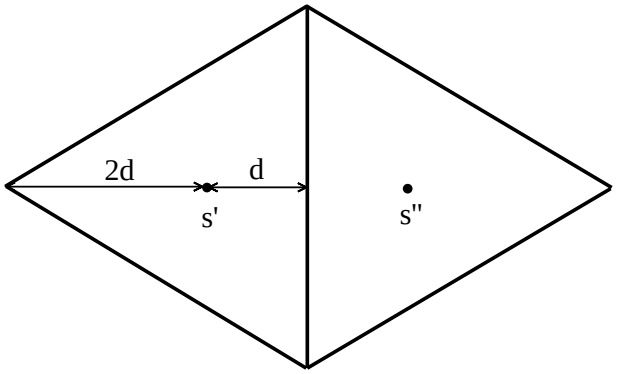

FIGURE 2.3: The two triangles S_k^i and S_{k+1}^i

In order to keep the analytical calculations simple, we do some simplifications. We assume that surface i is triangulated by equilateral triangles of equal area. The software we use for triangulating surfaces in this thesis is *Netgen*, which is an open source based mesh generator. Even though mesh generators, such as Netgen, output triangles of unequal size, we believe that this discussion will give us some insight about the self pressure.

Let d be the shortest distance from the center of mass to the edges of the triangles. We define $\boldsymbol{s}$ as the distance between the two centers of mass $\boldsymbol{s'} = \boldsymbol{s}_k$ and $\boldsymbol{s''} = \boldsymbol{s}_{k+1}$, i.e

$$\begin{aligned} \boldsymbol{s} &= \boldsymbol{s'} - \boldsymbol{s''}, \\ s &= \|\boldsymbol{s}\|. \end{aligned} \tag{2.153}$$

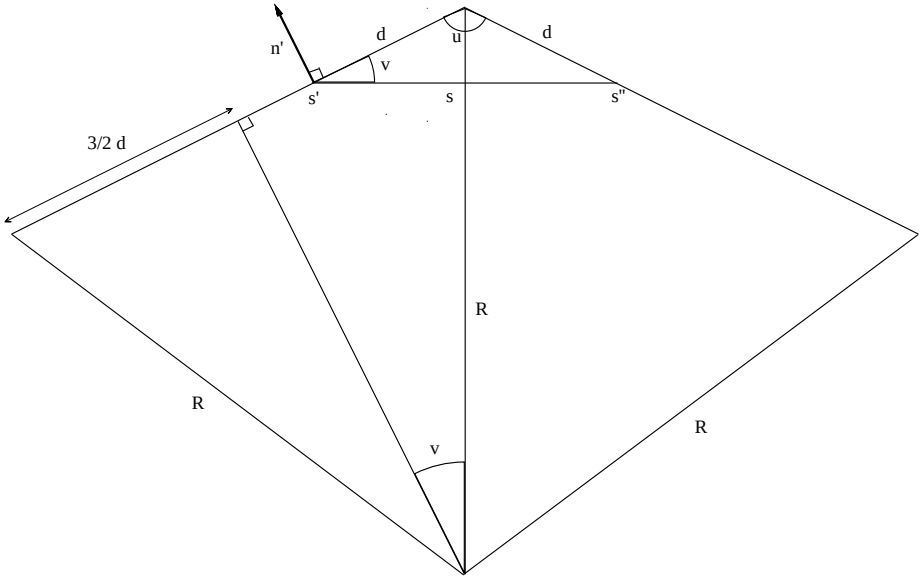

FIGURE 2.4: Looking at the two triangles S_k^i and S_{k+1}^i from the side. The angle between them is u. R is the radius of curvature.

The intersection between the surface and a plane containing the normal at a given point on the surface will be a curve. This curve is called a *normal section*. We refer to the curvature of a normal section as the *sectional curvature*. In general, a surface has different sectional curvatures in different sections. The maximal and minimal sectional curvature is called the *principal curvature*. It will be assumed that the largest of the principal curvatures, κ, is obtained at the edge where the triangles S_k^i and S_{k+1}^i intersect, and points in the same direction as $\boldsymbol{s}$. Let v be the angle between $\boldsymbol{s}$ and the plane that the triangle S_k^i lies in. Elementary trigonometry gives that

$$s = 2d \cos v. \tag{2.154}$$

The radius of curvature is related to the curvature κ by

$$\kappa = \frac{1}{R}. \tag{2.155}$$

R is a measure of the radius of the circular arc that best approximates the curve at that point.

Let's take a look at how the matrix elements, corresponding to these two triangles, depend on the curvature κ and the resolution of the discretization. Looking to figure 2.4, we see that the distance d decreases when the size of the triangles decreases. Thus the distance d is a measure of the resolution of the triangulation.

The matrix element $y^{ii}_{k,k+1}$ becomes

$$y^{ii}_{k,k+1} = -\boldsymbol{n}' \cdot \left(\boldsymbol{s}' - \boldsymbol{s}''\right) \frac{e^{-\omega\|\boldsymbol{s}'-\boldsymbol{s}''\|}}{4\pi\|\boldsymbol{s}'-\boldsymbol{s}''\|^3} \left(1+\omega\|\boldsymbol{s}'-\boldsymbol{s}''\|\right) = -\boldsymbol{n}' \cdot \boldsymbol{s} \frac{e^{-\omega s}}{4\pi s^3} \left(1+\omega s\right). \quad (2.156)$$

Using the definition of the dot product and assuming that $\boldsymbol{n}'$ points upwards, we find that

$$\boldsymbol{n}' \cdot \boldsymbol{s} = \|\boldsymbol{n}'\|\|\boldsymbol{s}\| \cos(\frac{\pi}{2} + v) = -s \sin v. \quad (2.157)$$

Thus

$$y^{ii}_{k,k+1} = \frac{\sin v}{4\pi s^2} e^{-\omega s} \left(1+\omega s\right) = \frac{\sin v}{16\pi d^2 \cos^2 v} e^{-\omega s} \left(1+\omega s\right). \quad (2.158)$$

Using basic trigonometry again, we find that

$$\sin v = \frac{3d}{2R} = \frac{3d\kappa}{2}, \quad (2.159)$$

$$\cos v = \sqrt{1-\sin^2 v} = \sqrt{1-\left(\frac{3d\kappa}{2}\right)^2}. \quad (2.160)$$

Thus

$$y^{ii}_{k,k+1} = \frac{3\kappa}{8\pi d\left(4-9d^2\kappa^2\right)} e^{-\omega d\sqrt{4-9d^2\kappa^2}} \left(1+\omega d\sqrt{4-9d^2\kappa^2}\right). \quad (2.161)$$

We see that $y^{ii}_{k,k+1} = 0$ if the curvature is zero. The main contribution to the pressure and self-pressure comes from quite small ω. For small d, the exponential is of order 1 and we have that

$$y^{ii}_{k,k+1} \approx \frac{3\kappa}{32\pi d}. \quad (2.162)$$

Thus $y^{ii}_{k,k+1}$ is proportional to κ and inversely proportional to d. We therefore expect that this quantity can be quite large, especially if the resolution of the triangulation is high, and the surface is very curved in the region where S^i_k and S^i_{k+1} are placed.

The expression for the particular matrix element $y^{ii}_{k,k+1}$ in equation (2.161) holds for a general surface. In order to keep the calculations simple, we for the rest of this section assume that surface i is a sphere of radius R. A sphere has the special property that the curvature is constant all over the surface; all sectional and principal curvatures equal the inverse of the radius of the sphere. Thus at any section on the sphere, the curvature is equal to the maximal principal curvature κ. Then there are several elements $y^{ii}_{k,k+1}$, $k = 1, 2, ...$, in the matrix Y^{ii} that are given by equation (2.161). These elements are the largest in the matrix and therefore these will drive the changes of the right hand side of the equation when the resolution or the curvature is changed. The other elements will play a minor role than these elements, and therefore we don't find it necessary to analyse their dependence on the curvature and the resolution of the discretization.

Since the surface is a sphere, we can find an explicit expression for the resolution dependence in d. Using basic trigonometry, we find that the area of the triangles is given by

$$A = A_k^i = A_{k+1}^i = 3\sqrt{3}d^2. \tag{2.163}$$

The number of triangles, N, on the sphere is given by

$$N = \frac{4\pi R^2}{A} = \frac{4\pi R^2}{3\sqrt{3}d^2}. \tag{2.164}$$

Solving for d we obtain

$$d = \sqrt{\frac{\pi}{3\sqrt{3}}}\frac{2R}{\sqrt{N}} = \sqrt{\frac{\pi}{3\sqrt{3}}}\frac{2}{\kappa\sqrt{N}}. \tag{2.165}$$

Thus we see that, in addition to being a measure of resolution, the distance d also depends on the curvature κ.

The matrix elements $a_{k,k+1}^{ii}$ are given by equation (2.134),

$$a_{k,k+1}^{ii} = -\frac{A_k^i}{4\pi}\frac{e^{-\omega\|\boldsymbol{s}'-\boldsymbol{s}''\|}}{\|\boldsymbol{s}'-\boldsymbol{s}''\|} = -\frac{A_k^i}{4\pi}\frac{e^{-\omega s}}{s}. \tag{2.166}$$

The fact that $s = 2d\cos v$, and equation (2.160), gives that

$$a_{k,k+1}^{ii} = -\frac{3\sqrt{3}d^2}{4\pi}\frac{e^{-2\omega d\sqrt{1-\left(\frac{3d\kappa}{2}\right)^2}}}{2d\sqrt{1-\left(\frac{3d\kappa}{2}\right)^2}} = -\frac{3\sqrt{3}d}{4\pi}\frac{e^{-\omega d\sqrt{4-9d^2\kappa^2}}}{\sqrt{4-9d^2\kappa^2}}. \tag{2.167}$$

When the resolution of the discretization is high, we have that

$$a_{k,k+1}^{ii} \approx -\frac{3\sqrt{3}d}{8\pi}. \tag{2.168}$$

We see that $a_{k,k+1}^{ii}$ is proportional to d. The distance d, and therefore also $a_{k,k+1}^{ii}$, depend on both curvature and resolution.

In order to find the resolution and curvature dependence in the self pressure, we consider the other elements in the matrix A^{ii} as well. The diagonal elements a_{kk}^{ii} are given by equation (2.150);

$$a_{kk}^{ii} \approx -\frac{A_k^i}{6\pi\omega}\int_0^1 dt\sum_{j=1}^{3}\frac{1-e^{-\omega\|\boldsymbol{\gamma}_{\boldsymbol{j_k}}(t)-\boldsymbol{s_k}\|}}{\|\boldsymbol{\gamma}_{\boldsymbol{j_k}}(t)-\boldsymbol{s_k}\|^2}. \tag{2.169}$$

The distance $\|\boldsymbol{\gamma}_{\boldsymbol{j_k}}(t) - \boldsymbol{s_k}\|$ is of the same size as d and therefore

$$a_{kk}^{ii} \approx -\frac{3\sqrt{3}d^2}{6\pi\omega} \int_0^1 dt \sum_{j=1}^{3} \frac{1 - e^{-\omega d}}{d^2} \approx -\frac{3\sqrt{3}d^2}{6\pi\omega} \sum_{j=1}^{3} \frac{\omega d}{d^2} \sim d. \tag{2.170}$$

The other matrix elements go as

$$a_{kk''}^{ii} = -\frac{A_k^i}{4\pi} \frac{e^{-\omega\|\boldsymbol{s}_k - \boldsymbol{s}_{k''}\|}}{\|\boldsymbol{s}_k - \boldsymbol{s}_{k''}\|} = -\frac{3\sqrt{3}d^2}{4\pi} \frac{e^{-\omega\|\boldsymbol{s}_k - \boldsymbol{s}_{k''}\|}}{\|\boldsymbol{s}_k - \boldsymbol{s}_{k''}\|} \sim d^2 \frac{e^{-\omega\|\boldsymbol{s}_k - \boldsymbol{s}_{k''}\|}}{\|\boldsymbol{s}_k - \boldsymbol{s}_{k''}\|}. \tag{2.171}$$

Thus there is a d^2-dependence. We also observe that when we move away from the tridiagonal, the exponential and the denominator come into play and the elements become progressively smaller.

According to the discussion above, the matrix A^{ii} have elements with a d-dependence close to the diagonal and elements that get smaller when moving away from the diagonal. The largest elements in the matrix Y^{ii} go as $\frac{\kappa}{d}$. Therefore the self-pressure equation $A^{ii}B^{ii} = Y^{ii}$ roughly can be written as

$$d^t A\, B = \frac{\kappa}{d} Y, \tag{2.172}$$

where $t \geq 1$ and A, Y are matrices with elements of order 1. We get

$$B = \frac{\kappa}{d^{1+t}} A^{-1} Y. \tag{2.173}$$

We therefore expect that the self pressure go as

$$b_{kk''}^{ii} \sim \frac{\kappa}{d^{1+t}} = \frac{1}{Rd^{1+t}} \sim \frac{N^{(1+t)/2}}{R^{2+t}}, \quad t \geq 1, \tag{2.174}$$

where equation (2.165) is used. The correct value of t is more difficult to determine. Since the biggest elements in A^{ii} is of order d^1, we are pretty sure that t is greater or equal to one. It is reasonable to think that the d-dependent elements close to the diagonal will dominate such that t is close to 1. However, we should keep in mind that the d^2- dependent elements depend more on the curvature and resolution than the d-dependent elements, and there are more of them.

In order to investigate whether the estimate (2.174) is correct, we do some numerical calculations. If it is, we can also determine the value of t more accurately. Consider a configuration consisting of two concentric spheres. The radius of the outer sphere is kept constant at a radius of 3 units, whereas the radius of the inner sphere is varied in the range from 1.4 to 2.8 units. The self pressure is calculated on the inner sphere. A disadvantage with the mesh generator Netgen is that one can't control exactly the number of triangles in the discretization. Typically, the roughest triangulation of a

surface consists of about a hundred triangles. When one increases the resolution once, the number of triangles is quadrupled, then quadrupled again and so it continues. Thus the 6 first triangulations of a surface generated by *Netgen* can consist of for example 100, 400, 1600, 6400, 25600 and 102400 triangles. The first, and maybe also the second, triangulation is usually so rough that it doesn't give any valuable information. Typically, the triangulations after the fifth contain so many triangles that the computer doesn't have enough memory do calculations. Thus there are only 3 or 4 different resolutions that we are able to do calculations for.

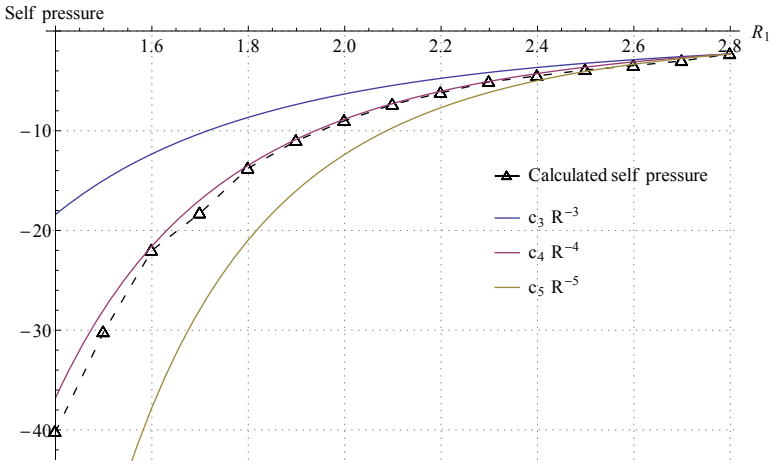

FIGURE 2.5: Self pressure on the inner sphere plotted against its radius. The number of triangles on the inner sphere is about 1900.

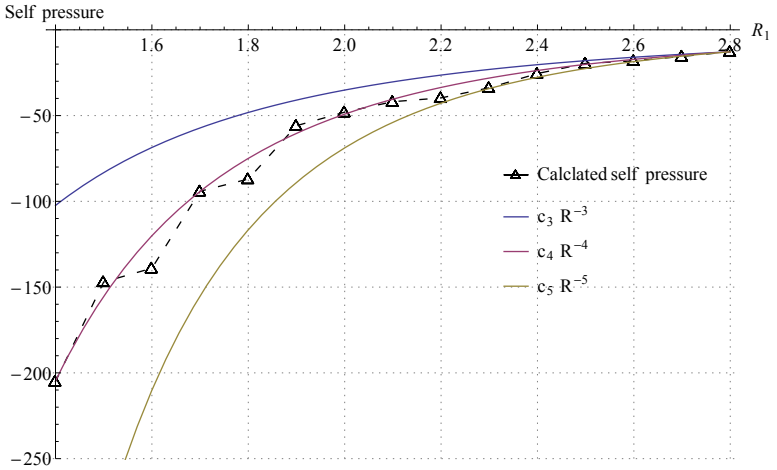

FIGURE 2.6: Self pressure on the inner sphere plotted against its radius. The number of triangles on the inner sphere is about 7500.

In figures 2.5, 2.6 and 2.7 the self pressure on the inner sphere is plotted as function of radius. There are, respectively, about 1900, 7500 and 30000 triangles on the inner sphere. The self pressure is plotted versus the three functions

$$p_n(R) = c_n R^{-n}, \quad n = 3, 4, 5, \tag{2.175}$$

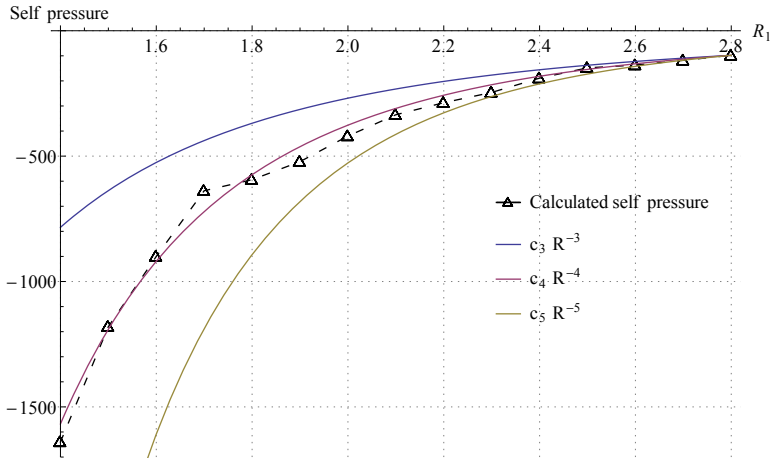

FIGURE 2.7: Self pressure on the inner sphere plotted against its radius. The number of triangles on the inner sphere is about 30000.

where c_n is chosen such that $p_n(2.8)$ equals the calculated self pressure for $R = 2.8$. These three plots, quite clearly, predicts that $b^{ii}_{kk''} \sim R^{-4}$ when the number of triangles is constant. This suggests that the value of t in equation (2.174) is approximately 2.

We investigate the dependence on the resolution in the self pressure by keeping the radius of the spheres constant and calculating the self pressure for 4 different resolutions. The self pressure will be calculated for two different radii, $R = 1.7$ and $R = 2.3$. The results are plotted in a kind of a log-log plot, shown in figure 2.8. We mentioned above that the number of triangles in the x-th refinement of the triangulation of a surface generated by *Netgen*, is given by

$$N = N_1 \cdot 4^x, \tag{2.176}$$

where N_1 is the number of triangles in the first triangulation of the surface. The label on the horizontal axis is x, which equals $\frac{\log(N/N_1)}{\log 4}$. We plot the logarithm of the calculated self pressure versus the function $\log(P_i(N))$, where

$$P_i(N) = c \cdot N^{(1+t)/2}. \tag{2.177}$$

The constant c is chosen such that $P_i(N_1)$ equals the calculated self pressure for N_1 triangles. Our investigation of the curvature dependence suggests the choice $t = 2$ in equation (2.174). Therefore we plot $\log(P_i(N))$ for $t = 2$. Figure 2.8 shows that the self pressure is close to having an $N^{3/2}$ dependence, which was estimated. Optimally, the green line should have been straight and covered the blue line entirely, and the black should have covered the red entirely. Thus it seems like the number α is close to 3/2, but slightly less. However, these numerical calculations of the curvature and resolution dependence, suggest that the value of t in equation (2.174) is close to 2.

We have now investigated the curvature and resolution dependence in the self pressure. Our analytical calculations suggest that the self pressure is determined by equation

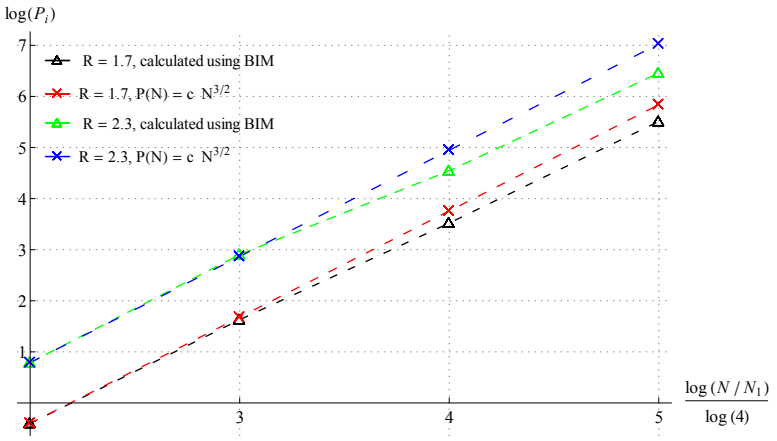

FIGURE 2.8: LogLog plot of self pressure on two different spheres with radius 1.7 and 2.3 units respectively.

(2.174), but can't determine the value of t more accurately $t \geq 1$. However, our numerical calculations verify that the analytical calculations are correct and that $t \approx 2$. Thus

$$b^{ii}_{kk''} \sim \frac{N^{3/2}}{R^4}. \tag{2.178}$$

The consistence between the numerical and analytical calculations is a little surprising, especially because of the simplifications we did. Among other things we assumed that the triangles were of equal size and equilateral, which they in reality not are. However, when looking at a triangulation of a sphere (see for example figure B.3), we see that many of the triangles in fact are close to being of equal size and equilateral.

A consequence of the $N^{3/2}R^{-4}$ dependency is that the self pressure can be very large for spheres with much curvature, i.e. small radius, especially if the resolution of the triangulation is high. The largest absolute value of the self pressure in the three figures 2.5, 2.6 and 2.7 is 1640, which corresponds to a radius of 1.4 units and a triangulation consisting of 29696 triangles. On the other hand, the lowest absolute value of the self pressure is 2.3, which corresponds to a radius of 2.8 units and a triangulation consisting of 1792 triangles. Thus we see that the self pressure can vary enormously, depending on the size of the curvature and the resolution. In principle, there is no limit for how large the self pressure can be.

2.8.1 Consequences of a large self-pressure

Consider a configuration of two objects, where object 2 is a sphere. The pressure on the sphere is determined by

$$\begin{bmatrix} A^{11} & A^{21} \\ A^{12} & A^{22} \end{bmatrix} \begin{bmatrix} X^{12} \\ X^{22} \end{bmatrix} = \begin{bmatrix} Y^{21} - A^{21}B^{22} \\ 0 \end{bmatrix}. \tag{2.179}$$

Thus the self pressure come into play on the right hand side of the equation. We know that the self pressure matrix B^{22} contains elements that go as $N^{3/2}R^{-4}$, which can be very large. The elements in the matrix A^{21} are approximations of double integrals over the free Green's function D_0 via the midpoint rule;

$$a^{21}_{kk''} = -\frac{A_k^2}{4\pi}\frac{e^{-\omega\|\boldsymbol{s}_k-\boldsymbol{s}_{k''}\|}}{\|\boldsymbol{s}_k-\boldsymbol{s}_{k''}\|} \sim d^2\frac{e^{-\omega\|\boldsymbol{s}_k-\boldsymbol{s}_{k''}\|}}{\|\boldsymbol{s}_k-\boldsymbol{s}_{k''}\|} \sim N^{-1}R^2\frac{e^{-\omega\|\boldsymbol{s}_k-\boldsymbol{s}_{k''}\|}}{\|\boldsymbol{s}_k-\boldsymbol{s}_{k''}\|}. \tag{2.180}$$

We should keep in mind that $\boldsymbol{s}_k$ and $\boldsymbol{s}_{k''}$ belong to different spheres so that the distance $\|\boldsymbol{s}_k-\boldsymbol{s}_{k''}\|$, in most cases, is much larger than the distance d. The function $\frac{e^{\omega s}}{s}$ decrease rapidly and therefore will the matrix A^{21} consist of elements that are very small. This means that the calculation of the matrix $A^{21}B^{22}$ involves multiplication of small numbers with large numbers. Since the elements of A^{ij} are approximations of some integrals, this can cause numerical challenges.

Let the matrix A represent the exact values of the double integrals that determine the left hand side of equation (2.179) and ϵE represent the error from the approximations. ϵ is a small constant. Similarly, we let A_0 be the exact value of the double integrals on the right hand side and ϵE_0 the error. Define $\sigma = N^{3/2}R^{-4}$ and let σB represent the self pressure contribution. Then equation (2.179) can be written as

$$(A+\epsilon E)X = Y - (A_0+\epsilon E_0)\sigma B. \tag{2.181}$$

The inverse of the lhs. is found by

$$\begin{aligned}(A+\epsilon E)^{-1} &= \big(A(I+\epsilon A^{-1}E)\big)^{-1} = (I+\epsilon A^{-1}E)^{-1}A^{-1}\\ &= (I-\epsilon A^{-1}E)A^{-1} = A^{-1}-\epsilon A^{-1}EA^{-1}.\end{aligned} \tag{2.182}$$

Thus the pressure is determined by

$$\begin{aligned}X &= \left(A^{-1}-\epsilon A^{-1}EA^{-1}\right)\left(Y-(A_0+\epsilon E_0)\sigma B\right)\\ &= A^{-1}Y-\sigma A^{-1}A_0B-\epsilon A^{-1}EA^{-1}Y+\epsilon\sigma(A^{-1}EA^{-1}A_0B-A^{-1}E_0B).\end{aligned} \tag{2.183}$$

Since $\epsilon\sigma > \epsilon$, the error in X is controlled by the size of $\epsilon\sigma$. Thus the errors of the approximations have to decrease faster than the self pressure increases when the resolution increases. In other words; we must have that $\epsilon\sigma \to 0$ when $N \to \infty$. If this isn't the case, it could be that the calculated pressure is just noise from the numerical errors. Then the matrix elements would have to be calculated using more accurate methods.

The resolution and curvature dependence in the error ϵ can be found: We know that the error when calculating a two dimensional integral over a square of area h^2 using the midpoint rule, is of order h^4 (see for example [17]), i.e. area to the power of two. The error when approximating an integral over a triangle will also be of order area to the

power of two. Thus

$$\epsilon \sim (A_k^i)^2 = A^2 \sim d^4 \sim R^4 N^{-2} \tag{2.184}$$

and therefore

$$\epsilon\sigma \sim R^4 N^{-2} N^{3/2} R^{-4} = \frac{1}{\sqrt{N}}. \tag{2.185}$$

This means that, no matter which curvature the surface has, we can make the error in X as small as we want by just increasing the resolution. Thus our analysis indicates that it will be sufficient to calculate the matrix elements using the midpoint rule. It will therefore be expected that the calculated pressure will converge towards the pressure found using other methods when the resolution is increased.

It is difficult to find a general, explicit expression for the curvature and resolution dependence in the self pressure for surfaces with varying curvature, and it is therefore tempting to ask whether the BIM is limited to geometries with constant curvature? However, we should keep in mind that a sphere can be made as curved as we want just by decreasing its radius. We therefore expect that we actually have covered the "worst case scenario" in our discussion. As long as the surfaces are smooth, the local curvature and resolution dependence in the self pressure won't get any worse (it won't increase faster) than for a sphere. It will therefore be sufficient to calculate the matrix elements using the midpoint rule for general surfaces as well. Thus, if the calculated pressure converges towards the pressure found using other methods for spheres, then it is also expected to converge for general surfaces. In order to test whether the BIM outputs a correct pressure, we are going to do numerical calculations for different test configurations. We will start by considering the flat configuration consisting of two parallel plates. The next step will be to consider concentric and adjacent spheres. To check whether it is the property of constant curvature that give rise to a (eventual) correct pressure, we will also consider configurations of varying curvature; adjacent and concentric ellipsoids. After having considered these configurations, we should be able to conclude on the validity of the BIM.

2.9 Symmetry reduction

We have shown that the Casimir pressure is found by solving the regularized boundary integral equation

$$\iint\limits_{Q} dA_{\boldsymbol{x}} D_0(\boldsymbol{x}, \boldsymbol{x}'')\mathcal{P}(\boldsymbol{x}, \boldsymbol{x}') = -\partial_{\boldsymbol{n}'} D_0(\boldsymbol{x}', \boldsymbol{x}'') - \iint\limits_{Q_i} dA_{\boldsymbol{x}} D_0(\boldsymbol{x}, \boldsymbol{x}'')\mathcal{P}_i(\boldsymbol{x}, \boldsymbol{x}'), \tag{2.186}$$

where $\boldsymbol{x}' \in Q_i$, $i = 1, .., r$ and $\mathcal{P}_i(\boldsymbol{x}, \boldsymbol{x}')$ is the unique solution to the self pressure equation

$$-\partial_{\boldsymbol{n}'} D_0(\boldsymbol{x}', \boldsymbol{x}'') = PV_{\boldsymbol{x}''} \iint_{Q_i} dA_{\boldsymbol{x}} D_0(\boldsymbol{x}, \boldsymbol{x}'') \mathcal{P}_i(\boldsymbol{x}, \boldsymbol{x}') \quad \boldsymbol{x}', \boldsymbol{x}'' \in Q_i. \tag{2.187}$$

These equations are solved numerically. In this section we show that it is possible to reduce the computational load if there is any symmetry in the configuration Q.

The set of isometries of $\mathbb{R}^3$ form a group under composition, which usually is called the Euclidian group E_3. We are interested in the subgroup, $H \subset E_3$, that preserves the surfaces Q. Let h be an element in H. Since h is an isometry, it is also a bijection. Thus h will map the surface Q_i onto Q_j for some j.

Define a function $F_j : Q_j \times Q_j \to \mathbb{R}$ by

$$F_j(\boldsymbol{x}, \boldsymbol{x}') = \mathcal{P}_i(h^{-1}\boldsymbol{x}, h^{-1}\boldsymbol{x}'), \tag{2.188}$$

and the functional I by

$$I[F_j] = PV_{\boldsymbol{x}''} \iint_{Q_j} dA_{\boldsymbol{x}} D_0(\boldsymbol{x}, \boldsymbol{x}'') F_j(\boldsymbol{x}, \boldsymbol{x}'). \tag{2.189}$$

Use the definition (2.188) and introduce a change of variables $\boldsymbol{y} = h^{-1}\boldsymbol{x}$ to get

$$\begin{aligned} I[F_j] &= PV_{\boldsymbol{x}''} \iint_{Q_j} dA_{\boldsymbol{x}} D_0(\boldsymbol{x}, \boldsymbol{x}'') \mathcal{P}_i(h^{-1}\boldsymbol{x}, h^{-1}\boldsymbol{x}') \\ &= PV_{\boldsymbol{x}''} \iint_{Q_i} dA_{\boldsymbol{y}} D_0(h\boldsymbol{y}, \boldsymbol{x}'') \mathcal{P}_i(\boldsymbol{y}, h^{-1}\boldsymbol{x}'). \end{aligned} \tag{2.190}$$

The isometry h preserves the norm, thus $D_0(h\boldsymbol{x}, h\boldsymbol{x}'') = D_0(\boldsymbol{x}, \boldsymbol{x}'')$, and

$$I[F_j] = PV_{h^{-1}\boldsymbol{x}''} \iint_{Q_i} dA_{\boldsymbol{y}} D_0(\boldsymbol{y}, h^{-1}\boldsymbol{x}'') \mathcal{P}_i(\boldsymbol{y}, h^{-1}\boldsymbol{x}'). \tag{2.191}$$

Equation (2.187) gives

$$I[F_j] = -\partial_{\boldsymbol{n}(h^{-1}\boldsymbol{x}')} D_0(h^{-1}\boldsymbol{x}', h^{-1}\boldsymbol{x}'') = -\nabla_{h^{-1}\boldsymbol{x}'} D_0(h^{-1}\boldsymbol{x}', h^{-1}\boldsymbol{x}'') \boldsymbol{n}(h^{-1}\boldsymbol{x}'). \tag{2.192}$$

Use the chain rule to obtain

$$I[F_j] = -\nabla_{\boldsymbol{x}'} D_0(h^{-1}\boldsymbol{x}', h^{-1}\boldsymbol{x}'') (Dh^{-1}(\boldsymbol{x}'))^{-1} \boldsymbol{n}(h^{-1}\boldsymbol{x}'), \tag{2.193}$$

where $Dh^{-1}(\boldsymbol{x}') = \left(\frac{\partial h^{-1}\boldsymbol{x}'}{\partial \boldsymbol{x}'} \right)$ is the Jacobian matrix of size 3×3.

Let $\boldsymbol{p} \in Q$ and $T_{\boldsymbol{p}}\mathbb{R}^3$ be the tangent space at $\boldsymbol{p}$. An element $\boldsymbol{\eta}$ in $T_{\boldsymbol{p}}\mathbb{R}^3$ is mapped

to the element $\boldsymbol{\xi}$ in the tangent space at $h\boldsymbol{p}$ by the pushforward (total derivative), i.e. $\boldsymbol{\xi} = Dh(\boldsymbol{x})\boldsymbol{\eta}$. In particular, this means that the normal is mapped from $\boldsymbol{x}'$ to $h^{-1}(\boldsymbol{x}')$ as $\boldsymbol{n}(h^{-1}\boldsymbol{x}') = Dh^{-1}(\boldsymbol{x}')\boldsymbol{n}(\boldsymbol{x}')$. Thus

$$\begin{aligned} I[F_j] &= -\nabla_{\boldsymbol{x}'} D_0(h^{-1}\boldsymbol{x}', h^{-1}\boldsymbol{x}'')(Dh^{-1}(\boldsymbol{x}'))^{-1} Dh^{-1}(\boldsymbol{x}')\boldsymbol{n}(\boldsymbol{x}') \\ &= -\nabla_{\boldsymbol{x}'} D_0(h^{-1}\boldsymbol{x}', h^{-1}\boldsymbol{x}'')\, \boldsymbol{n}(\boldsymbol{x}'). \end{aligned} \tag{2.194}$$

The norm preserving property is used once again;

$$I[F_j] = -\nabla_{\boldsymbol{x}'} D_0(\boldsymbol{x}', \boldsymbol{x}'')\boldsymbol{n}(\boldsymbol{x}') = -\partial_{\boldsymbol{n}'} D_0(\boldsymbol{x}', \boldsymbol{x}''). \tag{2.195}$$

Thus we have shown that

$$-\partial_{\boldsymbol{n}'} D_0(\boldsymbol{x}', \boldsymbol{x}'') = PV_{\boldsymbol{x}''} \iint\limits_{Q_j} dA_{\boldsymbol{x}} D_0(\boldsymbol{x}, \boldsymbol{x}'') F_j(\boldsymbol{x}, \boldsymbol{x}'). \tag{2.196}$$

This means that $F_j(\boldsymbol{x}, \boldsymbol{x}') = \mathcal{P}_i(h^{-1}\boldsymbol{x}, h^{-1}\boldsymbol{x}')$ is a solution to equation (2.187) for $i = j$. However, we already know that $\mathcal{P}_j(\boldsymbol{x}, \boldsymbol{x}')$ is a solution for $i = j$. Uniqueness gives that

$$\mathcal{P}_j(\boldsymbol{x}, \boldsymbol{x}') = \mathcal{P}_i(h^{-1}\boldsymbol{x}, h^{-1}\boldsymbol{x}'). \tag{2.197}$$

Let $\mathcal{P}(\boldsymbol{x}, \boldsymbol{x}')$ be the unique solution to equation (2.186) and define the function $F : Q \times Q \to \mathbb{R}$ by

$$F(\boldsymbol{x}, \boldsymbol{x}') = \mathcal{P}(h^{-1}\boldsymbol{x}, h^{-1}\boldsymbol{x}'). \tag{2.198}$$

We do similar calculations as above;

$$\begin{aligned}
&\iint\limits_{Q} dA_{\boldsymbol{x}} D_0(\boldsymbol{x},\boldsymbol{x}'')F(\boldsymbol{x},h\boldsymbol{x}') = \iint\limits_{Q} dA_{\boldsymbol{x}} D_0(\boldsymbol{x},\boldsymbol{x}'')\mathcal{P}(h^{-1}\boldsymbol{x},\boldsymbol{x}') \\
&\quad = \iint\limits_{Q} dA_{\boldsymbol{y}} D_0(h\boldsymbol{y},\boldsymbol{x}'')\mathcal{P}(\boldsymbol{y},\boldsymbol{x}') = \iint\limits_{Q} dA_{\boldsymbol{y}} D_0(\boldsymbol{y},h^{-1}\boldsymbol{x}'')\mathcal{P}(\boldsymbol{y},\boldsymbol{x}') \\
&\quad = -\partial_{\boldsymbol{n}(\boldsymbol{x}')} D_0(\boldsymbol{x}',h^{-1}\boldsymbol{x}'') - \iint\limits_{Q_i} dA_{\boldsymbol{x}} D_0(\boldsymbol{x},h^{-1}\boldsymbol{x}'')\mathcal{P}_i(\boldsymbol{x},\boldsymbol{x}') \\
&\quad = -\nabla_{\boldsymbol{x}'} D_0(\boldsymbol{x}',h^{-1}\boldsymbol{x}'')\boldsymbol{n}(\boldsymbol{x}') - \iint\limits_{Q_j} dA_{\boldsymbol{y}} D_0(h^{-1}\boldsymbol{y},h^{-1}\boldsymbol{x}'')\mathcal{P}_i(h^{-1}\boldsymbol{y},\boldsymbol{x}') \\
&\quad = -\nabla_{h^{-1}(h\boldsymbol{x}')} D_0(h^{-1}(h\boldsymbol{x}'),h^{-1}\boldsymbol{x}'')\boldsymbol{n}(h^{-1}(h\boldsymbol{x}')) - \iint\limits_{Q_j} dA_{\boldsymbol{y}} D_0(\boldsymbol{y},\boldsymbol{x}'')\mathcal{P}_j(\boldsymbol{y},h\boldsymbol{x}') \\
&\quad = -\nabla_{h^{-1}(h\boldsymbol{x}')} D_0(h^{-1}(h\boldsymbol{x}'),h^{-1}\boldsymbol{x}'')Dh^{-1}(h\boldsymbol{x}')\boldsymbol{n}(h\boldsymbol{x}') - \iint\limits_{Q_j} dA_{\boldsymbol{y}} D_0(\boldsymbol{y},\boldsymbol{x}'')\mathcal{P}_j(\boldsymbol{y},h\boldsymbol{x}') \\
&\quad = -\nabla_{h\boldsymbol{x}'} D_0(h^{-1}(h\boldsymbol{x}'),h^{-1}\boldsymbol{x}'')(Dh^{-1}(h\boldsymbol{x}'))^{-1}Dh^{-1}(h\boldsymbol{x}')\boldsymbol{n}(h\boldsymbol{x}') \\
&\qquad - \iint\limits_{Q_j} dA_{\boldsymbol{y}} D_0(\boldsymbol{y},\boldsymbol{x}'')\mathcal{P}_j(\boldsymbol{y},h\boldsymbol{x}') \\
&\quad = -\nabla_{h\boldsymbol{x}'} D_0(h\boldsymbol{x}',\boldsymbol{x}'')\boldsymbol{n}(h\boldsymbol{x}') - \iint\limits_{Q_j} dA_{\boldsymbol{y}} D_0(\boldsymbol{y},\boldsymbol{x}'')\mathcal{P}_j(\boldsymbol{y},h\boldsymbol{x}') \qquad (2.199)
\end{aligned}$$

Thus $F(\boldsymbol{x},h\boldsymbol{x}')$ is a solution to

$$\iint\limits_{Q} dA_{\boldsymbol{x}} D_0(\boldsymbol{x},\boldsymbol{x}'')F(\boldsymbol{x},h\boldsymbol{x}') = -\partial_{\boldsymbol{n}(h\boldsymbol{x}')} D_0(h\boldsymbol{x}',\boldsymbol{x}'') - \iint\limits_{Q_j} dA_{\boldsymbol{y}} D_0(\boldsymbol{y},\boldsymbol{x}'')\mathcal{P}_j(\boldsymbol{y},h\boldsymbol{x}'), \qquad (2.200)$$

where $h\boldsymbol{x}' \in Q_j$. Uniqueness gives that $F(\boldsymbol{x},h\boldsymbol{x}') = \mathcal{P}(\boldsymbol{x},h\boldsymbol{x}')$, and by definition of F we conclude that

$$\mathcal{P}(h^{-1}\boldsymbol{x},\boldsymbol{x}') = \mathcal{P}(\boldsymbol{x},h\boldsymbol{x}') \qquad (2.201)$$

Remember from the derivation of the boundary integral equation (2.186) that $\boldsymbol{x}'$ is the position of one of the sources. Originally we have to solve equation (2.186) for all $\boldsymbol{x}' \in Q$. But equations (2.197) and (2.201) say that if there exists an isometry h that connects two source locations, $\boldsymbol{x}'$ and $h\boldsymbol{x}'$, then equation (2.186) only have to be solved for one of the them. The contribution to the Casimir pressure for the other source location is thereafter found using the identity (2.201).

Every isometry of $\mathbb{R}^3$ can be written as a composition of a translation and an orthogonal map. This means that an isometry can be a translation, a rotation about a line, a reflection about a plane or a composition these. We know that if the configuration Q is symmetric, then there is also an isometry lurking in the background. More mathematically; if there exist some kind of symmetry in the configuration, then there also exist a subset S of Q such that $Q = H(S)$. That is, Q is generated by the action

of the subgroup H on S. The identity (2.201) then says that it is enough to calculate the pressure on S in order to find the pressure on Q. Thus the computational load for finding the Casimir pressure can be reduced a lot if the subset S is much smaller than Q. Some of the configurations we are considering in this thesis are examples of configurations where S is very small. For the case of two parallel plates S consists of only a single point. When the configuration consists of two concentric spheres, Q is generated from two points, one on each sphere.

It is possible to reduce the computational load even more for symmetric configurations; also the integration domain in the regularized boundary integral equation (2.186) can be reduced. Pick a source location $\boldsymbol{x}'$ in S. Let G be the subgroup of H that fixes the point $\boldsymbol{x}'$, i.e for $g \in G$ we have that $g\boldsymbol{x}' = \boldsymbol{x}'$. Assume T is a subset of Q that generates Q under the action of G, i.e $Q = G(T)$. Similar calculations like the ones we did above show that the integration domain can be reduced to T. Thus the computational load can be reduced even more. When the configuration consist of parallel plates or concentric spheres the integration domain can be cut into half.

Chapter 3

Functional integral method

3.1 Relation between the Casimir energy and a functional integral

Consider the massless scalar field $\varphi(\boldsymbol{x}, t)$ that satisfies the classical wave equation (2.27). Assume that the field satisfies the boundary conditions

$$\begin{aligned} \varphi(\boldsymbol{x}, t) &= \varphi(\boldsymbol{x}) \\ \varphi(\boldsymbol{x}, t') &= \varphi'(\boldsymbol{x}), \end{aligned} \tag{3.1}$$

where $t' > t$. The dynamics of the field is described by the *action* S,

$$S[\varphi] = \int_t^{t'} d\tau \int_{\mathbb{R}^3} d^3\boldsymbol{x}\, \mathcal{L}(\varphi(\boldsymbol{x}, \tau)), \tag{3.2}$$

where $\mathcal{L}$ is the Lagrangian density given in equation (2.28).

Within the formalism of canonical quantization, the field φ is converted into the operator $\hat{\varphi}$, which satisfies the usual commutation relations (see eq. (2.2)). In the Heisenberg picture the field operator $\hat{\varphi}(\boldsymbol{x}, t)$ is related to the energy operator $\hat{H}$ via the equation of motion

$$-i\hbar \frac{d}{dt}\hat{\varphi}(\boldsymbol{x}, t) = [\hat{H}, \hat{\varphi}(\boldsymbol{x}, t)], \tag{3.3}$$

and to the classical field φ via the eigenstate-equation

$$\hat{\varphi}(\boldsymbol{x}, t)|\varphi(\boldsymbol{x}),\, t\rangle = \varphi(\boldsymbol{x}, t)|\varphi(\boldsymbol{x}),\, t\rangle. \tag{3.4}$$

The time dependence of the eigenstates is given by

$$|\varphi(\boldsymbol{x}), t\rangle = e^{\frac{it}{\hbar}\hat{H}}|\varphi(\boldsymbol{x})\rangle. \tag{3.5}$$

The amplitude of making a transition between two states can be written as

$$\langle \varphi',\, t' | \varphi,\, t \rangle = \langle \varphi' | e^{-\frac{i}{\hbar}(t'-t)\hat{H}} | \varphi \rangle. \tag{3.6}$$

This is the probability amplitude of making a transition from the field configuration $\varphi(\boldsymbol{x})$ at the time t and ending up in $\varphi'(\boldsymbol{x})$ at t'.

The transition amplitude can be found by summing over all possible connecting paths between the two configurations. This "sum" is a path- or a functional integral. Thus

$$\langle \varphi' | e^{-\frac{i}{\hbar}(t'-t)\hat{H}} | \varphi \rangle = \int D\varphi \, e^{\frac{i}{\hbar}S[\varphi]} \equiv Z. \tag{3.7}$$

The integration runs over fields satisfying the boundary conditions $\varphi(\boldsymbol{x}, t) = \varphi(\boldsymbol{x})$ and $\varphi(\boldsymbol{x}, t') = \varphi'(\boldsymbol{x})$. Due to the close relation to the partition function in statistical physics, the letter Z is used for the functional integral.

The interesting configurations for us are

$$\varphi(\boldsymbol{x}) = \varphi'(\boldsymbol{x}) = 0. \tag{3.8}$$

Thus the integration will be performed over fields that start in the vacuum configuration at time t and end up in the same configuration at time t'. The constraints in equation (3.8) also imply that the fields in the integration domain are $T = t' - t$ periodic. However, in order to relate the transition amplitude to the Casimir energy, we will let $T \to \infty$ in the end. In addition, it will be assumed that the fields satisfy some boundary conditions $\mathcal{C}$ on a space time surface $\mathcal{S}$. Denote the transition amplitude satisfying these conditions by

$$Z[\mathcal{S}_{\mathcal{C}}, T] = \int D\varphi_{\mathcal{C},T} e^{\frac{i}{\hbar}S[\varphi]}, \tag{3.9}$$

where $D\varphi_{\mathcal{C},T}$ indicates that the integration is over T-periodic fields satisfying the boundary conditions $\mathcal{C}$. The boundary conditions we are interested in are

$$\mathcal{C}: \quad \varphi|_{\mathcal{S}} = 0. \tag{3.10}$$

In order to relate Z to the Casimir energy, introduce a complete set of energy eigenstates, $\{|\phi_n\rangle\}$. Thus $\hat{H}|\phi_n\rangle = E_n|\phi_n\rangle$. General field configurations can be expanded in the energy basis $\{|\phi_n\rangle\}$. Thus the ground (vacuum) state can be written as

$$|0\rangle = \sum_{\alpha} \langle 0 | \phi_\alpha \rangle | \phi_\alpha \rangle. \tag{3.11}$$

$\langle 0|...\rangle$ is a functional itself on the space of classical configurations. The vacuum to vacuum transition amplitude $Z[\mathcal{S}_\mathcal{C}, T]$ becomes

$$\begin{aligned} Z[\mathcal{S}_\mathcal{C}, T] &= \langle 0|e^{-\frac{i}{\hbar}(t'-t)\hat{H}}|0\rangle \\ &= \sum_\alpha \langle 0|\phi_\alpha\rangle\big\langle \phi_\alpha\big|e^{-\frac{iT}{\hbar}\hat{H}}\big|\sum_\beta \langle 0|\phi_\beta\rangle|\phi_\beta\big\rangle \\ &= \sum_{\alpha,\beta} \langle 0|\phi_\alpha\rangle\langle 0|\phi_\beta\rangle^*\big\langle \phi_\alpha\big|e^{-\frac{iT}{\hbar}\hat{H}}\big|\phi_\beta\big\rangle \\ &= \sum_{\alpha,\beta} \langle 0|\phi_\alpha\rangle\langle 0|\phi_\beta\rangle^*\langle \phi_\alpha|\phi_\beta\rangle e^{-\frac{iT}{\hbar}E_\beta} \\ &= \sum_\alpha |\langle 0|\phi_\alpha\rangle|^2 e^{-\frac{iT}{\hbar}E_\alpha}. \end{aligned} \tag{3.12}$$

In order to obtain a convergent series, we do an analytical continuation of the partition function $Z[\mathcal{S}_\mathcal{C}, T]$ into the complex plane, $T = -is$

$$Z[\mathcal{S}_\mathcal{C}, -is] = \sum_\alpha |\langle 0|\phi_\alpha\rangle|^2 e^{-\frac{s}{\hbar}E_\alpha}. \tag{3.13}$$

It will be assumed that the spectrum of the Hamiltonian is bounded from below and that the lowest energy state is E_0. When s is large,

$$Z[\mathcal{S}_\mathcal{C}, -is] \approx |\langle 0|\phi_0\rangle|^2 e^{-\frac{s}{\hbar}E_0}. \tag{3.14}$$

Take the logarithm;

$$\ln Z[\mathcal{S}_\mathcal{C}, T] \approx 2\ln|\langle 0|\phi_0\rangle| - \frac{s}{\hbar}E_0. \tag{3.15}$$

Solve for E_0 and let $s \to \infty$,

$$E_0 = \lim_{s\to\infty}\left(\frac{2\hbar}{s}\ln|\langle 0|\phi_0\rangle| + \frac{\hbar}{s}\ln Z[\mathcal{S}_\mathcal{C}, -is]\right) = -\lim_{s\to\infty}\frac{\hbar}{s}\ln Z[\mathcal{S}_\mathcal{C}, -is]. \tag{3.16}$$

E_0 is called the ground state energy and is the lowest possible energy level for the quantum system. In general, this quantity is infinite.

We now assume that perfect conductors are located at the surface $\mathcal{S}$. Then the field φ satisfies the boundary conditions $\mathcal{C}$, given in equation (3.10) and the *Casimir energy* for the system is obtained by subtracting the ground state energy when the objects have been removed to infinite separation from E_0,

$$\mathcal{E} = E_0 - E_\infty = -\lim_{s\to\infty}\frac{\hbar}{s}\ln\frac{Z[\mathcal{S}_\mathcal{C}, -is]}{Z_\infty[-is]}. \tag{3.17}$$

This quantity will turn out to be finite. In the following sections we will derive expressions for $\ln Z[\mathcal{S}_\mathcal{C}, T]$ and $\ln Z_\infty[T]$, evaluate them at $T = -is$ and in the end let $s \to \infty$.

3.2 Implementation of spatial boundary conditions via delta functionals

In this section we illustrate how we are going implement the boundary condition $\mathcal{C}$: $\varphi|_\mathcal{S} = 0$ in the functional integrals. We want to keep things simple and therefore just illustrates the implementation on a simplified situation. Assume that the space-time surface $\mathcal{S}$ can be parametrized by

$$\eta : \, B \to \mathcal{S}, \tag{3.18}$$

where $B = [a_1, b_1] \times [a_2, b_2] \times [a_3, b_3]$ is a box. Using the notation from the previous section, we want to define how to perform the functional integral

$$I[\mathcal{S}_\mathcal{C}] = \int D\varphi_\mathcal{C} F[\varphi], \tag{3.19}$$

where $F[\varphi]$ is some functional. Discretize $\mathcal{S}$ by splitting the box B into small boxes $B_{\boldsymbol{k}}$. Let $\{\boldsymbol{\alpha_j}\}$, given by

$$\boldsymbol{\alpha_j} = (a_1 + j_1\Delta u_1, a_2 + j_2\Delta u_2, a_3 + j_3\Delta u_3), \quad \boldsymbol{j} = (j_1, j_2, j_3), \quad j_i = 0, 1, ..., N_i, \tag{3.20}$$

be the set of vertices for the boxes. Let all of the boxes $B_{\boldsymbol{k}}$ be of equal size. Δu_i specifies the length of the edges of the boxes, and is given by $\Delta u_i = \frac{b_i - a_i}{N_i}$, $i = 1, 2, 3$. Define $B_{\boldsymbol{j}}$ as the box where $\boldsymbol{\alpha_j}$ is the vertex closest to the point $\boldsymbol{a} = (a_1, a_2, a_3)$ and the midpoint $\boldsymbol{s_j}$ is given by

$$\boldsymbol{s_j} = (a_1, a_2, a_3) + \left((j_1 - \tfrac{1}{2})\Delta u_1, (j_2 - \tfrac{1}{2})\Delta u_2, (j_3 - \tfrac{1}{2})\Delta u_3\right). \tag{3.21}$$

Let $\varphi_{\boldsymbol{j}} = \varphi(\eta(\boldsymbol{s_j}))$. Introduce the abbreviation

$$\prod_{\boldsymbol{j}} \equiv \prod_{j_1=1}^{N_1} \prod_{j_2=1}^{N_2} \prod_{j_3=1}^{N_3}. \tag{3.22}$$

Inserting a finite product of Dirac-delta functions into the functional integral in equation (3.19) gives

$$\int D\varphi \prod_{\boldsymbol{j}} \delta(\varphi_{\boldsymbol{j}}) F[\varphi]. \tag{3.23}$$

Because of the properties of the delta, the only contribution to the integral is when $\varphi_{\boldsymbol{j}} = 0$. But when $N_i \to \infty$, $i = 1, 2, 3$, the parametrization will be dense on $\mathcal{S}$ and the integral will be restricted to fields such that $\varphi|_{\mathcal{S}} = 0$. Defining the *delta functional* $\delta(\varphi|_{\mathcal{S}})$ by

$$\int D\varphi\, \delta(\varphi|_{\mathcal{S}}) F[\varphi] = \lim_{\substack{N_i \to \infty \\ i=1,2,3}} \int D\varphi \prod_{\boldsymbol{j}} \delta(\varphi_{\boldsymbol{j}}) F[\varphi], \tag{3.24}$$

we can implement the boundary conditions $\mathcal{C}$: $\varphi|_{\mathcal{S}} = 0$ as

$$I[\mathcal{S}_{\mathcal{C}}] = \int D\varphi\, \delta(\varphi|_{\mathcal{S}}) F[\varphi]. \tag{3.25}$$

The Dirac-delta can be represented as an integral,

$$\delta(x) = \frac{1}{2\pi} \int_{\mathbb{R}} d\lambda\, e^{i\lambda x}. \tag{3.26}$$

Therefore

$$\prod_{\boldsymbol{j}} \delta(\varphi_{\boldsymbol{j}}) = \int_{\mathbb{R}^N} \left(\prod_{\boldsymbol{j}} \frac{d\lambda_{\boldsymbol{j}}}{2\pi} \right) e^{i \sum_{\boldsymbol{j}} \lambda_{\boldsymbol{j}} \varphi_{\boldsymbol{j}}}, \tag{3.27}$$

where $\boldsymbol{j} = (j_1, j_2, j_3)$ and $N = N_1 N_2 N_3$. Let $\eta_{\boldsymbol{j}} \equiv \eta(\boldsymbol{s}_{\boldsymbol{j}})$. Define two functions on $\mathcal{S}$ by

$$\Delta u(\eta_{\boldsymbol{j}}) = \left| \frac{\partial \eta_{\boldsymbol{j}}}{\partial u_1} \wedge \frac{\partial \eta_{\boldsymbol{j}}}{\partial u_2} \wedge \frac{\partial \eta_{\boldsymbol{j}}}{\partial u_3} \right| \Delta u_1 \Delta u_2 \Delta u_3 \tag{3.28}$$

and

$$\varrho(\eta_{\boldsymbol{j}}) = \varrho(\eta(\boldsymbol{s}_{\boldsymbol{j}})) = \frac{\lambda_{\boldsymbol{j}}}{\Delta u(\eta_{\boldsymbol{j}})}. \tag{3.29}$$

Inserting equations (3.28) and (3.29) into equation (3.27) gives

$$\prod_{\boldsymbol{j}} \delta(\varphi_{\boldsymbol{j}}) = \int_{\mathbb{R}^N} \prod_{\boldsymbol{j}} \tfrac{\Delta u(\eta_{\boldsymbol{j}})}{2\pi} d\varrho(\eta_{\boldsymbol{j}}) e^{i \sum_{\boldsymbol{j}} \varrho(\eta_{\boldsymbol{j}}) \varphi(\eta_{\boldsymbol{j}}) \Delta u(\eta_{\boldsymbol{j}})}. \tag{3.30}$$

Formally

$$\prod_{\boldsymbol{j}} \tfrac{\Delta u(\eta_{\boldsymbol{j}})}{2\pi} d\varrho(\eta_{\boldsymbol{j}}) \to D\varrho \qquad \text{as } N_i \to \infty \text{ for } i = 1, 2, 3, \tag{3.31}$$

and

$$\sum_{\boldsymbol{j}} \varrho(\eta_{\boldsymbol{j}}) \varphi(\eta_{\boldsymbol{j}}) \Delta u(\eta_{\boldsymbol{j}}) \to \int_{\mathcal{S}} du\, \varrho\varphi, \tag{3.32}$$

where du is the volume element given by $du = \left| \frac{\partial \eta}{\partial u_1} \wedge \frac{\partial \eta}{\partial u_2} \wedge \frac{\partial \eta}{\partial u_3} \right| du_1\, du_2\, du_3$. Thus the delta functional can be expressed as

$$\delta(\varphi|_{\mathcal{S}}) = \int D\varrho\, e^{i \int_{\mathcal{S}} du\, \varrho\varphi}, \tag{3.33}$$

and the functional integral $I[\mathcal{S}_\mathcal{C}]$ becomes

$$I[\mathcal{S}_\mathcal{C}] = \int D\varphi D\varrho \, e^{i\int_\mathcal{S} du\, \varrho\varphi} F[\varphi]. \tag{3.34}$$

The field ϱ becomes a source "living" on the surface $\mathcal{S}$.

We now use the delta functional to implement boundary conditions to the transition amplitude given in equation (3.9). The space time surface $\mathcal{S}$ now consists of r disjoint objects, $\mathcal{S} = \bigcup_\alpha \mathcal{S}_\alpha$. Let ϱ^α be the source living on the object $\mathcal{S}_\alpha$. The delta functional is modified a little and can be expressed as

$$\delta(\varphi|_\mathcal{S}) = \int \prod_\alpha D\varrho^\alpha e^{\frac{i}{\hbar}\sum_\alpha \int_{\mathcal{S}_\alpha} du\, \varrho^\alpha\varphi}, \tag{3.35}$$

where the exponent now is measured in units of $\hbar$. Inserting this delta functional into the transition amplitude given in equation (3.9), we obtain

$$Z[\mathcal{S}_\mathcal{C}, T] = \int D\varphi_T \prod_\alpha D\varrho^\alpha_T \, e^{\frac{i}{\hbar}\left(S[\varphi]+\sum_\alpha \int_{\mathcal{S}_\alpha} du\, \varrho^\alpha\varphi\right)}. \tag{3.36}$$

3.3 Implementation of periodic boundary conditions

In the following section it will be showed how the periodic property $\varphi(\boldsymbol{x}, t') = \varphi(\boldsymbol{x}, t) = 0$ will be implemented into the transition amplitude given in equation (3.36). We are considering static configurations of objects. Thus the boundary $\mathcal{S}$ is fixed in time and can be written as $\mathcal{S} = \bigcup_\alpha \mathcal{S}_\alpha = \bigcup_\alpha (Q_\alpha \times [0, T])$. Let ϱ^α be the source living on $Q_\alpha \times [0, T]$. Note that also the field ϱ^α is T-periodic since the boundaries are static. Since the fields φ and ϱ^α are T-periodic, they can be expanded as Fourier series;

$$\begin{aligned} \varphi(\boldsymbol{x}, t) &= \sum_{n=-\infty}^{\infty} \varphi_n(\boldsymbol{x}) e^{2\pi i n t/T}, \\ \varrho^\alpha(\boldsymbol{x}, t) &= \sum_{n=-\infty}^{\infty} \varrho^\alpha_n(\boldsymbol{x}) e^{2\pi i n t/T}. \end{aligned} \tag{3.37}$$

The fact that the fields are real, implies that $\varphi_{-n} = \varphi_n^*$ and $\varrho^\alpha_{-n} = \varrho^{\alpha *}_n$. We now start to explore how equation (3.36) changes under the change of variables introduced

in equation (3.37). The integrals inside the exponential will change as

$$\begin{aligned}\int\limits_{\mathcal{S}_\alpha} du\, \varrho^\alpha(\boldsymbol{x},t)\varphi(\boldsymbol{x},t) &= \int\limits_{Q_\alpha} dA \int\limits_0^T dt \sum_{m,n} \varrho_m^\alpha(\boldsymbol{x})\varphi_n(\boldsymbol{x}) e^{2\pi i(m+n)t/T} \\ &= \sum_{m,n} \int\limits_{Q_\alpha} dA\, \varrho_m^\alpha \varphi_n \int\limits_0^T dt\, e^{2\pi i(m+n)t/T} \\ &= T \sum_n \int\limits_{Q_\alpha} dA\, \varrho_{-n}^\alpha \varphi_n,\end{aligned} \tag{3.38}$$

where the result

$$\int\limits_0^T dt\, e^{2\pi i(m+n)t/T} = \begin{cases} T & m = -n \\ 0 & m \neq -n \end{cases} \tag{3.39}$$

is used. The action can be simplified using the same result;

$$\begin{aligned} S[\varphi] &= \int\limits_t^{t'} d\tau \int\limits_{\mathbb{R}^3} dV\, \mathcal{L}(\varphi(\boldsymbol{x},\tau)) = \int\limits_0^T d\tau \int\limits_{\mathbb{R}^3} dV\, \frac{1}{2}\left(\varphi_t^2(\boldsymbol{x},\tau) - \nabla\varphi^2(\boldsymbol{x},\tau)\right) \\ &= \int\limits_0^T d\tau \int\limits_{\mathbb{R}^3} dV\, \frac{1}{2} \sum_{m,n} \left(\tfrac{2\pi i m}{T}\tfrac{2\pi i n}{T}\varphi_m(\boldsymbol{x})\varphi_n(\boldsymbol{x}) - \nabla\varphi_m(\boldsymbol{x})\cdot\nabla\varphi_n(\boldsymbol{x})\right) e^{\frac{2\pi i(m+n)\tau}{T}} \\ &= \sum_n \int\limits_{\mathbb{R}^3} dV\, \frac{T}{2}\left(\left(\tfrac{2\pi n}{T}\right)^2 \varphi_n\varphi_{-n} - \nabla\varphi_n\cdot\nabla\varphi_{-n}\right). \end{aligned} \tag{3.40}$$

The differentials in equation (3.36) may be written as

$$\begin{aligned} D\varphi_T &= \prod_{n=-\infty}^{\infty} D\varphi_n, \\ D\varrho_T^\alpha &= \prod_{n=-\infty}^{\infty} D\varrho_n^\alpha. \end{aligned} \tag{3.41}$$

The Jacobian is omitted because it is common to both $Z[\mathcal{S}_\mathcal{C}, T]$ and $Z_\infty[T]$ and therefore will cancel.

Inserting the equations (3.38), (3.40) and (3.41) into the partition function given by equation (3.36) and taking the logarithm, we obtain

$$\ln Z[\mathcal{S}_\mathcal{C}, T] = \sum_{n=-\infty}^{\infty} \ln \int D\varphi_n \prod_\alpha D\varrho_n^\alpha e^{\frac{iT}{\hbar}\left(\int\limits_{\mathbb{R}^3} d\boldsymbol{x}\, \frac{1}{2}\left(\left(\frac{2\pi n}{T}\right)^2\varphi_n\varphi_{-n} - \nabla\varphi_n\cdot\nabla\varphi_{-n}\right) + \sum\limits_\alpha \int\limits_{Q_\alpha} dA\, \varrho_{-n}^\alpha\varphi_n\right)}. \tag{3.42}$$

As $T \to \infty$, the sum $\sum_{n=-\infty}^{\infty}$ can be replaced by $\frac{T}{2\pi}\int_{-\infty}^{\infty} dk$, where $k = \frac{2\pi n}{T}$ and $\varphi_n(\boldsymbol{x})$ is replaced by $\varphi_k(\boldsymbol{x})$. Thus

$$\ln Z[\mathcal{S}_{\mathcal{C}}, T] = \frac{T}{2\pi}\int_{-\infty}^{\infty} dk \ln \int D\varphi_k \prod_{\alpha} D\varrho_k^{\alpha} e^{\frac{iT}{\hbar}\left(\int_{\mathbb{R}^3} dV\, \frac{1}{2}\left(k^2\varphi_k\varphi_{-k} - \nabla\varphi_k\cdot\nabla\varphi_{-k}\right) + \sum_{\alpha}\int_{Q_\alpha} dA\, \varrho_{-k}^{\alpha}\varphi_k\right)}. \tag{3.43}$$

Split into negative and positive part, make the substitution $k \to -k$ on the negative part and use the fact that $\varphi_{-k} = \varphi_k^*$, $\varrho_{-k}^{\alpha} = \varrho_k^{\alpha *}$;

$$\begin{aligned}\ln Z[\mathcal{S}_{\mathcal{C}}, T] = \frac{T}{2\pi}\int_0^{\infty} dk \ln \int D\varphi_k^* \prod_{\alpha} D\varrho_k^{\alpha *} e^{\frac{iT}{\hbar}\left(\int_{\mathbb{R}^3} dV\, \frac{1}{2}\left(k^2|\varphi_k|^2 - |\nabla\varphi_k|^2\right) + \int_{Q_\alpha} dA\, \varrho_k^{\alpha}\varphi_k^*\right)} \\ + \frac{T}{2\pi}\int_0^{\infty} dk \ln \int D\varphi_k \prod_{\alpha} D\varrho_k^{\alpha} e^{\frac{iT}{\hbar}\left(\int_{\mathbb{R}^3} dV\, \frac{1}{2}\left(k^2|\varphi_k|^2 - |\nabla\varphi_k|^2\right) + \int_{Q_\alpha} dA\, \varrho_k^{\alpha *}\varphi_k\right)}.\end{aligned} \tag{3.44}$$

Use the property $\ln a + \ln b = \ln(ab)$ to obtain

$$\ln Z[\mathcal{S}_{\mathcal{C}}, T] = \frac{T}{2\pi}\int_0^{\infty} dk \ln \Pi_Q(k), \tag{3.45}$$

where

$$\Pi_Q(k) = \int D\varphi_k D\varphi_k^* \prod_{\alpha=1}^{r} D\varrho_k^{\alpha} D\varrho_k^{\alpha *} e^{\frac{iT}{\hbar}\tilde{S}}, \tag{3.46}$$

and the *effective action* $\tilde{S}$ is

$$\tilde{S} = \tilde{S}[\varphi_k, \varphi_k^*, \varrho_k^{\alpha}, \varrho_k^{\alpha *}] = \int_{\mathbb{R}^3} dV\ \left(k^2|\varphi_k|^2 - |\nabla\varphi_k|^2\right) + \sum_{\alpha=1}^{r}\int_{Q_\alpha} dA\, (\varrho_k^{\alpha *}\varphi_k + \varrho_k^{\alpha}\varphi_k^*). \tag{3.47}$$

Similarly we find that

$$\ln Z_{\infty}[T] = \frac{T}{2\pi}\int_0^{\infty} dk \ln \Pi_{\infty}(k). \tag{3.48}$$

To obtain the expression for the Casimir energy, let $T = -is$ and do a Wick rotation $k = i\kappa$ in equation (3.45). Inserting this into (3.17), we obtain

$$\mathcal{E} = -\lim_{s\to\infty}\frac{\hbar}{s}\ln\frac{Z[\mathcal{S}_{\mathcal{C}}, -is]}{Z_{\infty}[-is]} = -\lim_{s\to\infty}\frac{\hbar}{2\pi}\int_0^{\infty} d\kappa \ln\frac{\Pi_Q(i\kappa)}{\Pi_{\infty}(i\kappa)}\bigg|_{T=-is}. \tag{3.49}$$

3.4 Classical equations of motion

In order to perform the integration over φ_k and φ_k^* in $\Pi_Q(i\kappa)$ and $\Pi_{\infty}(i\kappa)$, the fields will be decomposed into a classical part and a fluctuating part. The classical part is

a solution to the *classical equations of motion*. We are going to derive the classical equations of motion by taking the variational derivative of $\tilde{S}$ with respect to φ_k^*, and require it to be zero.

Make the abbreviations $\phi = \varphi_{cl,k}$ and $\tilde{S}_{cl} = \tilde{S}[\varphi_{cl,k}, \varphi^*_{cl,k}, \varrho_k^\alpha, \varrho_k^{\alpha *}]$. Consider a small variation $\delta\phi^*$ from the classical solution ϕ^* and insert it into the effective action in equation (3.47);

$$\begin{aligned}\tilde{S}[\phi, \phi^* + \delta\phi^*, \varrho_k^\alpha, \varrho_k^{\alpha *}] &= \tilde{S}_{cl} + \int\limits_{\mathbb{R}^3} dV \ \left(k^2\phi\,\delta\phi^* - \nabla\phi\cdot\nabla\delta\phi^*\right) + \sum_{\alpha=1}^{r}\int\limits_{Q_\alpha} dA\ \varrho_k^\alpha\delta\phi^* \\ &= \tilde{S}_{cl} + \int\limits_{\mathbb{R}^3} dV\ k^2\phi\,\delta\phi^* - \sum_{i=0}^{r}\int\limits_{V_i} dV\ \nabla\phi\cdot\nabla\delta\phi^* + \sum_{\alpha=1}^{r}\int\limits_{Q_\alpha} dA\ \varrho_k^\alpha\delta\phi^*, \end{aligned} \tag{3.50}$$

where the fact that $\mathbb{R}^3 = V_0 \bigcup \sum_{\alpha=1}^{r} V_\alpha = \bigcup_{i=0}^{r} V_i$ is used. The boundary of the compact object V_α is $\partial V_\alpha = Q_\alpha$. The boundary of the complement to the objects is $\partial V_0 = \sum_{\alpha=1}^{r} Q_\alpha$. Using Green's first identity, the volume integrals over the regions V_i can be written

$$\begin{aligned}\sum_{i=0}^{r}\int\limits_{V_i} dV\ \nabla\phi\cdot\nabla\delta\phi^* &= \sum_{\alpha=1}^{r}\int\limits_{\partial V_\alpha} dA\ (\partial_{\boldsymbol{n}}\phi_-)\,\delta\phi^* - \int\limits_{\partial V_0} dA\ (\partial_{\boldsymbol{n}}\phi_+)\,\delta\phi^* - \sum_{i=0}^{r}\int\limits_{V_i} dV\ \nabla^2\phi\,\delta\phi^* \\ &= \sum_{\alpha=1}^{r}\int\limits_{Q_\alpha} dA\ (\partial_{\boldsymbol{n}}\phi_-)\,\delta\phi^* - \sum_{\alpha=1}^{r}\int\limits_{Q_\alpha} dA\ (\partial_{\boldsymbol{n}}\phi_+)\,\delta\phi^* - \int\limits_{\mathbb{R}^3} dV\ (\nabla^2\phi)\,\delta\phi^* \\ &= \sum_{\alpha=1}^{r}\int\limits_{Q_\alpha} dA\ (\Delta\partial_{\boldsymbol{n}}\phi)\,\delta\phi^* - \int\limits_{\mathbb{R}^3} dV\ (\nabla^2\phi)\,\delta\phi^*, \end{aligned} \tag{3.51}$$

where the normals $\boldsymbol{n}$ point out of the compact objects V_α, $\alpha = 1, ..., r$ and $\Delta\partial_{\boldsymbol{n}}\phi(\boldsymbol{x}) = \partial_{\boldsymbol{n}}\phi_-(\boldsymbol{x}) - \partial_{\boldsymbol{n}}\phi_+(\boldsymbol{x})$. The fields $\phi_\pm$ are the defined as

$$\phi_-(\boldsymbol{x}) = \lim_{\substack{\boldsymbol{x'}\to\boldsymbol{x}\\ \boldsymbol{x'}\in V_\alpha}} \phi(\boldsymbol{x'}) \quad \text{and} \quad \phi_+(\boldsymbol{x}) = \lim_{\substack{\boldsymbol{x'}\to\boldsymbol{x}\\ \boldsymbol{x'}\in V_0}} \phi(\boldsymbol{x'}) \qquad \boldsymbol{x}\in Q_\alpha,\ \alpha = 1, ..., r. \tag{3.52}$$

Inserting equation (3.51) into (3.50) we obtain

$$\tilde{S}[\phi, \phi^* + \delta\phi^*, ..] = \tilde{S}_{cl} + \int\limits_{\mathbb{R}^3} dV\ \left(k^2\phi + \nabla^2\phi\right)\delta\phi^* + \sum_{\alpha=1}^{r}\int\limits_{Q_\alpha} dA\ (\varrho_k^\alpha - \Delta\partial_{\boldsymbol{n}}\phi)\,\delta\phi^*. \tag{3.53}$$

We require that the classical solution is continuous. Thus $\Delta\varphi_{cl,k} = 0$. Requiring that $\delta\tilde{S}/\delta\phi^* = 0$, we get the "equations of motion"

$$\begin{aligned} \nabla^2\varphi_{cl,k} + k^2\varphi_{cl,k} = 0 \qquad & \boldsymbol{x} \notin Q_\alpha \\ \Delta\varphi_{cl,k} = 0 \qquad & \boldsymbol{x} \in Q_\alpha \\ \Delta\partial_{\boldsymbol{n}}\varphi_{cl,k} = \varrho_k^\alpha \qquad & \boldsymbol{x} \in Q_\alpha. \end{aligned} \tag{3.54}$$

3.5 Integration over the unconstrained fields φ_k and φ_k^*

In order to integrate over φ_k and φ_k^*, we introduce the change of variables we mentioned above; φ_k and φ_k^* is decomposed into a classical part and a fluctuating part,

$$\begin{aligned} \varphi_k &= \varphi_{cl,k} + \delta\varphi_k, \\ \varphi_k^* &= \varphi_{cl,k}^* + \delta\varphi_k^*. \end{aligned} \tag{3.55}$$

The effective action in equation (3.47) then can be written as,

$$\begin{aligned} \tilde{S}[\varphi_{cl,k} + \delta\varphi_k, \varphi_{cl,k}^* + \delta\varphi_k^*, \varrho_k^\alpha, \varrho_k^{\alpha*}] = \int_{\mathbb{R}^3} dV \, \big\{ & k^2(\varphi_{cl,k} + \delta\varphi_k)(\varphi_{cl,k}^* + \delta\varphi_k^*) \\ - \nabla(\varphi_{cl,k} + \delta\varphi_k) \cdot \nabla(\varphi_{cl,k}^* + \delta\varphi_k^*) \big\} + \sum_{\alpha=1}^{r} \int_{Q_\alpha} dA \, & \left(\varrho_k^{\alpha*}(\varphi_{cl,k} + \delta\varphi_k) + \varrho_k^\alpha(\varphi_{cl,k}^* + \delta\varphi_k^*) \right). \end{aligned} \tag{3.56}$$

Proceeding similarly as we did when we derived the equations of motion, i.e. by using Green's first identity and the equations of motion (3.54) themselves, we obtain

$$\tilde{S}[\varphi_{cl,k} + \delta\varphi_k, \varphi_{cl,k}^* + \delta\varphi_k^*, \varrho_k^\alpha, \varrho_k^{\alpha*}] = \tilde{S}_{cl} + \int_{\mathbb{R}^3} dV \, \left(k^2|\delta\varphi_k|^2 - |\nabla\delta\varphi_k|^2 \right). \tag{3.57}$$

The classical equations of motion and Green's first identity can also be used to simplify the expression for the classical action $\tilde{S}_{cl}$. Using equation (3.47), we can write $\tilde{S}_{cl}$ as

$$\tilde{S}_{cl} = \frac{1}{2}\int_{\mathbb{R}^3} dV \, k^2\varphi_{cl,k}\varphi_{cl,k}^* - \frac{1}{2}\int_{\mathbb{R}^3} dV \, \nabla\varphi_{cl,k} \cdot \nabla\varphi_{cl,k}^* + \sum_{\alpha=1}^{r} \int_{Q_\alpha} dA \, \varrho_k^\alpha\varphi_{cl,k}^* + c.c. \tag{3.58}$$

Green's first identity applied to the second integral gives

$$\int_{\mathbb{R}^3} dV \, \nabla\varphi_{cl,k} \cdot \nabla\varphi_{cl,k}^* = \sum_{\alpha=1}^{r} \int_{Q_\alpha} dA \, (\Delta\partial_{\boldsymbol{n}}\varphi_{cl,k}) \, \varphi_{cl,k}^* - \int_{\mathbb{R}^3} dV \, (\nabla^2\varphi_{cl,k})\varphi_{cl,k}^*. \tag{3.59}$$

Thus

$$\tilde{S}_{cl} = \int_{\mathbb{R}^3} dV \, \left(\tfrac{k^2\varphi_{cl,k} + \nabla^2\varphi_{cl,k}}{2} \right) \varphi^*_{cl,k} + \sum_{\alpha=1}^{r} \int_{Q_\alpha} dA \, \left(\varrho^\alpha_k - \tfrac{\Delta \partial_{\boldsymbol{n}} \varphi_{cl,k}}{2} \right) \varphi^*_{cl,k} + c.c. \tag{3.60}$$

The equations of motion (3.54) give the following expression for the classical action:

$$\tilde{S}_{cl} = \frac{1}{2} \sum_{\alpha=1}^{r} \int_{Q_\alpha} dA \, \varrho^\alpha_k \varphi^*_{cl,k} + c.c = \frac{1}{2} \sum_{\alpha=1}^{r} \int_{Q_\alpha} dA \, \left(\varrho^\alpha_k \varphi^*_{cl,k} + \varrho^{\alpha *}_k \varphi_{cl,k} \right). \tag{3.61}$$

By inserting the effective action, given in equation (3.57), into equation (3.46) we get

$$\mathit{\Pi}_Q(k) = \int \prod_{\alpha=1}^{r} D\varrho^\alpha_k D\varrho^{\alpha *}_k e^{\frac{s}{\hbar}\tilde{S}_{cl}} \int D(\delta\varphi_k) D(\delta\varphi^*_k) e^{\frac{s}{\hbar} \int_{\mathbb{R}^3} dV \left(k^2 |\delta\varphi_k|^2 - |\nabla \delta\varphi_k|^2 \right)}. \tag{3.62}$$

Notice that part of the functional integral which involves $\delta\varphi_k$ is geometry independent. This part is common to $\mathit{\Pi}_Q(k)$ and $\mathit{\Pi}_\infty(k)$ and will therefore cancel. Thus the integration over φ_k gives no contribution to the Casimir energy.

Therefore, after we have performed the integration over φ_k and φ^*_k, equation (3.46) have reduced to

$$\mathit{\Pi}_Q(k) = \int \prod_{\alpha=1}^{r} D\varrho^\alpha_k D\varrho^{\alpha *}_k e^{\frac{s}{\hbar}\tilde{S}_{cl}}, \tag{3.63}$$

and $\mathit{\Pi}_\infty(k)$ is given by

$$\mathit{\Pi}_\infty(k) = \int \prod_{\alpha=1}^{r} D\varrho^\alpha_k D\varrho^{\alpha *}_k e^{\frac{s}{\hbar}\tilde{S}_{\infty}}, \tag{3.64}$$

where $\tilde{S}_\infty$ is the classical action when the objects have been removed to infinite separation.

3.6 Integration over the sources ϱ^α_k and $\varrho^{\alpha *}_k$

In order to perform the integration over ϱ^α_k and $\varrho^{\alpha *}_k$, we are going to introduce a change of variables. First, choose coordinate systems $\mathcal{O}_\alpha$ in each object V_α. Let $\boldsymbol{x}_\alpha$ be coordinates in $\mathcal{O}_\alpha$. See figure 3.1. In each of the coordinate systems, choose a complete set of functions, $\{q^\alpha_{\boldsymbol{i}_\alpha}(\boldsymbol{x}_\alpha)\}$, defined on the boundaries Q_α. At the end we are going to discretize the boundaries, and then it is easy to choose the functions such that they are orthonormal. However, to start with, we only assume that the functions $\{q^\alpha_{\boldsymbol{i}_\alpha}(\boldsymbol{x}_\alpha)\}$ form a complete set. Introduce the linear change of variables

$$\varrho^\alpha(\boldsymbol{x}_\alpha) = \sum_{\boldsymbol{j}_\alpha} \varrho^\alpha_{\boldsymbol{j}_\alpha} q^\alpha_{\boldsymbol{j}_\alpha}(\boldsymbol{x}_\alpha) \tag{3.65}$$

in equation (3.63).

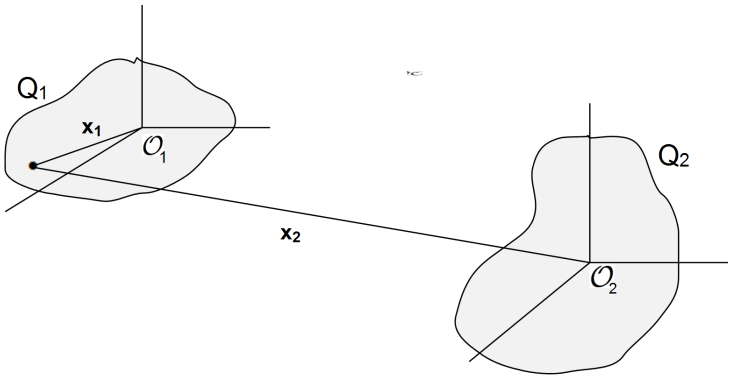

FIGURE 3.1: Coordinate system for the situation with two objects.

In order to perform the integration, we are also going to use the property that the equations (3.54) are linear, which means that the solution can be written as a linear superposition

$$\varphi_{cl,k} = \sum_{\beta} \varphi_{\beta}, \tag{3.66}$$

where φ_β satisfies (3.54) when all the sources are set to zero, except for ϱ_β. Thus if we define

$$\tilde{S}_{\alpha\beta} = \int\limits_{Q_\alpha} dA \, \left(\varrho_k^{\alpha *} \varphi_\beta + \varrho_k^{\alpha} \varphi_\beta^* \right), \tag{3.67}$$

the integrand in equation (3.63) can be written as

$$e^{\frac{s}{\hbar}\tilde{S}_{cl}} = e^{\frac{s}{2\hbar}\sum\limits_{\alpha\beta}\tilde{S}_{\alpha\beta}}. \tag{3.68}$$

The terms $\tilde{S}_{\alpha\beta}$ we call *interaction* terms. In particular, we call the terms $\tilde{S}_{\alpha\alpha}$ for *self-interaction* terms. When the conductors have been removed to infinite separation there is no interaction between them. Thus only the self-interaction terms contribute to $\tilde{S}_\infty$. The integrand in equation (3.64) can be written

$$e^{\frac{s}{\hbar}\tilde{S}_{\infty}} = e^{\frac{s}{2\hbar}\sum\limits_{\alpha}\tilde{S}_{\alpha\alpha}}. \tag{3.69}$$

In order to be able to compute the interaction terms, we are going to use Green's functions. The differential operator corresponding to the equations of motion (3.54) is $\mathcal{L} = \nabla^2 + k^2$. Let $G^\alpha(\boldsymbol{x}_\alpha, \boldsymbol{x}'_\alpha)$ be a Green's function for $\mathcal{L}$ in the coordinate system $\mathcal{O}_\alpha$, i.e

$$\mathcal{L}_\alpha G^\alpha(\boldsymbol{x}_\alpha, \boldsymbol{x}'_\alpha) = -\delta_\alpha(\boldsymbol{x}_\alpha - \boldsymbol{x}'_\alpha). \tag{3.70}$$

A Green's function corresponding to this equation is

$$G^\alpha(\boldsymbol{x}_\alpha, \boldsymbol{x}'_\alpha) = \frac{e^{ik\|\boldsymbol{x}_\alpha - \boldsymbol{x}_\alpha\|}}{4\pi\|\boldsymbol{x}_\alpha - \boldsymbol{x}_\alpha\|}. \tag{3.71}$$

Before we can perform the integration, we must find expressions for the interaction terms $\tilde{S}_{\alpha\beta}$, $\alpha, \beta = 1, ..., r$.

3.6.1 Self interaction terms $\tilde{S}_{\alpha\alpha}$

$\tilde{S}_{\alpha\alpha}$ is the contribution to the action from the field φ_α, generated by the source ϱ_α, integrated over the surface Q_α. From equation (3.67) we get

$$\tilde{S}_{\alpha\alpha} = \int\limits_{Q_\alpha} dA \ (\varrho_k^{\alpha *} \varphi_\alpha + \varrho_k^\alpha \varphi_\alpha^*) \,. \tag{3.72}$$

The field φ_α is a solution to equation (3.54) and can therefore be written using the Green's function and the sources as

$$\varphi_\alpha(\boldsymbol{x}_\alpha) = \int_{Q_\alpha} dA_{\boldsymbol{x}'_\alpha} G^\alpha(\boldsymbol{x}_\alpha, \boldsymbol{x}'_\alpha) \varrho^\alpha(\boldsymbol{x}'_\alpha). \tag{3.73}$$

Expand the Green's function G^α using the functions $\{q^\alpha_{\boldsymbol{i}_\alpha}(\boldsymbol{x}_\alpha)\}$ in the coordinate system $\mathcal{O}_\alpha$;

$$G^\alpha(\boldsymbol{x}_\alpha, \boldsymbol{x}'_\alpha) = \sum_{\boldsymbol{i}_\alpha} G^\alpha_{\boldsymbol{i}_\alpha}(\boldsymbol{x}'_\alpha) q^\alpha_{\boldsymbol{i}_\alpha}(\boldsymbol{x}_\alpha). \tag{3.74}$$

Inserting equations (3.65) and (3.74) into equation (3.73), we get

$$\varphi_\alpha(\boldsymbol{x}_\alpha) = \sum_{\boldsymbol{i}_\alpha \boldsymbol{j}_\alpha} G^\alpha_{\boldsymbol{i}_\alpha \boldsymbol{j}_\alpha} \varrho^\alpha_{\boldsymbol{j}_\alpha} q^\alpha_{\boldsymbol{i}_\alpha}(\boldsymbol{x}_\alpha), \tag{3.75}$$

where

$$G^\alpha_{\boldsymbol{i}_\alpha \boldsymbol{j}_\alpha} = \int_{Q_\alpha} dA_{\boldsymbol{x}'_\alpha} G^\alpha_{\boldsymbol{i}_\alpha}(\boldsymbol{x}'_\alpha) q^\alpha_{\boldsymbol{j}_\alpha}(\boldsymbol{x}'_\alpha). \tag{3.76}$$

Using the expansions of the field φ_α and the source ϱ^α given in equations (3.65) and (3.75), the self-interaction terms can be written as

$$\tilde{S}_{\alpha\alpha} = \int\limits_{Q_\alpha} dA \ (\varrho_k^{\alpha *} \varphi_\alpha + \varrho_k^\alpha \varphi_\alpha^*) = \sum_{\boldsymbol{i}_\alpha \boldsymbol{k}_\alpha} \varrho^{\alpha *}_{\boldsymbol{i}_\alpha} \mathcal{G}^\alpha_{\boldsymbol{i}_\alpha \boldsymbol{k}_\alpha} \varrho^\alpha_{\boldsymbol{k}_\alpha} + \sum_{\boldsymbol{i}_\alpha \boldsymbol{k}_\alpha} \varrho^\alpha_{\boldsymbol{i}_\alpha} \mathcal{G}^{\alpha *}_{\boldsymbol{i}_\alpha \boldsymbol{k}_\alpha} \varrho^{\alpha *}_{\boldsymbol{k}_\alpha}, \tag{3.77}$$

where

$$\mathcal{G}^\alpha_{\boldsymbol{i}_\alpha \boldsymbol{k}_\alpha} = \sum_{\boldsymbol{j}_\alpha} D^\alpha_{\boldsymbol{i}_\alpha \boldsymbol{j}_\alpha} G^\alpha_{\boldsymbol{j}_\alpha \boldsymbol{k}_\alpha} \tag{3.78}$$

and

$$D^\alpha_{\boldsymbol{i}_\alpha \boldsymbol{j}_\alpha} = \int_{Q_\alpha} dA_{\boldsymbol{x}_\alpha} q^{\alpha *}_{\boldsymbol{i}_\alpha}(\boldsymbol{x}_\alpha) q^\alpha_{\boldsymbol{j}_\alpha}(\boldsymbol{x}_\alpha). \tag{3.79}$$

Observe that if the set $\{q^\alpha_{\boldsymbol{i}_\alpha}(\boldsymbol{x}_\alpha)\}$ is orthonormal, we get

$$D^\alpha_{\boldsymbol{i}_\alpha \boldsymbol{j}_\alpha} = \delta_{\boldsymbol{i}_\alpha \boldsymbol{j}_\alpha}. \tag{3.80}$$

Defining

$$T^\alpha_{\boldsymbol{i}_\alpha \boldsymbol{k}_\alpha} = \mathcal{G}^\alpha_{\boldsymbol{i}_\alpha \boldsymbol{k}_\alpha} + \mathcal{G}^{\alpha *}_{\boldsymbol{k}_\alpha \boldsymbol{i}_\alpha}, \tag{3.81}$$

and interchanging dummy variables in the second sum in equation (3.77), the contribution to the action from the self interaction reduces to

$$\tilde{S}_{\alpha\alpha} = \sum_{\boldsymbol{i}_\alpha \boldsymbol{k}_\alpha} \varrho^{\alpha *}_{\boldsymbol{i}_\alpha} T^\alpha_{\boldsymbol{i}_\alpha \boldsymbol{k}_\alpha} \varrho^\alpha_{\boldsymbol{k}_\alpha}. \tag{3.82}$$

3.6.2 Interaction terms $\tilde{S}_{\alpha\beta}$, $\alpha \neq \beta$

We want to find the contribution to the action from the field φ_β, generated by the source ϱ_α, integrated over the surface Q_α. Here we can proceed almost as we did in the previous section. Let $\boldsymbol{x}_\alpha$ be coordinates in $\mathcal{O}_\alpha$. In the coordinate system $\mathcal{O}_\beta$ these coordinates can be written as $\boldsymbol{x}_\beta(\boldsymbol{x}_\alpha)$. Define

$$\varphi_\beta(\boldsymbol{x}_\alpha) \equiv \varphi_\beta(\boldsymbol{x}_\beta(\boldsymbol{x}_\alpha)). \tag{3.83}$$

$\varphi_\beta(\boldsymbol{x}_\alpha)$ can be written using the Green's function and the sources,

$$\varphi_\beta(\boldsymbol{x}_\alpha) = \varphi_\beta(\boldsymbol{x}_\beta(\boldsymbol{x}_\alpha)) = \int_{Q_\beta} dA_{\boldsymbol{x}'_\beta} G^\beta(\boldsymbol{x}_\beta(\boldsymbol{x}_\alpha), \boldsymbol{x}'_\beta) \varrho^\beta(\boldsymbol{x}'_\beta). \tag{3.84}$$

Make the expansion

$$G^\beta(\boldsymbol{x}_\beta(\boldsymbol{x}_\alpha), \boldsymbol{x}'_\beta) = \sum_{\boldsymbol{i}_\alpha} G^{\alpha\beta}_{\boldsymbol{i}_\alpha}(\boldsymbol{x}'_\beta) q^\beta_{\boldsymbol{i}_\alpha}(\boldsymbol{x}_\alpha). \tag{3.85}$$

Inserting this expression, together with the source expansion given in equation (3.65), into equation (3.84) we get

$$\varphi_\beta(\boldsymbol{x}_\alpha) = \sum_{\boldsymbol{i}_\alpha \boldsymbol{j}_\beta} G^{\alpha\beta}_{\boldsymbol{i}_\alpha \boldsymbol{j}_\beta} \varrho^\beta_{\boldsymbol{j}_\beta} q^\beta_{\boldsymbol{i}_\alpha}(\boldsymbol{x}_\alpha), \tag{3.86}$$

where

$$G^{\alpha\beta}_{\boldsymbol{i}_\alpha \boldsymbol{j}_\beta} = \int_{Q_\beta} dA_{\boldsymbol{x}'_\beta} G^{\alpha\beta}_{\boldsymbol{i}_\alpha}(\boldsymbol{x}'_\beta) q^\beta_{\boldsymbol{j}_\beta}(\boldsymbol{x}'_\beta). \tag{3.87}$$

Using equations (3.65) and (3.86), the interaction terms become

$$\tilde{S}_{\alpha\beta} = \int_{Q_\alpha} dA \, \left(\varrho^{\alpha *}_k \varphi_\beta + \varrho^\alpha_k \varphi^*_\beta \right) = \sum_{\boldsymbol{i}_\alpha \boldsymbol{k}_\beta} \varrho^{\alpha *}_{\boldsymbol{i}_\alpha} \mathcal{G}^{\alpha\beta}_{\boldsymbol{i}_\alpha \boldsymbol{k}_\beta} \varrho^\beta_{\boldsymbol{k}_\beta} + \sum_{\boldsymbol{i}_\alpha \boldsymbol{k}_\beta} \varrho^\alpha_{\boldsymbol{i}_\alpha} \mathcal{G}^{\alpha\beta *}_{\boldsymbol{i}_\alpha \boldsymbol{k}_\beta} \varrho^{\beta *}_{\boldsymbol{k}_\beta}, \tag{3.88}$$

where

$$\mathcal{G}^{\alpha\beta}_{\boldsymbol{i}_\alpha \boldsymbol{k}_\beta} = \sum_{\boldsymbol{j}_\alpha} D^{\alpha}_{\boldsymbol{i}_\alpha \boldsymbol{j}_\alpha} G^{\alpha\beta}_{\boldsymbol{j}_\alpha \boldsymbol{k}_\beta}. \tag{3.89}$$

Defining

$$U^{\alpha\beta}_{\boldsymbol{i}_\alpha \boldsymbol{k}_\beta} = \mathcal{G}^{\alpha\beta}_{\boldsymbol{i}_\alpha \boldsymbol{k}_\beta} + \mathcal{G}^{\beta\alpha *}_{\boldsymbol{k}_\beta \boldsymbol{i}_\alpha}, \tag{3.90}$$

we get

$$\tilde{S}_{\alpha\beta} = \sum_{\boldsymbol{i}_\alpha \boldsymbol{k}_\beta} \varrho^{\alpha *}_{\boldsymbol{i}_\alpha} U^{\alpha\beta}_{\boldsymbol{i}_\alpha \boldsymbol{k}_\beta} \varrho^{\beta}_{\boldsymbol{k}_\beta}. \tag{3.91}$$

3.6.3 Classical action

Combining the interaction and the self-interaction terms, the classical action becomes

$$\begin{aligned} \tilde{S}_{cl} &= \frac{1}{2} \sum_{\alpha\beta} \tilde{S}_{\alpha\beta} = \frac{1}{2} \left(\sum_{\alpha} \tilde{S}_{\alpha\alpha} + \sum_{\substack{\alpha\beta \\ \alpha \neq \beta}} \tilde{S}_{\alpha\beta} \right) \\ &= \frac{1}{2} \left(\sum_{\alpha} \sum_{\boldsymbol{i}_\alpha \boldsymbol{k}_\alpha} \varrho^{\alpha *}_{\boldsymbol{i}_\alpha} T^{\alpha}_{\boldsymbol{i}_\alpha \boldsymbol{k}_\alpha} \varrho^{\alpha}_{\boldsymbol{k}_\alpha} + \sum_{\substack{\alpha\beta \\ \alpha \neq \beta}} \sum_{\boldsymbol{i}_\alpha \boldsymbol{k}_\beta} \varrho^{\alpha *}_{\boldsymbol{i}_\alpha} U^{\alpha\beta}_{\boldsymbol{i}_\alpha \boldsymbol{k}_\beta} \varrho^{\beta}_{\boldsymbol{k}_\beta} \right). \end{aligned} \tag{3.92}$$

Observe that, by definition (equations (3.81) and (3.90)), the matrices T^α and $U^{\alpha\beta}$ are self-adjoint.

Define the block matrix $A = A(k)$ by

$$A^{\alpha\beta} = -T^{\alpha}\delta_{\alpha\beta} - U^{\alpha\beta}(1 - \delta_{\alpha\beta}), \qquad \alpha, \beta = 1, ..., r. \tag{3.93}$$

Thus the entries of A are also matrices. The fact that T^α and $U^{\alpha\beta}$ are self-adjoint implies that A is self-adjoint. The matrix A is positive definite since the Helmholtz operator $\nabla^2 + k^2$ is a positive operator for $k = i\kappa$. Using equation (3.93), the action can be written as

$$\tilde{S}_{cl} = -\frac{1}{2} \sum_{\alpha\beta} \sum_{\boldsymbol{i}_\alpha \boldsymbol{k}_\beta} \varrho^{\alpha *}_{\boldsymbol{i}_\alpha} A^{\alpha\beta}_{\boldsymbol{i}_\alpha \boldsymbol{k}_\beta} \varrho^{\beta}_{\boldsymbol{k}_\beta} = -\frac{1}{2} \langle \varrho, A\varrho \rangle, \tag{3.94}$$

where $\langle \, , \, \rangle$ is the standard inner product in $\mathbb{C}^n$. The action in the infinite separation case becomes

$$\begin{aligned} \tilde{S}_{\infty} &= \frac{1}{2} \sum_{\alpha} \tilde{S}_{\alpha\alpha} = \frac{1}{2} \sum_{\alpha} \sum_{\boldsymbol{i}_\alpha \boldsymbol{k}_\alpha} \varrho^{\alpha *}_{\boldsymbol{i}_\alpha} T^{\alpha}_{\boldsymbol{i}_\alpha \boldsymbol{k}_\alpha} \varrho^{\alpha}_{\boldsymbol{k}_\alpha} \\ &= -\frac{1}{2} \sum_{\alpha\beta} \sum_{\boldsymbol{i}_\alpha \boldsymbol{k}_\beta} \varrho^{\alpha *}_{\boldsymbol{i}_\alpha} B^{\alpha\beta}_{\boldsymbol{i}_\alpha \boldsymbol{k}_\beta} \varrho^{\beta}_{\boldsymbol{k}_\beta} = -\frac{1}{2} \langle \varrho, B\varrho \rangle, \end{aligned} \tag{3.95}$$

where the block matrix $B = B(k)$ is defined by

$$B^{\alpha\beta} = -T^{\alpha}\delta_{\alpha\beta}, \qquad \alpha, \beta = 1, ..., r. \tag{3.96}$$

Notice that also B is self-adjoint and positive definite.

3.6.4 Performing the integration

Under the change of variables $\varrho^{\alpha}(\boldsymbol{x}_{\alpha}) = \sum\limits_{\boldsymbol{i}_{\alpha}} \varrho^{\alpha}_{\boldsymbol{i}_{\alpha}} q^{\alpha}_{\boldsymbol{i}_{\alpha}}(\boldsymbol{x}_{\alpha})$, the differentials change as

$$\int \prod_{\alpha=1}^{r} D\varrho^{\alpha} D\varrho^{\alpha *} \to J \int \prod_{\alpha=1}^{r} \prod_{\boldsymbol{i}_{\alpha}} d\varrho^{\alpha}_{\boldsymbol{i}_{\alpha}} d\varrho^{\alpha *}_{\boldsymbol{i}_{\alpha}} = J' \int \prod_{\alpha=1}^{r} \prod_{\boldsymbol{i}_{\alpha}} \tfrac{d\varrho^{\alpha}_{\boldsymbol{i}_{\alpha}} d\varrho^{\alpha *}_{\boldsymbol{i}_{\alpha}}}{2\pi i}, \tag{3.97}$$

where J is the Jacobian of the coordinate change and $J' = J \prod\limits_{\boldsymbol{i}_{\alpha}} 2\pi i$. Defining the block matrices $A' = A'(k)$ and $B' = B'(k)$ as

$$\begin{aligned} A' &= \frac{s}{2\hbar} A, \\ B' &= \frac{s}{2\hbar} B, \end{aligned} \tag{3.98}$$

the equations (3.63) and (3.64) can be written as

$$\Pi_Q(k) = J' \int \prod_{\alpha=1}^{r} \prod_{\boldsymbol{i}_{\alpha}} \tfrac{d\varrho^{\alpha}_{\boldsymbol{i}_{\alpha}} d\varrho^{\alpha *}_{\boldsymbol{i}_{\alpha}}}{2\pi i} e^{-\langle \varrho, A'\varrho \rangle} \tag{3.99}$$

and

$$\Pi_{\infty}(k) = J' \int \prod_{\alpha=1}^{r} \prod_{\boldsymbol{i}_{\alpha}} \tfrac{d\varrho^{\alpha}_{\boldsymbol{i}_{\alpha}} d\varrho^{\alpha *}_{\boldsymbol{i}_{\alpha}}}{2\pi i} e^{-\langle \varrho, B'\varrho \rangle}. \tag{3.100}$$

Using the integral result for self-adjoint and positive-definite and matrices,

$$\int \prod_{j} \tfrac{dz_j dz_j^*}{2\pi i} e^{-\langle \boldsymbol{z}, A\boldsymbol{z} \rangle} = \frac{1}{\det A}, \tag{3.101}$$

from Appendix A we get

$$\Pi_Q(k) = \frac{J'}{\det A'(k)}, \tag{3.102}$$

$$\Pi_{\infty}(k) = \frac{J'}{\det B'(k)}. \tag{3.103}$$

3.7 Casimir energy

Remember the expression for the Casimir energy;

$$\mathcal{E} = -\frac{\hbar}{2\pi}\lim_{s\to\infty}\int_0^\infty d\kappa \ln\frac{\Pi_Q(i\kappa)}{\Pi_\infty(i\kappa)}\bigg|_{T=-is} = \frac{\hbar}{2\pi}\lim_{s\to\infty}\int_0^\infty d\kappa \ln\frac{\Pi_\infty(i\kappa)}{\Pi_Q(i\kappa)}\bigg|_{T=-is}. \quad (3.104)$$

The integrand can be calculated using the results in equations (3.102) and (3.103);

$$\frac{\Pi_\infty(i\kappa)}{\Pi_Q(i\kappa)} = \frac{J'}{J'}\frac{\det A'}{\det B'} = \det\left(B'^{-1}A'\right) = \det\left(\frac{2\hbar}{s}B^{-1}\frac{s}{2\hbar}A\right) = \det\left(B^{-1}A\right). \quad (3.105)$$

Let $M = M(i\kappa)$ be the block matrix given by

$$M(i\kappa) = B^{-1}(i\kappa)A(i\kappa). \quad (3.106)$$

B is the diagonal block matrix defined in equation (3.96). Thus the inverse of B is also diagonal, and the block entries are given by

$$[B^{\alpha\beta}]^{-1} = -[T^\alpha]^{-1}\delta_{\alpha\beta}. \quad (3.107)$$

This result, together with the definition of A in equation (3.93), gives that

$$M^{\alpha\beta} = \mathbf{1}\delta_{\alpha\beta} + [T^\alpha]^{-1}U^{\alpha\beta}(1-\delta_{\alpha\beta}) \qquad \alpha,\beta = 1,...,r. \quad (3.108)$$

Observe that there is no time dependence (s is cancelled) in M. Inserting equation (3.105) into equation (3.104), we finally obtain an expression for the Casimir energy,

$$\mathcal{E} = \frac{\hbar}{2\pi}\int_0^\infty d\kappa \ln\det M(i\kappa). \quad (3.109)$$

For the special case when the configuration consists of two objects, the Casimir energy is given by

$$\mathcal{E} = \frac{\hbar}{2\pi}\int_0^\infty d\kappa \ln\det(\mathbf{1} - \left[T^1\right]^{-1}U^{12}\left[T^2\right]^{-1}U^{21}). \quad (3.110)$$

3.8 Formulas needed to calculate the Casimir energy

Long calculations led up to the expression for the Casimir energy in equation (3.109). In this section we collect the expressions and formulas that are necessary to calculate the Casimir energy.

The Green's function corresponding to equation (3.70) with $k = i\kappa$ is

$$G^\alpha(\boldsymbol{x}_\alpha, \boldsymbol{x}'_\alpha) = \frac{e^{-\kappa\|\boldsymbol{x}_\alpha - \boldsymbol{x}_\alpha\|}}{4\pi\|\boldsymbol{x}_\alpha - \boldsymbol{x}_\alpha\|}. \quad (3.111)$$

Given a configuration of r compact objects $\{V_\alpha\}$. Choose an orthonormal basis $\{q^\alpha_{\boldsymbol{i}_\alpha}(\boldsymbol{x}_\alpha)\}$ on the surfaces Q_α. We discuss how to find this basis in the next section. Because of orthogonality things simplify a little. The elements in the matrix D^α, given in equation (3.79), can be written as

$$D^\alpha_{\boldsymbol{i}_\alpha \boldsymbol{j}_\alpha} = \int_{Q_\alpha} dA_{\boldsymbol{x}_\alpha} q^{\alpha *}_{\boldsymbol{i}_\alpha}(\boldsymbol{x}_\alpha) q^\alpha_{\boldsymbol{j}_\alpha}(\boldsymbol{x}_\alpha) = \delta_{\boldsymbol{i}_\alpha \boldsymbol{j}_\alpha}, \tag{3.112}$$

and the matrices $\mathcal{G}^\alpha$ and $\mathcal{G}^{\alpha\beta}$, given in equation (3.78) and (3.89), become

$$\begin{aligned} \mathcal{G}^\alpha_{\boldsymbol{i}_\alpha \boldsymbol{k}_\alpha} &= \sum_{\boldsymbol{j}_\alpha} D^\alpha_{\boldsymbol{i}_\alpha \boldsymbol{j}_\alpha} G^\alpha_{\boldsymbol{j}_\alpha \boldsymbol{k}_\alpha} = \sum_{\boldsymbol{j}_\alpha} \delta_{\boldsymbol{i}_\alpha \boldsymbol{j}_\alpha} G^\alpha_{\boldsymbol{j}_\alpha \boldsymbol{k}_\alpha} = G^\alpha_{\boldsymbol{i}_\alpha \boldsymbol{k}_\alpha}, \\ \mathcal{G}^{\alpha\beta}_{\boldsymbol{i}_\alpha \boldsymbol{k}_\beta} &= \sum_{\boldsymbol{j}_\alpha} D^\alpha_{\boldsymbol{i}_\alpha \boldsymbol{j}_\alpha} G^{\alpha\beta}_{\boldsymbol{j}_\alpha \boldsymbol{k}_\beta} = \sum_{\boldsymbol{j}_\alpha} \delta_{\boldsymbol{i}_\alpha \boldsymbol{j}_\alpha} G^{\alpha\beta}_{\boldsymbol{j}_\alpha \boldsymbol{k}_\beta} = G^{\alpha\beta}_{\boldsymbol{i}_\alpha \boldsymbol{k}_\beta}. \end{aligned} \tag{3.113}$$

The final formula for the Casimir energy is

$$\mathcal{E} = \frac{\hbar}{2\pi} \int_0^\infty d\kappa \ln \det M(i\kappa), \tag{3.114}$$

where the matrix $M(i\kappa)$ is given by

$$M^{\alpha\beta} = \mathbf{1}\delta_{\alpha\beta} + [T^\alpha]^{-1} U^{\alpha\beta}(1 - \delta_{\alpha\beta}) \qquad \alpha, \beta = 1, ..., r, \tag{3.115}$$

and the elements in the self-adjoint matrices T^α and $U^{\alpha\beta}$ are given by

$$\begin{aligned} T^\alpha_{\boldsymbol{i}_\alpha \boldsymbol{k}_\alpha} &= \mathcal{G}^\alpha_{\boldsymbol{i}_\alpha \boldsymbol{k}_\alpha} + \mathcal{G}^{\alpha *}_{\boldsymbol{k}_\alpha \boldsymbol{i}_\alpha} = \mathcal{G}^\alpha_{\boldsymbol{i}_\alpha \boldsymbol{k}_\alpha} + \mathcal{G}^\alpha_{\boldsymbol{k}_\alpha \boldsymbol{i}_\alpha} = G^\alpha_{\boldsymbol{i}_\alpha \boldsymbol{k}_\alpha} + G^\alpha_{\boldsymbol{k}_\alpha \boldsymbol{i}_\alpha}, \\ U^{\alpha\beta}_{\boldsymbol{i}_\alpha \boldsymbol{k}_\beta} &= \mathcal{G}^{\alpha\beta}_{\boldsymbol{i}_\alpha \boldsymbol{k}_\beta} + \mathcal{G}^{\beta\alpha *}_{\boldsymbol{k}_\beta \boldsymbol{i}_\alpha} = \mathcal{G}^{\alpha\beta}_{\boldsymbol{i}_\alpha \boldsymbol{k}_\beta} + \mathcal{G}^{\beta\alpha}_{\boldsymbol{k}_\beta \boldsymbol{i}_\alpha} = G^{\alpha\beta}_{\boldsymbol{i}_\alpha \boldsymbol{k}_\beta} + G^{\beta\alpha}_{\boldsymbol{k}_\beta \boldsymbol{i}_\alpha}. \end{aligned} \tag{3.116}$$

The elements of the matrices G^α and $G^{\alpha\beta}$ are given by equation (3.76) and (3.87);

$$\begin{aligned} G^\alpha_{\boldsymbol{i}_\alpha \boldsymbol{j}_\alpha} &= \int_{Q_\alpha} dA_{\boldsymbol{x}'_\alpha} G^\alpha_{\boldsymbol{i}_\alpha}(\boldsymbol{x}'_\alpha) q^\alpha_{\boldsymbol{j}_\alpha}(\boldsymbol{x}'_\alpha), \\ G^{\alpha\beta}_{\boldsymbol{i}_\alpha \boldsymbol{j}_\beta} &= \int_{Q_\beta} dA_{\boldsymbol{x}'_\beta} G^{\alpha\beta}_{\boldsymbol{i}_\alpha}(\boldsymbol{x}'_\beta) q^\beta_{\boldsymbol{j}_\beta}(\boldsymbol{x}'_\beta), \end{aligned} \tag{3.117}$$

where $G^\alpha_{\boldsymbol{i}_\alpha}(\boldsymbol{x}'_\alpha)$ and $G^{\alpha\beta}_{\boldsymbol{i}_\alpha}(\boldsymbol{x}'_\beta)$ are defined as the coefficients of the expansion of the Green's function in the basis $q^\alpha_{\boldsymbol{i}_\alpha}(\boldsymbol{x}_\alpha)$ (see equations (3.85) and (3.74)). Since the basis is orthonormal, these coefficients are given by

$$\begin{aligned} G^\alpha_{\boldsymbol{i}_\alpha}(\boldsymbol{x}'_\alpha) &= \int_{Q_\alpha} dA_{\boldsymbol{x}_\alpha} G^\alpha(\boldsymbol{x}_\alpha, \boldsymbol{x}'_\alpha) q^\alpha_{\boldsymbol{j}_\alpha}(\boldsymbol{x}_\alpha), \\ G^{\alpha\beta}_{\boldsymbol{i}_\alpha}(\boldsymbol{x}'_\beta) &= \int_{Q_\alpha} dA_{\boldsymbol{x}_\alpha} G^\beta(\boldsymbol{x}_\alpha, \boldsymbol{x}'_\beta) q^\alpha_{\boldsymbol{j}_\alpha}(\boldsymbol{x}_\alpha). \end{aligned} \tag{3.118}$$

Thus we get

$$\begin{aligned} G^{\alpha}_{\boldsymbol{i}_\alpha \boldsymbol{j}_\alpha} &= \int_{Q_\alpha} dA_{\boldsymbol{x}'_\alpha} \int_{Q_\alpha} dA_{\boldsymbol{x}_\alpha}\, q^{\alpha}_{\boldsymbol{i}_\alpha}(\boldsymbol{x}_\alpha) G^{\alpha}(\boldsymbol{x}_\alpha, \boldsymbol{x}'_\alpha) q^{\alpha}_{\boldsymbol{j}_\alpha}(\boldsymbol{x}'_\alpha), \\ G^{\alpha\beta}_{\boldsymbol{i}_\alpha \boldsymbol{j}_\beta} &= \int_{Q_\beta} dA_{\boldsymbol{x}'_\beta} \int_{Q_\alpha} dA_{\boldsymbol{x}_\alpha}\, q^{\alpha}_{\boldsymbol{i}_\alpha}(\boldsymbol{x}_\alpha) G^{\beta}(\boldsymbol{x}_\alpha, \boldsymbol{x}'_\beta) q^{\beta}_{\boldsymbol{j}_\beta}(\boldsymbol{x}'_\beta). \end{aligned} \tag{3.119}$$

When looking at equation (3.119), it seems like it is going be very expensive to fill the matrix M. However, as we will see in the next section, by discretizing the surfaces Q_α, it becomes an easy task to find an orthonormal basis $\{q^{\alpha}_{\boldsymbol{i}_\alpha}(\boldsymbol{x}_\alpha)\}$. The fact that the basis is orthonormal, implies that the integration domain in equation (3.119) reduces a lot.

3.9 Discretization

The functional integral method is designed for arbitrary configurations of conductors. The general configurations will be discretized using triangles, but we also for the FIM use two different discretizations for the special configuration consisting of two parallel plates, namely both standard grids of squares and triangulations consisting of triangles. Doing this we can test how much the method depend on the discretization. In this section we take a look at how to find the orthonormal basis $\{q^{\alpha}_{\boldsymbol{i}_\alpha}(\boldsymbol{x}_\alpha)\}$ and how to calculate the matrices G^α and $G^{\alpha\beta}$ for the two different discretizations.

3.9.1 Square discretization of the parallel plates

Fix a coordinate system such that the plates are lying in the planes $z = z_1 = -\frac{a}{2}$ and $z = z_2 = \frac{a}{2}$. Let the plates have length L in both x- and y-direction. Fix two grids such that S^{α}_{kl} is the square with center in $\boldsymbol{s}_{kl} = ((k - \frac{1}{2})h, (l - \frac{1}{2})h, z_\alpha)$ and edges of length $h = \frac{L}{N}$, where N is the number of discretization points in both x- and y-direction. $\alpha = 1, 2$ and $k, l = 1, ..., N$. The double indices kl are made into single indices by letting $i = k + N(l - 1)$. Then i runs from 1 to N^2.

The complete set of functions $\{q^{\alpha}_i(\boldsymbol{x})\}$ defined on the plates Q_α, $\alpha = 1, 2$, is chosen to be

$$q^{\alpha}_i(\boldsymbol{x}) = \begin{cases} \frac{1}{h} & \boldsymbol{x} \in S^{\alpha}_i \\ 0 & \text{else.} \end{cases} \tag{3.120}$$

With this basis we get

$$D^{\alpha}_{ij} = \iint\limits_{Q_\alpha} dA_{\boldsymbol{x}} q^{\alpha}_i(\boldsymbol{x}) q^{\alpha}_j(\boldsymbol{x}) = \frac{1}{h^2} \iint\limits_{S^{\alpha}_i} dA_{\boldsymbol{x}} = \delta_{ij}. \tag{3.121}$$

We see that the basis is orthonormal.

3.9.1.1 Matrix elements $G_{ij}^{\alpha\beta}$

For $\alpha \neq \beta$

$$\begin{aligned} G_{ij}^{\alpha\beta} &= \iint\limits_{Q_\beta} dA_{\boldsymbol{x'}} \iint\limits_{Q_\alpha} dA_{\boldsymbol{x}} q_i^\alpha(\boldsymbol{x}) G^\beta(\boldsymbol{x}, \boldsymbol{x'}) q_j^\beta(\boldsymbol{x'}) \\ &= \frac{1}{4\pi h^2} \iint\limits_{S_j^\beta} dA_{\boldsymbol{x'}} \iint\limits_{S_i^\alpha} dA_{\boldsymbol{x}} \frac{e^{-\kappa\|\boldsymbol{x}-\boldsymbol{x'}\|}}{\|\boldsymbol{x}-\boldsymbol{x'}\|}. \end{aligned} \tag{3.122}$$

This integral is non singular and can be approximated using the midpoint rule,

$$G_{ij}^{\alpha\beta} \approx \frac{h^2}{4\pi} \frac{e^{-\kappa\|\boldsymbol{s}_i^\alpha - \boldsymbol{s}_j^\beta\|}}{\|\boldsymbol{s}_i^\alpha - \boldsymbol{s}_j^\beta\|}. \tag{3.123}$$

3.9.1.2 Matrix elements G_{ij}^{α}

$$\begin{aligned} G_{ij}^{\alpha} &= \iint\limits_{Q_\alpha} dA_{\boldsymbol{x'}} \iint\limits_{Q_\alpha} dA_{\boldsymbol{x}} q_i^\alpha(\boldsymbol{x}) G^\alpha(\boldsymbol{x}, \boldsymbol{x'}) q_j^\alpha(\boldsymbol{x'}) \\ &= \frac{1}{4\pi h^2} \iint\limits_{S_j^\alpha} dA_{\boldsymbol{x'}} \iint\limits_{S_i^\alpha} dA_{\boldsymbol{x}} \frac{e^{-\kappa\|\boldsymbol{x}-\boldsymbol{x'}\|}}{\|\boldsymbol{x}-\boldsymbol{x'}\|}. \end{aligned} \tag{3.124}$$

When $i \neq j$, there is no singularity in the integrand, and the integral can be approximated using the midpoint rule,

$$G_{ij}^{\alpha} \approx \frac{h^2}{4\pi} \frac{e^{-\kappa\|\boldsymbol{s}_i^\alpha - \boldsymbol{s}_j^\alpha\|}}{\|\boldsymbol{s}_i^\alpha - \boldsymbol{s}_j^\alpha\|}. \tag{3.125}$$

If $i = j$;

$$G_{ii}^{\alpha} = \frac{1}{4\pi h^2} \iint\limits_{S_i^\alpha} dA_{\boldsymbol{x'}} \iint\limits_{S_i^\alpha} dA_{\boldsymbol{x}} \frac{e^{-\kappa\|\boldsymbol{x}-\boldsymbol{x'}\|}}{\|\boldsymbol{x}-\boldsymbol{x'}\|}. \tag{3.126}$$

Wee see that there is a singularity in the integrand when $\boldsymbol{x} = \boldsymbol{x'}$, thus we have to define how to perform the integral. We are going to calculate the integral almost the same way as we calculated the diagonal elements in the boundary integral method. Keep $\boldsymbol{x'}$ fixed and look at the inner integral, abbreviated I_{inner}. Let D_ϵ be the hemisphere with radius ϵ, centered around $\boldsymbol{x'}$. We define the inner integral as

$$I_{\text{inner}} = PV_{\boldsymbol{x'}} \iint\limits_{S_i^\alpha} dsdt \, \frac{e^{-\kappa\|\boldsymbol{x}-\boldsymbol{x'}\|}}{\|\boldsymbol{x}-\boldsymbol{x'}\|} + \lim_{\epsilon\to 0} \iint\limits_{D_\epsilon} dsdt \, \frac{e^{-\kappa\|\boldsymbol{x}-\boldsymbol{x'}\|}}{\|\boldsymbol{x}-\boldsymbol{x'}\|}. \tag{3.127}$$

Similar calculations to those done in section 2.4 give that the contribution from integrating over D_ϵ is zero when $\epsilon \to 0$.

Thus

$$G_{ii}^{\alpha} = \frac{1}{4\pi h^2} \iint\limits_{S_i^{\alpha}} dA_{\boldsymbol{x'}} \left(PV_{\boldsymbol{x'}} \iint\limits_{S_i^{\alpha}} dA_{\boldsymbol{x}} \frac{e^{-\kappa\|\boldsymbol{x}-\boldsymbol{x'}\|}}{\|\boldsymbol{x}-\boldsymbol{x'}\|} \right). \tag{3.128}$$

Define $\boldsymbol{s} = (s,t)$ and $\boldsymbol{s}_3 = (s,t,0)$. A parametrization of the squares is given by

$$\boldsymbol{X}_i^{\alpha}(\boldsymbol{s}) = \boldsymbol{s}_i^{\alpha} + \boldsymbol{s}_3, \quad \boldsymbol{s} = (s,t) \in S = \left[-\tfrac{h}{2}, \tfrac{h}{2}\right] \times \left[-\tfrac{h}{2}, \tfrac{h}{2}\right]. \tag{3.129}$$

Thus

$$\|\boldsymbol{N}\| = \|\partial_s \boldsymbol{X}_i^{\alpha} \times \partial_t \boldsymbol{X}_i^{\alpha}\| = 1. \tag{3.130}$$

Doing the same for the primed coordinates, we obtain

$$\|\boldsymbol{x}-\boldsymbol{x'}\| = \|\boldsymbol{X}_i^{\alpha}(\boldsymbol{s}) - \boldsymbol{X}_i'^{\alpha}(\boldsymbol{s'})\| = \|\boldsymbol{s}_i^{\alpha} + \boldsymbol{s}_3 - (\boldsymbol{s}_i^{\alpha} + \boldsymbol{s}_3')\| = \|\boldsymbol{s}_3 - \boldsymbol{s}_3'\| = \|\boldsymbol{s}-\boldsymbol{s'}\|, \tag{3.131}$$

and the integral changes to

$$G_{ii}^{\alpha} = \frac{1}{4\pi h^2} \iint\limits_{S} ds'dt' \left(PV_{\boldsymbol{s'}} \iint\limits_{S} dsdt \, \frac{e^{-\kappa\|\boldsymbol{s}-\boldsymbol{s'}\|}}{\|\boldsymbol{s}-\boldsymbol{s'}\|} \right). \tag{3.132}$$

Using the function f, given by

$$f(r;\omega) = \frac{e^{-\omega r}}{r}, \tag{3.133}$$

the inner integral can be written as

$$I_{\text{inner}} = PV_{\boldsymbol{s'}} \iint\limits_{S} dsdt \; f(\|\boldsymbol{s}-\boldsymbol{s'}\|;\kappa). \tag{3.134}$$

Use the fact that $f(r;\omega) = \nabla \cdot \boldsymbol{g}(\boldsymbol{r};\omega)$, where $\boldsymbol{g}$ is given in equation (2.124), and the divergence theorem to obtain

$$I_{\text{inner}} = \oint\limits_{\partial S} dl_{\boldsymbol{s}} \, \boldsymbol{n} \cdot \boldsymbol{g}(\boldsymbol{s}-\boldsymbol{s'};\kappa) + \lim_{\epsilon\to 0} \oint\limits_{C_\epsilon} dl_{\boldsymbol{s}} \, \boldsymbol{n} \cdot \boldsymbol{g}(\boldsymbol{s}-\boldsymbol{s'};\kappa), \tag{3.135}$$

where $\partial S = C_1 \cup C_2 \cup C_3 \cup C_4$ is boundary of the square S, and C_ϵ is the boundary of the hemisphere D_ϵ. Calculations very similar to equations (2.127) - (2.128), show that there is no contribution from the integration around C_ϵ. Thus

$$I_{\text{inner}} = \oint\limits_{\partial S} dl_{\boldsymbol{s}} \, \boldsymbol{n} \cdot \frac{\boldsymbol{s}-\boldsymbol{s'}}{\kappa\|\boldsymbol{s}-\boldsymbol{s'}\|^2} \left(1 - e^{-\kappa\|\boldsymbol{s}-\boldsymbol{s'}\|}\right). \tag{3.136}$$

Inserting this into equation (3.132) and changing order of integration gives

$$G_{ii}^{\alpha} = \frac{1}{4\pi h^2} \oint\limits_{\partial S} dl_{\boldsymbol{s}} \int\limits_{-\frac{h}{2}}^{\frac{h}{2}} \int\limits_{-\frac{h}{2}}^{\frac{h}{2}} ds' dt' \, \boldsymbol{n} \cdot \frac{\boldsymbol{s} - \boldsymbol{s'}}{\kappa \|\boldsymbol{s} - \boldsymbol{s'}\|^2} \left(1 - e^{-\kappa \|\boldsymbol{s} - \boldsymbol{s'}\|}\right). \tag{3.137}$$

Since the singularity is removed, the integrals over s' and t' can be approximated using the midpoint rule;

$$G_{ii}^{\alpha} \approx \frac{1}{4\pi} \oint\limits_{\partial S} dl \, \boldsymbol{n} \cdot \frac{\boldsymbol{s}}{\kappa \|\boldsymbol{s}\|^2} \left(1 - e^{-\kappa \|\boldsymbol{s}\|}\right). \tag{3.138}$$

Using the parametrization of ∂S given in equation (2.130), we get

$$\begin{aligned} G_{ii}^{\alpha} &\approx \frac{1}{4\pi} \int\limits_{-h/2}^{h/2} dt \sum_{i=1}^{4} \boldsymbol{n}_i \cdot \frac{\boldsymbol{\gamma}_i(t)}{\kappa \|\boldsymbol{\gamma}_i(t)\|^2} \left(1 - e^{-\kappa \|\boldsymbol{\gamma}_i(t)\|}\right) \\ &= \frac{h}{2\pi\kappa} \int\limits_{-h/2}^{h/2} dt \, \frac{1 - e^{-\kappa \sqrt{t^2 + (\frac{h}{2})^2}}}{t^2 + (\frac{h}{2})^2}. \end{aligned} \tag{3.139}$$

Observe that this result is very similar to the expression for the diagonal elements in the boundary integral method (see equation (2.131)), the only difference is the sign. The integral is calculated numerically using the midpoint rule or a Gaussian quadrature.

3.9.2 Triangulation of surfaces of arbitrary shape

Let S_i^{α} be a triangle represented by its vertices $\boldsymbol{x_{1_i}}, \boldsymbol{x_{2_i}}, \boldsymbol{x_{3_i}}$.

The orthonormal basis is chosen to be

$$q_i^{\alpha}(\boldsymbol{x}) = \begin{cases} \frac{1}{\sqrt{A_i^{\alpha}}} & \boldsymbol{x} \in S_i^{\alpha} \\ 0 & \text{else,} \end{cases} \tag{3.140}$$

where A_i^{α} is the area of the triangle S_i^{α}.

3.9.2.1 Matrix elements $G_{ij}^{\alpha\beta}$

For $\alpha \neq \beta$

$$\begin{aligned} G_{ij}^{\alpha\beta} &= \iint\limits_{Q_\beta} dA_{\boldsymbol{x'}} \iint\limits_{Q_\alpha} dA_{\boldsymbol{x}} q_i^{\alpha}(\boldsymbol{x}) G^{\beta}(\boldsymbol{x}, \boldsymbol{x'}) q_j^{\beta}(\boldsymbol{x'}) \\ &= \frac{1}{4\pi \sqrt{A_i^{\alpha} A_j^{\beta}}} \iint\limits_{S_j^{\beta}} dA_{\boldsymbol{x'}} \iint\limits_{S_i^{\alpha}} dA_{\boldsymbol{x}} \frac{e^{-\kappa \|\boldsymbol{x} - \boldsymbol{x'}\|}}{\|\boldsymbol{x} - \boldsymbol{x'}\|}. \end{aligned} \tag{3.141}$$

This integral is approximated using the midpoint rule

$$G_{ij}^{\alpha\beta} \approx \frac{A_i^\alpha A_j^\beta}{4\pi\sqrt{A_i^\alpha A_j^\beta}} \frac{e^{-\kappa\|\boldsymbol{s_i}-\boldsymbol{s_j}\|}}{\|\boldsymbol{s_i}-\boldsymbol{s_j}\|} = \frac{\sqrt{A_i^\alpha A_j^\beta}}{4\pi} \frac{e^{-\kappa\|\boldsymbol{s_i}-\boldsymbol{s_j}\|}}{\|\boldsymbol{s_i}-\boldsymbol{s_j}\|}, \tag{3.142}$$

where $\boldsymbol{s_i}$ is the center of mass, i.e. $\boldsymbol{s_i} = \frac{1}{3}\left(\boldsymbol{x_{1_i}} + \boldsymbol{x_{2_i}} + \boldsymbol{x_{3_i}}\right)$.

3.9.2.2 Matrix elements G_{ij}^α

$$\begin{aligned} G_{ij}^\alpha &= \iint\limits_{Q_\alpha} dA_{\boldsymbol{x'}} \iint\limits_{Q_\alpha} dA_{\boldsymbol{x}} q_i^\alpha(\boldsymbol{x}) G^\alpha(\boldsymbol{x},\boldsymbol{x'}) q_j^\alpha(\boldsymbol{x'}) \\ &= \frac{1}{4\pi\sqrt{A_i^\alpha A_j^\alpha}} \iint\limits_{S_j^\alpha} dA_{\boldsymbol{x'}} \iint\limits_{S_i^\alpha} dA_{\boldsymbol{x}} \frac{e^{-\kappa\|\boldsymbol{x}-\boldsymbol{x'}\|}}{\|\boldsymbol{x}-\boldsymbol{x'}\|}. \end{aligned} \tag{3.143}$$

When $i \neq j$ we use the midpoint rule;

$$G_{ij}^\alpha \approx \frac{\sqrt{A_i^\alpha A_j^\alpha}}{4\pi} \frac{e^{-\kappa\|\boldsymbol{s_i}-\boldsymbol{s_j}\|}}{\|\boldsymbol{s_i}-\boldsymbol{s_j}\|}. \tag{3.144}$$

When $i = j$ we do the same as for the squares. We extend the triangle into a triangle and a hemisphere centered around $\boldsymbol{x'}$. The integral over the hemisphere doesn't contribute when the radius goes to zero, thus G_{ii}^α is given as the principal value integral

$$G_{ii}^\alpha = \frac{1}{4\pi A_i^\alpha} \iint\limits_{S_i^\alpha} dA_{\boldsymbol{x'}} \left(PV_{\boldsymbol{x'}} \iint\limits_{S_i^\alpha} dA_{\boldsymbol{x}} \frac{e^{-\kappa\|\boldsymbol{x}-\boldsymbol{x'}\|}}{\|\boldsymbol{x}-\boldsymbol{x'}\|} \right). \tag{3.145}$$

We now proceed almost as we did when we calculated the diagonal elements a_{kk}^{ij} in the BIM. Choose coordinates such that the triangle S_i^α is lying in the xy-plane with the vertex $\boldsymbol{x_{1_i}}$ in the origin and the vertex $\boldsymbol{x_{2_i}}$ on the positive part of the x axis. Let $\boldsymbol{r_i} = \boldsymbol{x_{2_i}} - \boldsymbol{x_{1_i}}$ and $\boldsymbol{q_i} = \boldsymbol{x_{3_i}} - \boldsymbol{x_{1_i}}$. In more detail,

$$\boldsymbol{x_{1_i}} \to \boldsymbol{0} = (0,0), \tag{3.146}$$

$$\boldsymbol{x_{2_i}} \to \boldsymbol{u_i} = (u_i, 0) = (\|\boldsymbol{r_i}\|, 0), \tag{3.147}$$

$$\boldsymbol{x_{3_i}} \to \boldsymbol{v_i} = (v_i, w_i) = \frac{1}{\|\boldsymbol{r_i}\|}\left(\boldsymbol{r_i}\cdot\boldsymbol{q_i}, \|\boldsymbol{r_i}\times\boldsymbol{q_i}\|\right). \tag{3.148}$$

In these coordinates the triangle S_i^α has the vertexes $\boldsymbol{0}$, $\boldsymbol{u_i}$ and $\boldsymbol{v_i}$. The center of mass becomes $\boldsymbol{s_i} = \frac{1}{3}(\boldsymbol{u_i} + \boldsymbol{v_i})$. Using these coordinates and the function f, given in equation

(3.133), we obtain

$$G_{ii}^{\alpha} = \frac{1}{4\pi A_i^{\alpha}} \iint\limits_{S_i^{\alpha}} dA_{\boldsymbol{x'}} \left(PV_{\boldsymbol{x'}} \iint\limits_{S_i^{\alpha}} dA_{\boldsymbol{x}} f(\|\boldsymbol{x} - \boldsymbol{x'}\|; \kappa) \right). \tag{3.149}$$

Using the fact that $f(r;\kappa) = \nabla \cdot \boldsymbol{g}(\boldsymbol{r};\kappa)$, where $\boldsymbol{g}$ is given in equation (2.124), and the divergence theorem, the principal value integral becomes

$$\oint\limits_{\partial S_i^{\alpha}} dl_{\boldsymbol{x}}\, \boldsymbol{n} \cdot \boldsymbol{g}(\boldsymbol{x} - \boldsymbol{x'}; \kappa) + \lim_{\epsilon \to 0} \oint\limits_{C_{i,\epsilon}^{\alpha}} dl_{\boldsymbol{x}}\, \boldsymbol{n} \cdot \boldsymbol{g}(\boldsymbol{x} - \boldsymbol{x'}; \kappa), \tag{3.150}$$

where $\partial S_i^{\alpha} = C_{1_i} \cup C_{2_i} \cup C_{3_i}$ is boundary of the triangle S_i^{α} and $C_{i,\epsilon}^{\alpha}$ is the boundary of the hemisphere $D_{i,\epsilon}^{\alpha}$. There is no contribution from the second integral. Thus, changing order of integration, we obtain

$$G_{ii}^{\alpha} = \frac{1}{4\pi A_i^{\alpha}} \oint\limits_{\partial S_i^{\alpha}} dl_{\boldsymbol{x}} \iint\limits_{S_i^{\alpha}} dA_{\boldsymbol{x'}}\, \boldsymbol{n} \cdot \frac{\boldsymbol{x} - \boldsymbol{x'}}{\kappa \|\boldsymbol{x} - \boldsymbol{x'}\|^2} \left(1 - e^{-\kappa \|\boldsymbol{x} - \boldsymbol{x'}\|}\right). \tag{3.151}$$

Use the midpoint rule to approximate the double integral;

$$G_{ii}^{\alpha} \approx \frac{1}{4\pi} \oint\limits_{\partial S_i^{\alpha}} dl_{\boldsymbol{x}}\, \boldsymbol{n} \cdot \frac{\boldsymbol{x} - \boldsymbol{s_i}}{\kappa \|\boldsymbol{x} - \boldsymbol{s_i}\|^2} \left(1 - e^{-\kappa \|\boldsymbol{x} - \boldsymbol{s_i}\|}\right). \tag{3.152}$$

Using the parametrization given in equation (2.147),

$$\begin{aligned} C_{1_i}: &\quad \boldsymbol{\gamma_{1_i}}(t) = \boldsymbol{u_i} t, \quad t \in [0,1], \\ C_{2_i}: &\quad \boldsymbol{\gamma_{2_i}}(t) = \boldsymbol{u_i} + (\boldsymbol{v_i} - \boldsymbol{u_i}) t, \quad t \in [0,1] \\ C_{3_i}: &\quad \boldsymbol{\gamma_{3_i}}(t) = \boldsymbol{v_i}(1 - t), \quad t \in [0,1], \end{aligned} \tag{3.153}$$

and the calculations done in equations (2.148) and (2.149), we obtain

$$G_{ii}^{\alpha} \approx \frac{A_i^{\alpha}}{6\pi\kappa} \int\limits_0^1 dt \sum_{j=1}^{3} \frac{1 - e^{-\kappa \|\boldsymbol{\gamma_{j_i}}(t) - \boldsymbol{s_i}\|}}{\|\boldsymbol{\gamma_{j_i}}(t) - \boldsymbol{s_i}\|^2}, \tag{3.154}$$

where

$$A_i^{\alpha} = \frac{u_i w_i}{2} \tag{3.155}$$

is the area of the triangle S_i^{α}. Observe that also here, the only difference from equation (2.150) is the sign. The integral is calculated numerically using the midpoint rule or a Gaussian quadrature.

Chapter 4

Mode summation method

We mentioned in chapter 1 that, in principle, the method of mode summation applies to any configuration. However, in most cases it is very hard to find the full frequency spectrum and a way to regularize the sum that determines the Casimir energy. Thus in practice, the method is limited to very symmetric configurations. In this chapter we use mode summation to derive expressions for the Casimir energy for two special symmetric configurations, namely parallel plates and concentric spheres.

4.1 Parallel plates

We are going to derive an expression the Casimir energy using two different alternatives. In the first alternative the regularization of the frequency sum is done by first applying *the argument principle* and then subtracting the high frequency part, whereas in the second *zeta-function regularization* is used.

Consider two parallel plates separated by a distance a. Assume that the plates are of infinite length and width. Let V_0 be the region between the two plates;

$$V_0 = \{\boldsymbol{x} = (x, y, z) \in \mathbb{R}^3 \mid 0 < z < a\}. \tag{4.1}$$

The two infinitely thin plates are located in the planes

$$Q_1 = \{\boldsymbol{x} \in \mathbb{R}^3 \mid z = 0\}, \tag{4.2}$$

$$Q_2 = \{\boldsymbol{x} \in \mathbb{R}^3 \mid z = a\}. \tag{4.3}$$

4.1.1 Alternative 1: Using the argument principle

Let V_- be the region below the plates and V_+ be the region above them,

$$V_- = \{\boldsymbol{x} \in \mathbb{R}^3 \mid z < 0\}, \tag{4.4}$$

$$V_+ = \{\boldsymbol{x} \in \mathbb{R}^3 \mid z > a\}. \tag{4.5}$$

The scalar field φ that "lives" in the different regions, we define as

$$\varphi(\boldsymbol{x}, t) = \begin{cases} \varphi_-(\boldsymbol{x}, t), & \boldsymbol{x} \in V_- \\ \varphi_0(\boldsymbol{x}, t), & \boldsymbol{x} \in V_0 \\ \varphi_+(\boldsymbol{x}, t), & \boldsymbol{x} \in V_+ \end{cases} \tag{4.6}$$

and the defining equation for the field is

$$\varphi_{tt}(\boldsymbol{x}, t) - c^2(z)\nabla^2\varphi(\boldsymbol{x}, t) = 0, \quad \boldsymbol{x} \in \mathbb{R}^3, \tag{4.7}$$

where

$$c(z) = \begin{cases} c_0, & z \in (0, a) \\ c_1, & \text{else.} \end{cases} \tag{4.8}$$

A Fourier transform of equation (4.7) in the time domain gives

$$\omega^2\varphi(\boldsymbol{x}) - c^2(z)\nabla^2\varphi(\boldsymbol{x}) = 0. \tag{4.9}$$

Continue by taking Fourier transforms in the $x-$ and $y-$direction;

$$-\varphi''(z) + \left(k^2 - \frac{\omega^2}{c^2(z)}\right)\varphi(z) = 0, \tag{4.10}$$

where $\boldsymbol{k} = (k_x, k_y)$ and $k^2 = \boldsymbol{k} \cdot \boldsymbol{k}$. By defining

$$q_j^2 = k^2 - \frac{\omega^2}{c_j^2}, \quad j = 0, 1, \tag{4.11}$$

we can write down equation (4.10) explicitly for the three different regions;

$$\begin{aligned} V_- : &\quad -\varphi_-''(z) + q_1^2\varphi_-(z) = 0, \\ V_0 : &\quad -\varphi_0''(z) + q_0^2\varphi_0(z) = 0, \\ V_+ : &\quad -\varphi_+''(z) + q_1^2\varphi_+(z) = 0. \end{aligned} \tag{4.12}$$

On the plates Q_1 and Q_2 we require the solution to be continuous;

$$\lim_{z\to 0^-} \varphi_-(z) = \lim_{z\to 0^+} \varphi_0(z), \tag{4.13}$$

$$\lim_{z\to a^-} \varphi_0(z) = \lim_{z\to a^+} \varphi_+(z). \tag{4.14}$$

We also require that the time derivative of the field, φ_t, is continuous here. The other boundary conditions will be derived from the requirement that no energy should be deposited into the boundaries. Following the steps we did in equations (2.27) - (2.34), but instead using wave equation (4.7), we obtain the energy flux

$$\boldsymbol{S}_e = -c^2(z)\varphi_t \nabla\varphi. \tag{4.15}$$

The normal component of the energy flux must be continuous across the plates if there is no energy deposition. Using the fact that the normal points in the z-direction and that φ_t is continuous, this requirement can be written as

$$\lim_{z\to 0^-} c_1^2\varphi_-'(z) = \lim_{z\to 0^+} c_0^2\varphi_0'(z), \tag{4.16}$$

$$\lim_{z\to a^-} c_0^2\varphi_0'(z) = \lim_{z\to a^+} c_1^2\varphi_+'(z). \tag{4.17}$$

The general solutions of equation (4.12) are

$$\begin{aligned} V_-: &\quad \varphi_-(z) = A_1 e^{q_1 z} + A_2 e^{-q_1 z}, \\ V_0: &\quad \varphi_0(z) = B_1 e^{q_0 z} + B_2 e^{-q_0 z}, \\ V_+: &\quad \varphi_+(z) = C_1 e^{q_1 z} + C_2 e^{-q_1 z}. \end{aligned} \tag{4.18}$$

Let $A_2 = C_1 = 0$ such that there is no exponential growth when $z \to \pm\infty$. The boundary conditions at $z = 0$ give

$$\begin{aligned} A_1 &= B_1 + B_2, \\ c_1^2 q_1 A_1 &= c_0^2 q_0 (B_1 - B_2). \end{aligned} \tag{4.19}$$

and for $z = a$ we obtain

$$\begin{aligned} B_1 e^{q_0 a} + B_2 e^{-q_0 a} &= C_2 e^{-q_1 a}, \\ c_0^2 q_0 (B_1 e^{q_0 a} - B_2 e^{-q_0 a}) &= -c_1^2 q_1 C_2 e^{-q_1 a}. \end{aligned} \tag{4.20}$$

We eliminate A_1 and C_2 and get the linear system

$$M\boldsymbol{B} = \boldsymbol{0}, \tag{4.21}$$

where

$$M = \begin{bmatrix} c_1^2 q_1 - c_0^2 q_0 & c_1^2 q_1 + c_0^2 q_0 \\ (c_1^2 q_1 + c_0^2 q_0) e^{q_0 a} & (c_1^2 q_1 - c_0^2 q_0) e^{-q_0 a} \end{bmatrix} \text{ and } \boldsymbol{B} = \begin{bmatrix} B_1 \\ B_2 \end{bmatrix}. \tag{4.22}$$

Equation (4.21) has non-trivial solutions if and only if

$$\det M = 0. \tag{4.23}$$

This relation determines the possible frequencies ω and can more conveniently be written as

$$g(\omega, k) = -e^{-q_1 a} \det M = e^{-q_1 a} \left((c_0^2 q_0 + c_1^2 q_1)^2 e^{q_0 a} - (c_0^2 q_0 - c_1^2 q_1)^2 e^{-q_0 a} \right) = 0, \tag{4.24}$$

where q_i is given by equation (4.11).

The energy of the system can be expressed as a sum over the frequencies, ω_n, which are roots of $g(\omega, k)$;

$$E = \frac{\hbar}{2} \int_{-\infty}^{\infty} \frac{dk_x}{2\pi} \int_{-\infty}^{\infty} \frac{dk_y}{2\pi} \sum_n \omega_n(\boldsymbol{k}) = \frac{\hbar}{8\pi^2} \iint_{\mathbb{R}^2} d\boldsymbol{k} \sum_n \omega_n(\boldsymbol{k}) \tag{4.25}$$

The sum $\sum_n \omega_n$ will be evaluated using the *argument principle*, which says the following:

Let h be an analytic function with no poles inside a positively oriented contour C and f a meromorphic function with no poles or zeros on C. Then

$$\frac{1}{2\pi i} \oint_C dz\, h(z) \frac{d}{dz} \ln f(z) = \sum_n m_n h(z_n^0) - k_n h(z_n^p), \tag{4.26}$$

where z_n^0 are the zeros, and z_n^p the poles of f inside the contour, and m_n and k_n are their respective multiplicity.

We are going to apply this principle to our problem by defining a contour $C = C_1 \bigcup C_R$, where

$$\begin{aligned} C_1 &= \left\{ ix \middle| \, x \in [-R, R] \right\}, \\ C_R &= \left\{ z = x + iy \in \mathbb{C} \middle| \, |z| = R, x > 0 \right\}. \end{aligned} \tag{4.27}$$

Let $h(z) = z$. Since the function $g(\omega, k)$ has no poles, the argument principle gives that

$$\sum_n \omega_n = \frac{1}{2\pi i} \lim_{R \to \infty} \oint_C d\omega\, \omega \frac{d}{d\omega} \ln g(\omega, k). \tag{4.28}$$

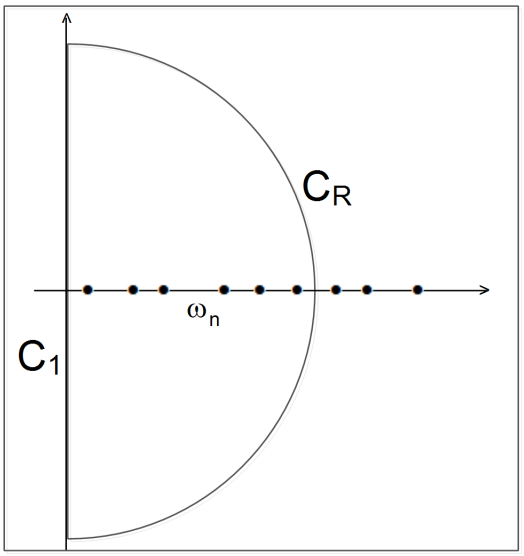

FIGURE 4.1: The integration contour $C = C_1 \cup C_R$

The energy is therefore

$$E = \frac{\hbar}{16\pi^3 i} \iint\limits_{\mathbb{R}^2} d\boldsymbol{k} \lim_{R\to\infty} \left(\int\limits_{iR}^{-iR} d\omega\, \omega \frac{d}{d\omega} \ln g(\omega, k) + \int\limits_{C_R} d\omega\, \omega \frac{d}{d\omega} \ln g(\omega, k) \right). \tag{4.29}$$

This expression is divergent and must be regularized. The regularization consists of subtracting the high frequency contribution. It will be assumed that the system is dispersive. This means that the response of the material in the boundaries to the modes is frequency-dependent, i.e $c_i = c_i(\omega)$. For large ω it is natural to assume that $c_0 = c_1 = c$ (c is the speed of light). The physical explanation is that the modes don't see the atoms in the boundaries because their frequencies are so high. Normal sized frequency modes experience the boundaries as perfectly conducting, i.e. $c_0 = c$ and $c_1 = 0$. Thus, for large ω, we have

$$q_j \approx \sqrt{k^2 - \frac{\omega^2}{c^2}} \approx i\frac{\omega}{c}, \quad j = 0, 1, \tag{4.30}$$

and therefore

$$g(\omega, k) \approx (c_0^2 q_0 + c_1^2 q_1)^2 e^{(q_0 - q_1)a} \approx (2ic\omega)^2 e^{i(\frac{1}{c} - \frac{1}{c})\omega a} \to -4c^2\omega^2, \tag{4.31}$$

$$g'(\omega, k) \to -8c^2\omega. \tag{4.32}$$

Thus $\frac{d}{d\omega}\ln g(\omega,k) = \omega\frac{g'(\omega,k)}{g(\omega,k)} \to 2$ along C_∞. The energy can therefore be written as

$$E = \frac{\hbar}{16\pi^3 i}\iint\limits_{\mathbb{R}^2} d\boldsymbol{k}\left(-\lim_{R\to\infty}\int\limits_{-iR}^{iR} d\omega\,\omega\frac{d}{d\omega}\ln(g(\omega,k)) + 2\int\limits_{C_\infty} d\omega\right). \tag{4.33}$$

Observe that there is no geometry dependence in the second integral and therefore this term will cancel when we subtract the high frequency part. The dominating contribution to the energy for large ω is

$$g_\infty(\omega,k) = (c_0^2 q_0 + c_1^2 q_1)^2 e^{(q_0-q_1)a}. \tag{4.34}$$

The energy associated to this contribution is

$$E_\infty = \frac{\hbar}{16\pi^3 i}\iint\limits_{\mathbb{R}^2} d\boldsymbol{k}\left(-\lim_{R\to\infty}\int\limits_{-iR}^{iR} d\omega\,\omega\frac{d}{d\omega}\ln(g_\infty(\omega,k)) + 2\int\limits_{C_\infty} d\omega\right). \tag{4.35}$$

Define the regularized Casimir energy as

$$\mathcal{E} = E - E_\infty = -\frac{\hbar}{16\pi^3 i}\iint\limits_{\mathbb{R}^2} d\boldsymbol{k}\lim_{R\to\infty}\int\limits_{-iR}^{iR} d\omega\,\omega\frac{d}{d\omega}\ln\left(\frac{g(\omega,k)}{g_\infty(\omega,k)}\right) \tag{4.36}$$

Integration by parts, followed by a change of variable $\omega = iu$, results in

$$\mathcal{E} = \frac{\hbar}{16\pi^3}\iint\limits_{\mathbb{R}^2} d\boldsymbol{k}\int\limits_{-\infty}^{\infty} du\,\ln\left(\frac{g(iu,k)}{g_\infty(iu,k)}\right), \tag{4.37}$$

where

$$\frac{g(iu,k)}{g_\infty(iu,k)} = 1 - \left(\frac{(c_0^2 q_0 - c_1^2 q_1)}{(c_0^2 q_0 + c_1^2 q_1)}\right)^2 e^{-2q_0 a}\Big|_{\omega=iu}. \tag{4.38}$$

We take the limit $c_0 \to c$ and $c_1 \to 0$ to simulate a perfect conductor. Then

$$\frac{g(iu,k)}{g_\infty(iu,k)} \to 1 - e^{-2q_1 a}\big|_{\omega=iu} = 1 - e^{-2\sqrt{\boldsymbol{k}^2 + \left(\frac{u}{c}\right)^2}a}. \tag{4.39}$$

By first changing to spherical coordinates and thereafter letting $v = 2\rho a$, we obtain

$$\begin{aligned}
\mathcal{E} &= \frac{\hbar}{16\pi^3} \int_{-\infty}^{\infty} dk_x \int_{-\infty}^{\infty} dk_y \int_{-\infty}^{\infty} du \, \ln\left(1 - e^{-2\sqrt{\boldsymbol{k}^2 + \left(\frac{u}{c}\right)^2}a}\right) \\
&= \frac{\hbar c}{16\pi^3} \int_0^{2\pi} d\theta \int_0^{\pi} d\phi \, \sin\phi \int_0^{\infty} d\rho \, \rho^2 \ln\left(1 - e^{-2\rho a}\right) \\
&= \frac{\hbar c}{16\pi^3} 2\pi \cdot 2 \int_0^{\infty} \frac{dv}{2a} \, \frac{v^2}{(2a)^2} \ln\left(1 - e^{-v}\right) \\
&= \frac{\hbar c}{32\pi^2 a^3} \int_0^{\infty} dv \, v^2 \ln\left(1 - e^{-v}\right). \qquad (4.40)
\end{aligned}$$

This integral is most easily calculated using *Mathematica*. We obtain $\pi^4/45$. Thus the Casimir energy for two parallel plates is given by

$$\mathcal{E}(a) = -\frac{\hbar c}{32\pi^2 a^3} \frac{\pi^4}{45} = -\frac{\pi^2 \hbar c}{1440 a^3} \approx -0.006854 \frac{\hbar c}{a^3}. \qquad (4.41)$$

4.1.2 Alternative 2: Zeta function regularization

We also derive the Casimir energy for two perfectly conducting parallel plates using zeta function regularization.

With this alternative it is only necessary to define the scalar field φ in the region between and on the plates;

$$\begin{aligned}
\varphi_{tt}(\boldsymbol{x}, t) - c^2 \nabla^2 \varphi(\boldsymbol{x}, t) = 0, \quad \boldsymbol{x} \in V_0, \\
\varphi|_{Q_j} = 0.
\end{aligned} \qquad (4.42)$$

Fourier transforms of equation (4.7) in the time domain and the x and y direction give

$$\varphi''(z) + q^2 \varphi(z) = 0, \qquad (4.43)$$

$$\varphi(0) = \varphi(a) = 0, \qquad (4.44)$$

where

$$q^2 = \frac{\omega^2}{c^2} - k^2 \qquad (4.45)$$

and $\boldsymbol{k} = (k_x, k_y)$ and $k^2 = \boldsymbol{k} \cdot \boldsymbol{k}$. Notice that q is defined oppositely of the previous section here. The general solution is

$$\varphi(z) = A \sin(qz) + B \cos(qz). \qquad (4.46)$$

The boundary conditions (4.44) give $B = 0$ and

$$q_n = \frac{n\pi}{a}, \quad n = 1, 2, 3, ... \tag{4.47}$$

Thus

$$\omega = \omega_n = c\sqrt{k_x^2 + k_y^2 + \left(\frac{n\pi}{a}\right)^2}, \quad n = 1, 2, 3, ... \tag{4.48}$$

and the energy is

$$E = \frac{\hbar}{2} \int_{-\infty}^{\infty} \frac{dk_x}{2\pi} \int_{-\infty}^{\infty} \frac{dk_y}{2\pi} \sum_{n=1}^{\infty} \omega_n. \tag{4.49}$$

This expression is of course divergent. We regularize by multiplying by ω_n^{-2s} and in the end letting $s \to 0$;

$$\mathcal{E} = \frac{\hbar}{2} \int_{-\infty}^{\infty} \frac{dk_x}{2\pi} \int_{-\infty}^{\infty} \frac{dk_y}{2\pi} \sum_{n=1}^{\infty} \omega_n^{1-2s}. \tag{4.50}$$

Introducing polar coordinates, we obtain

$$\mathcal{E} = \frac{\hbar}{2} \int_0^{\infty} \frac{dr}{2\pi}\, r \sum_{n=1}^{\infty} c\left(r^2 + \left(\frac{n\pi}{a}\right)^2\right)^{\frac{1}{2}-s}. \tag{4.51}$$

Interchange sum and integral, and then substitute $y = \frac{ar}{n\pi}$ to obtain

$$\begin{aligned}
\mathcal{E} &= \frac{\hbar c}{2} \frac{1}{2\pi} \sum_{n=1}^{\infty} \int_0^{\infty} \frac{n\pi dy}{a}\, \frac{n\pi y}{a} \left(\left(\frac{n\pi y}{a}\right)^2 + \left(\frac{n\pi}{a}\right)^2\right)^{\frac{1}{2}-s} \\
&= \frac{\hbar c}{4\pi} \sum_{n=1}^{\infty} \int_0^{\infty} dy\, y \left(y^2+1\right)^{\frac{1}{2}-s} \left(\frac{n\pi}{a}\right)^{3-2s} \\
&= \frac{\hbar c}{4\pi} \left(\frac{\pi}{a}\right)^{3-2s} \int_0^{\infty} dy\, y \left(y^2+1\right)^{\frac{1}{2}-s} \sum_{n=1}^{\infty} \frac{1}{n^{2s-3}}.
\end{aligned} \tag{4.52}$$

Both the integral and the sum diverge when $s \to 0$. However, we observe that both converge for $s > \frac{3}{2}$. We therefore are going to evaluate each of them in their domain of convergence and thereafter analytically continue to $s = 0$.

The integral can be calculated using the substitution $u = y^2 + 1$;

$$\int_0^{\infty} dy\, y \left(y^2+1\right)^{\frac{1}{2}-s} = \int_1^{\infty} \frac{du}{2}\, u^{\frac{1}{2}-s} = \frac{1}{2} \frac{u^{\frac{3}{2}-s}}{\frac{3}{2}-s} \Bigg|_{u=1}^{\infty} = -\frac{1}{3-2s} \Bigg|_{s=0} = -\frac{1}{3}. \tag{4.53}$$

The sum we recognize as a well-studied mathematical function, namely the Riemann zeta function ζ (see for example [18] and [19])

$$\sum_{n=1}^{\infty} \frac{1}{n^{2s-3}} = \zeta(2s-3)\Big|_{s=0} = \zeta(-3). \tag{4.54}$$

The series that defines the zeta function $\zeta(s)$ is divergent for $Re(s) \leq 1$. However, the zeta function $\zeta(s)$ can be uniquely analytically continued to the whole complex plane. There is a close relation between the zeta function and the Bernoulli polynomials B_n for integers n;

$$\zeta(-n) = -\frac{B_{n+1}(1)}{n+1}. \tag{4.55}$$

Thus

$$\zeta(-3) = -\frac{B_4(1)}{4} = \frac{1}{120}. \tag{4.56}$$

By inserting the results (4.53) and (4.56) into equation (4.52), we obtain

$$\mathcal{E} = \frac{\hbar c}{4\pi}\left(\frac{\pi}{a}\right)^3\left(-\frac{1}{3}\right)\frac{1}{120} = -\frac{\hbar c \pi^2}{1440 a^3}. \tag{4.57}$$

This of course the same result that we got using the first alternative. Note that we didn't subtract anything explicitly from the energy, using the zeta function regularization. In some sense the zeta regularization corresponds to the subtraction.

4.2 Two concentric spheres

The following derivation is based on a paper by M. Ozcan [20].

Consider two concentric spheres with radius R_1 and R_2, where $R_1 < R_2$. The defining equation for the scalar field in the space, V_0, between the two spheres is

$$\begin{aligned} \varphi_{tt}(\boldsymbol{x}, t) - c^2\nabla^2\varphi(\boldsymbol{x}, t) &= 0, \\ \varphi|_{Q_j} &= 0. \end{aligned} \tag{4.58}$$

A Fourier transform in time gives

$$\omega^2\varphi(\boldsymbol{x}) + c^2\nabla^2\varphi(\boldsymbol{x}) = 0. \tag{4.59}$$

In spherical coordinates the Laplace operator become

$$\nabla^2 = \frac{1}{r^2}\frac{\partial}{\partial r}\left(r^2\frac{\partial}{\partial r}\right) + \frac{1}{r^2\sin\theta}\frac{\partial}{\partial\theta}\left(\sin\theta\frac{\partial}{\partial\theta}\right) + \frac{1}{r^2\sin^2\theta}\frac{\partial^2}{\partial\phi^2}. \tag{4.60}$$

Let $k = \omega/c$. Then equation (4.58) can be written as

$$\frac{1}{r^2}\frac{\partial}{\partial r}\left(r^2\frac{\partial\varphi}{\partial r}\right) + \frac{1}{r^2\sin\theta}\frac{\partial}{\partial\theta}\left(\sin\theta\frac{\partial\varphi}{\partial\theta}\right) + \frac{1}{r^2\sin^2\theta}\frac{\partial^2\varphi}{\partial\phi^2} + k^2\varphi = 0, \tag{4.61}$$

where $\varphi = \varphi(r,\theta,\phi)$, $r \in [R_1, R_2]$, $\theta \in [0, 2\pi)$ and $\phi \in [0, \pi)$. The boundary condition become

$$\varphi(R_1,\theta,\phi) = \varphi(R_2,\theta,\phi) = 0. \tag{4.62}$$

4.2.1 Solution of equation (4.61)

Separation of variables will be used to solve equation (4.61);

$$\varphi(r,\theta,\phi) = R(r)\Theta(\theta)\Phi(\phi). \tag{4.63}$$

Multiply equation (4.61) by $r^2/R\Theta\Phi$,

$$\frac{1}{R}\frac{d}{dr}\left(r^2\frac{dR}{dr}\right) + k^2r^2 + \frac{1}{\Theta\sin\theta}\frac{d}{d\theta}\left(\sin\theta\frac{d\Theta}{d\theta}\right) + \frac{1}{\Phi\sin^2\theta}\frac{d^2\Phi}{d\phi^2} = 0. \tag{4.64}$$

We first try to find the angular part of the field φ. When we multiply equation (4.64) by $\sin^2\theta$, only the last term involves ϕ, whereas the first three involves r and θ. Therefore the last term must be constant,

$$\frac{1}{\Phi}\frac{d^2\Phi}{d\phi^2} = -m^2. \tag{4.65}$$

The solution is

$$\Phi_m(\phi) = c_m e^{im\phi}, \quad m \in \mathbb{Z}. \tag{4.66}$$

The condition $\Phi(\phi) = \Phi(\phi + 2\pi)$ implies that m must be an integer. We can wlog. choose $c_m = 1$. Substituting (4.65) into equation (4.64), we obtain

$$\frac{1}{R}\frac{d}{dr}\left(r^2\frac{dR}{dr}\right) + k^2r^2 + \frac{1}{\Theta\sin\theta}\frac{d}{d\theta}\left(\sin\theta\frac{d\Theta}{d\theta}\right) - \frac{m^2}{\sin^2\theta} = 0. \tag{4.67}$$

The third and fourth terms only depend on θ, whereas the first and second term only depend on r. Therefore the sum of the third and fourth term must be a constant, which we write as $-l(l+1)$;

$$\frac{1}{\Theta\sin\theta}\frac{d}{d\theta}\left(\sin\theta\frac{d\Theta}{d\theta}\right) - \frac{m^2}{\sin^2\theta} = -l(l+1). \tag{4.68}$$

Multiply by Θ to get

$$\frac{1}{\sin\theta}\frac{d}{d\theta}\left(\sin\theta\frac{d\Theta}{d\theta}\right) + \left(l(l+1) + \frac{m^2}{\sin^2\theta}\right)\Theta = 0. \tag{4.69}$$

Make the substitution $x = \cos\theta$;

$$\frac{d}{dx}\left[(1-x^2)\frac{d\Theta(x)}{dx}\right] + \left(l(l+1) + \frac{m^2}{1-x^2}\right)\Theta(x) = 0. \tag{4.70}$$

Equation (4.70) is the *Associated Legendre Equation*, and the solution is

$$\Theta_l^m(\cos\theta) = P_l^m(\cos\theta), \tag{4.71}$$

where P_l^m are the *Associated Legendre Polynomials*. Only the choices $l = 0, 1, 2...$ and $m = -l, -l+1, ..., l-1, l$ will make sure that the solution is finite for $-l \leq \cos\theta \leq 1$. The two solutions Φ_m and Θ_l^m can be combined into a *Spherical Harmonic*, $Y_l^m(\theta, \phi)$, given by

$$Y_l^m(\theta,\phi) = C_l^m P_l^m(\cos\theta)e^{im\phi}, \quad l = 0, 1, 2..., m = -l, -l+1, ..., l-1, l, \tag{4.72}$$

where C_l^m is a normalization constant.

By substituting equation (4.68) back into equation (4.67), only the radial part remains;

$$r^2\frac{d^2R}{dr^2} + 2r\frac{dR}{dr} + \left[k^2r^2 + l(l+1)\right]R = 0. \tag{4.73}$$

Define a function Z by

$$R(r) = \frac{Z(r)}{\sqrt{kr}}. \tag{4.74}$$

Substituting this into equation (4.73), we get

$$r^2\frac{d^2Z}{dr^2} + r\frac{dZ}{dr} + \left[k^2r^2 - \left(l+\frac{1}{2}\right)^2\right]Z = 0. \tag{4.75}$$

This is a *Bessel equation* of order $l + 1/2$. The complete solution is

$$Z(r) = A_l' J_{l+1/2}(kr) + B_l' N_{l+1/2}(kr), \tag{4.76}$$

where $J_{l+1/2}$ and $N_{l+1/2}$ are *Bessel's functions* of first and second kind, respectively.

Thus the solution to equation (4.61) is

$$\varphi(r,\theta,\phi) = \sum_{k,l,m}(kr)^{-1/2}\left[A_l J_{l+1/2}(kr) + B_l N_{l+1/2}(kr)\right]Y_l^m(\theta,\phi). \tag{4.77}$$

By inserting the boundary conditions

$$\begin{aligned}\varphi(R_1,\theta,\phi) &= 0,\\ \varphi(R_2,\theta,\phi) &= 0,\end{aligned} \tag{4.78}$$

we obtain

$$\varphi(r,\theta,\phi) = \sum_{k,l,m} (kr)^{-1/2} A_l \left[J_{l+1/2}(kr) - \frac{J_{l+1/2}(kR_1)}{N_{l+1/2}(kR_1)} N_{l+1/2}(kr) \right] Y_l^m(\theta,\phi) \tag{4.79}$$

where $r \in [R_1, R_2]$, $\theta \in [0, 2\pi)$, $\phi \in [0, \pi)$, A_l is a normalization constant and k are the roots of the equation

$$J_{l+1/2}(kR_2)N_{l+1/2}(kR_1) - J_{l+1/2}(kR_1)N_{l+1/2}(kR_2) = 0. \tag{4.80}$$

4.2.2 Expression for the Casimir energy

The Casimir energy is given by

$$E_C = \frac{1}{2}\hbar \sum_{l=0}^{\infty} \sum_{m=-l}^{l} \sum_{n=1}^{\infty} \omega_{nl} = \hbar c \sum_{l=0}^{\infty} \nu \sum_{n=1}^{\infty} k_{nl}, \tag{4.81}$$

where $\nu = l + 1/2$, $\omega_{nl} = k_{nl}c$. k_{nl} are eigenfrequencies, determined by solving the transcendental frequency equation (4.80). Note that for fixed l, there is an infinite number of solutions k_{nl} to the frequency equation. Also note that the complete solution of Bessel's equation involves the Bessel functions $J_{l+1/2}$ and $N_{l+1/2}$. These functions can be represented as infinite series' of ascending powers of k, but for large $|k|$ the series' converge slowly and therefore the initial terms give no information about the sum. In order to describe the frequency spectrum at fixed l and large $|k|$, we therefore introduce uniform asymptotic expansions of the Bessel's functions. The asymptotic expansions converges rapidly in the sense that the series rapidly approaches a constant as $l \to \infty$. Thus, to carry out the summation with respect to l in E_C, the sum $\sum_{n=1}^{\infty} k_{nl}$ will be replaced by $\sum_{n=1}^{\infty} k_{nl} + \sum_{n=1}^{\infty} \tilde{k}_{nl}$, where $\tilde{k}_{nl}$ is the eigenvalue spectrum in the limit $k \to \infty$ at fixed l. k_{nl} represents the rest of the spectrum. The Casimir energy then can be written as

$$E_C = \bar{E}_C + \tilde{E}_C = \hbar c \sum_{l=0}^{\infty} \nu \sum_{n=1}^{\infty} k_{nl} + \hbar c \sum_{l=0}^{\infty} \nu \sum_{n=1}^{\infty} \tilde{k}_{nl}. \tag{4.82}$$

The expression for the energy is of course divergent and must be regularized. As we will see in the next subsections, the regularization will involve both Abel Plana formulas, exponential cutoffs and zeta functions.

4.2.3 Calculation of $\tilde{E}_C$

In order to calculate the eigen frequencies for large arguments at fixed ν, we use Hankel's asymptotic expansion for $x \gg 1$;

$$\begin{aligned} J_\nu(x) &\simeq \sqrt{\frac{2}{\pi x}}\left[\cos\left(x-\frac{\nu\pi}{2}-\frac{\pi}{4}\right)-\frac{4\nu^2-1}{8x}\sin\left(x-\frac{\nu\pi}{2}-\frac{\pi}{4}\right)\right], \\ N_\nu(x) &\simeq \sqrt{\frac{2}{\pi x}}\left[\cos\left(x-\frac{\nu\pi}{2}-\frac{\pi}{4}\right)+\frac{4\nu^2-1}{8x}\sin\left(x-\frac{\nu\pi}{2}-\frac{\pi}{4}\right)\right]. \end{aligned} \tag{4.83}$$

Inserting these into the frequency equation (4.80), we get

$$\begin{aligned} &R_1\sin\left(R_2\tilde{k}-\frac{\nu\pi}{2}-\frac{\pi}{4}\right)\cos\left(R_1\tilde{k}-\frac{\nu\pi}{2}-\frac{\pi}{4}\right) \\ &-R_2\sin\left(R_1\tilde{k}-\frac{\nu\pi}{2}-\frac{\pi}{4}\right)\cos\left(R_2\tilde{k}-\frac{\nu\pi}{2}-\frac{\pi}{4}\right)=0. \end{aligned} \tag{4.84}$$

Graphically we see that this equation have approximately the same roots as

$$R_2\sin((R_2-R_1)\tilde{k})=0, \tag{4.85}$$

i.e $\tilde{k}_{nl}\approx\frac{n\pi}{R_2-R_1}$. However, the zeros aren't entirely evenly spaced and a better approximation (see [20]) is

$$\tilde{k}_{nl}^2\simeq\left(\frac{n\pi}{R_2-R_1}\right)^2+\frac{\nu^2}{R_2R_1}\quad n=1,2,... \tag{4.86}$$

Thus

$$\tilde{E}_C=\hbar c\sum_{l=0}^{\infty}\nu\sum_{n=1}^{\infty}\left[\left(\frac{n\pi}{R_2-R_1}\right)^2+\frac{\nu^2}{R_2R_1}\right]^{\frac{1}{2}}. \tag{4.87}$$

This divergent sum can be regularized using the *Abel-Plana sum formula* , which is given by

$$\mathrm{Reg}\left[\sum_{n=0}^{\infty}f(n)\right]\equiv\sum_{n=0}^{\infty}f(n)-\int_0^{\infty}f(x)dx=\frac{1}{2}f(0)+i\int_0^{\infty}dt\,\frac{f(it)-f(-it)}{e^{2\pi t}-1}, \tag{4.88}$$

where f is an analytic function for Re $[z]>0$ and *Reg* refers to the regularized value of the sum. The Abel-Plana sum formula for half integers will also be used;

$$\sum_{n=0}^{\infty}f(n+1/2)=\int_0^{\infty}f(x)dx-i\int_0^{\infty}dt\,\frac{f(it)-f(-it)}{e^{2\pi t}+1}. \tag{4.89}$$

Define

$$G(z;A,B)=\sqrt{(Az)^2+B^2}. \tag{4.90}$$

This function has branch points $z = \pm i\frac{B}{A}$. By going around the branch points, one can prove the equality (see p. 23 in [7])

$$G(it; A, B) - G(-it; A, B) = 2i\sqrt{(At)^2 - B^2}\theta(At - B), \tag{4.91}$$

where $\theta(x)$ is the Heaviside step function. We regularize $\tilde{E}_C$ using this identity and equation (4.88);

$$\begin{aligned}
\tilde{E}_C &= \hbar c \sum_{l=0}^{\infty} \nu \,\mathrm{Reg}\left[\sum_{n=1}^{\infty} G\left(n; \tfrac{\pi}{d}, \tfrac{\nu}{\sqrt{R_1R_2}}\right)\right] \\
&= \hbar c \sum_{l=0}^{\infty} \nu \left[-\left(\frac{\nu^2}{R_1R_2}\right)^{\frac{1}{2}} + i\, 2i \int_0^{\infty} dt \left\{\left(\frac{t\pi}{d}\right)^2 - \frac{\nu^2}{R_2R_1}\right\}^{\frac{1}{2}} \frac{\theta\left(\frac{\pi t}{d} - \frac{\nu}{\sqrt{R_1R_2}}\right)}{e^{2\pi t} - 1}\right] \\
&= -\frac{\hbar c}{2\sqrt{R_1R_2}} \sum_{l=0}^{\infty} \nu^2 - 2\hbar c \sum_{l=0}^{\infty} \nu \int_{\frac{\nu\xi}{2\pi}}^{\infty} dt \left\{\left(\frac{t\pi}{d}\right)^2 - \frac{\nu^2}{R_2R_1}\right\}^{\frac{1}{2}} \frac{1}{e^{2\pi t} - 1},
\end{aligned} \tag{4.92}$$

where $d = R_2 - R_1$, $\xi = \frac{2d}{\sqrt{R_1R_2}}$ and $\nu = l + 1/2$. The first divergent sum can be analytically continued using the *Hurwitz zeta function* (see [19]);

$$\sum_{l=0}^{\infty} \nu^2 = \sum_{l=0}^{\infty} \left(l + \frac{1}{2}\right)^2 = \zeta\left(-2, 1/2\right). \tag{4.93}$$

The property

$$\zeta\left(-2n, 1/2\right) = 0, \tag{4.94}$$

for $n = 1, 2, ..$, gives that equation (4.92) becomes

$$\tilde{E}_C = -2\hbar c \sum_{l=0}^{\infty} F(\nu), \tag{4.95}$$

where

$$F(\nu) = \nu \int_{\frac{\nu\xi}{2\pi}}^{\infty} dt \left\{\left(\frac{t\pi}{d}\right)^2 - \frac{\nu^2}{R_2R_1}\right\}^{\frac{1}{2}} \frac{1}{e^{2\pi t} - 1}. \tag{4.96}$$

Using the half integer Abel-Plana sum formula given in equation (4.89), we get

$$\tilde{E}_C = -2\hbar c \int_0^{\infty} dx\, F(x) + 2\hbar c i \int_0^{\infty} dx\, \frac{F(ix) - F(-ix)}{e^{2\pi x} + 1} \tag{4.97}$$

The first integral is solved using several substitutions;

$$\begin{aligned}
\int_0^\infty dx\, F(x) &= \hbar c \int_0^\infty dx\, x \int_{\frac{x\xi}{2\pi}}^\infty dt\, \left\{ \left(\frac{t\pi}{d}\right)^2 - \frac{x^2}{R_2 R_1} \right\}^{\frac{1}{2}} \frac{1}{e^{2\pi t}-1} \\
&= \hbar c R_1 R_2 \int_0^\infty dv\, v^2 \int_{\frac{vd}{\pi}}^\infty dt\, \left\{ \left(\frac{t\pi}{vd}\right)^2 - 1 \right\}^{\frac{1}{2}} \frac{1}{e^{2\pi t}-1} \\
&= \hbar c R_1 R_2 \frac{d}{2\pi} \int_0^\infty dv\, v^3 \int_0^\infty du\, \sqrt{\frac{u}{u+1}} \frac{1}{e^{2d\sqrt{u+1}v}-1} \\
&= \hbar c R_1 R_2 \frac{d}{2\pi} \frac{1}{2^4 d^4} \int_0^\infty du\, \sqrt{\frac{u}{u+1}} \frac{1}{(u+1)^2} \int_0^\infty dy\, \frac{y^3}{e^y-1} \\
&= \hbar c \frac{R_1 R_2}{2^5 \pi d^3} \int_0^1 dq\, \sqrt{q}\, \frac{\pi^4}{15} = \frac{R_1 R_2}{2^5 \pi d^3} \frac{2}{3} \frac{\pi^4}{15} = \frac{R_1 R_2 \pi^3}{720 d^3}
\end{aligned} \tag{4.98}$$

The second integral in equation (4.97) is divergent. This integral is regularized by substituting $\nu - i\epsilon$ for ν and letting $\epsilon \to 0$ at the end. This results in

$$2\hbar c i \int_0^\infty dt\, \frac{F(it) - F(-it)}{e^{2\pi t}+1} = -\frac{5\hbar c \pi}{1440 d}. \tag{4.99}$$

Thus

$$\tilde{E}_C = -\frac{\hbar c R_1 R_2 \pi^3}{360 d^3} \left[1 + \frac{5}{4\pi^2} \frac{d^2}{R_1 R_2} \right]. \tag{4.100}$$

4.2.4 Calculation of $\bar{E}_C$

In order to regularize the expression for $\bar{E}_C$, we introduce an exponential cutoff. I.e we define $\bar{E}_C$ as

$$\bar{E}_C = \hbar c \sum_{l=0}^\infty \nu \sum_{n=1}^\infty k_{nl} e^{-\alpha k_{nl}} = \hbar c \sum_{l=0}^\infty \left(l + \frac{1}{2} \right) S_l, \tag{4.101}$$

where $S_l = \sum_{n=1}^\infty k_{nl} e^{-\alpha k_{nl}}$ and the original expression is recovered by letting $\alpha \to 0$. Define

$$f_\nu(x; a, b) = J_\nu(bx) N_\nu(ax) - J_\nu(ax) N_\nu(bx). \tag{4.102}$$

Thus the frequencies k_{nl} are the roots of $f_\nu(\nu k; R_1, R_2)$. To evaluate the sum S_l, we use the argument principle given in equation (4.26). Choose $h(z) = z e^{-\alpha z}$. The principle

then states that

$$\frac{1}{2\pi i}\oint_C dk\, e^{-\alpha k} k \frac{d}{dk} \ln f_\nu(k) = \sum_{n=1}^{\infty} k_{nl} e^{-\alpha k_{nl}} = S_l. \tag{4.103}$$

Thus the sum S_l can be replaced by a contour integral, and the expression for $\bar{E}_C$ becomes

$$\bar{E}_C = \hbar c \sum_{l=0}^{\infty} \nu \frac{1}{2\pi i}\oint_C dk\, e^{-\alpha k} k \frac{d}{dk} \ln f_\nu(\nu k). \tag{4.104}$$

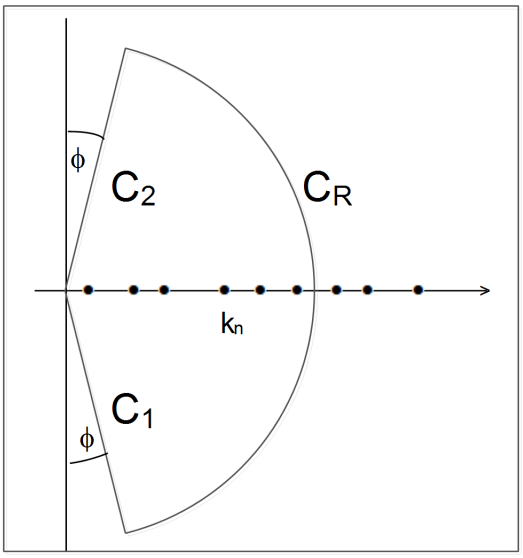

FIGURE 4.2: The integration contour $C = C_1 \cup C_2 \cup C_R$

Let the contour C be given by $C = C_1 \cup C_2 \cup C_R$, where

$$\begin{aligned} C_R &= \{z = x + iy \in \mathbb{C} |\, |z| = R, x > 0\} \\ C_1 &= \left\{-iye^{i\phi} | y \in [0, R]\right\} \\ C_2 &= \left\{iye^{-i\phi} | y \in [0, R]\right\}. \end{aligned} \tag{4.105}$$

For fixed R, the contour C encloses a finite number of roots of $f_\nu(\nu k)$, but when we take the limit $R \to \infty$, C encloses all of them. Provided that $\phi \neq 0$, the contribution from C_∞ vanishes because of the exponential cutoff. The contributions from C_1 and C_2 are complex conjugated of each other, and therefore only the real part gives a contribution. Equation (4.104) reduces to

$$\bar{E}_C = -\frac{\hbar c}{\pi} \lim_{\alpha \to 0} \sum_{l=0}^{\infty} \nu\, \mathrm{Re}\, e^{-i\phi} \int_0^{\infty} dy\, e^{-i\alpha y e^{-i\phi}} y \frac{d}{dy} \ln f_\nu(i\nu y; R_1, R_2). \tag{4.106}$$

Well known relations between the Bessel functions J_ν, N_ν and the modified Bessel functions I_ν and K_ν will be used to calculate the integral in equation (4.106);

$$J_\nu(iz) = i^\nu I_\nu(z), \tag{4.107}$$

$$K_\nu(iz) = \frac{\pi}{2} i^{\nu+1} \left[J_\nu(z) + i N_\nu(x) \right]. \tag{4.108}$$

These relations give that

$$f_\nu(ix; a, b) = g_\nu(x; a, b), \tag{4.109}$$

where

$$g_\nu(x; a, b) = -\frac{2}{\pi} \left[I_\nu(bx) K_\nu(ax) - I_\nu(ax) K_\nu(bx) \right]. \tag{4.110}$$

Define $\lambda = \frac{R_1}{R_2}$ and rescale the integration variable with $yR_2 \to y$ in equation (4.106);

$$\bar{E}_C = -\frac{\hbar c}{R_2 \pi} \lim_{\alpha \to 0} \sum_{l=0}^{\infty} \nu \, \mathrm{Re} \; e^{-i\phi} \int_0^\infty dy \, e^{-i\alpha y e^{-i\phi}/R_2} \, y \frac{d}{dy} \ln g_\nu(\nu y; \lambda), \tag{4.111}$$

where $g_\nu(x; \lambda) \equiv g_\nu(x; \lambda, 1)$. Lommel's expansions (or the multiplication theorem) for the function $g_\nu(x; \lambda)$ gives

$$g_\nu(x; \lambda) = \lambda^{-\nu} \sum_{k=0}^{\infty} \frac{(\lambda^2-1)^k}{k! 2^k} x^{2k-\nu} \left[I_\nu(x) \left(\tfrac{d}{x \, dx} \right)^k \{ x^\nu K_\nu(x) \} - K_\nu(x) \left(\tfrac{d}{x \, dx} \right)^k \{ x^\nu I_\nu(x) \} \right], \tag{4.112}$$

where $|\lambda^2 - 1| < 1$. Long calculations give that

$$\begin{aligned} \nu y \frac{d}{dy} \ln g_\nu(z; \lambda) = \Bigg[& \frac{(1-\lambda^2)^2}{12} z^2 + \frac{(1-\lambda^2)^3}{24} z^2 + \frac{(1-\lambda^2)^4}{720} \left[z^2(19 - \nu^2) - z^4 \right] \\ & - \frac{(1-\lambda^2)^5}{1440} \left[3z^2(\nu^2 - 9) + 2z^4 \right] + [\text{Terms in even powers of z}] \Bigg]_{z = \nu y e^{-i\phi}}. \end{aligned} \tag{4.113}$$

Inserting equation (4.113), and using the integral result

$$\begin{aligned} I(2n) &= e^{-i\phi} \int_0^\infty dy \, e^{-i\alpha y e^{-i\phi}/R_2} \left(\nu y e^{-i\phi} \right)^{2n} = \int_0^\infty \left(-i \tfrac{R_2}{\alpha} dx \right) \, e^{-x} \, \left(-\nu i \tfrac{R_2}{\alpha} x \right)^{2n} \\ &= (-1)^{n+1} i \nu^{2n} \left(\tfrac{R_2}{\alpha} \right)^{2n+1} \Gamma(2n) = (-1)^{n+1} i (2n)! \nu^{2n} \left(\tfrac{R_2}{\alpha} \right)^{2n+1}, \quad n = 0, 1, .., \end{aligned} \tag{4.114}$$

equation (4.111) becomes

$$\begin{aligned}\bar{E}_C = &-\frac{\hbar c}{R_2\pi}\lim_{\alpha\to 0}\sum_{l=0}^{\infty}\mathrm{Re}\left[i\frac{(1-\lambda^2)^2}{6}\nu^2\left(\frac{R_2}{\alpha}\right)^3 + i\frac{(1-\lambda^2)^3}{12}\nu^2\left(\frac{R_2}{\alpha}\right)^3\right.\\ &+ i\frac{(1-\lambda^2)^4}{720}\left[2\nu^2(19-\nu^2)\left(\frac{R_2}{\alpha}\right)^3 + 24\nu^4\left(\frac{R_2}{\alpha}\right)^5\right]\\ &+ i\frac{(1-\lambda^2)^5}{720}\left[-6\nu^2(\nu^2-9)\left(\frac{R_2}{\alpha}\right)^3 + 48\nu^4\left(\frac{R_2}{\alpha}\right)^5\right]\\ &\left.+ [\text{Terms in imaginary number and even powers of } \nu]\right].\end{aligned} \tag{4.115}$$

All terms in the above expression have a singular term in the regulation parameter α, but the fact that they are purely imaginary implies that

$$\bar{E}_C = 0. \tag{4.116}$$

4.2.5 Final expression for the Casimir energy

Inserting the expressions for $\tilde{E}_C$ and $\bar{E}_C$ into equation (4.82), we obtain

$$E_C = \bar{E}_C + \tilde{E}_C = -\frac{\hbar c R_1 R_2 \pi^3}{360 d^3}\left[1 + \frac{5}{4\pi^2}\frac{d^2}{R_1 R_2}\right], \tag{4.117}$$

where $d = R_2 - R_1$. This is the Casimir energy for two concentric spheres.

Chapter 5

Relation between Casimir energy and pressure

In the previous chapter we used the method of mode summation to find the Casimir energy for some configurations. We also remember that the FIM outputs the Casimir energy of a system, whereas the BIM gives the Casimir pressure and force. In order to be able to compare the three different methods, we therefore must find a relation between the energy of a system and the force/pressure on the objects in the system.

The energy in a system is a function of several parameters, $r_1, ..., r_n$. Thus the energy is given by $E(\boldsymbol{r}) = E(r_1, .., r_n)$. Let $\boldsymbol{\gamma}(s) = (r_1(s), ..., r_n(s))$ be a one parameter curve through the argument space. Then

$$dE(\boldsymbol{\gamma}(s)) = \nabla E \cdot \boldsymbol{\gamma}'(s) ds \tag{5.1}$$

is the relation between the change in the parameter s and the change in energy. Let $Q = \cup_j Q_j$, where Q_j are the boundaries of a set of compact objects V_j in $\mathbb{R}^3$. The force on the surface element dA on Q_j is related to the pressure via

$$\boldsymbol{F}_j = \boldsymbol{n}_j P_j dA, \tag{5.2}$$

where $\boldsymbol{n}_j$ is a unit normal pointing into the region $V_0 = \mathbb{R}^3 \setminus \{V_k\}$. The change in the energy related to a deformation, $d\boldsymbol{r}$, of one ore more of the objects, is given by

$$dE = -\oiint_Q \boldsymbol{F} \cdot d\boldsymbol{r} = -\oiint_Q dA\, P\boldsymbol{n} \cdot d\boldsymbol{r} = -\sum_j \oiint_{Q_j} dA P_j \boldsymbol{n}_j \cdot d\boldsymbol{r}_j, \tag{5.3}$$

where the sum involves the objects that are deformed. Combining equations (5.1) and (5.3), we obtain

$$-\nabla E \cdot \boldsymbol{\gamma}'(s) ds = \sum_j \oiint_{Q_j} dA\, P_j \boldsymbol{n}_j \cdot d\boldsymbol{r}_j. \tag{5.4}$$

This relation holds for general configurations and will be used to find explicit relations between the Casimir energy and force/pressure for configurations that are of particular interest for us.

5.1 Two parallel plates

Let the two plates lie in the planes $z = z_1$ and $z = z_2$, with $z_2 - z_1 = a > 0$. Keeping the upper plate fixed, the position of the plates is determined by the parameter s via the parametrization $\boldsymbol{\gamma}(s) = (z_1 \pm s, z_2)$. For a change ds in the parameter, the change in energy will be

$$dE(\boldsymbol{\gamma}(s)) = \nabla E(z_1, z_2) \cdot \boldsymbol{\gamma}'(s) ds = \left(\frac{\partial E}{\partial z_1}, \frac{\partial E}{\partial z_2} \right) \cdot (\pm 1, 0) ds = \pm \frac{\partial E}{\partial z_1} ds. \tag{5.5}$$

A parametrization of the lower plate is given by $\boldsymbol{r}_1(u, v) = (u, v, z_1)$, while $\boldsymbol{r}_1(u, v, s) = (u, v, z_1 \pm s)$ describe deformations of it. The unit normal is given by $\boldsymbol{n}_1 = (0, 0, 1)$. Under the parameter change ds, the change in position of the plate is given by the differential

$$d\boldsymbol{r}_1 = \boldsymbol{r}_1'(s) ds = (0, 0, \pm ds). \tag{5.6}$$

We assume that the area of the plates is A and that $a \ll \sqrt{A}$ such that the boundary effects can be neglected. Then the symmetry of the configuration gives that the pressure is constant on the surface. Equation (5.3) gives the relation between the pressure and the change in energy;

$$dE(\boldsymbol{\gamma}(s)) = -\iint\limits_{Q_1} dA \, P_1 \boldsymbol{n}_1 \cdot d\boldsymbol{r}_1 = \mp ds \iint\limits_{Q_1} dA \, P_1 = \mp ds \, A \, P_1. \tag{5.7}$$

The energy per area is therefore given by

$$\mp \frac{\partial E}{\partial z_1} ds = \pm ds \, P_1. \tag{5.8}$$

Thus

$$P_1 = -\frac{\partial E}{\partial z_1}. \tag{5.9}$$

Similar calculations are done for the upper plate, and we get

$$P_2 = \frac{\partial E}{\partial z_2}, \tag{5.10}$$

because the normal is pointing in the opposite direction. Using the fact that $a = z_2 - z_1$, we get that $E = E(a)$ and

$$\begin{aligned} P_1 &= -\frac{\partial E}{\partial z_1} = -\frac{\partial a}{\partial z_1}\frac{dE}{da} = \frac{dE}{da}, \\ P_2 &= \frac{\partial E}{\partial z_2} = \frac{\partial a}{\partial z_2}\frac{dE}{da} = \frac{dE}{da}. \end{aligned} \tag{5.11}$$

Using mode summation we found that the Casimir energy for two parallel plates is given by

$$\mathcal{E} = -\frac{\hbar c \pi^2}{1440 a^3}. \tag{5.12}$$

Thus the pressure is

$$P_1 = P_2 = \frac{d\mathcal{E}}{da} = \frac{\hbar c \pi^2}{480 a^4}, \tag{5.13}$$

where positive direction is along the normals that point into the region between the plates, V_0. Thus the force between the plates is attractive.

5.2 Concentric spheres

Let R_1 and R_2, $R_2 > R_1$, be the radii of the two spheres. Since the spheres are concentric, the configuration is fully described by their radii. To start with, we keep the outer sphere fixed. Thus the configuration is described by the one parameter curve $\boldsymbol{\gamma}(s) = (R_1 \pm s, R_2)$. Under a change in radius of the inner sphere by ds, the change in energy will be

$$\nabla E(R_1, R_2) \cdot \boldsymbol{\gamma}'(s) ds = \left(\frac{\partial E}{\partial R_1}, \frac{\partial E}{\partial R_2} \right) \cdot (\pm 1, 0) ds = \pm \frac{\partial E}{\partial R_1} ds. \tag{5.14}$$

A parametrization of the inner sphere is given by $\boldsymbol{r}_1(\varphi, \theta) = R_1 \left(\sin\varphi\cos\theta, \sin\varphi\sin\theta, \cos\varphi\right) = R_1 \boldsymbol{n}_1$, where $\boldsymbol{n}_1$, given by

$$\boldsymbol{n}_1 = \left(\sin\varphi\cos\theta, \sin\varphi\sin\theta, \cos\varphi\right), \tag{5.15}$$

is the unit normal of the sphere. A deformation of the sphere is described by $\boldsymbol{r}_1(\varphi, \theta, s) = (R_1 \pm s)\boldsymbol{n}_1$. Under a parameter change, ds, the change in position of the inner sphere is given by the differential

$$d\boldsymbol{r}_1 = \frac{\partial \boldsymbol{r}_1}{\partial s} ds = \pm ds \boldsymbol{n}_1. \tag{5.16}$$

The relation between the pressure and the change in energy is given by equation (5.3);

$$dE(\boldsymbol{\gamma}(s)) = -\iint_{Q_1} dA\, P_1 \boldsymbol{n}_1 \cdot \pm ds \boldsymbol{n}_1 = \mp ds \iint_{Q_1} dA\, P_1 = \mp ds 4\pi R_1^2 P_1, \tag{5.17}$$

where it is used that, because of symmetry, the pressure is constant on the surface. We get

$$\pm \frac{\partial E}{\partial R_1} ds = \mp ds\, 4\pi R_1^2 P_1. \tag{5.18}$$

Thus the pressure on the inner sphere is given by

$$P_1 = -\frac{1}{4\pi R_1^2} \frac{\partial E}{\partial R_1}. \tag{5.19}$$

For the outer sphere, similar calculations give

$$P_2 = \frac{1}{4\pi R_2^2} \frac{\partial E}{\partial R_2}. \tag{5.20}$$

The sign is opposite since the outer normal is pointing inwards.

Remember that using mode summation, we found that the Casimir energy for this configuration is

$$E_C = -\frac{\hbar c R_1 R_2 \pi^3}{360 d^3} \left[1 + \frac{5}{4\pi^2} \frac{d^2}{R_1 R_2}\right], \tag{5.21}$$

where $d = R_2 - R_1$.

Using equation (5.19), we find that the pressure on the inner sphere is given by

$$P_1 = -\frac{1}{4\pi R_1^2} \frac{\partial E_C}{\partial R_1} = \frac{\hbar c \pi^2 R_2}{480 d^4 R_1} \left[1 + \frac{d}{3R_1} + \frac{5}{12\pi^2} \frac{d^2}{R_1 R_2}\right]. \tag{5.22}$$

Equation (5.20) gives that the pressure on the outer sphere is

$$P_2 = \frac{1}{4\pi R_2^2} \frac{\partial E_C}{\partial R_2} = \frac{\hbar c \pi^2 R_1}{480 d^4 R_2} \left[1 - \frac{d}{3R_2} + \frac{5}{12\pi^2} \frac{d^2}{R_1 R_2}\right]. \tag{5.23}$$

Consider a situation where the spheres are very close to each other, i.e let $R_2 \to R_1$. Then $\frac{d}{R_i} \ll 1$ and therefore

$$P_1 \to \frac{\hbar c \pi^2}{480 d^4} \tag{5.24}$$

and

$$P_2 \to \frac{\hbar c \pi^2}{480 d^4}. \tag{5.25}$$

We recognize this as the same result as we obtained for the parallel plates. The explanation is that the contribution to the Casimir effect mainly comes from the nearby regions. When the objects are close to each other, locally there is almost no difference between the two configurations.

5.3 Adjacent objects

Consider two objects whose centers of mass are determined by $\boldsymbol{s}_1 = (x_1, 0, 0)$ and $\boldsymbol{s}_2 = (x_2, 0, 0)$. We keep object 2 fixed and move object 1 along the x-axis. The positions of the objects are described by the one parameter curve $\boldsymbol{\gamma}(s) = (x_1 \pm s, x_2)$. Under a change in position, determined by ds, the change in energy will be

$$dE(\boldsymbol{\gamma}(s)) = \nabla E(x_1, x_2) \cdot \boldsymbol{\gamma}'(s) ds = \left(\frac{\partial E}{\partial x_1}, \frac{\partial E}{\partial x_2} \right) \cdot (\pm 1, 0) ds = \pm \frac{\partial E}{\partial x_1} ds. \tag{5.26}$$

Assume $\boldsymbol{r}_1(\varphi, \theta) = (x_1, 0, 0) + \boldsymbol{X}_1(\varphi, \theta)$ is a parametrization of object 1. Allowing the object to move along the x-axis, the object is determined by $\boldsymbol{r}_1(s, \varphi, \theta) = (x_1 \pm s, 0, 0) + \boldsymbol{X}_1(\varphi, \theta)$. The differential change is $d\boldsymbol{r}_1 = \boldsymbol{r}_1'(s) ds = (\pm ds, 0, 0)$. In this situation, it is more convenient to relate the energy to the force since the pressure isn't constant. Using equation (5.3), we obtain

$$dE(\boldsymbol{\gamma}(s)) = -\iint_{Q_1} dA \, P_1 \boldsymbol{n}_1 \cdot (\pm ds, 0, 0) = \mp ds \iint_{Q_1} dA \, P_1 \boldsymbol{n}_{1,x} = \mp ds \boldsymbol{F}_{1,x}. \tag{5.27}$$

Thus

$$\pm \frac{\partial E}{\partial x_1} ds = \mp ds \boldsymbol{F}_{1,x}. \tag{5.28}$$

The force is therefore given by

$$\boldsymbol{F}_{1,x} = -\frac{\partial E}{\partial x_1}. \tag{5.29}$$

Similar calculations give

$$\boldsymbol{F}_{2,x} = \frac{\partial E}{\partial x_2}. \tag{5.30}$$

Thus it is clear that the force on the object will be oriented along the x-axis.

Chapter 6

Numerical implementations

In this chapter we consider the implementations of the boundary integral method (BIM) and the functional integral method (FIM). The implementations of the methods will be written in C, using both MPI and pthreads for parallel support. The implementations are designed for r conductors.

6.1 Boundary integral method

Remember that the BIM outputs the pressure,

$$P(\boldsymbol{x}) = \frac{1}{2\pi} \int_0^\infty d\omega \, \mathcal{P}(\boldsymbol{x}, \boldsymbol{x}, \omega). \tag{6.1}$$

The integral over ω will be calculated using an n-point Gaussian quadrature. The integral will be truncated at some point ω_{max}. We can't give formula for how large ω_{max} has to be chosen, but a suitable choice can be found by solving the boundary integral equations for a rough discretization of the boundaries of the conductors.

We now consider the algorithm for calculating the density $\mathcal{P}(\boldsymbol{x}, \boldsymbol{x}, \omega)$ on the k-th of the r conductors, for a particular ω. For simplicity, we assume that each of the conductors are discretized using N elements. In order to find this density, we have to solve the linear system of equations given in equations (2.105) and (2.106), for $i = k$. In general, the matrix on the right hand side of equation (2.105) consists of N columns. However, according to our discussion in chapter 2.9, the number of columns can be reduced enormously if there are any symmetries apparent. Both for parallel plates (assuming infinite length, such that there are no boundary effects) and concentric spheres, the number of columns can be reduced to a single column. In addition, symmetry gives that the pressure on both plates in the parallel plates configuration is of equal size. This means that the equation only have to be solved for $i = 1$, and not $i = 2$. These examples indicate that it is possible to reduce the computational load substantially for symmetric

configurations. We let N_R, $1 \leq N_R \leq N$, be the number of columns on the rhs. of equations (2.105) and (2.106).

Under the above mentioned assumptions and in accordance with chapter 2, an implementation of the BIM will involve 4 steps:

1. Fill r^2 matrices A^{ij} of size $N \times N$ each, and a rhs. of size $N \times N_R$.
2. Solve the linear system $A^{kk}B^{kk} = Y^{kk}$ of size $N \times N$ for N_R different right hand sides.
3. Perform $r-1$ matrix multiplications, $A^{kj}B^{kk}$, for $j = 1, 2, .., r$, $j \neq k$.
4. Solve the linear system (2.105) of size $rN \times rN$ for N_R different right hand sides.

Taking a closer look at the steps we have to go through, we see that most of them are well suited for being programmed in parallel. The implementation will be parallelized the obvious way; each of the matrices A^{ij} will be stored on different nodes. These r^2 nodes we call worker nodes. The right hand side of the equations will be stored on a master node. Only by looking at step 1, we see that it is an advantage parallelizing. When the resolution of the discretization is high, the matrix on the left hand side of equation (2.105), $A = \left(A^{ij}\right)$, easily becomes too large for being stored on a single node computer. Thus by storing the lhs. on r^2 different nodes, one has the opportunity of working with higher resolution of the discretizations. In addition, one reduces the computational time by filling each of the matrices A^{ij} at the same time, instead of serially. Step 2 and 3 are clearly possible to perform even though the matrices A^{ij} are stored on different nodes, but what about step 4? Since there are many different columns on the rhs. of the equation, the obvious way to solve the equation in step 4, is to use a linear solver based on LU-decomposition. However, such a method will require that the entire lhs., $A = \left(A^{ij}\right)$, is stored on a single node. LU-decomposition is therefore out of the question. Fortunately, there exist linear solvers that can be applied even though the lhs. of the equation is stored on different nodes. An example is the iterative linear solver based on the *generalized minimal residue method* (GMRES). Public domain implementations of GMRES can be found on the internet (See for example the routine written in fortran77 [21]). Using the GMRES, the matrix A will only be involved in a matrix-vector product. Such a product can easily be performed in parallel by storing the different block matrices A^{ij} on different nodes. Thus also step 4 is well suited for being parallelized.

The $r-1$ matrix multiplications in step 3 are easily parallelized. Step 2, which is to solve the self pressure equation, is harder to perform in parallel. The reason is that only the node where the matrix A^{kk} is stored, can be used to solve the equation. All other nodes are unoccupied during this step and therefore this step may speed down the implementation. Normally the number of nodes one has in hand is 1,2,4,8,16 and so on.

This fact can be used to speed up step 2. For example if $r = 2$, the method described above only involves 5 nodes. Thus there are 3 more nodes where the matrix A^{kk} can be stored. Thus, instead of solving the self-pressure equation serially, column by column, one can for example solve it for 4 different rhs. at the same time.

The computer that I used had a memory of 32 GB available on the largest nodes. Using double precision every element of a matrix requires 8 bytes. This should imply, if the entire node is used for storing a matrix, that it is possible to store matrices slightly larger than 60000×60000 on each node. If one want to work with larger matrices, and doesn't have a larger computer available, it is possible to split the matrices A^{ij} into even smaller submatrices. This will require that there are enough nodes available, because then more than r^2 nodes is needed for storing the lhs. of equation (2.105). We also observe that if there is no symmetry reduction, the matrix on the rhs. of the equation can be large. Fortunately the memory isn't a problem here, since the different columns are independent of each other and therefore one can consider one column at the time, i.e. the equations can be solved for each column serially.

6.2 Functional integral method

Remember that the FIM gives the Casimir energy. In the BIM, the pressure is given as an integral from 0 to ∞, and similarly the energy is;

$$\mathcal{E} = \frac{\hbar}{2\pi} \int_0^\infty d\kappa \, \ln \det M(i\kappa). \tag{6.2}$$

The integral will be calculated using a Gaussian quadrature and will be truncated at a suitable choice κ_{max}, for example at ω_{max}. The matrix M consist of r^2 block matrices $M^{\alpha\beta}$ of size $N \times N$, where

$$M^{\alpha\beta} = \mathbf{1}\delta_{\alpha\beta} + [T^\alpha]^{-1} U^{\alpha\beta}(1 - \delta_{\alpha\beta}) \qquad \alpha, \beta = 1, ..., r. \tag{6.3}$$

We consider the algorithm for calculating the energy density once. To simplify, we also here assume that all conductors are discretized using N elements.

1. Fill the matrices T^α and $U^{\alpha\beta}$ of size $N \times N$ each, for $\alpha = 1, .., r$, $\beta \neq \alpha$. Thus r^2 matrices have to be filled.

2. Calculate the matrices $M^{\alpha\beta} = [T^\alpha]^{-1} U^{\alpha\beta}$, $\beta \neq \alpha$, by solving the $r(r-1)$ linear systems $T^\alpha M^{\alpha\beta} = U^{\alpha\beta}$. The size of the lhs. is $N \times N$, and there are N columns on the rhs.

3. Calculate the determinant of a $rN \times rN$ matrix.

This algorithm outputs the energy density for a particular κ. Since the force or pressure involve a derivative of the energy, a minimum of two calculations of the energy is required. Thus the algorithm has to be repeated twice for each κ.

Step 3 is hard to implement in parallel since it involves calculation of a determinant. As far as we know, the determinant of the matrix M of size $rN \times rN$ must be calculated by storing the entire matrix M on the same node. This reduces the size of the matrices that we are able to do calculations for, and implies that we can't apply the FIM on as high resolutions as the BIM. The fact that it is hard to parallelize the calculations of the density is a big limitation of the FIM. It could be mentioned that it is still possible to parallelize the calculations of the energy itself. This can be done by calculating the integral over κ in parallel, i.e by calculating the energy density for different κ's on different nodes. Such a parallelization doesn't imply that it is possible to do calculations for higher resolutions, since one still have to store the entire matrix $M(i\kappa)$ on the same node, but the computational time will be reduced. However, this can't be seen as an advantage of the FIM compared to the BIM, since exactly the same is possible for the BIM.

By looking closer at step 2, we observe that there are only r different lhs. in the linear equations. For each lhs. there are $r-1$ different matrices on the rhs. Such linear systems are effectively solved using LU-decomposition. The determinant will also be calculated using LU-decomposition.

6.3 Complexity considerations

From the discussion in the two previous sections, we see that there are similarities between the two implementations. Since both the BIM and the FIM are based on Green's functions, the elements in the matrices will be very similar. The primary difference between the implementations is that the BIM ends up solving a large linear system, whereas one with the FIM has to calculate a determinant of a large matrix in the end. However, this difference is important; the former is well suited for being parallelized using GMRES as the linear solver, whereas the latter is not.

The implementation of the FIM is based on LU-decomposition, and therefore it is easy to estimate the total asymptotic floating point operation cost:

1. Fill r^2 matrices. Cost: cr^2N^2, for some constant c.
2. Solve r linear systems with $r-1$ different matrices on the rhs. Cost: $r\frac{2}{3}N^3 + r^2(r-1)2N^3$.
3. Calculate the determinant of a $rN \times rN$ matrix. Cost: $\frac{2}{3}(rN)^3$.

Thus the total cost is $\left(\frac{8}{3}r^3 - 2r^2 + \frac{2}{3}r\right)N^3$.

Since the implementation of the BIM is based on GMRES, it is difficult to give a general estimate of the total cost of this method. Step 1 is to fill $r^2 + 1$ matrices and therefore the cost is $cr^2N^2 + cNN_R$. The constant c is almost equal for the BIM and the FIM because both are based on Green's functions. Step 3 consists of $r - 1$ matrix multiplications and the cost, using the standard formula, is $(r - 1)N^2N_R$. We observe that the cost of step 3 is $\mathcal{O}(N^3)$ if $N_R = N$, i.e if there is no symmetry reduction.

The cost of step 2 and 4 depend strongly on the number of iterations the GMRES routine has to perform. There are several parameters that determine how fast the GMRES routine converges. A property of the GMRES routine is that it is exact after at most n iterations, for a system of size $n \times n$. However, it turns out that in our case, far fewer than n iterations are required. If this wasn't the case, the GMRES routine would have been to slow for us. An important speed-up factor of the GMRES routine is the use of an initial guess. Remember that we integrate over ω from 0 to ∞. This means that for a particular value of ω, ω_k, we can use the solution obtained from ω_{k-1} as initial guess. Since the value of ω_{k-1} is close to ω_k, we expect that the pressure density at ω_{k-1} is a good guess of the value of the pressure density at ω_k. The result is that the routine will require fewer iterations. However, the most important factor when it comes to the cost of step 2 and 4 is how much symmetry reduce the problem size. This is because, unlike solvers based on LU-decomposition, the cost and computational time of the GMRES grows linearly with the number of columns, N_R, on the right hand side of the equations.

The above discussion indicates that we can't obtain an explicit expression for the total asymptotic floating point operation cost in the implementation of the BIM. We have mentioned that there are two important features of the method that can reduce the computational time, namely parallelization and symmetry reduction, and therefore make the method competitive with other methods such as the FIM. The fact that the implementation is designed for being parallelized, implies that one can work with higher resolutions since the main matrix is split and stored on different nodes. Even though the floating point operation cost isn't reduced, the computational time will be reduced since the computations are done at the same time. Symmetry reduction implies reduction of total cost and therefore also computational time.

Chapter 7

Results and discussion

The implementations will first be tested on two parallel plates, a configuration without curvature. Since the exact pressure on the plates is known, we can use this configuration as a test on whether the implementations calculates the pressure correctly. For this particular configuration, we have developed implementations using both structured discretizations consisting of squares and unstructured discretizations consisting of triangles. We will investigate whether the different discretizations affect the calculated pressure or not.

After having considered a flat configuration, we start investigating whether the BIM calculates the pressure correctly for curved surfaces. We consider the configuration consisting of two concentric spheres. The exact solution for this configuration is known, and will be compared to the numerical solutions. The BIM will be further investigated by considering configurations consisting of adjacent spheres, adjacent ellipsoids and concentric ellipsoids.

I. Kilen found that the pressure calculated using the BIM, was off by a factor of two in the 2D case. He concluded that this factor was lost somewhere in the theory. We haven't found the source to this error yet and we therefore expect that also our results will have a missing factor. The question is whether the factor is still two or whether it has a dimensional dependence.

The integrals over κ and ω in the FIM and BIM, respectively, will be calculated using an n-point Gaussian quadrature. An error estimate for the quadrature is given by

$$R_n = \frac{(b-a)^{(2n+1)}(n!)^4}{(2n+1)[(2n)!]^3} f^{(2n)}(\xi), \quad a < \xi < b, \tag{7.1}$$

(see chapter 5.2 in [22]). We don't have explicit expressions for the integrands and therefore we can't calculate $f^{(2n)}(\xi)$. However, we will assume that the choice $f^{(2n)}(\xi) = 100$ is large enough. It turns out that for our test configurations, the choice $\omega_{max} =$

$\kappa_{max} = 60$ makes the truncation error small enough. By letting $n = 32$, we get

$$R_{32} = \frac{60^{65}(32!)^4}{65[(64)!]^3}\, 100 \approx 10^{-10}, \tag{7.2}$$

which is a better accuracy than required.

When the force is calculated using the FIM, a first order central difference will be used to approximate the derivative of the energy. We choose the variation parameter to be $da = 10^{-4}$.

In order to reduce notation, we introduce abbreviations such as BIM_tri_mp. This means "boundary integral method where the objects are discretized using triangles and the diagonal elements of the matrices are calculated using the midpoint rule". Similarly FIM_sq_gauss means "functional integral method where the objects are discretized using squares and the diagonal elements of the matrices are calculated using an 8-point Gaussian quadrature".

7.1 Parallel plates

Consider two parallel plates that are located at $z = -\frac{a}{2}$ and $z = \frac{a}{2}$. We let the length of the edges be $L = 10$ and consider separation distances in the range from $a = 0.7$ to $a = 2.2$. It turns out that the numerical solutions depend on how the diagonal elements in the matrices are calculated. We therefore decide to approximate the integrals that determine these elements both using a 1-point midpoint rule and much more accurate 8-point Gaussian quadrature. Thus, for the square discretizations, the pressure is calculated using both BIM_sq_mp, BIM_sq_gauss, FIM_sq_mp and FIM_sq_gauss. Since the plates are not of infinite size, we expect some boundary effects. However, by keeping the ratio a/L small, these will be constrained to the edges. We want to compare the methods to the exact solution and therefore, to start with, we only compute the pressure on squares in the middle of the plates, when applying the BIM. The resolution is chosen such that there are 10000 squares of equal size on each of the plates.

7.1.1 Square discretization

Figure 7.1 shows the pressure calculated using the BIM_sq_mp, BIM_sq_gauss, FIM_sq_mp and FIM_sq_gauss for different separation distances. The exact solution is plotted in the same figure. The relative errors between the numerical solutions and the exact solution are shown in figure 7.2. The best results are obtained using the BIM_sq_mp, where the error is less than 1% for all separation distances. We also observe FIM_sq_mp gives better results than the FIM_sq_gauss. Since an 8-point Gaussian quadrature calculates the diagonal elements more accurately than the 1-point midpoint rule, these results are surprising. An explanation may be that all other elements in the matrices are calculated

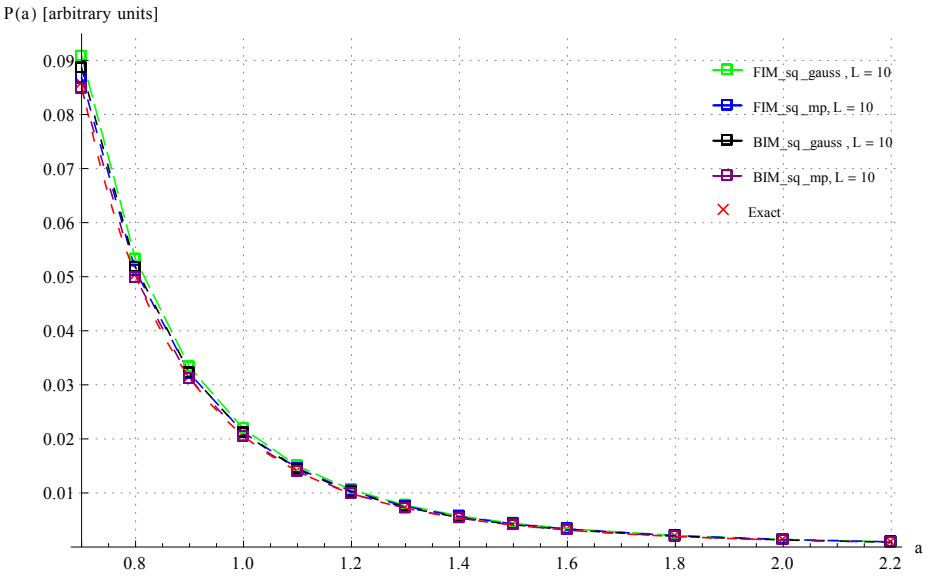

FIGURE 7.1: Pressure on one of the plates. Square discretization.

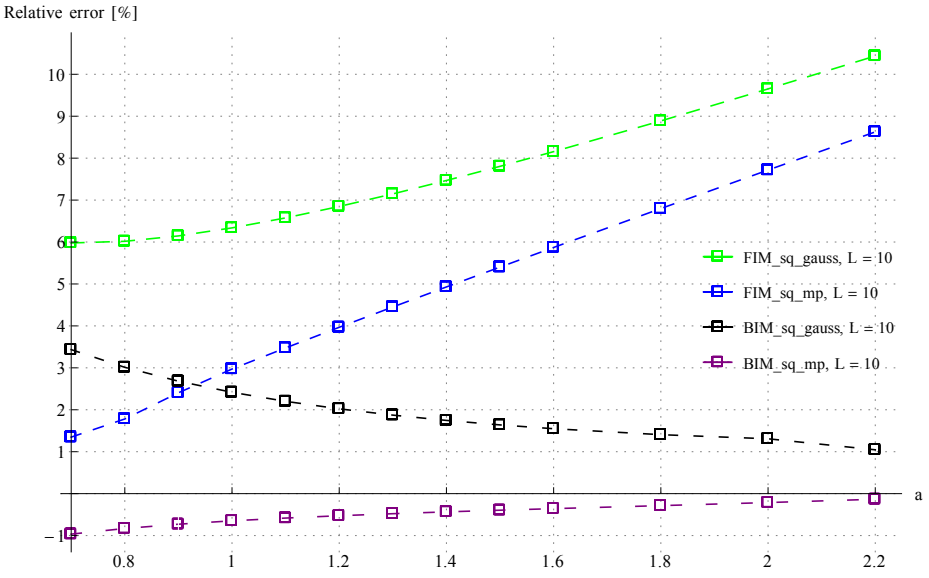

FIGURE 7.2: Relative error between the numerical and exact solutions. Square discretization.

using the midpoint rule. Thus the errors of the approximations become of the same size in all elements if the diagonal elements are calculated using the midpoint rule.

We have multiplied the pressure, obtained using the BIM, by a factor of two. The fact that the relative error in the BIM_sq_mp approaches zero from below when the separation distance increases, whereas the relative error from the BIM_sq_gauss approaches zero from above, verifies that the missing factor is two. We therefore correct our implementations of the BIM for this factor before doing more calculations.

It is worth noting that whereas the accuracy of the BIM improves when the separation distance increases using the BIM, the opposite occurs in the FIM. The behaviour

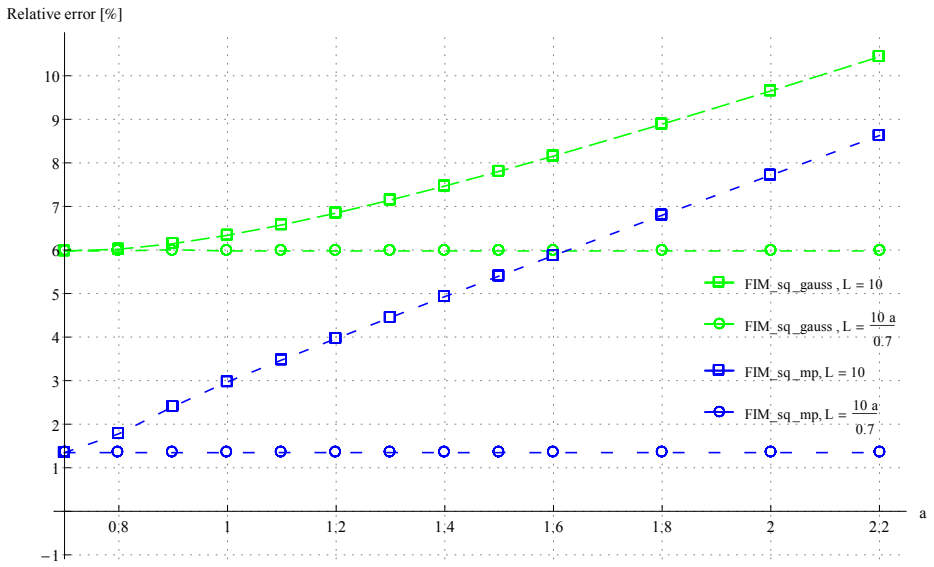

FIGURE 7.3: Relative error for the FIM, both fixed and varying length of the plates.

of the error in the BIM is expected since the same resolution is used for all separations. At shorter separation distances, the discretization is more visible for the equations. The behaviour of the FIM is more difficult to explain, but we should keep in mind that both the BIM and the FIM are designed for compact objects in $\mathbb{R}^3$. The parallel plates configuration is therefore outside the scope of both methods. It seems like the non-compactness of this configuration affect the FIM more than the BIM. However, our results are completely in accordance with the results Isak Kilen [1] found for corresponding configuration in two dimensions. He showed that it is possible to keep the error constant by varying the length of the edges linearly with the separation distance a, but keeping the number of elements in the discretization constant. We check whether the same is true in the three dimensional case.

Figure 7.3 shows the relative error for the FIM with both $L = 10$ and $L = \frac{10a}{0.7}$. The total number of squares on each plate is kept constant at 10000. We see that the error is constant when we increase the length of the edges linearly with a. Since the ratio L/a is constant, it is expected that the contribution to the error from the boundaries is constant. However, since the resolution decreases, we expect a slight increase in the error when the separation distance increases. This is seen to be of little effect and therefore we conclude that the boundary effects give the main contribution to the error and not the resolution. This suggests that the FIM is more sensitive to edge effects than the BIM.

With the BIM one has the possibility to compute the pressure on each of the elements in the discretization. In figures 7.4 and 7.5 the pressure distribution on the plates is illustrated. We see that the boundary effects give rise to a large pressure close to the edges.

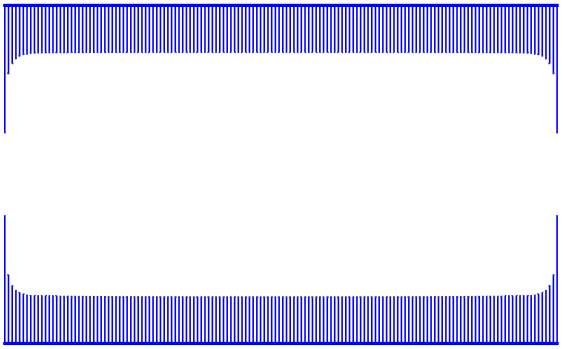

FIGURE 7.4: 2D cut of the plates and the pressure on them. The strength of pressure is represented via a line segment.

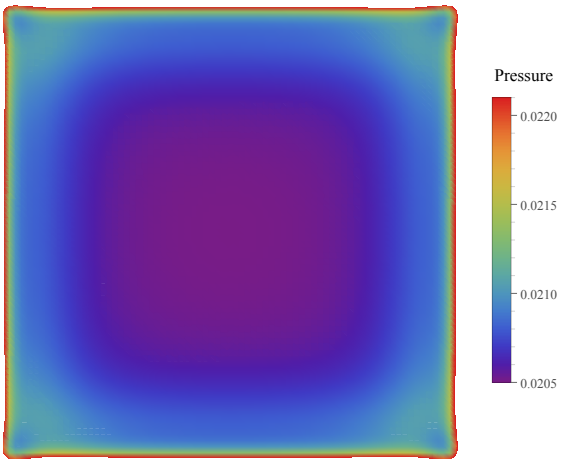

FIGURE 7.5: Illustration of the pressure distribution on one of the plates.

7.1.2 Triangle discretization

The boundary effects don't influence the middle region of the plates and therefore is the pressure constant here. Using the BIM_sq, we found very small variations in calculated pressure on the different squares in the middle region, typically of size $10^{-4}\%$ or less. However, using the BIM_tri, we find a larger variation in the pressure on the different triangles.

Figure 7.6 shows that the pressure on some of the triangles, calculated using the BIM_tri_mp, is deviating with as much as 8 % from the mean, whereas for the BIM_tri_gauss the variation in the calculated pressure is less than 0.2%. The extreme variations we obtain using the BIM_tri_mp, have a certain reason: Remember that the diagonal elements in the matrices are approximations of line integrals on the edges of the triangles. It is not obvious how to approximate these integrals using the midpoint rule. We tried to evaluate the integrand both at the middle of the edges and by minimizing the distance from the edges to the center of mass. The results for the latter are presented in figure 7.6, and the results for the former were even worse. We therefore decide only to

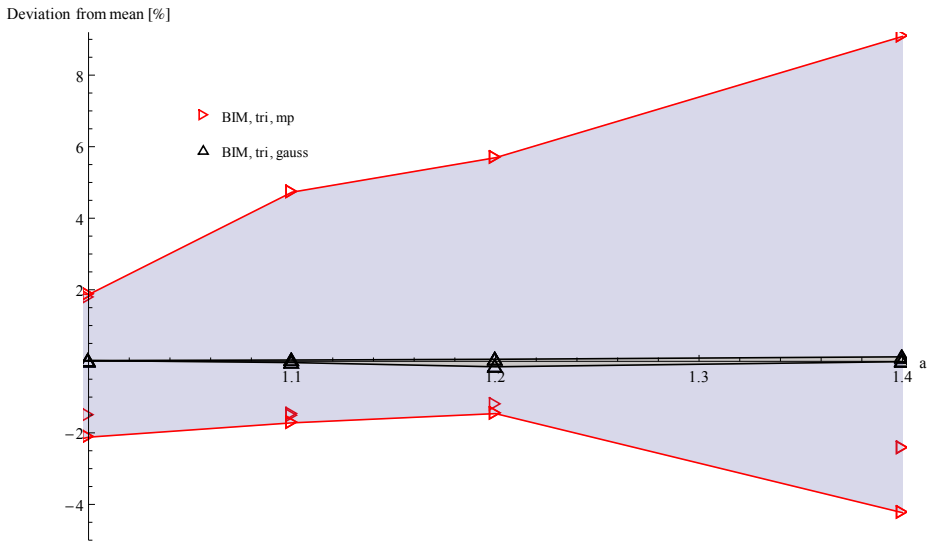

FIGURE 7.6: Variation from mean pressure for a sample of triangles.

calculate the diagonal elements using a Gaussian quadrature in the BIM_tri and discard the BIM_tri_mp. For the same reason we discard the FIM_tri_mp. We observe that also the BIM_tri_gauss gives more varying results than the square versions. This probably has something to do with the fact that the triangulations are unstructured and that the triangles vary in size and shape.

We now compare the BIM_tri_gauss to the BIM_sq and the exact solution. In the BIM_sq we use 40000 squares. Thus each of them are of size 0.05×0.05. As we have mentioned earlier, we can't control exactly the number of triangles in a triangulation outputted from the mesh generator *Netgen*. For this particular configuration it turns out that the resolution vary pretty much for the different separation distances. However, we use as high resolution as possible for each separation distance. The number of triangles on the plate where the pressure is calculated, is plotted in figure 7.8. The relative errors between the numerical solutions and the exact solution are shown in figure 7.7.

We see that the errors for the BIM_tri_gauss and the BIM_sq_gauss are approximately equal in the range from $a = 0.9$ to $a = 1.5$ units, whereas for the other separation distances the errors for the BIM_tri_gauss are 0.3-0.7 percentage points larger. The explanation can be found by looking to figure 7.8: In the range from $a = 0.9$ to $a = 1.5$ the number of triangles is approximately the same as the number of squares. However, for the other separation distances there are only about half as many triangles as squares in the respective discretizations. It seems like the resolution is to low at these separation distances to get the same accuracy as for the squares. Thus differences in resolution explain the small variations in the errors. Therefore it appears that the type of discretization used in implementation of the BIM, isn't very relevant to the value of the pressure.

The FIM_tri will also be compared to the BIM_tri. We indicated in the previous

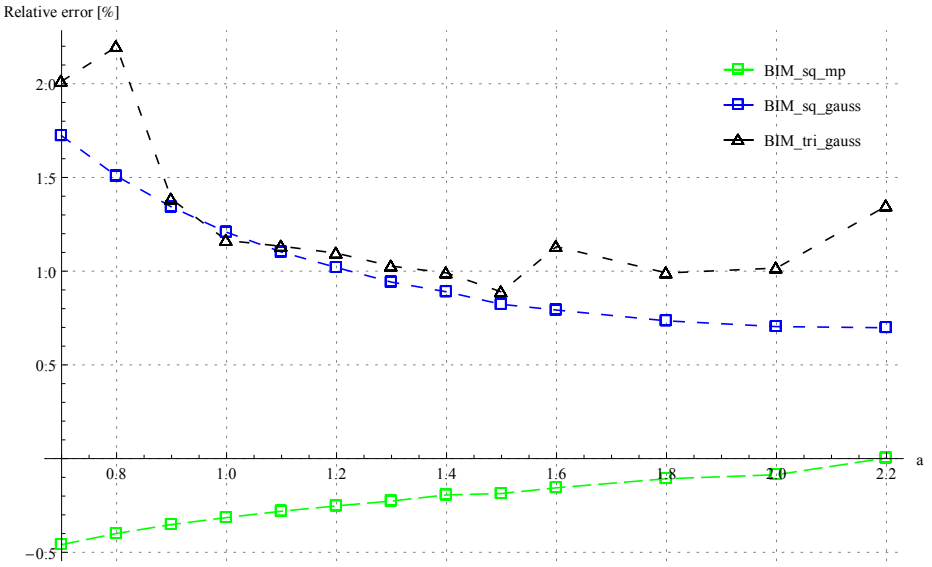

FIGURE 7.7: Relative error between the solutions found using the BIM_tri_gauss, BIM_sq_mp/gauss and the exact solution.

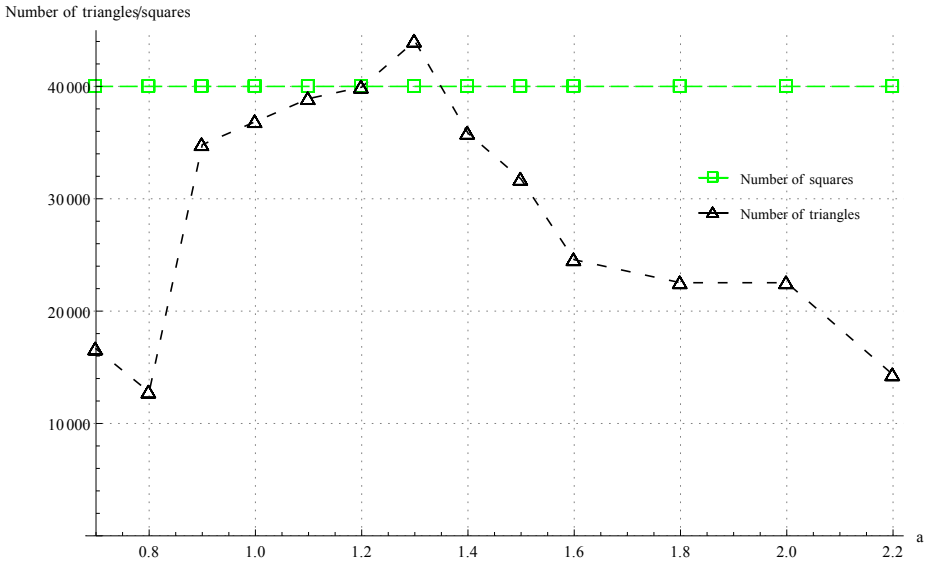

FIGURE 7.8: Number of elements in each of the discretizations for the BIM.

chapter that our implementation of the FIM can't do calculations with the same high resolution as the BIM. Figure 7.10 shows the number of elements in the discretization for the different separations distances. In figure 7.9 we plot the relative error for the FIM_tri_gauss and the FIM_sq_gauss compared to the exact solution. We see that the relative error is approximately equal for the two different discretizations. The differences that appear at the three shortest separation distances can be explained by differences in the resolution. Unlike the BIM, there is almost no difference between the errors at the larger separation distances, even though the resolutions of the two discretizations differ for both methods.

We conclude that both the BIM and FIM calculate the Casimir pressure correctly, and

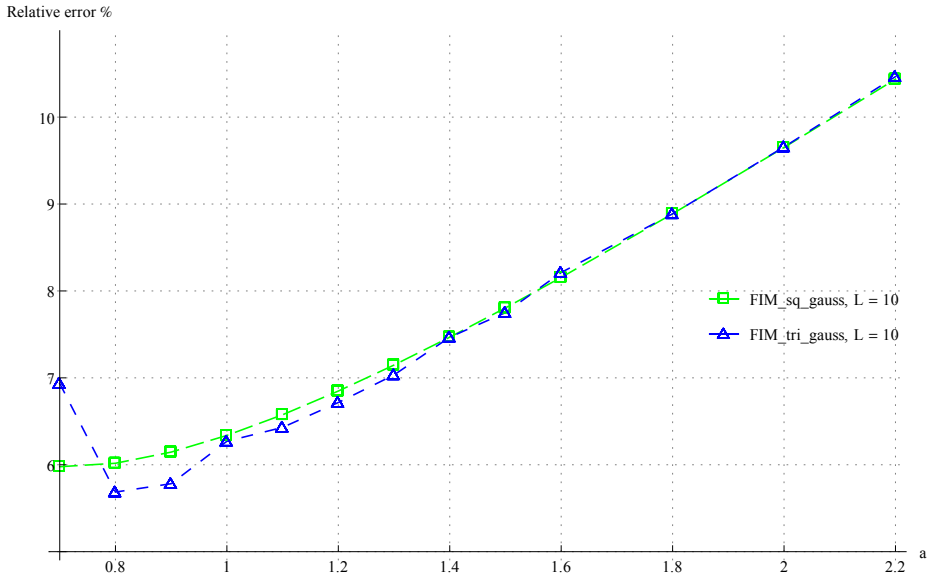

FIGURE 7.9: Relative error between the solutions found using FIM_tri_gauss, FIM_sq_mp/gauss and the exact solution.

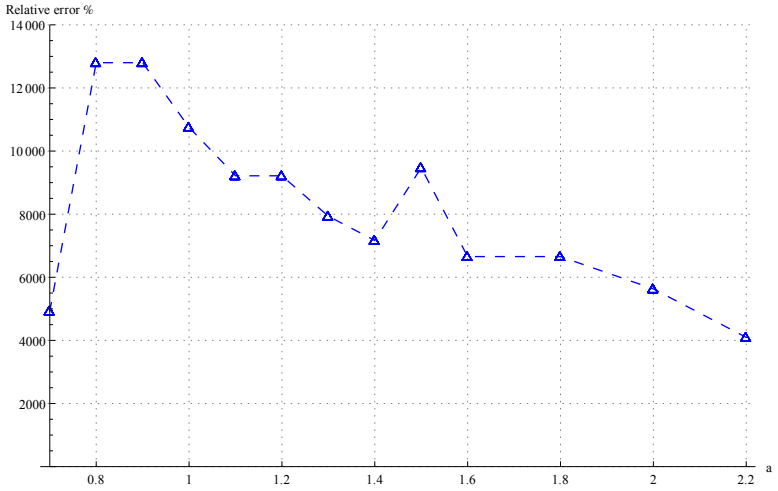

FIGURE 7.10: Number of elements in each of the discretizations for the FIM.

that the obtained results do not depend significantly on the type of discretization used. Even though unstructured meshes of triangles give somewhat more uncertain results, we decide to hereafter only discretize the surfaces using triangles. The BIM_tri_gauss will therefore be referred to as the BIM and the FIM_tri_gauss as the FIM. We choose to use triangulations since these are more flexible in fitting to surfaces of arbitrary shape.

7.2 Concentric spheres

In order to investigate whether the BIM calculates the pressure correctly for curved objects, we consider the configuration consisting of two concentric spheres. In chapters 4.2 and 5.2 we found exact expressions for the pressure on the inner and the outer sphere.

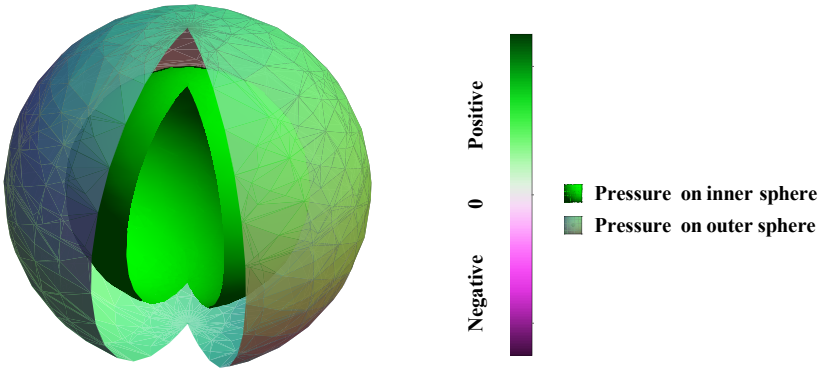

FIGURE 7.11: Illustration of the two concentric spheres. The colour indicates the strength of the pressure on the spheres.

An illustration of the configuration, and the pressure on the spheres, is shown in figure 7.11. The pressure on the inner sphere is larger than the pressure on the outer sphere. By integrating over each sphere, we find that the total force is zero on each of them. We also observe that the pressure on both spheres is positive. This means that locally the force points in the same direction as the normal vector, namely into the region between the spheres.

7.2.1 Behaviour of pressure for fixed curvature and increased resolution

We investigate whether the pressure is approaching the exact solution when the resolution is increased for three different curvatures, namely spheres of radii $R_1 = 2.3$ and $R_2 = 3.0$, $R_1 = 1.7$ and $R_2 = 3.0$ and the more extreme situation $R_1 = 0.5$ and $R_2 = 1.0$. In order to get a picture of the importance of the subtraction of the self pressure from the boundary integral equations, we also solve the discretized boundary integral equation (2.108) with the self pressure equal to zero, i.e. $B^{22} = 0$. The equations will be solved for as many different resolutions as possible, but unfortunately (as we explained in chapter 2.8) there are only 4. The results are shown in figures 7.12, 7.13, 7.14 and 7.15.

In figure 7.15 we see that for $R = 0.5$, the pressure is reduced by more than 30 % when the self pressure is set to zero, for $R = 1.7$ about 25 % and for $R = 2.3$ about 10 %. Thus the importance of the removal of the self pressure contribution, is relatively larger for spheres with much curvature. This is of course expected since the self pressure on the sphere goes as curvature to the power of 4. Figures 7.12, 7.13 and 7.14 show that, no matter how curved the sphere is, the calculated pressure is converging towards the exact pressure when the number of triangles increases. It is remarkable that this happens also for the $R_1 = 0.5$, $R_2 = 1.0$ configuration, where the curvature is very large. At the highest resolution, which means 30720 triangles on the inner sphere, the self pressure

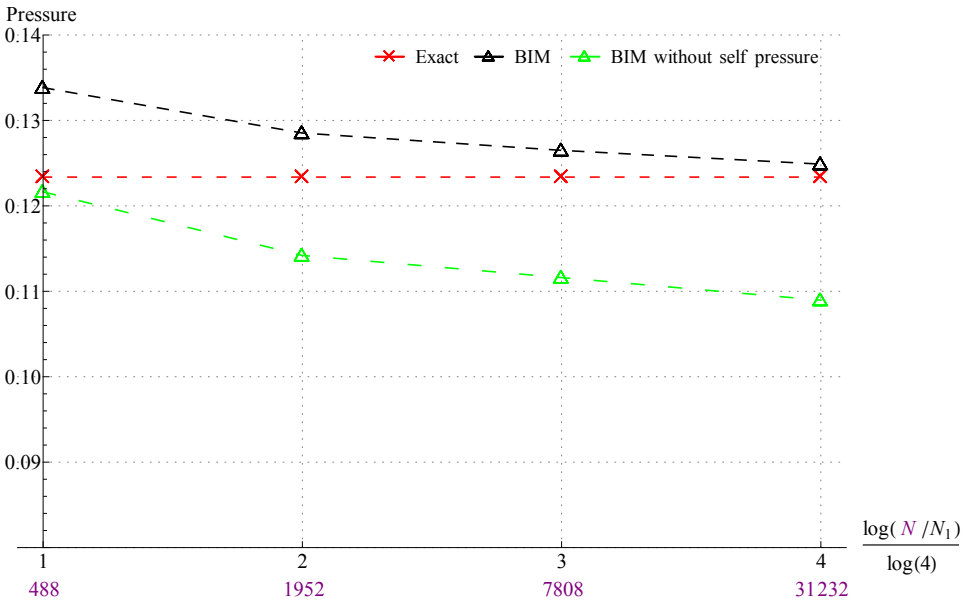

FIGURE 7.12: Pressure on inner sphere as function of resolution. $R_1 = 2.3$, $R_2 = 3.0$.

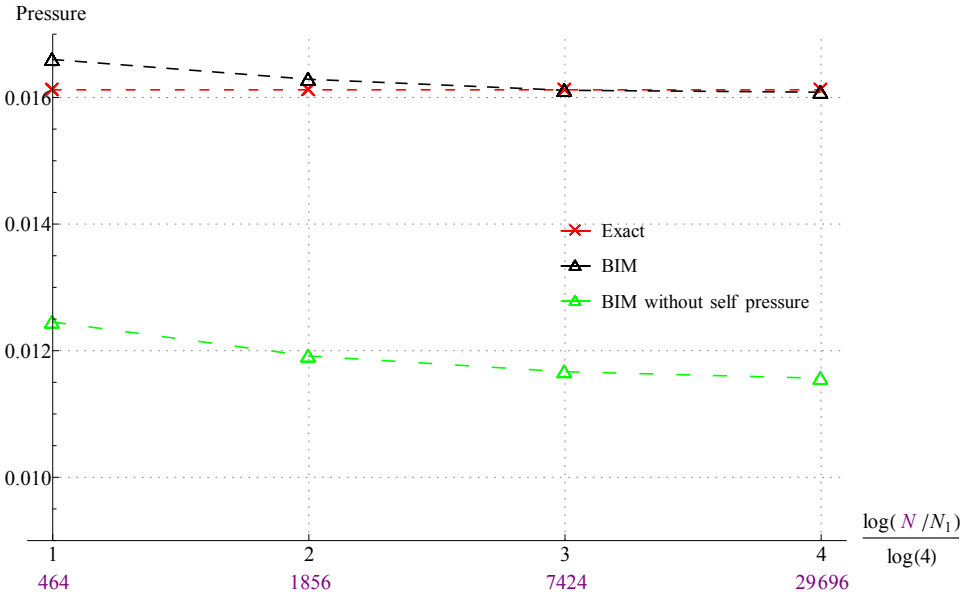

FIGURE 7.13: Pressure on inner sphere as function of resolution. $R_1 = 1.7$, $R_2 = 3.0$.

has a value of -94766, whereas the exact pressure is 0.8912 of the same units. Thus the absolute value of the self pressure is over 10^5 times larger than the pressure.

We also notice that it is the subtraction of the self pressure from the boundary integral equation that make the pressure converging towards the exact pressure. When the self pressure is not subtracted from the equations, the calculated pressure diverges away from the correct pressure when the resolution increases.

Thus our calculations show that, independently of the size of the curvature and the self pressure, the BIM outputs a pressure that is approaching the exact pressure when the resolution is increased. These calculations verify that the boundary integral equations

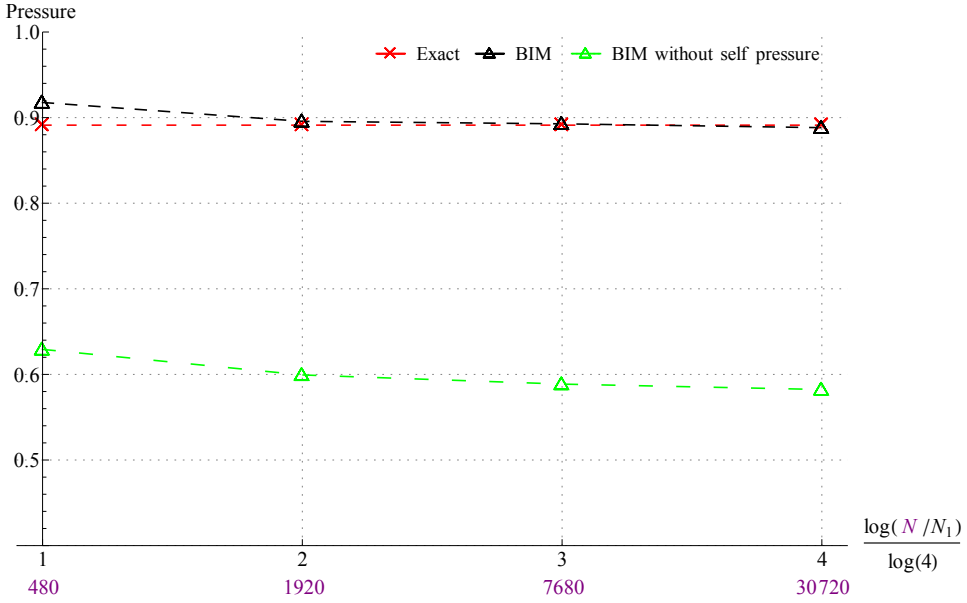

FIGURE 7.14: Pressure on inner sphere as function of resolution. $R_1 = 0.5$, $R_2 = 1.0$.

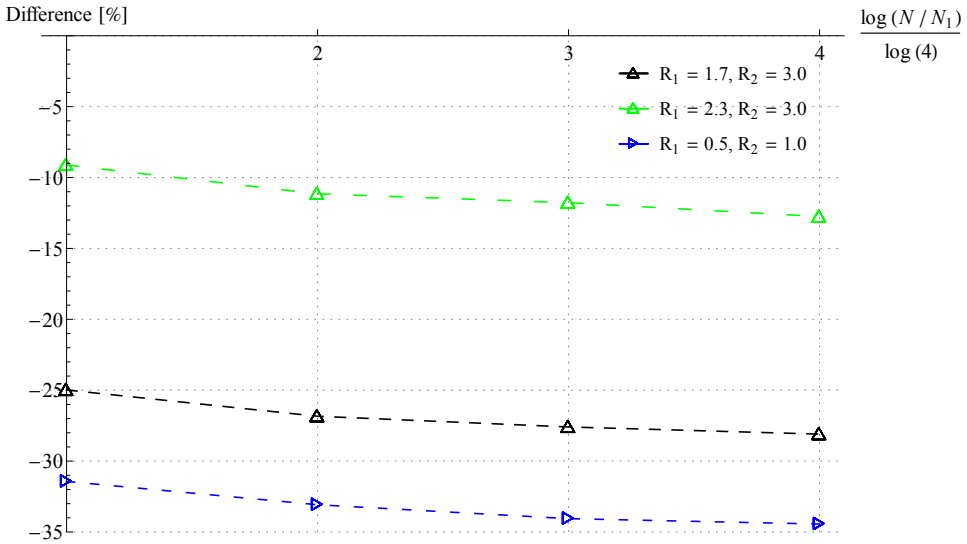

FIGURE 7.15: Difference in percent between calculated pressure on inner sphere with and without self pressure in the equations.

are correctly regularized for curved surfaces as well. However, in order to make sure that it is not the special property of constant curvature that gives rise to a correct pressure, we also do some calculations for configurations with varying curvature. These configurations will consist of ellipsoids and the results are presented in section 7.4.

7.2.2 Behaviour of pressure for different separation distances

To check how the error of the BIM behaves for different separation distances, we consider a configuration where the radius of the outer sphere is kept fixed, $R_2 = 3.0$. The radius of the inner sphere will be varied in the range from $R_1 = 1.4$ to $R_2 = 2.8$

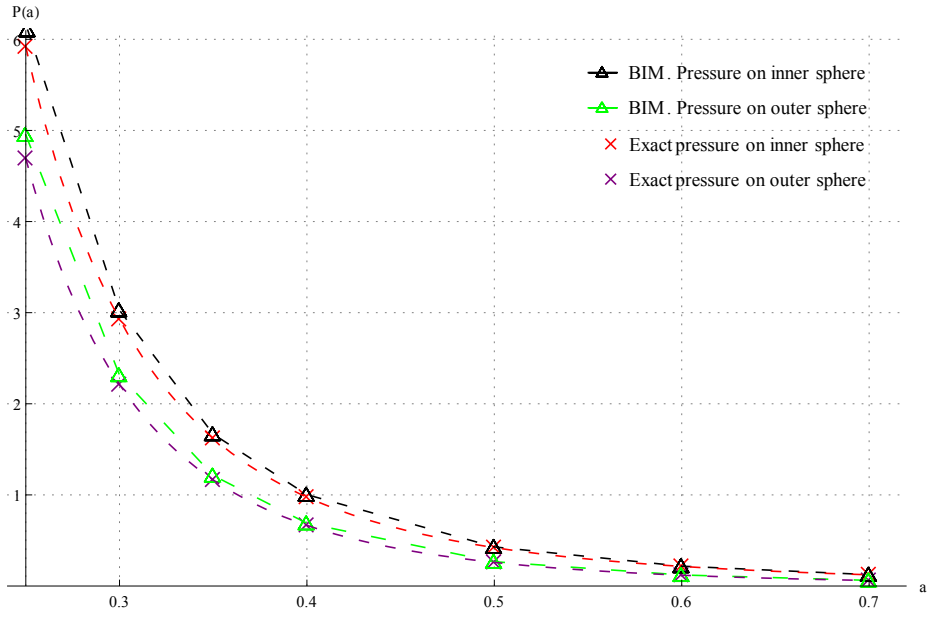

FIGURE 7.16: Pressure on each of the concentric spheres for $a = 0.25$ to $a = 0.7$.

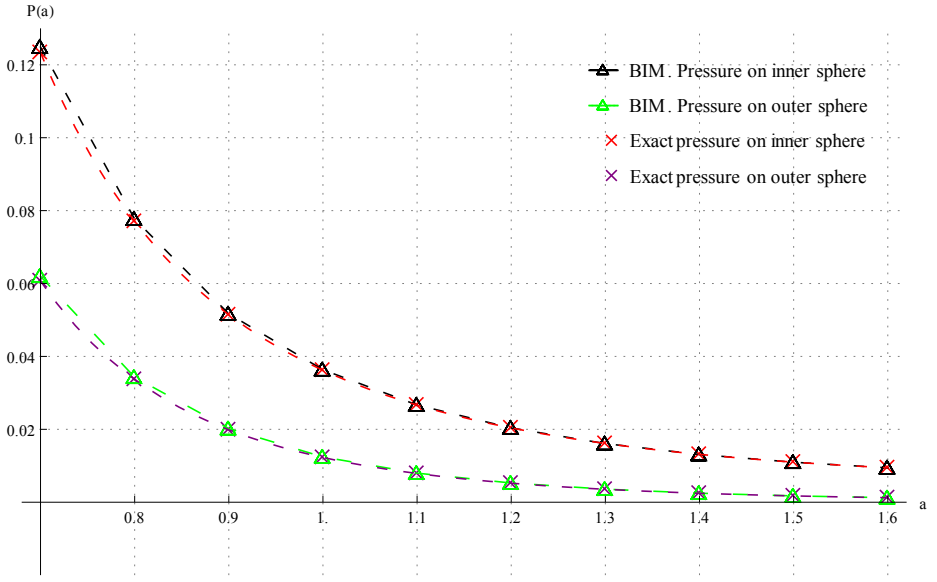

FIGURE 7.17: Pressure on each of the concentric spheres for $a = 0.7$ to $a = 1.6$.

units. For each pair of radii we calculate the pressure on both the inner and the outer sphere, using both the BIM and the FIM. Figures 7.16 and 7.17 show the pressure on both spheres, calculated using the BIM, compared to the exact solution obtained using mode summation. For this configuration Netgen managed to output triangulations with approximately the same number of triangles on each sphere, independently of the radius on the inner sphere. Thus there are about 30000 triangles on each of the discretized spheres.

Figure 7.18 shows the relative errors in the pressure on the inner sphere compared to the exact solution, whereas figure 7.19 shows the errors in the pressure on the outer

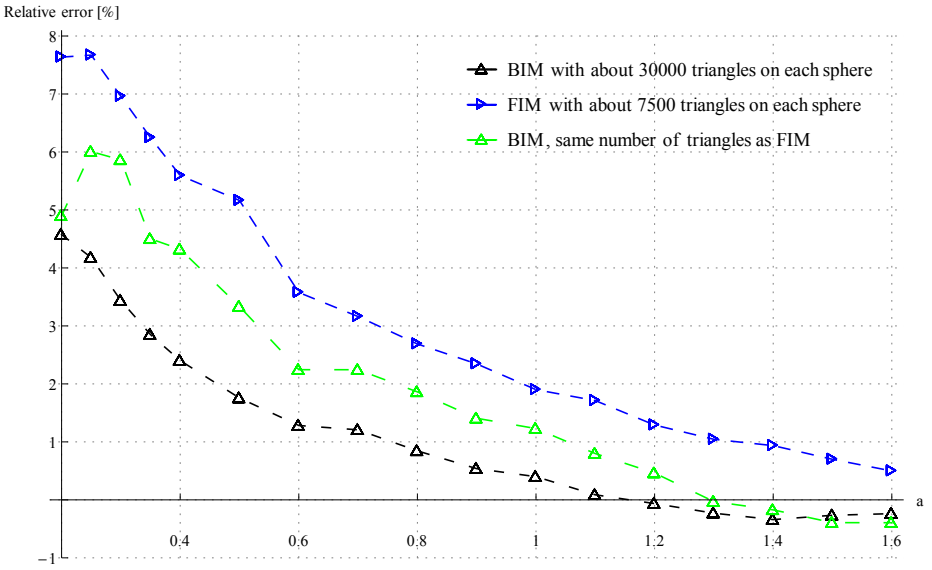

FIGURE 7.18: Error in calculated pressure on inner sphere relative to exact pressure.

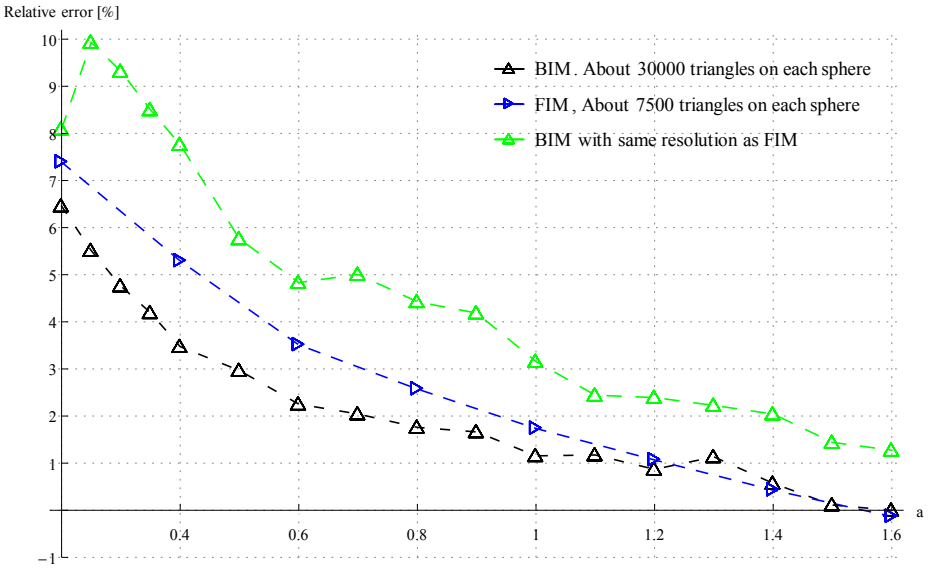

FIGURE 7.19: Error in calculated pressure on outer sphere relative to exact pressure.

sphere. As for the parallel plates, we see that the relative errors are largest at the shortest separation distances. We also observe that, for all distances where we have done measurements, the implementation of the BIM calculates the pressure more accurately at the 30000 resolution than the 7500 resolution. This is a another verification of what we found in the previous subsection.

We notice that on the inner sphere, the relative error in the pressure, found using the BIM, is 1-2 percentage points less than error in the FIM when the resolution is the same. On the outer sphere it is opposite. This is not in accordance with what I. Kilen found for the corresponding configuration in two dimensions, namely two concentric circles. He found that the FIM was, quite clearly, more accurate than the BIM on both circles.

Our results could indicate that the BIM is an even better alternative in three than in two dimensions.

Nevertheless, the fact that the BIM outputs a pressure that is approximately equal to the exact pressure and is even closer to the pressure calculated using the FIM, when corrected for the missing factor of two, supports the claim that our boundary integral equations are fully regularized, also for curved surfaces.

7.3 Adjacent spheres

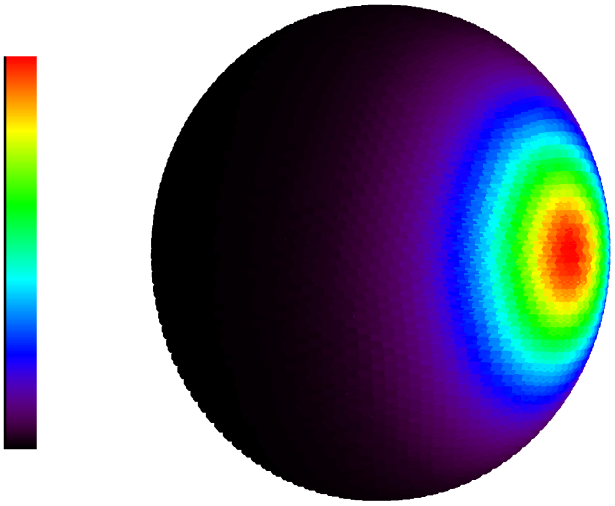

FIGURE 7.20: Force on one of the adjacent spheres.

We consider two spheres with radius $R = 1.0$, centered in $\boldsymbol{s}_1 = (0, 0, 0)$ and $\boldsymbol{s}_2 = (x, 0, 0)$. The separation distance between the two spheres is $a = x - 2$. The distance a will be varied in the range from $a = 1$ to $a = 2.2$. The main difference between this configuration and the concentric spheres is that the total force on each of the spheres isn't zero. This is a configuration where we don't have an exact solution. However, we can test the BIM versus the FIM. The corresponding configuration in two dimensions is two adjacent circles. I. Kilen found that the circles attracted each other. We expect that also the spheres will attract each other.

Figure 7.20 shows the pressure distribution, found using the BIM, on the sphere on the left hand side in the configuration. The red region, where the pressure is largest, is the region on the left sphere that is closest to the right sphere. When integrating over the pressure on each triangle, we find that the total force points directly towards the right sphere. The force on the right sphere is found to be of exactly equal size as the force on the left sphere, just oppositely directed. Thus the spheres attract each other.

In figure 7.21 the size of the total force on the left sphere is plotted for several separation distances a. We see that the force decreases as the separation distance increases. Figure 7.22 shows how much the force, found using the FIM, differs from the

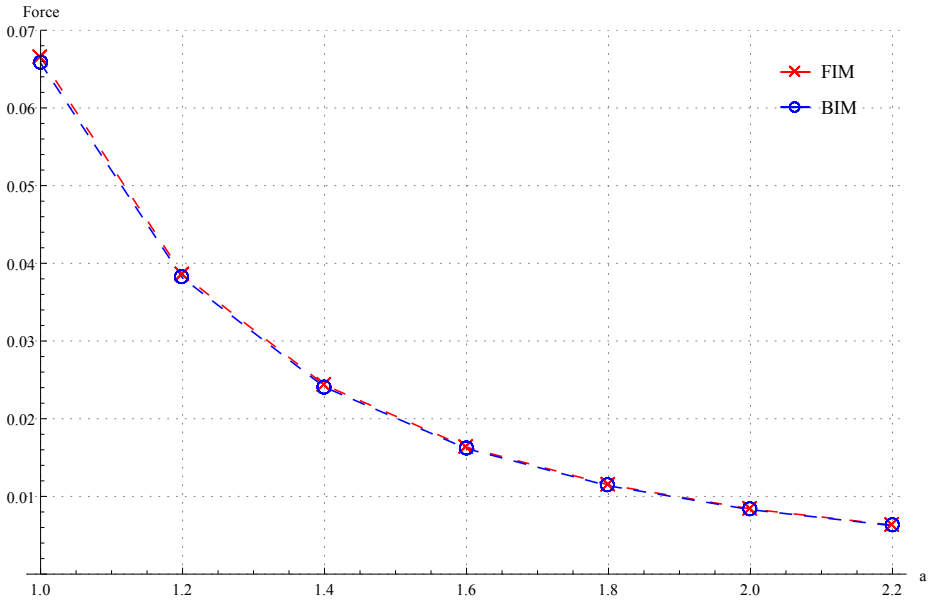

FIGURE 7.21: Force on the left sphere as function of separation distance.

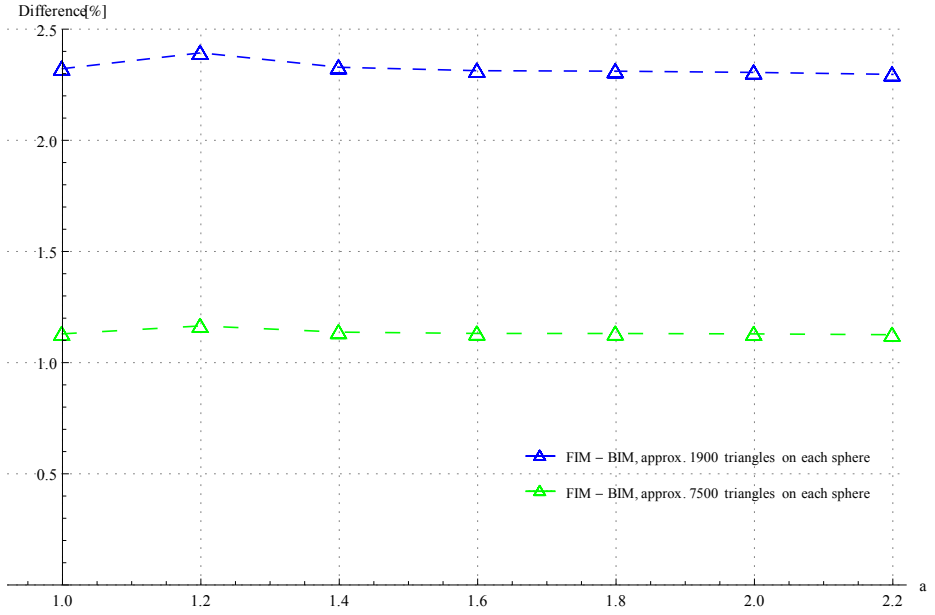

FIGURE 7.22: Difference in the force calculated using the FIM relative to the BIM.

force calculated with the BIM. We see that when there are about 1900 triangles on each sphere, the force calculated using the FIM is almost constantly about 2.3% larger than the force from the BIM. When there are about 7500 triangles on each sphere, the difference reduces to about 1.1%. Since we don't have an exact solution for this configuration, we can't decide which method is the better. However, the fact that the two methods give approximately the same results and that the difference between the two methods is getting smaller when the resolution increases, is another verification of that the implementations are correct.

7.4 Ellipsoids

The equation for an ellipsoid with center in the origin is given by

$$\left(\frac{x}{a}\right)^2 + \left(\frac{y}{b}\right)^2 + \left(\frac{z}{c}\right)^2 = 1. \tag{7.3}$$

We remember that a principal curvature is either a maximal or a minimal sectional curvature. Under the assumption $b = c = R < a = 1$, the maximal principal curvature on an ellipsoid is found at all sections through the points $(\pm 1, 0, 0)$ and is given by (see equation (59) in [23])

$$\kappa_{\max} = \frac{ab}{b^3} = \frac{1}{R^2}. \tag{7.4}$$

The minimal principal curvature is found at all sections that go through a point on the circle $(0, R\cos t, R\sin t)$ and is pointing in the x-direction. It is given by

$$\kappa_{\min} = \frac{ab}{a^3} = R. \tag{7.5}$$

Thus $\kappa_{\max} \to \infty$ and $\kappa_{\min} \to 0$ when $R \to 0$. This means that we can design an ellipsoid with as varying curvature as we want by choosing a small enough value of R.

7.4.1 Adjacent ellipsoids

Consider two adjacent ellipsoids centered in $\boldsymbol{s}_1 = (0, 0, 0)$ and $\boldsymbol{s}_2 = (x, 0, 0)$. The two ellipsoids will be of equal size and determined by the parameters $a = 1.0$, $b = c = 0.4$. Thus the curvature on the objects vary in the range from $\kappa_{\min} = 0.4$ to $\kappa_{\max} = \frac{1}{0.4^2} = 6.25$. The separation distance between the two ellipsoids is $d = x - 2$. We will calculate the force on the ellipsoids, using both the BIM and the FIM, for distances in the range from $d = 0.4$ to $d = 1.2$.

Figure 7.23 shows the size of the force on the ellipsoid that is centered around the origin for different separation distances. The force points directly towards the other sphere. Symmetry gives that the force on the other ellipsoid is of equal size, but oppositely directed. Thus the ellipsoids attract each other. Figure 7.24 shows the differences in the outputs from the two methods. For the resolution of 1300 triangles, the force calculated using the FIM is about 6% larger than the force from the BIM. When the resolution increase to 5200 triangles, the difference reduces to about 3%. We can't decide which method is the better, but we see that the two methods give approximately the same results and that the difference between the two methods is getting smaller when the resolution increases. When comparing to the adjacent spheres, we see that the difference between the FIM and the BIM is larger for ellipsoids. This indicates that, in order to get the same accuracy, one has to use a higher resolution for configurations with varying curvature than for configurations with constant curvature. However, based

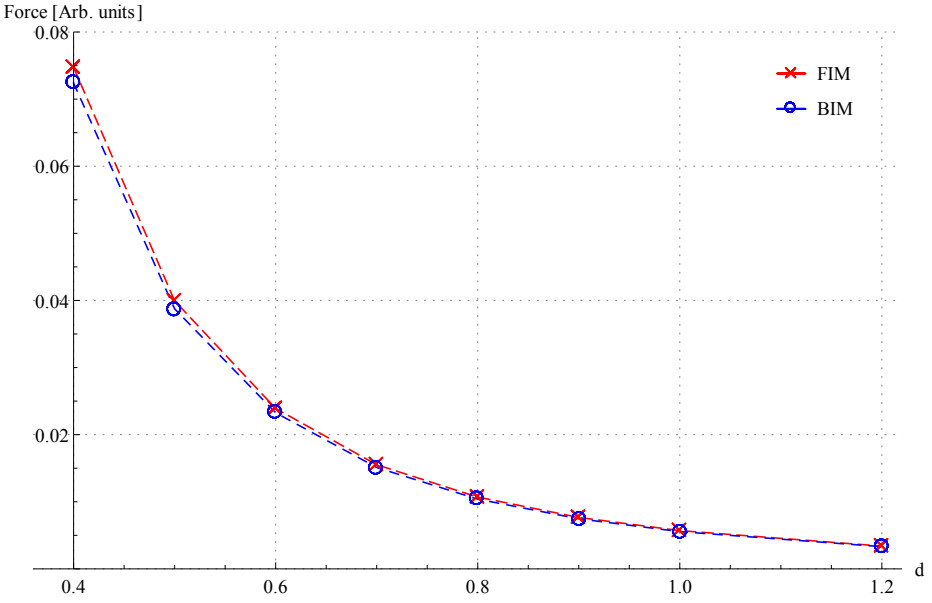

FIGURE 7.23: Force on the ellipsoid with center in the origin.

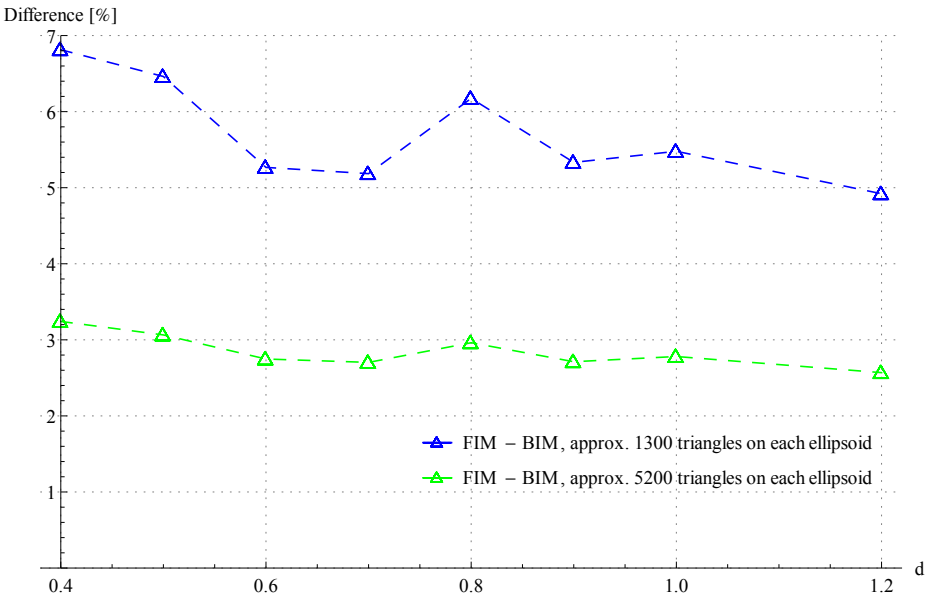

FIGURE 7.24: Difference in the force calculated using the FIM relative to the BIM.

on the calculations for adjacent ellipsoids, there is nothing that indicates that the BIM won't calculate the pressure/force correctly for configurations with varying curvature. The calculated force approaches the force obtained using an other method when the resolution is increased.

7.4.2 Concentric ellipsoids

Consider two concentric ellipsoids. Choose the parameters for the outer ellipsoid to be $a = 2$ and $b = c = 0.8$. For the inner ellipsoid we let $a = 1$ and $b = c = R$. The parameter R will be varied. We first use the BIM to calculate the pressure distribution

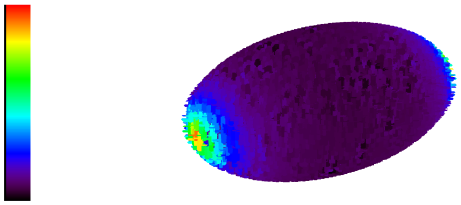

FIGURE 7.25: Illustration of the pressure distribution on the inner ellipsoid when $R = 0.4$

on the inner ellipsoid for $R = 0.4$. The pressure distribution is illustrated in figure 7.25. Even though we have used a rough discretization, we see that the pressure is largest around the points $(\pm 1, 0, 0)$. This is expected since the curvature is largest in these regions.

We now consider some situations where the variation in curvature is large. This is achieved by first letting $R = 0.4$, and then letting R approach zero. It turns out that $R = 0.2$ is the smallest value for which we are able to do calculations for at least two different resolutions. The extremal principal curvatures are then $\kappa_{\min} = 0.2$ and $\kappa_{\max} = \frac{1}{0.2^2} = 25$. We calculate the pressure and self pressure on the triangle that is closest to the point $(1, 0, 0)$, i.e. on the triangle where the pressure is largest. Since the pressure isn't constant on the ellipsoids, it is difficult to compare to the FIM. However, we saw in the previous subsection that the BIM calculates the force correctly, with increasing accuracy for increasing resolution, for a configuration with varying curvature as well. We therefore know that if we obtain a pressure that converges when the number of triangles increases, then it is the correct pressure on the object. Thus we have to compute the pressure on the ellipsoid for different resolutions.

TABLE 7.1: Two concentric ellipsoids. Parameters inner ellipsoid: $a = 1$, $b = c = 0.4$.

Resolution [Number of triangles]	1306	5224	20896
Pressure at the point (1,0,0)[Arb. units]	1.0473	1.0585	1.0671
Self pressure at the point (1,0,0)[Arb. units]	-4669	-27357	-134973

TABLE 7.2: Two concentric ellipsoids. Parameters inner ellipsoid: $a = 1$, $b = c = 0.3$.

Resolution [Number of triangles]	3170	12680
Pressure at the point (1,0,0)[Arb. units]	1.9804	2.0461
Self pressure at the point (1,0,0) [Arb. units]	-37612	-186126

TABLE 7.3: Two concentric ellipsoids. Parameters inner ellipsoid: $a = 1$, $b = c = 0.2$.

Resolution [Number of triangles]	9860	39440
Pressure at the point (1,0,0)[Arb. units]	5.7796	5.8561
Self pressure at the point (1,0,0)[Arb. units]	-587103	-2533434

Tables 7.1, 7.2 and 7.3 show that whereas the self pressure grows rapidly, the pressure is relatively stable for the different resolutions at constant $b = c = R$. For $R = 0.2$, we see that the absolute value of self pressure increases from 587103 to 2533434 when the number of triangles is increased from 9860 to 39440, whereas the pressure changes from 5.7796 to 5.8561. The small increase in pressure is partly due to the fact that the triangle where the pressure is calculated, is closer to the point $(1, 0, 0)$ the higher the resolution is. For $R = 0.2$ the centers of mass of the triangles are respectively (0.9979, 0.0076, 0.0044) and (0.9995, 0.0039, 0.0022). We see that the latter is closer to the point $(1, 0, 0)$ and therefore should the pressure be larger here. Therefore, when taking into account that an increase in resolution should improve the accuracy of the solution as well, it seems like the pressure converges. Thus the results obtained in this subsection is another verification of that the BIM calculates the pressure correctly for general configurations.

Chapter 8

Conclusion

We have in this thesis developed the boundary integral method for the special case of a 3D massless scalar field, subject to Dirichelet boundary conditions. The first step was to derive a boundary integral equation for the Casimir pressure. The regularization of the equation involved several steps:

1. Treat integrals that involve singularities as principal value integrals.
2. Take the limit $\boldsymbol{x}' \to \boldsymbol{x}''$ by first letting $\boldsymbol{x}'$ approach the same surface as $\boldsymbol{x}''$, then discretizing the surface and finally taking the limit along the discretized surface.
3. Subtract the self-pressure contribution from the equations.

In order to test whether the equations are fully regularized, the method has been implemented numerically and applied to several test configurations. For all test configurations, the calculated pressure was off by a factor of two compared to other methods. Except for this factor, the method has correctly predicted the geometry dependence of the test cases.

Our results are in accordance with the results I. Kilen [1] obtained in the two dimensional case. The missing factor has the same value in both two and three dimensions. We conclude that, in addition to being independent of the geometry, the factor is also independent of dimensionality. The source to this factor haven't been found yet, but we know that it is lost somewhere in the theory. A natural question to ask is whether it is also independent of the spin of the field? However, in practice, such a missing factor isn't a problem since we can renormalize the value of the pressure by multiplying by two.

There are differences between the methods in two and three dimensions. The largest difference is that, if taking the limit $\boldsymbol{x}' \to \boldsymbol{x}''$ correctly, the self-pressure is finite in two dimensions, whereas in 3D it is not. To obtain a finite self-pressure, we therefore included the discretization of the surfaces as a part of the regularization procedure. Despite this, we have seen that the self-pressure increases when the curvature or resolution increases.

A large self-pressure has given rise to some numerical challenges, but nevertheless, after renormalization, the value of the Casimir pressure/force has been correct for all test configurations.

We conclude that our boundary integral equations are fully regularized. The boundary integral method calculates the Casimir pressure correctly in the case of a 3D massless scalar field.

8.1 Further work

The missing factor of two is not a problem in practice. However, it would have been nice to find its source. The BIM has not been tested on configurations where boundaries of the objects are non-differentiable. Many devices have vertices and therefore it would be interesting to consider how the BIM behaves for such configurations as well.

It would also be interesting to extend the method to other boundary conditions such as von Neumann boundary conditions. A natural next step is to extend to the case of electromagnetic fields, which physically, is a more realistic situation.

Appendix A

Gaussian integrals

A.1 Real situation

Let $I(\lambda)$ be the one dimensional Gaussian integral

$$I(\lambda) = \int_{-\infty}^{\infty} dx\, e^{-\lambda x^2}, \quad \lambda > 0. \tag{A.1}$$

By squaring and introducing polar coordinates, we obtain

$$\begin{aligned} I^2(\lambda) &= \int_{-\infty}^{\infty} dx\, e^{-\lambda x^2} \int_{-\infty}^{\infty} dy\, e^{-\lambda y^2} = \int_{-\infty}^{\infty}\int_{-\infty}^{\infty} dxdy\, e^{-\lambda(x^2+y^2)} \\ &= \int_0^{2\pi} d\theta \int_0^{\infty} dr\, re^{-\lambda r^2} \overset{u=\lambda r^2}{=} 2\pi \frac{1}{2\lambda} \int_0^{\infty} du\, e^{-u} = \frac{\pi}{\lambda}. \end{aligned} \tag{A.2}$$

Thus

$$I(\lambda) = \int_{-\infty}^{\infty} dx\, e^{-\lambda x^2} = \sqrt{\frac{\pi}{\lambda}}. \tag{A.3}$$

Let $D = (d_{ij}) = \mathrm{diag}(\lambda_j)$ be a $n \times n$ diagonal matrix. Assume that D is positive definite, i.e. $\lambda_j > 0\ \forall j$. Define $\boldsymbol{x}^T = (x_1, ..., x_n)$ and let $\langle \boldsymbol{x}, \boldsymbol{y} \rangle = \boldsymbol{x}^T \boldsymbol{y}$ denote the standard inner product in $\mathbb{R}^n$. Then

$$\langle \boldsymbol{x}, D\boldsymbol{x} \rangle = \sum_{i,j} x_i d_{ij} x_j = \sum_j .\lambda_j x_j^2 \tag{A.4}$$

The determinant of D is given by

$$\det D = \prod_j \lambda_j. \tag{A.5}$$

Let $I_n(D)$ be the n-dimensional Gaussian integral,

$$I_n(D) = \int_{\mathbb{R}^n} d\boldsymbol{x}\, e^{-\langle \boldsymbol{x}, D\boldsymbol{x}\rangle}. \tag{A.6}$$

Using the results (A.3), (A.4) and (A.5), we can calculate the integral $I_n(D)$;

$$\begin{aligned} I_n(D) &= \int_{\mathbb{R}^n} d\boldsymbol{x}\, e^{-\sum_j \lambda_j x_j^2} = \int_{-\infty}^{\infty} dx_1\, e^{-\lambda_1 x_1^2} \cdots \int_{-\infty}^{\infty} dx_n\, e^{-\lambda_n x_n^2} \\ &= \sqrt{\frac{\pi}{\lambda_1}} \cdots \sqrt{\frac{\pi}{\lambda_n}} = \sqrt{\frac{\pi^n}{\prod_j \lambda_j}} = \frac{\pi^{n/2}}{(\det D)^{1/2}}. \end{aligned} \tag{A.7}$$

Next, assume A is a real, positive definite, symmetric matrix. Then there exists a rotation (orthogonal) matrix R, with the properties

$$\begin{aligned} R^T &= R^{-1}, \\ R^T A R &= D, \\ \det R &= 1, \end{aligned} \tag{A.8}$$

where $D = \mathrm{diag}(\lambda_i)$ is a diagonal matrix consisting of the eigenvalues $\{\lambda_i\}$ of A, which are positive. The integral $I_n(A)$ can be calculated by introducing the change of variables $\boldsymbol{x}' = R^T\boldsymbol{x}$ and then using the properties (A.8) and the result in equation (A.7);

$$\begin{aligned} I_n(A) &= \int_{\mathbb{R}^n} d\boldsymbol{x}\, e^{-\langle \boldsymbol{x}, A\boldsymbol{x}\rangle} = \int_{\mathbb{R}^n} d(R\boldsymbol{x'})\, e^{-\langle R\boldsymbol{x}', AR\boldsymbol{x}'\rangle} \\ &= \det R \int_{\mathbb{R}^n} d\boldsymbol{x}'\, e^{-\langle \boldsymbol{x}', R^T AR\boldsymbol{x}'\rangle} = \int_{\mathbb{R}^n} d\boldsymbol{x}'\, e^{-\langle \boldsymbol{x}', D\boldsymbol{x}'\rangle} \\ &= \frac{\pi^{n/2}}{(\det D)^{1/2}}. \end{aligned} \tag{A.9}$$

The property

$$\det D = \det(R^T A R) = \det(ARR^T) = (\det A)\det(RR^{-1}) = \det A \tag{A.10}$$

gives that

$$I_n(A) = \int_{\mathbb{R}^n} d\boldsymbol{x}\, e^{-\langle \boldsymbol{x}, A\boldsymbol{x}\rangle} = \frac{\pi^{n/2}}{(\det A)^{1/2}}. \tag{A.11}$$

This holds for any real, positive definite, symmetric $n \times n$ matrix A.

A.2 Complex situation

Start by rewriting $I^2(\lambda)$ from the previous section;

$$\frac{\pi}{\lambda} = \iint\limits_{\mathbb{R}^2} dxdy\, e^{-\lambda(x^2+y^2)} = \iint\limits_{\mathbb{R}^2} dxdy\, e^{-\lambda(x-iy)(x+iy)}. \tag{A.12}$$

Introduce a change variables

$$\begin{aligned} z &= x + iy, \\ z^* &= x - iy. \end{aligned} \tag{A.13}$$

The volume form becomes

$$dx \wedge dy = \frac{dz + dz^*}{2} \wedge \frac{dz - dz^*}{2i} = \frac{dz \wedge dz^*}{2i}. \tag{A.14}$$

Thus

$$\int\limits_{\mathbb{C}} \tfrac{dzdz^*}{2\pi i}\, e^{-\lambda z^* z} = \frac{1}{\lambda}. \tag{A.15}$$

Let $D = (d_{ij}) = \operatorname{diag}(\lambda_j) \in \mathbb{R}^{n\times n}$ be a diagonal matrix, where $\lambda_j > 0$, $j = 1, ..., n$. Let $\langle \boldsymbol{z}, \boldsymbol{w} \rangle = \boldsymbol{z}^* \boldsymbol{w}$ denote the standard dot product in $\mathbb{C}^n$, where $\boldsymbol{z}^*$ is the conjugate transpose of the column vector $\boldsymbol{z}$. Using the abbreviation

$$[d\boldsymbol{z}d\boldsymbol{z}^*] = \prod_{j=1}^{n} \frac{dz_j dz_j^*}{2\pi i} \tag{A.16}$$

and the result in equation (A.15), we obtain

$$\int\limits_{\mathbb{C}^n} [d\boldsymbol{z}d\boldsymbol{z}^*]\, e^{-\langle \boldsymbol{z}, D\boldsymbol{z}\rangle} = \int\limits_{\mathbb{C}^n} [d\boldsymbol{z}d\boldsymbol{z}^*]\, e^{-\sum_j \lambda_j |z_j|^2} = \frac{1}{\det D}. \tag{A.17}$$

Let A be a positive definite, self-adjoint matrix. Then there exists a unitary matrix U, with properties

$$\begin{aligned} UU^* = U^*U &= I, \\ |\det U| &= 1, \\ U^*AU &= D, \end{aligned} \tag{A.18}$$

where $D = \operatorname{diag}(\lambda_i)$ is a diagonal matrix consisting of the eigenvalues $\{\lambda_i\}$ of A. Since A is positive definite and self-adjoint, the eigenvalues are real and positive. Introducing a change of variables, $\boldsymbol{z} = U\boldsymbol{z}'$, using the properties (A.18) and the result in equation

(A.17), we obtain

$$\begin{aligned}\int_{\mathbb{C}^n} [d\boldsymbol{z}d\boldsymbol{z}^*]\, e^{-\langle \boldsymbol{z}, A\boldsymbol{z}\rangle} &= \int_{\mathbb{C}^n} [d(U\boldsymbol{z}')d(U\boldsymbol{z}')^*]\, e^{-\langle U\boldsymbol{z}', AU\boldsymbol{z}'\rangle} \\ &= \det(UU^*) \int_{\mathbb{C}^n} [d\boldsymbol{z}'d\boldsymbol{z}'^*]\, e^{-\langle \boldsymbol{z}', U^*AU\boldsymbol{z}'\rangle} \\ &= \int_{\mathbb{C}^n} [d\boldsymbol{z}'d\boldsymbol{z}'^*]\, e^{-\langle \boldsymbol{z}', D\boldsymbol{z}'\rangle} \\ &= \frac{1}{\det D}.\end{aligned} \tag{A.19}$$

Using the property that

$$\begin{aligned}\det D = \det(U^*AU) = \det(AUU^*) &= (\det A)\det(UU^*) \\ = (\det A)\det(I) &= \det A,\end{aligned} \tag{A.20}$$

we get

$$\int_{\mathbb{C}^n} [d\boldsymbol{z}d\boldsymbol{z}^*]\, e^{-\langle \boldsymbol{z}, A\boldsymbol{z}\rangle} = \int_{\mathbb{C}^n} \prod_{j=1}^{n} \frac{dz_j dz_j^*}{2\pi i}\, e^{-\langle \boldsymbol{z}, A\boldsymbol{z}\rangle} = \frac{1}{\det A}. \tag{A.21}$$

This result holds for any positive definite, self-adjoint $n \times n$ matrix A.

Appendix B

Mesh generation and triangulation

Almost all of the differential equations that arises when doing physical simulation have to be solved numerically. Usually a continuous problem is replaced by a discrete problem that can be computed thanks to the power of currently available computers. The solution to the discrete problem is then an approximate solution to the initial problem whose accuracy is based on the various choices that are made in the numerical process. When going from a continuous to a discrete problem, one usually start with discretizing the domain of interest, i.e one divides the domain into a *mesh* or approximate it by a mesh. A mesh is a finite union of small, simple elements such as for example triangles, quads or tetrahedra depending on the complexity and the spatial dimension of the domain. Meshes of different kinds are so often used that mesh generation has become an own industry. There exists much software (both commercial and not, see [24]) developed for mesh generation. We have used the free software *Netgen* for meshing our surfaces into triangles.

A mesh can either be *structured* or *unstructured*. The primary difference is that a structured mesh has a regular topology, i.e it has a well known pattern, while an unstructured mesh has an irregular topology, which means that the topology has to be stored for every element of the mesh. A typical example of a structured mesh in two dimensions is a square grid that may be deformed by a coordinate transformation (see figure B.2). An unstructured mesh is often a *triangulation* with arbitrarily varying local neighbourhoods (see figure B.1).

There are some advantages using a structured mesh instead of an unstructured. The elements usually have a lower geometric complexity and require less computer memory because the coordinates can be calculated, rather than explicitly stored. A structured mesh also offers more direct control over the size and shape of the elements. The big disadvantage is its lack of flexibility in fitting a complex domain, it may require many

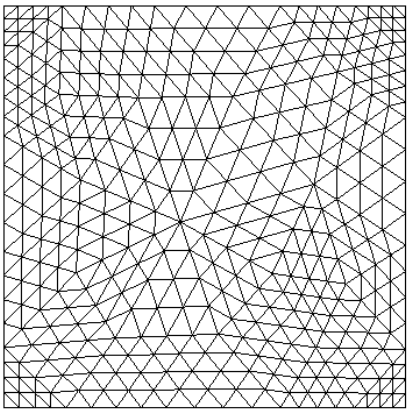

FIGURE B.1: Example of an unstructured mesh of a plane

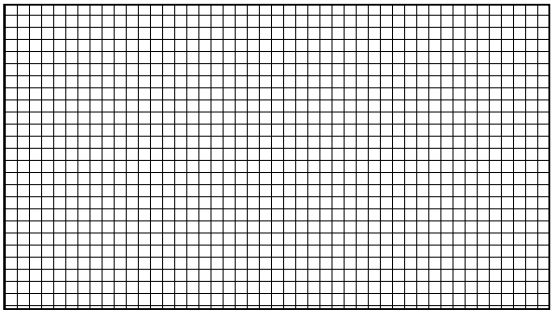

FIGURE B.2: Example of a structured mesh of a plane

elements and the elements themselves can be ill-shaped. Actually it may be impossible to find a structured mesh that fits a complicated domain acceptably well. On the contrary, an unstructured mesh can fit an arbitrarily complicated domain. Therefore, when the domain of interest is complex enough, it could be that the only option is to use an unstructured mesh.

As mentioned above, a typical example of an unstructured mesh is a triangulation. It is possible to define a triangulation in several ways, depending on how the geometric object that should be triangulated is represented. However, in general we can say that a triangulation of a geometric object is a subdivision into simplices. A simplex is a generalized triangle. We can also say that for a triangulation of a geometric object in $\mathbb{R}^n$ there are two properties that have to be satisfied;

1. Let S_i and S_j be two simplices in the triangulation and A be the intersection $A = S_i \bigcap S_j$. Then A either is the empty set or a simplex of dimension less than the dimension of S_i and S_j.

2. Any bounded set in $\mathbb{R}^n$ intersects only a finite number of simplices in the triangulation.

The geometric objects we are considering in this thesis are compact sets in $\mathbb{R}^3$. We are interested in triangulating the boundaries of such objects. A triangulation of such surfaces consists of triangles that intersect only at shared edges and vertices. An other example is a triangulation of a 3-dimensional object in $\mathbb{R}^3$ which consists of tetrahedrons that intersect at shared facets, edges and vertices. The triangulation of a polytope is a partition of simplices that covers the object exactly. Since a triangulation is a union of objects without curvature, the triangulation of a curved object will necessarily only be an approximation of the object.

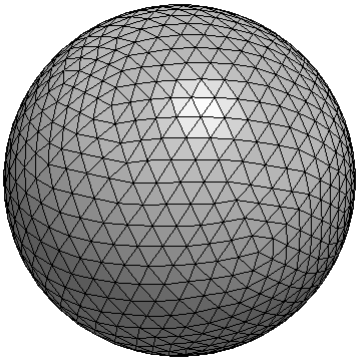

FIGURE B.3: Triangulation of a sphere

Triangulations can be used to approximate all kinds of objects; a sphere (see figure B.3), an aircraft, the shape of a teapot, a horse and so on. In fact, it has been proven that all surfaces can be triangulated [25]. However, to find such a triangulation can be a very hard problem. In addition, one usually isn't satisfied with only finding a triangulation, one also want to optimize the triangulation such that the numerical solution of the problem one has in hand actually is close to the exact solution of the problem.

An optimal triangulation is the one that is best according to some criterion that measures for example the size, shape, or number of simplices. These measures are often referred to as *quality measures*. For triangles typical quality measures are angles, length of edges, height and area. An example of a triangulation with bad quality is one where the minimal angle of some of the triangles is very small and the ratios of the length of the edges are far away from 1. Many different methods for triangulating objects have been developed in order to make optimal triangulations. The method that maybe is most known is the *Delaunay triangulation*, which is made such that no point in the point set that is triangulated, is inside the circum-hypersphere of any simplex in the triangulation. In the plane, a property of this triangulation is that it maximizes the minimal angle of the triangles. For more information about the Delaunay triangulation and other kinds of triangulations, see for example [26].

When using a software to triangulate an object one has to think through how to represent the object and how to store the mesh of the object. Usually the software supports

different kinds of both input and output file formats. If the object is a union, intersection or the complement of well-known primitives such as planes, spheres, ellipsoids etc. then there exists a file format, called constructive solid geometry (CSG) format, which is easy to use. For more advanced geometries, other file formats such as for example STL can be used. Information about the different file formats that the software supports is usually found in the documentation of the software. The *neutral file format* in the software Netgen is a simple format that is used to store the mesh. This format is easy to read into any program. A brief description of the format is given here. The two basic quantities in a triangulation are the nodes (points) and the triangles. Nodes are easy to represent, since they can be identified simply by their Cartesian coordinates. To represent the node information, one first writes the number of nodes and then the coordinates of each node line for line. The information about the triangles starts on the first line after the coordinates. First the number of triangles is written down. Then for each triangle there is a new line containing four integers. The first of the integers is the identifying number of the triangle, and the three other say where in the node list the three vertices are found. The vertices are oriented in such a way that the triangles have a counter clockwise orientation when looking at the object.

Appendix C

Programs and files used in the implementations

This appendix is written for them who want to use the programs we have developed to do more calculations than we have reported in this thesis. We therefore write down all of the programs that are used when doing the numerics, and give a short explanation of them.

Some remarks that may be helpful when running programs on the supercomputer *Stallo*: Infiles to the main programs must be saved at the location */global/work/$USER/* . Programs are started by sending a runscript to Stallo using for example *qsub runscript.sh*. This command must be typed from the directory where the program is saved. Before compilation of the programs, the library *gsl* must be loaded. This is done by typing the command *module load gsl* on the command line.

C.1 Boundary integral method

Table C.1 lists up programs used in the implementation of the boundary integral method with a discretization consisting of squares.

Table C.2 lists up programs used in the implementation of the boundary integral method with a discretization consisting of triangles.

C.2 Functional integral method

Table C.3 lists up programs used in the implementation of the functional integral method with a discretization consisting of squares.

Table C.4 lists up programs used in the implementation of the functional integral method with a discretization consisting of triangles.

Table C.1: BIM_sq

Program	**Description**
BIMsq.c	Main program.
indataBIMsq	Example of the only infile needed to run BIMsq.c
makefileBIMsq	File needed to compile the main program on an ordinary linux computer
makefileBIMsq_stallo	File needed to compile the main program on Stallo
runscript_BIMsq.sh	File that is sent to Stallo in order to run the program BIMsq.c.
fortran.f	GMRES-routine written in the language *fortran*, which is used by BIMsq.c
resBIMsq	Example of file outputted when running BIMsq.c.

Table C.2: BIM_tri

Program	**Description**
BIMtri.c	Main program.
indataBIMtri	The infile to BIMtri.c.
makefileBIMtri	File needed to compile the main program on an ordinary linux computer
makefileBIMtri_Stallo	File needed to compile the main program on Stallo.
runscript_BIMtri.sh	File that is sent into Stallo in order to run the program BIMtri.c.
fortran.f	GMRES-routine written in the language *fortran*, which is used by BIMtri.c
pressureBIMtri	Example of outdata.

Table C.3: FIM_sq

Program	**Description**
FIMsq.c	Main program for FIM_sq.
indataFIMsq	Example of indata
makefileFIMsq	Makefile ordinary linux computer
makefileFIMsq_stallo	Makefile on Stallo
runscript_FIMsq.sh	File that is sent into Stallo in order to run the program FIMsq.c.
resFIMsq	Example of outdata from FIMsq.

TABLE C.4: FIM_tri

Program	**Description**
FIMtri.c	Main program.
indataFIMtri	Example of the first of three infiles to FIMtri.c. Contains parameters.
surface_minusda	Example of the second infile. Contains the triangulation of the surfaces with separation distance a - da
surface_plussda	Example of the third infile. Contains the triangulation of the surfaces with separation distance a + da
makefileFIMtri	Makefile ordinary linux computer
makefileFIMtri_stallo	Makefile on Stallo
runscript_FIMtri.sh	File that is sent into Stallo in order to run the program FIMtri.c.
resFIMtri	Example of output from FIMtri.c.

Bibliography

[1] I.R Kilen. Numerical calculation of casimir forces. Master's thesis, University of Tromsø, June 2012. URL `http://hdl.handle.net/10037/4376`.

[2] H. B. G. Casimir. On the attraction between two perfectly conducting plates. *Kon. Ned. Akad. Wetensch.*, 51:793–795, 1948.

[3] Julian Schwinger. Casimir effect in source theory. *Lett. Math. Phys. 1*, pages 43–47, 1975.

[4] M. J. Sparnaay. Measurements of attractive forces between flat plates. *Physica, 24*, pages 751–764, 1958.

[5] S. K. Lamoreaux. Demonstration of the casimir force in the 0.6 μm to 6 mm range. *Phys. Rev. Lett. 78*, pages 5–8, 1997.

[6] U. Mohideen and A. Roy. Precision measurement of the casimir force from 0.1 to 0.9 mm. *Phys.Rev.Lett 81.*

[7] U. Mohideen M. Bordag, G.L. Klimchitskaya and V.M. Mostepanenko. Advances in the casimir effect. *Oxford Science Publications*, 2009.

[8] Federico Capasso J. N. Munday1 and V. Adrian Parsegian. Measured long-range repulsive casimir-lifshitz forces. *Nature*, 457:170–173, 2009. URL `http://www.nature.com/nature/journal/v457/n7226/suppinfo/nature07610_S1.html`.

[9] F.C. Lombardo F.D. Mazzitelli, D.A.R. Dalvit. Exact zero-point interaction energy between cylinders. *New J.Phys.8:240*, 2006. URL `http://arxiv.org/pdf/quant-ph/0610181.pdf`.

[10] Thorsten Emig, Andreas Hanke, Ramin Golestanian, and Mehran Kardar. Probing the strong boundary shape dependence of the casimir force. *Phys. Rev. Lett.*, 87: 260402, Dec 2001. doi: 10.1103/PhysRevLett.87.260402. URL `http://link.aps.org/doi/10.1103/PhysRevLett.87.260402`.

[11] Thorsten Emig, Andreas Hanke, Ramin Golestanian, and Mehran Kardar. Normal and lateral casimir forces between deformed plates. *Phys. Rev. A*, 67:022114, Feb

2003. doi: 10.1103/PhysRevA.67.022114. URL http://link.aps.org/doi/10.1103/PhysRevA.67.022114.

[12] R. L. Jaffe M. Kardar T. Emig, N. Graham. Casimir forces between arbitrary compact objects. *Phys.Rev.Lett.99:170403,2007*, 2007. URL http://arxiv.org/abs/0707.1862.

[13] R. L. Jaffe M. Kardar T. Emig, N. Graham. Casimir forces between compact objects: I. the scalar case. *Phys.Rev.D77:025005,2008*, 2008. URL arXiv:0710.3084.

[14] D. Iannuzzi J. D. Joannopoulos S. G. Johnson A. Rodriguez, M. Ibanescu. Virtual photons in imaginary time: Computing exact casimir forces via standard numerical-electromagnetism techniques. *Physical Review A, 76:032106, 2007.* URL http://arxiv.org/abs/0705.3661.

[15] S. M. Christensen. Vacuum expectation value of the stress tensor in an arbitrary curved background: The covariant point-separation method. *Phys. Rev. D*, 14: 2490–2501, Nov 1976. doi: 10.1103/PhysRevD.14.2490. URL http://link.aps.org/doi/10.1103/PhysRevD.14.2490.

[16] N. F. Svaiter V. A. De Lorenci, G. Menezes. Light-cone fluctuations and the renormalized stress tensor of a massless scalar field. *Int. J. Mod. Phys. A28 (2013) 1350001.* URL http://arxiv.org/abs/1208.3860.

[17] K.E. Schmidt. Introduction to some basic operations needed for numerical calculations in electromagnetism. URL http://fermi.la.asu.edu/PHY531/intro/node2.html.

[18] J. Sondow and E.W. Weisstein. Riemann zeta function. . URL http://mathworld.wolfram.com/RiemannZetaFunction.html. From MathWorld–A Wolfram Web Resource.

[19] J. Sondow and E.W. Weisstein. Hurwitz zeta function. . URL http://mathworld.wolfram.com/HurwitzZetaFunction.html. From MathWorld–A Wolfram Web Resource.

[20] M. Ozcan. Scalar casimir effect between two concentric spheres. *International Journal of Modern Physics A 27, 1250082 (2012)*, July 2012. URL http://arxiv.org/pdf/1207.4183v1.pdf.

[21] S. Gratton V. Frayssé, L. Giraud and J. Langou. A set of gmres routines for real and complex arithmetics. URL http://www.cerfacs.fr/algor/Softs/GMRES/index.html.

[22] D. Kahaner, C. B. Moler, and S. Nash. *Numerical Methods and Software*. Prentice-Hall, Englewood Cliffs, 1989. ISBN 0-13-627258-4.

[23] E. W. Weisstein. Ellipse. . URL `http://mathworld.wolfram.com/Ellipse.html`. From MathWorld–A Wolfram Web Resource.

[24] R. Schneider. URL `http://www.robertschneiders.de/meshgeneration/software.html`.

[25] E.W. Weisstein. Triangulation. . URL `http://mathworld.wolfram.com/Triangulation.html`. From MathWorld–A Wolfram Web Resource.

[26] M. W. Bern and D. Eppstein. Mesh generation and optimal triangulation. In Ding-Zhu Du and Frank Kwang-Ming Hwang, editors, *Computing in Euclidean Geometry*, number 4 in Lecture Notes Series on Computing, pages 47–123. World Scientific, second edition, 1995. URL `http://www.ics.uci.edu/~eppstein/pubs/BerEpp-CEG-95.pdf`.